Buckling Resistance of Single and Double Angle Compression Members

Ahmad Mfarreh M Alenezi

Thesis submitted to the University of Ottawa
in partial fulfillment of the requirements for the degree of
Doctor of Philosophy
in Civil Engineering

Department of Civil Engineering
Faculty of Engineering
University of Ottawa

uOttawa

ABSTRACT

The present dissertation contributes to advancing methods of determining the elastic and inelastic buckling resistance of compressive members with single angle and back-to-back double angle cross-sections with end conditions representative of those commonly used in steel construction.

The first contribution develops an elastic buckling solution for members with asymmetric sections, such as unequal-leg angle members, connected to gusset plates at both ends and subjected to pure compression. In this case, the gusset plate connections at the member ends provide a fixity restraint to the member within the plane of the gusset and nearly a pin restraint in a plane normal to the gusset. Since both directions do not coincide with the principal directions of the member, the classical flexural-torsional buckling solutions provided in standards become inapplicable. In this context, a variational principle is formulated based on non-principal directions and then used to derive the governing differential equations and associated boundary conditions for the problem. The coupled equations are then solved analytically subject to the boundary conditions, and the characteristic equations are recovered and solved for the flexural-torsional buckling load of the member. The validity of the solutions derived is assessed against 3D shell elastic eigen-value buckling models based on ABAQUS for benchmark cases and the solution is shown to accurately predict the elastic buckling load and mode shapes. The effect of non-principal end restraints on the buckling load of compression members is then investigated for members with angle and zed cross-sections in a parametric study. It is observed that when a member end is fixed about a non-principal direction and pinned about the orthogonal direction, the flexural-torsional buckling load of the member is significantly influenced by the angle of inclination between the fixity axis and the minor principal axis.

The second contribution aims to obtain the inelastic buckling resistance for single angle compression members with end gusset plate connections by taking into consideration the effects of material and geometric nonlinearity, initial out-of-straightness, residual stresses, and load eccentricity induced by the offset of the member centroidal axis from the end gusset plate connection. Towards this goal, a series of 3D shell models based on ABAQUS are developed and validated through comparisons against experimental results by others and then used to generate a database of compressive capacities for over 900 eccentrically loaded angle members with various geometrical dimensions and load eccentricities. The database is then used to investigate the effect of slenderness ratio, leg width ratio, connected leg width-to-thickness ratio and gusset plate-to-angle thickness ratio on the compressive resistance of the members, assess the accuracy of solutions available in present design standards, and develop improved design expressions for the compressive resistance for the members.

The third contribution develops solutions for predicting the elastic buckling resistance of back-to-back double angle assemblies with end gusset plates and intermediate interconnectors subjected to compressive loads. Towards this goal, two novel models are developed. (1) A thin-walled finite element buckling solution is formulated and implemented into a MATLAB code. The formulation treats each angle member as a line of 1D thin-walled beam elements where then both angle members are connected at intermediate points along the span at the locations of interconnectors. The formulation is equipped with a multi-point constraint feature to enforce the kinematic constraints at the interconnector locations and at both extremities of the member. The model captures the tendency of both angles to open relative to one another in between interconnectors while undergoing flexural-torsional buckling. (2) An analytical buckling solution is developed for the limiting case where enough interconnectors are provided between members to force the two

angles to essentially behave as a monolithic entity. The resistance predicted by the former model was then shown to asymptotically approach that predicted by the later model as the number of interconnectors is increased. The validity of the finite element model is assessed against 3D shell models based on ABAQUS and published experimental results, and then used to assess the validity of present design rules based on the effective slenderness concept. The present models are then used to carry out a parametric study of 1250 runs while varying the member slenderness ratio, leg width ratio, connected leg width-to-thickness ratio, and angle spacing-to-thickness ratio. The database of results generated is used to develop a simple expression to characterize the elastic buckling load/stress of the assembly. The possible integration of the new expression with present design provisions in standards to predict the inelastic buckling resistance of the member is illustrated through a design example.

Dedication

This dissertation is dedicated to my mother,

Turfa Alshebel,

and to the memory of my grandmother,

Latifa Alshammary.

Acknowledgements

I would like to express my deepest gratitude to my supervisor, Dr. Magdi Mohareb, for his valuable guidance, insightful advice, continuous support, and constant encouragement throughout this research. It was an absolute pleasure working with you.

I would also like to extend my gratitude to the Ministry of Education of Saudi Arabia, Qassim University and the Saudi Arabian Culture Bureau in Canada for their generous financial support and excellent technical assistance.

My greatest gratitude goes to my remarkable mother, Turfa Alshebel, for her love, patience, countless sacrifices, and endless support. Words cannot express how grateful I am for the extraordinary life you have given me.

I would also like to extend my gratitude to my father, uncles, aunts, sisters, brothers, nieces and nephews for their countless love and support.

Last but not least, I would like to thank all my friends and colleagues in Saudi Arabia and Canada for their continuous encouragement and support.

Table of Contents

Table of Figures

Table of Tables

Chapter 1: Introduction

1.1. Background and motivation

Angle members are widely used in structural systems such as trusses, transmission towers and braces in structural steel frames as compression and/or tension members. In such members, cross-sections may consist of a single angle or multiple angles arranged in configurations such as back-to-back double angles, star-shaped, etc. The use of angle cross-sections in axially loaded members is advantageous from an economic viewpoint owing to their light weight and from a constructability viewpoint as angles can be easily connected to other components of the structure typically through gusset plates through one of the angle legs. Such an angle-gusset plate connection restrains the member end from rotating within the plan of the gusset plate but offers little rotational restraints to the member end related to out of the plane rotation (Figure 1.1). Given that the axis of rotational fixity does not coincide with any of the principal directions $\hat{x}, \hat{y}$ of the cross-section, the accurate determination of the buckling resistance for such a member is beyond the scope of classical solutions and, consequently, the scope of the elastic buckling equation based on the classical solution adopted in design standards (e.g., CSA S16 2019 and ANSI/AISC 360 2016) as such solutions are intended for fixity conditions defined along the principal directions.

In angle-gusset plate connections, the connection is frequently detailed such that the line of action of the expected axial force provided by the gusset plate is aligned with the centre line of the angle (Figure 1.1a). This leads to a load eccentricity e_y along the y axis but no eccentricity along the x axis (Figure 1.1b). The presence of eccentricity induces additional moments into the compression member. Solutions for eccentrically loaded angles available in CSA S16-19 and ANSI/AISC 360-16 are either based on an empirical effective slenderness expression or on beam-column interaction equations. Despite the simplicity of the effective slenderness ratio expression,

it is limited to angle members (i) having a long-to-short leg width ratio larger than 1.7, (ii) connected to gusset plates through welding or through a minimum of two bolts at each end, (iii) connected/loaded at the same leg at both ends and (iv) not subjected to intermediate transfer loads. The interaction equation, on the other hand, has a more general scope of applicability and is thus applicable beyond these restrictions. The application of interaction equations however involves a relatively lengthy procedure and will, in general, grossly underestimate the compressive resistance of such a member.

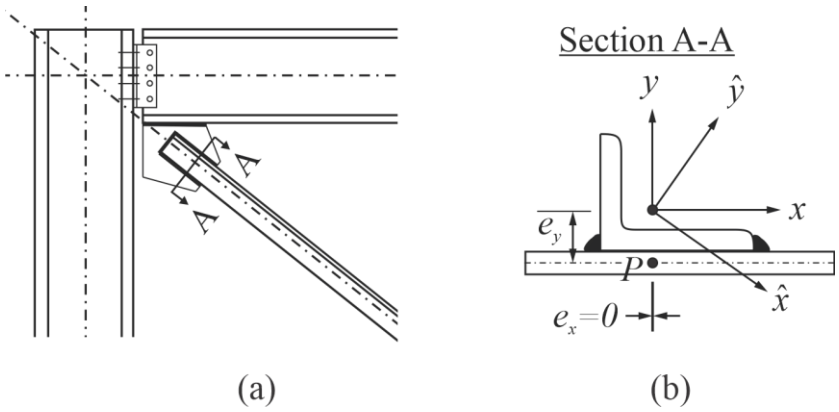

Figure 1.1 angle-gusset plate connection in bracing systems, (b) cross-sectional view A-A at the connection

When a compression assembly consists of two identical angles connected back-to-back (Figure 1.2), the challenges associated with non-principal end restraints and load eccentricity no longer arise as the gusset plate middle surface coincides with the axis of symmetry of the assembly (i.e., the y axis in Figure 1.2b). In this case, the gusset connection restrains the assembly along its the principal directions x, y and subjects the assembly to a concentric load P . Another challenge arises from providing interconnectors between both angles at discrete locations along the member span. The interconnectors provide local constraints that relate the displacements of the individual angles at discrete locations along the span and force both cross-sections to behave as a single monolithic entity (Figure 1.2b) at the locations of the interconnectors, but enable both angles to

deform independently away from the interconnectors (Figure 1.2c). Solutions available in CSA S16-19 and ANSI/AISC 360-16 for predicting the compressive resistance of such assemblies are based on a modified slenderness ratio expression originally intended for toe-to-toe double channel assemblies that are expected to buckle in a pure flexural mode. While the expression may be applicable to angle assemblies arranged as box-like pattern that are likely to buckle in a pure flexural mode, it may lead to inaccurate buckling predictions for a back-to-back double angle assemblies that are monosymmetric and are thus expected to buckle in a combined flexural-torsional mode.

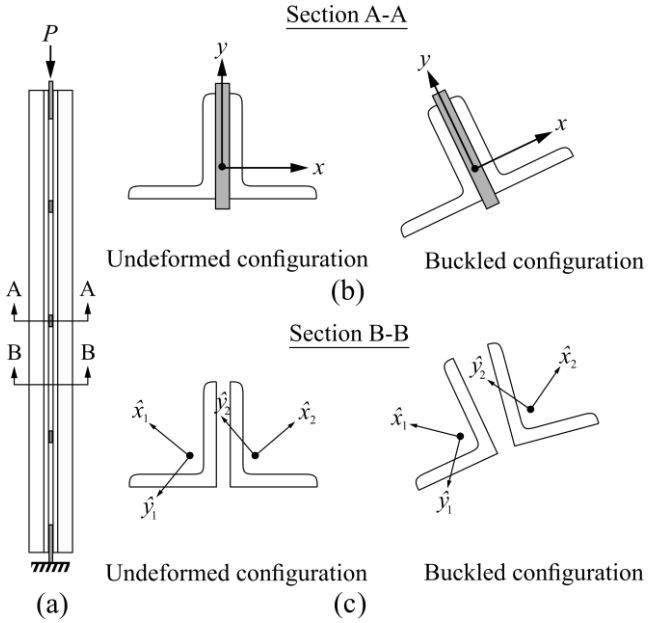

Figure 1.2 Back-to-back double angle assembly (a) Elevation view, (b) Cross-sectional view A-A at interconnector, (c) Cross-sectional view B-B away from interconnectors

1.2. Objectives

The aim of the present dissertation is to advance methodologies for predicting the elastic and inelastic compressive resistance of compression members with single angle and back-to-back double angle cross-sections with end restraints representative of those typically used in steel construction. Towards this goal, the present dissertation contributes to the following aspects:

(1) It derives a family of closed-form elastic buckling solutions for concentrically loaded compression members with end restraints defined along non-principal axes and uses the solutions to investigate the effect of end conditions on the elastic buckling load of members with angle and zed cross-sections

(2) It develops a series of 3D shell models based on ABAQUS that incorporate initial out-of-straightness, residual stresses, geometric and material nonlinear effects, and load eccentricity. The models are used to develop a large database of runs on eccentrically loaded single angle compression members with end conditions similar to those of gusset plate connections aimed to investigate the effect of various geometric parameters on the compressive resistance. The results are then used to develop a simple design expression to predict the compressive resistance of such members.

(3) It develops thin-walled beam analytical and finite element buckling solutions for predicting the elastic buckling load for back-to-back double angle assemblies and then uses the solutions to generate an extensive database of the elastic compressive resistance of members with for various sectional geometric parameters and spans to develop an improved design method that can be integrated into design standards to predict the inelastic compressive resistance of the assembly.

1.3. Dissertation overview

Following the present chapter (Chapter 1), the dissertation consists of a general literature review chapter (Chapter 2), three main chapters written in an article-based format (Chapters 3-5) and a closing chapter (Chapter 6) that provides a summary, conclusions, and recommendations for future research. Chapter 3 was published in Alenezi and Mohareb (2021) while Chapter 5 is currently under review by an international journal. A brief description of Chapters 2-6 follows:

Chapter 2 surveys the theoretical aspects related to the subject of the dissertation. It also presents provisions from the Canadian and American design standards that are relevant to the design of single and back-to-back double angle compression members.

Chapter 3 provides closed-form solutions for predicting the buckling loads of concentrically loaded compression members with end restraints defined along non-principal axes. The chapter also investigates the effect of non-principal end restraints on the buckling loads for members with single angle and zed sections. Detailed derivations of the general buckling solutions are presented in appendices to the chapter.

Chapter 4 presents the development of 3D finite element models based on ABAQUS for eccentrically loaded single angle compression members that incorporate initial out-of-straightness, residual stresses, geometric and material nonlinear effects and load eccentricity. The chapter also develops a database of compressive resistance for 936 members with gusset plate end connections and various geometries and load eccentricities. It also includes an assessment of the solutions available in CSA S16-19 for predicting the compressive resistance of such a member and proposes an improved design expression.

Chapter 5 provides a thin-walled beam finite element buckling formulation that captures the effect of discrete interconnectors in back-to-back double angle assemblies. The chapter also includes an analytical buckling solution for the assembly for the case where sufficient interconnectors are provided to constrain the assembly to behave as a monolithic entity. The study includes an investigation of the effect of interconnectors on the buckling of load of the assembly, an assessment of the validity of the solutions in CSA S16-19 and ANSI/AISC 360-16, and a database of 1250 buckling loads for assemblies with different geometric parameters. A simple design expression for predicting the buckling load of the assembly that captures interconnector effects is also proposed.

Chapter 6 summaries the main contributions of the dissertation, highlights the main conclusions and provides recommendations for future research.

References

AISC (American Institute of Steel Construction). (2016). "Specification for Structural Steel Buildings." ANSI/AISC 360-16, Chicago, IL.

Alenezi, A. M., and Mohareb, M. (2021). "Buckling solutions for compression members with end restraints defined along non-principal directions." *J. Constr. Steel Res.*, 181, 106505.

CSA (Canadian Standards Association). (2019). "Design of Steel Structures." CSA S16:19, Toronto, ON, Canada.

Chapter 2: Literature Review

2.1. Introduction

This chapter is intended to provide the theoretical background related to developing the buckling solutions in the main parts of the thesis along with relevant provisions in design standards relevant to compression angle members. A brief discussion on the type of response in structural systems and methods of analysis are presented in Section 2.2. The variational principles forming the basis of the buckling solutions developed in Chapter 3 and 5 are presented in Section 2.3 along with a summary of the methodologies relevant to the analytical and numerical buckling solutions in these chapters. Section 2.4 provides a review of the thin-walled beam theories relevant the developments in Chapter 3 and 5. Relevant design provisions in the Canadian and American standards to single and back-to-back double angle compression members are presented in Section 2.5. The present review is supplemented with more detailed reviews of literature that are included at the outset of each of Chapters 3-5 to specifically discuss studies related to the topics addressed in these chapters.

2.2. Types of response and methods of analysis

When a perfectly straight steel member is subjected to increasing loading, its deformational response can be determined from an elastic analysis as long as the material remains in the elastic range during deformation. In this case, a linearly elastic analysis predicts a deformation response that is directly proportional to the applied load (schematically represented by the dashed curve in Figure 2.1). An example would be the shortening of a perfectly straight column under the action of a gradually increasing concentric compressive force.

When the applied loads acting on the column attain a critical value, the column will reach a state of onset of buckling at which it tends to undergo sudden lateral displacements and/or twist under no increase in loading. This behaviour is characterized by an eigenvalue problem, in which the

magnitude of the buckling load is related to the eigenvalue and the buckling mode shapes are represented by the corresponding eigenvector. Since the amplitude of the eigenvector is indeterminate, multiple buckling configurations become possible at the buckling load, as represented by the horizontal line in Figure 2.1.

If the column possesses initial out-of-straightness, or if the line of action of the applied compressive load is shifted from the centroidal axis of the member, additional moments are induced in the member, which induce a nonlinear load deformation albeit the material may remain in the elastic range (solid curve in Figure 2.1). In this case, the slope of the load deformation response curve typically becomes milder as the applied forces increase and may asymptotically approach the buckling load as determined by the eigenvalue analysis. This type of nonlinear load deformation response can be characterized by a geometrically nonlinear analysis.

If the member enters into the inelastic range of deformation of the material, the load deformation response may peak at a load below the elastic critical load, and subsequently exhibit a negative slope (dotted curve in Figure 2.1). Such a response can be characterized by an analysis that accounts for geometric and material nonlinear effects.

The present study will investigate in Chapters 3 and 5 the elastic critical load for perfectly straight single angle and back-to-back double angle members with end gusset plate connections by formulating and developing eigenvalue type of solutions tailored for such end conditions. The effects of initial out-of-straightness, residual stresses, load eccentricity, geometric and material nonlinearities are also investigated for single angle compression members in Chapter 4 by conducting a series of finite element analysis that capture geometric and material nonlinear effects.

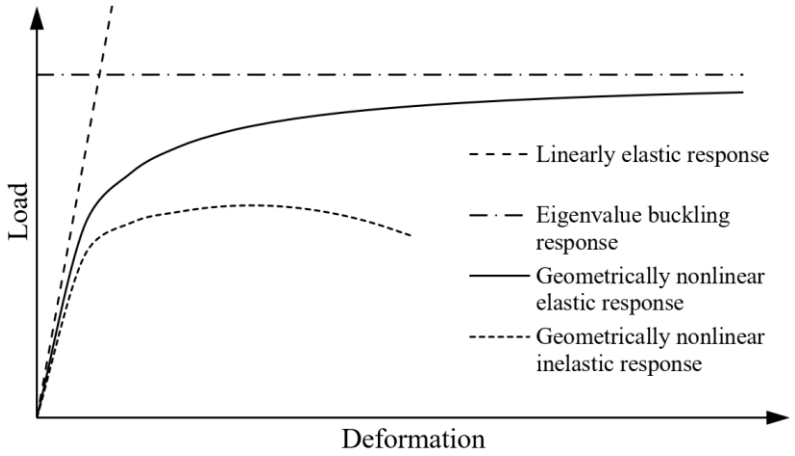

Figure 2.1 Load-deformation response for steel structures (adapted from Trahair 1993)

2.3. Buckling of compression members

A compression member can buckle in a pure flexural mode about one of its principal axes (Figure 2.2a), a pure torsional mode (Figure 2.2b) or in a combined flexural-torsional mode (Figure 2.2c), which involves simultaneous bending about one or both principal axes and twisting.

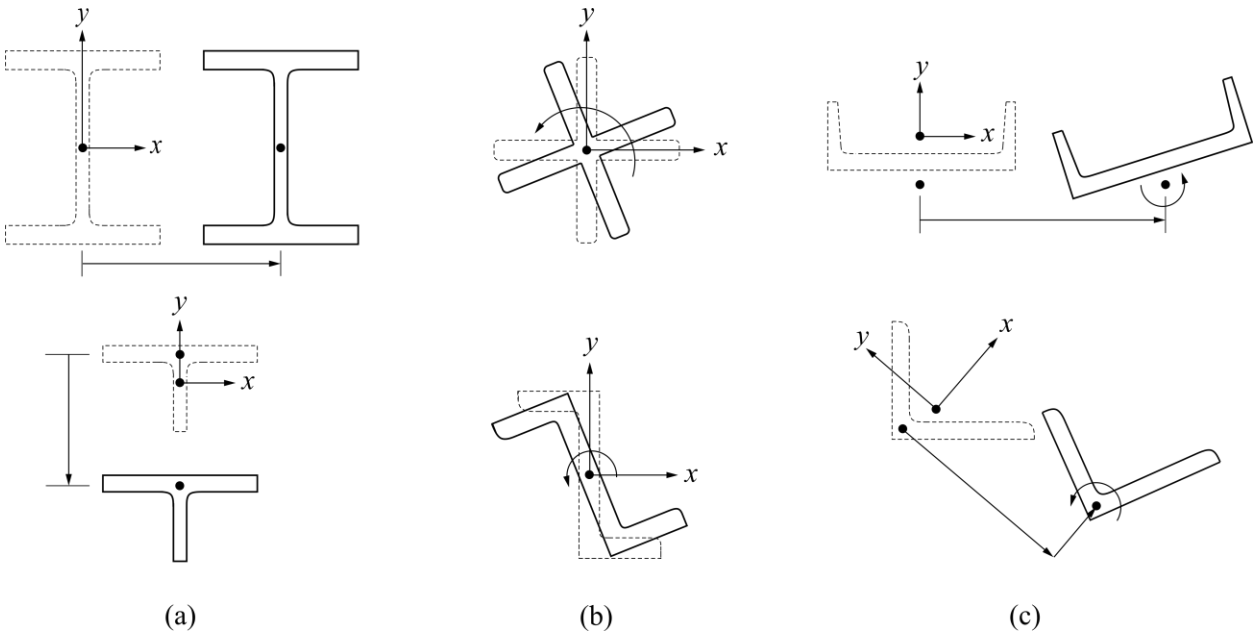

Figure 2.2 (a) Pure flexural buckling mode (b) pure torsional buckling mode and (c) flexural-torsional buckling mode

2.3.1. Variational principles

Variational principles provide the means to characterize the conditions of equilibrium and neutral stability of a system. For a stability problem with multiple degrees of freedom $q_i,(1,2,\ldots,n)$, the total potential energy $\Pi(q_1,q_2,\ldots,q_n)$ is obtained by summing the internal strain energy U stored in the member and the load potential gain V, i.e.,

$$\Pi(q_1,q_2,\ldots,q_n)=U(q_1,q_2,\ldots,q_n)+V(q_1,q_2,\ldots,q_n) \tag{2.1}$$

The variation principle can be used to find the equilibrium state of a member by exploring the variation Δ in the total potential energy $\Pi(q_1,q_2,\ldots,q_n)$ due to virtual displacements δq_i (Bazant and Cedolin 1991), i.e.,

$$\begin{aligned}\Pi(q_1,q_2,\ldots,q_n)&=\Pi(q_1+\delta q_1,q_2+\delta q_2,\ldots,q_n+\delta q_n)-\Pi(q_1,q_2,\ldots,q_n)\\&=\delta\Pi+\delta^2\Pi+\delta^3\Pi+\cdots\end{aligned} \tag{2.2}$$

where

$$\begin{aligned}\delta\Pi&=\sum_{i=1}^{n}\left(\frac{\partial\Pi}{\partial q_i}\right)\delta q_i\\ \delta^2\Pi&=\frac{1}{2!}\sum_{i=1}^{n}\sum_{j=1}^{n}\left(\frac{\partial^2\Pi}{\partial q_i\partial q_j}\right)\delta q_i\delta q_j\\ \delta^3\Pi&=\frac{1}{3!}\sum_{i=1}^{n}\sum_{j=1}^{n}\sum_{k=1}^{n}\left(\frac{\partial^3\Pi}{\partial q_i\partial q_j\partial q_k}\right)\delta q_i\delta q_j\delta q_k\end{aligned} \tag{2.3}\text{a-c}$$

The equilibrium position of a member subjected to a load is found by satisfying the condition $\delta\Pi=0$. Depending on the magnitude of the load applied, the attained equilibrium position can be either stable, unstable, or neutral. If $\delta^2\Pi>0$ for any arbitrary δq_i, the total potential energy has a minimum value, and the equilibrium is stable whereas if $\delta^2\Pi<0$ for any arbitrary δq_i, the

equilibrium is unstable. When the condition $\delta^2\Pi = 0$ is satisfied, the equilibrium of the member is neutrally stable.

In Chapter 3, the buckling solution is derived by setting to zero the variation of the second variation of the total potential energy, i.e.,

$$\delta\left(\delta^2\Pi/2\right) = 0 \tag{2.4}$$

Equation Eq. (2.4) is then integrated by parts to recover the governing differential equations and associated boundary conditions of the problem. The differential equations obtained are then solved subject to the boundary conditions to obtain an analytical solution for flexural-torsional buckling.

In Chapter 5, a finite element buckling solution is formulated by relating the buckling displacement fields to the nodal displacements through interpolation functions. The condition of neutral stability is then obtained in discretized form by evoking the stationarity condition of the functional $\delta^2\Pi/2 = \delta^2\left[\left(1/2\right)\mathbf{D}^{\mathbf{T}}\left(\mathbf{K_E} + \lambda\mathbf{K_G}\right)\mathbf{D}\right]$ subject to the constraints $\mathbf{CD} = \mathbf{0}$ where $\mathbf{K_E}$ is the elastic stiffness matrix, $\mathbf{K_G}$ is the geometric stiffness matrix which depends on the pre-buckling internal forces obtained from a linear static analysis, $\mathbf{C}$ is the buckling constraints matrix, $\mathbf{D}$ is the nodal buckling displacements vector, and λ is the buckling load multiplier. This leads to constructing an auxiliary functional $\delta^2\Pi^*/2$ by augmenting $\delta^2\Pi/2$ by a term of $\mathbf{CD}$ pre-multiplied by a Lagrange multipliers vector $\boldsymbol{\lambda}_\mathbf{L}$, i.e.,

$$\delta^2\Pi^*/2 = \left(1/2\right)\mathbf{D}^{\mathbf{T}}\left(\mathbf{K_E} + \lambda\mathbf{K_G}\right)\mathbf{D} - \boldsymbol{\lambda}_\mathbf{L}\mathbf{CD} \tag{2.5}$$

The stationary conditions of the constrained structure are then enforced, yielding

$$\left(\left[\begin{array}{c|c} \mathbf{K_E} & \mathbf{C}^{\mathbf{T}} \\ \hline \mathbf{C} & \mathbf{0} \end{array}\right] + \lambda\left[\begin{array}{c|c} \mathbf{K_G} & \mathbf{0} \\ \hline \mathbf{0} & \mathbf{0} \end{array}\right]\right)\left\{\begin{array}{c} \mathbf{D} \\ \hline \boldsymbol{\lambda}_\mathbf{L} \end{array}\right\} = \left\{\begin{array}{c} \mathbf{0} \\ \hline \mathbf{0} \end{array}\right\} \tag{2.6}$$

After enforcing the boundary conditions, the linearized eigenvalue problem in Eq. (2.6) is solved for the load multipliers λ and associated eigenvectors.

2.4. Thin-walled beam theories

As indicated in Section 2.3, compression members can buckle in a flexural-torsional mode (Figure 2.2c). When a thin-walled member with an open cross-section undergoes twisting deformation (Figure 2.3a), longitudinal displacements arise in the member, and, generally, the cross-section no longer remains planar after deformation. Such deformations are referred to as warping. The thin-walled beam theory of Vlasov (1961) provided the mathematical foundation of warping deformations along the middle surface of the cross-section, often referred to as global warping (Figure 2.3b). An extension for the Vlasov theory was developed by Gjelsvik (1981) to characterize the additional cross-section warping relative to the middle surface. Both Vlasov and Gjelsvik theories are intended for monolithic sections. The work was further extended to monosymmetric built-up assemblies of thin-walled beam cross-sections by Pezeshky et al. (2020).

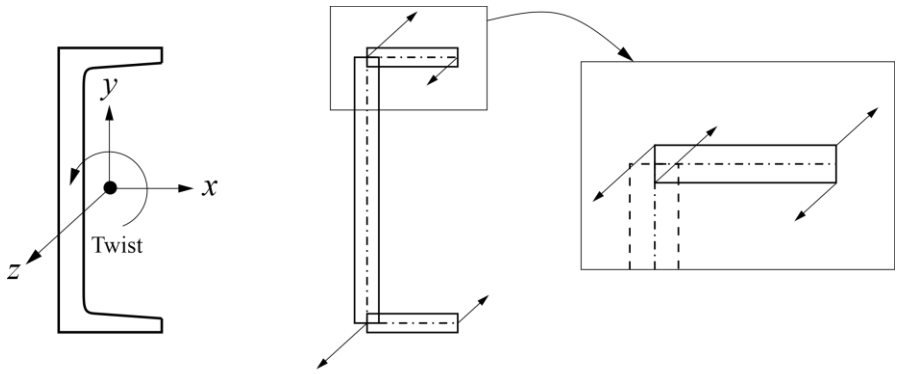

Figure 2.3 (a) Thin-walled cross-section under twisting, (b) global warping and (c) local warping

2.4.1. Vlasov theory

Vlasov (1961) developed a theory that characterizes the longitudinal displacement of a generic point along the middle surface (contour) of a thin-walled member with an open cross-section under

the assumptions that (i) the member cross-section displaces and rotates as a rigid disc throughout deformation and (ii) the shear strain vanishes at the middle surface of the cross-section. A generic thin-walled section is depicted in Figure 2.4a with a right-handed Cartesian coordinate system (x, y, z). The section has an arbitrary Pole R (x_R, y_R) and arbitrary sectorial origin B (x_B, y_B) lying on the contour. When point Q with coordinates $[x(s), y(s)]$, in which s is a curvilinear coordinate, moves within the plane of the section, the corresponding displacements u_Q, v_Q, along the x, y axes can be related to the displacements u, v of Pole R and the angle of twist θ of the cross-section as

$$\begin{aligned} u_Q(s,z) &= u(z) - [y(s) - y_R]\theta(z) \\ v_Q(s,z) &= v(z) + [x(s) - x_R]\theta(z) \end{aligned} \quad (2.7)\text{a,b}$$

The tangential and normal displacements t and n, respectively, of point Q can be defined as

$$\begin{aligned} t(s,z) &= u(z)\cos\alpha(s) + v(z)\sin\alpha(s) + r(s)\theta(z) \\ n(s,z) &= -u(z)\sin\alpha(s) + v(z)\cos\alpha(s) + q(s)\theta(z) \end{aligned} \quad (2.8)\text{a,b}$$

where $\alpha(s)$ is the angle of the tangent to the contour at the point of interest s relative to the x axis. The normal distance $r(s)$ from pole to the tangent to the contour and the tangent distance $q(s)$ from pole to the tangent to the contour (Figure 2.4b) are given by

$$\begin{aligned} r(s) &= [x(s) - x_R]\sin\alpha(s) - [y(s) - y_R]\cos\alpha(s) \\ q(s) &= [x(s) - x_R]\cos\alpha(s) + [y(s) - y_R]\sin\alpha(s) \end{aligned} \quad (2.9)\text{a,b}$$

The longitudinal displacement $w(s,z)$ is derived from the zero-strain assumption,

$$\partial w/\partial s + \partial t/\partial z \approx 0 \quad (2.10)$$

by integrating Eq. (2.10) with respect to s, yielding

$$w_Q(s,z) = w(z) - \int_s \left[\partial t(s,z)/dz\right] ds \tag{2.11}$$

From Figure 2.4c, one can define

$$\cos\alpha(s)\,ds = dx \qquad \sin\alpha(s)\,ds = dy \qquad r(s)\,ds = d\omega \tag{2.12)a-c}$$

By differentiating Eq. (2.8)a with respect to z, substituting the resulting equation into Eq. (2.11), inserting ds into the brackets, then substituting Eqs. (2.12)a-c into Eq. (2.11) and performing the integration in the right-hand side of the equation, the total longitudinal displacement including the warping effect is

$$w_Q(s,z) = w(z) - u'(z)x(s) - v'(z)y(s) - \theta'(z)\omega(s) \tag{2.13}$$

in which $\omega(s)$ is the sectorial coordinate of point Q calculated as twice the area enclosed between the arc BQ and the mobile radius RB and fixed radius RQ shown in Figure 2.4c. In Eq. (2.13), the first term is due to shortening/elongation, the second and third terms are due to bending about x, y axes and the last term is due to warping.

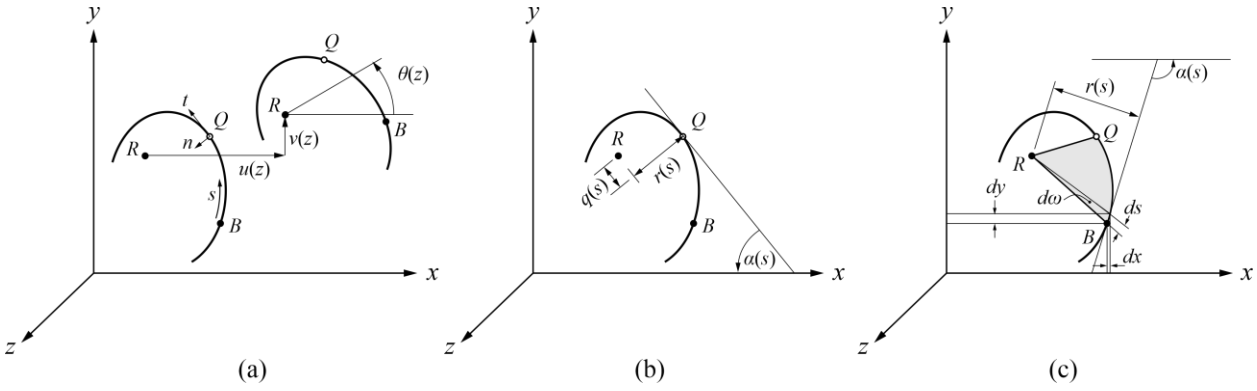

Figure 2.4 (a) in-plane displacements, (b) normal and tangential distances between R and Q (c) relations between the Cartesian and sectorial coordinates

2.4.2. Gjelsvik theory

For sections consisting of multiple straight elements intersecting at a single point such as angle or tee sections, the global warping function according to Vlasov theory tends to vanish. Gjelsvik

(1981) developed a theory that captures a thickness-related warping component (i.e., local warping) that characterizes the relative longitudinal displacement of a point offset from the middle surface (Figure 2.3c). The local warping gains significance as the thickness of the cross-section increases. The theory supplements both Vlasov assumptions with the Kirchhoff plate assumption whereby a line normal to the contour of the section is assumed to remain normal during deformation. For a point Q offset by a distance n from the contour, the total longitudinal displacement including local warping is given by

$$w_Q(n,s,z) = w(z) - u'(z)\left[x(s) + n\sin\alpha(s)\right] - v'(z)\left[y(s) - n\cos\alpha(s)\right] - \theta'(z)\left[\omega(s) - nq(s)\right] \tag{2.14}$$

where $-nq(s)$ is the local warping component, and one recalls that $q(s)$ is the tangent distance from pole to the tangent to the contour at the point of interest s.

2.4.3. The theory of Pezeshky et al.

Pezeshky et al. (2020) extended Vlasov's theory to monosymmetric built-up members with multiple thin-walled cross-sections whose shear centres pass through the symmetry axis of the assembly. The theory is based on the three kinematic assumptions of the Vlasov/Gjelsvik theories. In addition, the assembly has a unique shear centre while each of the cross-sections forming the built-up assembly has its own principal sectorial origin. Under these assumptions, the longitudinal displacement for a point Q_i offset from the contour of section $i = 1, 2...n$ was shown to take form

$$w_{Q_i}(n_i,s_i,z) = w(z) - u'(z)\left[x_i(s) + n_i\sin\alpha_i\right] - v'(z)\left[y_i(s) - n_i\cos\alpha_i\right] - \theta'(z)\left[\omega_i(s) - n_i q_i(s)\right] \tag{2.15}$$

The buckling formulation for single angle members developed in Chapter 3 and the finite element formulation for double angle assemblies in Chapter 5 both follow the Gjelsvik (1981) theory while

the monolithic formulation for back-to-back double angle assemblies in Chapter 5 further extends the theory of Pezeshky et al. (2020) to angles with shear centres that do not lie on the axis of symmetry of the assembly.

2.5. Design provisions in standards

The design provisions in the Canadian standards CSA S16-19 related to the design of compression members include (a) a treatment for concentrically loaded compression members, (b) effective slenderness equations for eccentrically loaded single angle members (c) an interaction equation approach for eccentrically loaded single angle members, and (d) an effective slenderness approach for concentrically loaded back-to-back double angle members with intermediate interconnectors. An overview of these procedures is presented in Subsection 2.5.1. The American standards ANSI/AISC 360-16 has similarities with the Canadian standards. The minor differences between standards are hence highlighted in Subsection 2.5.2.

2.5.1. Canadian standards CSA S16-19

2.5.1.1. Concentrically loaded compression members

The factored compressive resistance P_r of a concentrically loaded compression member is given by (Cl. 13.3.1.1)

$$P_r = \phi A F_Y \left[1 + \left(F_Y / F_e\right)^m\right]^{-1/m} \tag{2.16}$$

where ϕ is the resistance factor taken as 0.9, A is the sectional area, F_Y is the specified minimum yield strength, m is an empirical constant intended to reflect the reduction in strength due to residual stresses and initial out-of-straightness and is taken as 1.34 for hot-rolled fabricated structural sections (e.g., angles) and F_e is the smallest elastic buckling stress as determined from the cubic equation (Cl. 13.3.1.1c)

$$\left(F_e - F_{e\hat{x}}\right)\left(F_e - F_{e\hat{y}}\right)\left(F_e - F_{ez}\right) - F_e^2\left(F_e - F_{e\hat{y}}\right)\left(\hat{x}_S / r_0\right)^2 - F_e^2\left(F_e - F_{e\hat{x}}\right)\left(\hat{y}_S / r_0\right)^2 = 0 \qquad (2.17)$$

in which, $\hat{x}_S$ and $\hat{y}_S$ are the coordinates of the shear centre relative to the section centroid, r_0 is the polar radius of gyration about the shear centre given by $r_0 = \sqrt{\hat{x}_0^2 + \hat{y}_0^2 + r_{\hat{x}}^2 + r_{\hat{y}}^2}$, $r_{\hat{x}}, r_{\hat{y}}$ are the radii of gyration about the principal axes $\hat{x}, \hat{y}$, and (Cl. 13.3.1.2)

$$F_{e\hat{x}} = \frac{\pi^2 E}{\left(K_{\hat{x}} L_{\hat{x}} / r_{\hat{x}}\right)^2} \qquad F_{e\hat{y}} = \frac{\pi^2 E}{\left(K_{\hat{y}} L_{\hat{y}} / r_{\hat{y}}\right)^2} \qquad F_z = \left(\frac{\pi^2 E I_{\omega\omega}}{\left(K_z L_z\right)^2} + GJ\right)\frac{1}{A r_0^2} \qquad (2.18)\text{ a-c}$$

where E is the modulus of elasticity, G is the modulus of rigidity, $I_{\omega\omega}$ is the warping constant, J is the Saint-Venant torsional constant and $\left(K_{\hat{x}} L_{\hat{x}} / r_{\hat{x}}\right)$, $\left(K_{\hat{y}} L_{\hat{y}} / r_{\hat{y}}\right)$ are the slenderness ratios with respect to the principal directions $\hat{x}, \hat{y}$ and $K_z L_z$ is the effective length relative to twist. When applying Eq. (2.17) for simply supported columns ($K_{\hat{x}} = K_{\hat{y}} = K_z = 1.0$) with asymmetric sections ($\hat{x}_S \neq 0$ and/or $\hat{y}_S \neq 0$), the predicted buckling stress is in exact agreement with that based on the Vlasov thin-walled beam theory. For boundary conditions that are different in all three directions $K_{\hat{x}} \neq K_{\hat{y}} \neq K_z$, Eq. (2.17) predicts slightly conservative elastic buckling stress predictions. The application of Eq. (2.17) hinges on the designer's ability to quantify the type of end restraint along the principal directions and hence quantify appropriate values for the effective length factors $K_{\hat{x}}, K_{\hat{y}}$. This requirement, in principle, prevents the use of Eq. (2.17) in case of single angles with end gusset plate connections in which the gusset plate connection provides a fixation along a non-principal direction and a nearly pinned end condition along the orthogonal direction. In this respect, Chapter 3 develops a more general elastic buckling solution applicable to compression members with boundary conditions defined along non-principal directions.

2.5.1.2. Effective slenderness for eccentrically loaded single angle members

For a single angle compression member connected to a gusset plate by a single leg that is (i) compressively loaded through the same leg at both ends, (ii) attached by welding or a minimum of two-bolt connection, (iii) not subjected to intermediate transverse loads and (iv) have long-to-short leg width ratio $b_l/b_s < 1.7$, CSA S16 (2019) empirically accounts for the effect of eccentricity through an effective slenderness ratio to be used to directly estimate the compressive resistance of the member (Cl. 13.3.2.1). The effective slenderness ratio for an angle member with equal-leg or unequal-leg angle and connected through the longer leg is given by (Cl. 13.3.2.2)

$$\frac{KL}{r} = \begin{cases} 72 + 0.75\,L/r_x & 0 \le L/r_x \le 80 \\ 32 + 1.25\,L/r_x \le 200 & L/r_x > 80 \end{cases} \tag{2.19}$$

where r_x is the radius of gyration about an axis parallel to the connected leg. For a member with an unequal-leg angle connected through the shorter leg, the slenderness ratio is given by (Cl. 13.3.2.2)

$$\frac{KL}{r} = \begin{cases} 72 + 0.75L/r_x + 4\left[\left(b_l/b_s\right)^2 - 1\right] > 0.95L/r_{min} & 0 \le L/r_x \le 80 \\ 0.95L/r_{min} < 32 + 1.25L/r_x + 4\left[\left(b_l/b_s\right)^2 - 1\right] \le 200 & L/r_x > 80 \end{cases} \tag{2.20}$$

in which r_{min} is the minimum radius of gyration. The effective slenderness ratio obtained is then used to estimate the elastic buckling stress from (Cl. 13.3.2.1)

$$F_e = \pi^2 E \Big/ \left(KL/r\right)^2 \tag{2.21}$$

which is then substituted into Eq. (2.16) to obtain the compressive resistance of the member.

2.5.1.3. Interaction equation for eccentrically loaded single angle members

When the limitations of the effective slenderness solution in Section 2.5.1.2 are not satisfied for an eccentrically loaded member, and when the local buckling classification limit $b_l/t \le 250/\sqrt{F_Y}$

as specified by CSA S16-19 for single angle compression members is satisfied, the member is to be treated as Class 3 beam-column member with moments $M_{f\hat{x}} = Pe_{\hat{y}}, M_{f\hat{y}} = Pe_{\hat{x}}$. The relevant interaction equation takes the form (Cl. 13.8.4)

$$\frac{P}{P_r} + U_{\hat{x}} \frac{Pe_{\hat{y}}}{M_{r\hat{x}-i}} + U_{\hat{y}} \frac{Pe_{\hat{x}}}{M_{r\hat{y}-i}} \leq 1.0 \tag{2.22}$$

where P_r is the factored axial load resistance in the absence of moments, $M_{r\hat{x}-i}$ is the factored flexural resistance about the $\hat{x}$ axis based on corner point $i = 1,2,3$ (Figure 2.5) on the cross-section, $M_{r\hat{y}-i}$ is the factored flexural resistance about $\hat{y}$ axis based on the same corner point, $P_{e\hat{x}}$ and $P_{e\hat{y}}$ are the Euler buckling loads about both principal directions, and $U_{\hat{x}}, U_{\hat{y}}$ are amplification factors to be applied to the applied moments $M_{f\hat{x}} = Pe_{\hat{y}}, M_{f\hat{y}} = Pe_{\hat{x}}$ to account for the $P-\delta$ effect, and the equality of the left hand-side term of Eq. (2.22) to unity would lead to the sought axial load capacity P. Under CSA S16-19, Eq. (2.22) is to be applied to guard against failures due to (i) cross-sectional strength, (ii) overall member strength and (ii) lateral-torsional buckling strength. It is most likely that the resistance of an eccentrically loaded angle member will be governed by the lateral-torsional mode of failure. The following definitions of terms appearing in Eq. (2.22) when applied to the lateral torsional buckling mode of failure in braced frames.

(1) P_r is the factored compressive resistance of the member in the absence of moments as determined from Eq. (2.16) based on weak axis buckling load.

(2) $U_{\hat{x}} = 1/\left(1 - P/P_{e\hat{x}}\right)$ and $U_{\hat{y}} = 1/\left(1 - P/P_{e\hat{x}}\right)$ where $P_{e\hat{x}}$ and $P_{e\hat{y}}$ are the Euler buckling loads given by (Cl. 13.8.5)

$$P_{e\hat{x}} = \pi^2 EI_{\hat{x}\hat{x}} / L^2 \qquad P_{e\hat{y}} = \pi^2 EI_{\hat{y}\hat{y}} / L^2 \tag{2.23 a,b}$$

(3) The factored weak axis moment resistance $M_{r\hat{x}-i}$ is given by (Cl. 13.5b)

$$M_{r\hat{x}-i} = \phi S_{\hat{x}-i} F_Y \tag{2.24}$$

in which, $S_{\hat{x}-i}$ is the elastic section modulus associated with the $\hat{x}_i$ axis associated with a specific point $i = 1, 2, 3$ on the cross-section (taken at the three corner points in the case of an angle as shown in Figure 2.5).

(4) The factored strong axis moment resistance $M_{r\hat{y}-i}$ is based on the yield capacity of the section $M_{Y\hat{y}-i}$ and its elastic lateral torsional buckling moment $M_{U\hat{y}}$ as determined in the following steps:

(a) Determine the elastic yield capacity about the major axis $M_{Y\hat{y}-i} = S_{\hat{y}-i} F_Y$ (Cl. 13.5b), $S_{\hat{y}-i}$ being the elastic section modulus with respect to the $\hat{y}$ axis based on yielding on corner point i on the cross-section.

(b) Determine the elastic lateral-torsional buckling moment $M_{U\hat{y}}$ from (Cl. 13.6.1f)

$$M_{U\hat{y}} = \frac{4.9 E I_{\hat{x}}}{L^2} \left(\sqrt{\beta_{\hat{y}}^2 + 0.052 \left(\frac{Lt}{r_{\hat{x}}} \right)^2} + \beta_{\hat{y}} \right) \tag{2.25}$$

where $\beta_{\hat{y}}$ is the asymmetry parameter about the major principal axis defined by

$$\beta_{\hat{y}} = \left(1 / I_{\hat{y}\hat{y}} \right) \int_A \hat{x} \left(\hat{y}^2 + \hat{x}^2 \right) dA - 2\hat{x}_S \tag{2.26}$$

in which $\beta_{\hat{y}}$ is positive when the shear centre is in compression and negative otherwise.

(c) Given $M_{Y\hat{y}-i}$ and $M_{U\hat{y}}$, determine the factored moment resistance $M_{r\hat{y}-i}$ of the section about the strong axis including the lateral torsional buckling effects from the following empirical equations (Cl. 13.6.1f)

$$M_{r\hat{y}-i}=\begin{cases}\phi 1.15\left(1-0.79\dfrac{M_{U\hat{y}}}{M_{Y\hat{y}-i}}\right)M_{Y\hat{y}-i}\le M_{Y\hat{y}-i} & \dfrac{M_{U\hat{y}}}{M_{Y\hat{y}-i}}>0.67\\ \phi\left(0.92-0.17\dfrac{M_{U\hat{y}}}{M_{Y\hat{y}-i}}\right)M_{U\hat{y}} & \dfrac{M_{U\hat{y}}}{M_{Y\hat{y}-i}}\le 0.67\end{cases} \tag{2.27}$$

Interaction Eq. (2.22) should be evaluated at all three corner points of the cross-section while taking into consideration the appropriate sign of stresses (tension or compression). The capacity of the member is then governed by the lowest force P obtained.

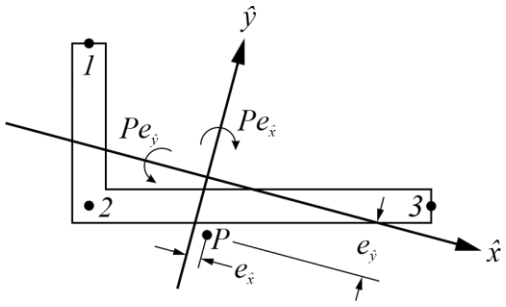

Figure 2.5 Combined loading in eccentrically loaded angles

2.5.1.4. Concentrically loaded back-to-back double angle members

A back-to-back double angle assembly has a monosymmetric configuration with $x_s=0$. In this case, the elastic buckling stress is the minimum of $F_{e\hat{x}}$ as provided by Eq. (2.18)a and (Cl. 13.3.1.2)

$$F_{e\hat{y}z}=\frac{F_{e\hat{y}}+F_{ez}}{2\left[1-\left(\hat{y}_S^2/r_0^2\right)\right]}\left(1-\sqrt{1-\frac{4F_{e\hat{y}}F_{ez}\left[1-\left(\hat{y}_S^2/r_0^2\right)\right]}{\left(F_{e\hat{y}}+F_{ez}\right)^2}}\right) \tag{2.28}$$

When determining $F_{e\hat{y}}$ in Eq. (2.18)b, the effective slenderness ratio $\left(K_{\hat{y}}L_{\hat{y}}/r_{\hat{y}}\right)_m$ depends on the overall slenderness of the member $\left(K_{\hat{y}}L_{\hat{y}}/r_{\hat{y}}\right)$ as well as the maximum slenderness $\left(a/r_{min}\right)$ of the angle in between interconnectors, a being the distance between interconnectors along the span, and r_{min} is the minimum radius of gyration of the individual angle. The effective slenderness of the member also depends on the types of interconnectors (Cl. 19.2.4), i.e.,

$$\left(K_{\hat{y}}L_{\hat{y}}/r_{\hat{y}}\right)_m = \begin{cases} \sqrt{\left(K_{\hat{y}}L_{\hat{y}}/r_{\hat{y}}\right)^2 + \left(a/r_{min}\right)^2} & \text{for snug-tight bolts} \\ \sqrt{\left(K_{\hat{y}}L_{\hat{y}}/r_{\hat{y}}\right)^2 + \left(0.65a/r_{min}\right)^2} & \text{for welds or pretensioned bolts} \end{cases} \quad (2.29)\text{a,b}$$

2.5.2. American standards ANSI/AISC 360-16

The design provisions of ANSI/AISC 360-16 are similar to those of CSA S16-19. The differences from Canadian Standards are provided in in the following:

1. ANSI/AISC 360-16 provides a different compressive resistance equation for compression member as (Cl. E3)

$$P_r = \phi A \times \begin{cases} \left(0.658^{F_Y/F_e}\right)F_Y & F_Y/F_e \le 2.25 \\ 0.877F_e & F_Y/F_e > 2.25 \end{cases} \quad (2.30)$$

where F_e is the buckling stress as given corresponding to the smallest root of Eq. (2.17).

2. ANSI/AISC 360-16 also adopt the empirical effective slenderness in Eqs. (2.19) and (2.20) for eccentrically loaded angles (Cl. E5). For the interaction equation Eq. (2.22), however, ANSI/AISC 360-16 uses slightly different definitions for the flexural strength $M_{r\hat{x}-i}$ and $M_{r\hat{y}-i}$, i.e., (Cl. F10)

$$M_{r\hat{x}-i} = \phi 1.5 S_{\hat{x}-i} F_Y \quad (2.31)$$

$$M_{r\hat{y}-i} = M_{r\hat{y}-i} = \begin{cases} \phi\left(1.92 - 1.17\dfrac{M_{U\hat{y}}}{M_{Y\hat{y}-i}}\right)M_{Y\hat{y}-i} \le 1.5M_{Y\hat{y}-i} & \dfrac{M_{U\hat{y}}}{M_{Y\hat{y}-i}} \ge 1 \\ \phi\left(0.92 - 0.17\dfrac{M_{U\hat{y}}}{M_{Y\hat{y}-i}}\right)M_{U\hat{y}} & \dfrac{M_{U\hat{y}}}{M_{Y\hat{y}-i}} < 1 \end{cases} \quad (2.32)$$

3. The modified slenderness ratio adopted by ANSI/AISC 360-16 for back-to-back double angle assembly with snug-tight bolted connections remains the same. However, for welded or bolted connections with pre-tensioned bolts, the modified slenderness ratio becomes (Cl. E6.1)

$$\left(K_{\hat{y}}L_{\hat{y}}/r_{\hat{y}}\right)_m = \begin{cases} K_{\hat{y}}L_{\hat{y}}/r_{\hat{y}} & a/r_{min} \le 40 \\ \sqrt{\left(K_{\hat{y}}L_{\hat{y}}/r_{\hat{y}}\right)^2 + \left(0.5a/r_{min}\right)^2} & a/r_{min} > 40 \end{cases} \quad \text{(2.33)a,b}$$

The present chapter presented the theoretical aspects most relevant to the developments presented in the thesis. It also summarized key design provisions in the Canadian and American design standards related to the design of single angle and back-to-back double angle compression members.

References

AISC (American Institute of Steel Construction). (2016). “Specification for Structural Steel Buildings.” ANSI/AISC 360-16, Chicago, IL.

Bazant, Z. P. and Cedolin, L. (1991) "Stability of Structures: Elastic, Inelastic, Fracture and Damage Theories", Oxford University Press, New York.

CSA (Canadian Standards Association). (2019). “Design of Steel Structures.” CSA S16:19, Toronto, ON, Canada.

Gjelsvik, A. (1981). *The theory of thin walled bars*, John Wiley & Sons, New York.

Pezeshky, P., Sahraei, A., Rong, F., Sasibut, S., and Mohareb, M. (2020). “Generalization of the Vlasov theory for lateral torsional buckling analysis of built-up monosymmetric assemblies.” *Eng. Struct*., 221, 111055.

Trahair, N. S. (1993). Flexural-Torsional Buckling of Structures, CRC Press, Boca Raton, FL.

Chapter 3: Buckling Solutions for Compression Members with End Restraints Defined along Non-Principal Directions[1]

3.1. Abstract

The classical flexural-torsional buckling solution for compression members with asymmetric cross-sections is intended for members with end fixity conditions defined along the principal directions. In a number of practical situations, member ends can be rotationally restrained about a non-principal direction and rotationally free about the orthogonal non-principal axis. This may occur, for example, when one of the legs of a compression member with an angle or the web of a zed cross-section is connected to a gusset plate. The buckling loads in such cases cannot be determined from the classical solution. Within this context, the present study formulates the variational principle, governing neutral stability conditions, and associated boundary terms based on general non-principal directions, and then develops analytical solutions for the resulting coupled equations. The validity of the solutions is then demonstrated though comparisons with shell and thin-walled beam-based finite element solutions. The solutions are then used to investigate the influence of the orientation of the restraining axes on the buckling load capacity and associated buckling modes for single angles and zed shaped compression members with common end conditions.

Keywords

Flexural-torsional buckling; asymmetric cross-sections; closed-form solution; compression member; inclined boundary conditions, non-principal axes.

[1]Alenezi, A. M. and Mohareb, M. (2021). "Buckling solutions for compression members with end restraints defined along non-principal directions." *J. Constr. Steel Res.*, 181, 106505.

3.2. Introduction and motivation

Concentrically loaded compression members with asymmetric cross-sections undergo flexural-torsional buckling characterized by simultaneous flexure about principal directions $\hat{x}, \hat{y}$ (e.g., Figure 3.1) and twist. Design standards (e.g., ANSI/AISC 360 2016 and CSA S16 2019) predict the elastic buckling strength P of an asymmetric column from the equation

$$\left(P-P_{\hat{x}}\right)\left(P-P_{\hat{y}}\right)\left(P-P_z\right)-P^2\left(P-P_{\hat{y}}\right)\left(\hat{x}_{SC}/r_0\right)^2-P^2\left(P-P_{\hat{x}}\right)\left(\hat{y}_{SC}/r_0\right)^2=0 \tag{3.1}$$

where $\hat{x}_{SC}$ and $\hat{y}_{SC}$ are the coordinates of the shear centre SC with respect to the centroid C, r_0 is the polar radius of gyration about the shear centre given by $r_0=\sqrt{\hat{x}_{SC}^2+\hat{y}_{SC}^2+r_{\hat{x}}^2+r_{\hat{y}}^2}$, and $r_{\hat{x}}, r_{\hat{y}}$ are the radii of gyration about $\hat{x}, \hat{y}$ axes, and

$$P_{\hat{x}}=\frac{\pi^2 EI_{\hat{x}\hat{x}}}{\left(K_{\hat{x}}L_{\hat{x}}\right)^2},\ P_{\hat{y}}=\frac{\pi^2 EI_{\hat{y}\hat{y}}}{\left(K_{\hat{y}}L_{\hat{y}}\right)^2}\ \text{ and }\ P_z=\left(\frac{\pi^2 EI_{\omega\omega}}{\left(K_zL_z\right)^2}+GJ\right)\frac{1}{r_0^2} \tag{3.2}\text{a-c}$$

in which E is the modulus of elasticity, G is the modulus of rigidity, $I_{\hat{x}\hat{x}}$ and $I_{\hat{y}\hat{y}}$ are the principal moments of inertia, $I_{\omega\omega}$ is the warping constant, J is the Saint-Venant torsional constant and $K_{\hat{x}}L_{\hat{x}}$, $K_{\hat{y}}L_{\hat{y}}$ are the effective lengths with respect to the principal directions $\hat{x}, \hat{y}$ and K_zL_z is the effective length relative to twist. Equation (3.1) provides an exact solution of the buckling equilibrium equations for the critical load P when the boundary conditions at both ends are defined along the principal directions $\hat{x}, \hat{y}$. For example, when both ends are pinned (i.e., $K_{\hat{x}}=K_{\hat{y}}=K_z=1.0$), Eq. (3.1) is known to lead to an exact solution of the governing differential equations (e.g., Vlasov 1961, Timoshenko and Gere 1961, Galambos 1968 and Trahair 1993). In a number of practical situations, however, end conditions may be defined along non-principal directions. This is the case, for example, in a member with an angle cross-section that is connected

to a gusset plate to one of its legs (Figure 3.1a). Such a connection provides a pin restraint about x axis and a fixity restraint about y axis, both x and y being non-principal. Another case is when the web of a member with a zed cross-section is connected to a gusset plate (Figure 3.1b). This connection provides a fixity restraint about x axis but a pin restraint about y axis. In such cases, Eq. (3.1) would be inapplicable. Within this context, the present study aims to develop closed-form solutions capable of treating similar cases where connection details at the member ends may lead to different boundary conditions along orthogonal non-principal directions.

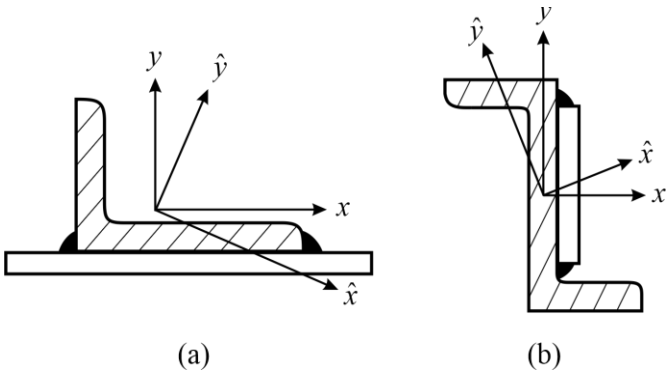

Figure 3.1[*] Typical end connections for members with (a) angle cross-section (b) zed cross-section

3.3. Literature review

The buckling of concentrically loaded members with open cross-sections was investigated in the early work of Wagner (1936), Kappus (1938) and Vlasov (1961). Using the direct equilibrium approach, Wagner (1936) derived the governing differential equations for the flexural-torsional buckling of asymmetric compression members. By adopting similar kinematic assumptions, Kappus (1938) formulated the governing differential equations using an energy approach. Goodier (1942) and Timoshenko (1945) extended Wagner's work to members under compression and

[*] Similar end conditions can be achieved in bolted connections by using pre-tensioned bolts.

biaxial bending, and solved the governing equations using approximate displacement functions. Renton (1960) derived a closed-form solution for the buckling load of asymmetric compression members with pinned restraints at both ends in flexure. Hone (1967) utilized Renton's solution to derive closed-form expressions for members with pinned and fixed end restraints about both principal axes and relative to twist. Culver (1966) analytically solved the differential equations for members under compression and biaxial bending and then numerically obtained the integration constants. Paavola and Salonen (1992) formulated a closed-form solution for the flexural-torsional buckling of beam-columns with elastic end restraints. The solution is valid only for members with mono-symmetric or point symmetric cross-sections, in which only two of the three governing equations are coupled. Xiang et al. (1992) developed a finite element formulation for columns with variable axial loading. Attard (1992) showed that the use of effective length factors based on the classical pure flexural buckling solution yields conservative estimates for the flexural-torsional buckling loads of monosymmetric members. Sallstrom (1996) formulated the static and geometric stiffness matrices for members with arbitrary open cross-sections subjected to compressive forces. Solutions for members under the combined compression and bending involve finite element formulations (e.g., Krajcinovic 1969, Barsoum and Gallagher 1970, Laudiero and Zaccaria 1988 and Kim et al. 1994), the finite strip method (e.g., Plank and Wittrick 1974, Smith and Sridharan 1978, Lau and Hancock 1986, Papangelis and Hancock 1995 and He et al. 2018), the constrained finite strip method (e. g., Ádány and Schafer 2006a,b Ádány and Schafer 2008 and Li and Schafer 2013) and the generalized beam (GBT) method (e.g., Davies et al. 1994, Dinis et al. 2006, and Camotim et al. 2008). The applications of the above solutions to column application were illustrated in the work of Ádány and Schafer (2006b) and Li and Schafer (2013).

Buckling solutions for members with end restraints defined along non-principal axes include the work of Trahair (1969) who provided a finite integral solution for members subjected to eccentric compression. Based on bifurcation analyses and geometrically non-linear analyses, Kitipornchai and Chan (1987) developed a finite element solution for angles and tee beam-columns, and for asymmetric beam-columns (Chan and Kitipornchai 1987). Kim et al. (2003) developed a shear-deformable stiffness solution for the buckling of asymmetric beam-column. Rasmussen and Trahair (2005) developed solutions for the flexural buckling of columns with doubly symmetric and point symmetric sections with inclined end restraints. Trahair and Rasmussen (2005) also developed a finite element solution for the buckling of concentrically loaded members with general cross-sections with rigid and elastic restraints along non-principal directions and eccentric from the shear centre. Based on power series expansions of the displacement fields, Kim et al. (2007) derived a stiffness solution for asymmetric members subjected to a linearly distributed compressive loading. Gluaz (2017) developed an approximate analytical buckling solution for concentrically loaded pin-ended members restrained about non-principal axes. Most recently, Liu et al. (2019) derived a thin-walled beam element for the geometric analysis of beam-columns with general open-sections which relates the sectional properties in the non-principal directions to those in the principal directions.

Some of the mentioned studies have focused on developing finite element solutions (e.g., Trahair and Rasmussen 2005 and Liu et al. 2019), while others have developed approximate solutions (e.g., Gluaz 2017). The studies that developed closed-form buckling solutions (e.g., Renton 1960 and Paavola and Salonen 1992) are limited to members with principal end restraints. The authors are unaware of any closed-form solutions for asymmetric compression members with end restraints defined along non-principal axes. In order to fill this gap, the present study (i) develops

the field equations and boundary conditions for compression members with restraints defined along non-principal directions, (ii) develops closed-form solutions for the resulting coupled system of differential equations, (iii) formulates the characteristic equations for cases involving different boundary conditions along non-principal directions, (iv) assesses the validity of the developed solution through comparisons with finite element analysis, and (v) adopts the new solution to determine the elastic buckling resistance and mode shapes for compression members with single angle and zed shaped cross-sections connected to gusset plates at both ends.

3.4. Statement of the problem

A prismatic member with an asymmetric cross-section is subjected to a compressive force acting at the section centroid. The boundary conditions of the member are defined along non-principal directions x and y. It is required to formulate a closed-form solution to predict the flexural-torsional buckling load of the member.

3.5. Assumptions

The formulation is based on the following assumptions:

(1) The member response follows the Vlasov assumptions (Vlasov 1961):
   i. The member cross-section does not deform in its plane throughout deformation (i.e., no cross-sectional distortion).
   ii. Shear strains at the mid-surface of the cross-section are negligible.

(2) The formulation is restricted to prismatic members

(3) Strains are small and rotations are moderate.

(4) Material is linearly elastic isotropic

(5) The origin is taken to coincide with the cross-section centroid. However, the orientation of the axes does not necessarily coincide with the principal directions. This feature is intended to enable enforcing boundary conditions along non-principal directions.

(6) The pole is taken to coincide with the shear centre of the cross-section.

(7) The sectorial origin is chosen to satisfy the condition $S_\omega = \int_A \omega dA = 0$ (i.e., a principal sectorial origin is adopted)

3.6. Formulation

Figure 3.2 depicts a member with an asymmetric cross-section subjected to a reference compressive force N_R. Under load N_R, the member deforms axially by going from Undeformed Configuration 1 to Deformed Configuration 2. The corresponding longitudinal displacement is $w_p(z)$. Load N_R is then assumed to increase to λN_R. As a result, the column shortens further by going from Configuration 2 to 3 and the longitudinal displacement increases to $\lambda w_p(z)$. At this state, the column is at the onset of buckling, where it has a tendency to buckle into a flexural-torsional mode without increase in load. Throughout buckling (i.e., in going from Configuration 3 to 4), the shear centre of the cross-section (with coordinates x_{SC}, y_{SC}) is assumed to undergo displacements $u(z)$ and $v(z)$ along the x and y directions, and the section undergoes an angle of twist $\theta(z)$. A local coordinate system (s,n) is defined in which s is the tangential coordinate along the contour and n is a coordinate normal to the section contour. Based on the first Vlasov assumption, displacements $\tilde{u}(s,n,z)$ and $\tilde{v}(s,n,z)$ defined along directions x, y for a point with coordinates $\left[x(s,n), y(s,n), \omega(s,n)\right]$ lying on the contour (e.g., Gjelsvik 1981 and Trahair 1993) is given by

$$\tilde{u}(s,n,z) = u(z) - \left[y(s,n) - y_{SC}\right]\theta(z) \tag{3.3}$$

$$\tilde{v}(s,n,z) = v(z) + \left[x(s,n) - x_{SC}\right]\theta(z) \tag{3.4}$$

Also, the longitudinal displacement

$$\begin{aligned}\tilde{w}(s,n,z) = \lambda w_p(z) - x(s,n)u'(z) - y(s,n)v'(z) + \omega(s,n)\theta'(z) \\ + y(s,n)u'(z)\theta(z) - x(s,n)v'(z)\theta(z)\end{aligned} \tag{3.5}$$

in which $\omega(s,n)$ is the sectorial coordinate and a prime indicates differentiation with respect to z. As a matter of notation, all fields with a subscript p pertain to the pre-buckling stage, while fields with no subscripts pertain to the buckling stage.

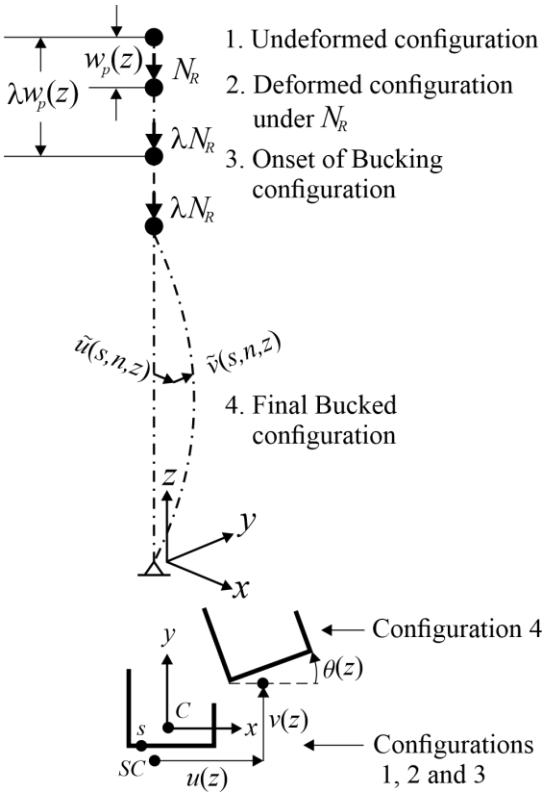

Figure 3.2 Stages of deformation throughout flexural-torsional buckling

3.6.1. Variational principle

The total potential energy at the final buckled configuration (Figure 3.2) is the sum of the internal strain energy due to longitudinal strains and due to shear strains induced by the Saint-Venant torsion (e.g. Trahair 1993), i.e.,

$$\Pi = \frac{1}{2}\int_0^L \iint_A \left[\left(\sigma_z + \lambda\sigma_{zp}\right)\left(\varepsilon_z + \lambda\varepsilon_{zp}\right) + \left(\tau_{sz} + \lambda\tau_{szp}\right)\left(\gamma_{sz} + \lambda\gamma_{szp}\right)\right] dA dz \tag{3.6}$$

where σ_z and ε_z are the longitudinal stresses and strains, and τ_{sz} and γ_{sz} are the shear stresses and strains, respectively. By taking the second variation of Eq. (3.6), one obtains

$$\frac{1}{2}\overline{\overline{\Pi}} = \frac{1}{2}\int_0^L \int_A \left(E\overline{\varepsilon}_z^2 + \lambda\sigma_{zp}\overline{\overline{\varepsilon}}_z + G\overline{\gamma}_{sz}^2 + \lambda\tau_{szp}\overline{\overline{\gamma}}_{sz} \right) dA dz \tag{3.7}$$

The last term in Eq. (3.7) vanishes for a pure compression member since the pre-buckling shear stresses τ_{szp} vanish. As a matter of notation, all single bars denote the first variation of the argument functional (or function) and all double bars denote the second variation. The longitudinal buckling strains is given by

$$\begin{aligned} \varepsilon_z \approx \tilde{w}' + \frac{1}{2}\left(\tilde{u}'^2 + \tilde{v}'^2\right) = \lambda w_p' - xu'' - yv'' + \omega\theta'' + y\left(u'\theta' + \theta u''\right) - x\left(v'\theta' + \theta v''\right) \\ + \frac{1}{2}\left[u' - \left(y - y_{SC}\right)\theta'\right]^2 + \frac{1}{2}\left[v' + \left(x - x_{SC}\right)\theta'\right]^2 \end{aligned} \tag{3.8}$$

and the shear strains of an open thin-walled section is given by (e.g., Gjelsvik 1981)

$$\gamma_{sz} = 2n\theta' \tag{3.9}$$

By taking the first and second variations of Eq. (3.8) and the first variation of Eq. (3.9) and noting that the buckling displacements (u, v and θ) and their derivatives vanish at the onset of buckling, one obtains

$$\overline{\varepsilon}_z = -x\overline{u}'' - y\overline{v}'' + \omega\overline{\theta}''$$

$$\begin{aligned} \overline{\overline{\varepsilon}}_z = \overline{u}'^2 + \overline{v}'^2 + 2y\left(\overline{u}'\overline{\theta}' + \overline{u}''\overline{\theta}\right) - 2x\left(\overline{v}'\overline{\theta}' + \overline{v}''\overline{\theta}\right) - 2\left(y - y_{SC}\right)\overline{u}'\overline{\theta}' + 2\left(x - x_{SC}\right)\overline{v}'\overline{\theta}' \\ + \left[\left(y - y_{SC}\right)^2 + \left(x - x_{SC}\right)^2\right]\overline{\theta}'^2 \end{aligned} \tag{3.10 a,b}$$

$$\overline{\gamma}_{sz} = 2n\overline{\theta}' \tag{3.11}$$

By adopting centroidal axes, taking the pole to coincide with the shear centre, and adopting a principal sectorial origin, one has

$$\int_A x dA = \int_A y dA = \int_A \omega x dA = \int_A \omega y dA = \int_A \omega dA = 0 \tag{3.12}$$

The present study will deviate from the conventional treatment (e.g., Trahair 1993), by adopting a general orientation for the x, y axes, as opposed to taking principal directions. Thus, the product of inertia $I_{xy} = \int_A xydA \neq 0$ will not vanish. From Eqs. (3.10) and (3.11) by substituting into Eq. (3.7), integrating over area, taking advantage of the orthogonality conditions in Eqs. (3.12), and adopting the notation $P = -\lambda \sigma_{zp} / A$, one can express the second variation of the total potential energy as

$$\frac{1}{2}\bar{\bar{\Pi}} = \frac{1}{2}\int_0^L \Big[EI_{yy}\bar{u}''^2 + EI_{xx}\bar{v}''^2 + 2EI_{xy}\bar{u}''\bar{v}'' + EI_{\omega\omega}\bar{\theta}''^2 + GJ\bar{\theta}'^2 - P\left(\bar{u}'^2 + \bar{v}'^2 + r_0^2\bar{\theta}'^2 + 2y_{SC}\bar{u}'\bar{\theta}' - 2x_{SC}\bar{v}'\bar{\theta}'\right)\Big] dz \tag{3.13}$$

where $J = \sum_{i=1}^{m} \int_{A_i} 4n_i^2 dA_i = \sum_{i=1}^{m} b_i t_i^3 / 3$ is the Saint Venant torsional constant, and b_i and t_i are the width and thickness of the rectangular segments $i = 1, 2, ...m$, respectively, that form the cross-section. The condition of neutral stability is then obtained by setting to zero the variation of Eq. (3.13), yielding

$$\delta\left(\frac{1}{2}\bar{\bar{\Pi}}\right) = \int_0^L \Big\{ \left(EI_{yy}\bar{u}'' + EI_{xy}\bar{v}''\right)\delta\bar{u}'' + \left(EI_{xx}\bar{v}'' + EI_{xy}\bar{u}''\right)\delta\bar{v}'' + EI_{\omega\omega}\bar{\theta}''\delta\bar{\theta}'' - \left(P\bar{u}' + Py_{SC}\bar{\theta}'\right)\delta\bar{u}' - \left(P\bar{v}' - Px_{SC}\bar{\theta}'\right)\delta\bar{v}' - \left(\left(Pr_0^2 - GJ\right)\bar{\theta}' + Py_{SC}\bar{u}' - Px_{SC}\bar{v}'\right)\delta\bar{\theta}' \Big\} dz = 0 \tag{3.14}$$

3.6.2. Governing equations

The governing differential equations and the associated boundary conditions are recovered by integration by parts of Eq. (3.14), yielding

$$EI_{yy}\bar{u}'''' + EI_{xy}\bar{v}'''' + P\bar{u}'' + Py_{SC}\bar{\theta}'' = 0 \tag{3.15}$$

$$EI_{xx}\bar{v}'''' + EI_{xy}\bar{u}'''' + P\bar{v}'' - Px_{SC}\bar{\theta}'' = 0 \tag{3.16}$$

$$EI_{\omega\omega}\bar{\theta}'''' + \left(Pr_0^2 - GJ\right)\bar{\theta}'' + Py_{SC}\bar{u}'' - Px_{SC}\bar{v}'' = 0 \tag{3.17}$$

and

$$\left[\left(EI_{yy}\bar{u}''+EI_{xy}\bar{v}''\right)\delta\bar{u}'\right]_0^L=0 \quad \left[\left(EI_{yy}\bar{u}'''+EI_{xy}\bar{v}'''+P\bar{u}'+Py_{SC}\bar{\theta}'\right)\delta\bar{u}\right]_0^L=0 \tag{3.18}$$

$$\left[\left(EI_{xx}\bar{v}''+EI_{xy}\bar{u}''\right)\delta\bar{v}'\right]_0^L=0 \quad \left[\left(EI_{xx}\bar{v}'''+EI_{xy}\bar{u}'''+P\bar{v}'-Px_{SC}\bar{\theta}'\right)\delta\bar{v}\right]_0^L=0 \tag{3.19}$$

$$\left[\left(EI_{\omega\omega}\bar{\theta}''\right)\delta\bar{\theta}'\right]_0^L=0 \quad \left[\left(EI_{\omega\omega}\bar{\theta}'''+\left(Pr_0^2-GJ\right)\bar{\theta}'+Py_{SC}\bar{u}'-Px_{SC}\bar{v}'\right)\delta\bar{\theta}\right]_0^L=0 \tag{3.20}$$

For the special case of orthogonal coordinates, one has $I_{xy}=0$ and it can be verified that the above equations lead to the classical flexural-torsional buckling governing equations and boundary conditions.

3.6.3. Closed-form solutions

3.6.3.1. Flexural-torsional buckling

For asymmetric members or mono-symmetric members with boundary conditions defined along non-principal axes ($x_{SC}\neq 0$ and $y_{SC}\neq 0$), the flexural-torsional buckling solution is derived by rearranging Eqs. (3.15), (3.16) and (3.17) in a matrix form and assuming an exponential form for the displacement functions, i.e., $\left\langle \bar{u}(z),\bar{v}(z),\bar{\theta}(z)\right\rangle=\left\langle \hat{A} \quad \hat{B} \quad \hat{C}\right\rangle e^{m_i z}$, yielding

$$\begin{bmatrix} EI_{yy}m_i^4+Pm_i^2 & EI_{xy}m_i^4 & Py_{SC}m_i^2 \\ EI_{xy}m_i^4 & EI_{xx}m_i^4+Pm_i^2 & -Px_{SC}m_i^2 \\ Py_{SC}m_i^2 & -Px_{SC}m_i^2 & EI_{\omega\omega}m_i^4+\left(Pr_o^2-GJ\right)m_i^2 \end{bmatrix}\begin{Bmatrix}\hat{A}\\ \hat{B}\\ \hat{C}\end{Bmatrix}e^{m_i z}=\begin{Bmatrix}0\\0\\0\end{Bmatrix} \tag{3.21}$$

For a non-trivial solution, the determinant of Eq. (3.21) must vanish, leading to

$$m_i^6\left[am_i^6+bm_i^4+cm_i^2+d\right]=0 \tag{3.22}$$

where

$$\begin{aligned} a &= E^3\left(I_{yy}I_{xx}-I_{xy}^2\right)I_{\omega\omega} \\ b &= E^2\left[\left(I_{yy}I_{xx}-I_{xy}^2\right)\left(Pr_o^2-GJ\right)+P\left(I_{yy}+I_{xx}\right)I_{\omega\omega}\right] \\ c &= PE\left[\left(I_{xx}+I_{yy}\right)\left(Pr_o^2-GJ\right)-P\left(I_{yy}x_{SC}^2+I_{xx}y_{SC}^2+2I_{xy}x_{SC}y_{SC}-I_{\omega\omega}\right)\right] \\ d &= P^2\left[P\left(r_o^2-x_{SC}^2-y_{SC}^2\right)-GJ\right] \end{aligned} \tag{3.23}$$

The possible solutions for the characteristic equation, Eq. (3.22), will depend on the sign of constant d. When $P<GJ/\left(r_o^2-x_{SC}^2-y_{SC}^2\right)$ (i.e., $d<0$), the roots of the characteristic equation are $m_{1-6}=0$, $m_{7,8}=\pm\alpha$, $m_{9,10}=\pm i\beta$ and $m_{11,12}=\pm i\gamma$, in which α, β and γ are obtained by a modified form of Cardan's method (Nickalls 1993) as

$$\alpha=\sqrt{\frac{-b}{3a}+2\sqrt{\frac{b^2-3ac}{9a^2}}\cos\left(\psi\right)} \qquad \beta=\sqrt{\frac{b}{3a}-2\sqrt{\frac{b^2-3ac}{9a^2}}\cos\left(\frac{2\pi}{3}+\psi\right)}$$
$$\gamma=\sqrt{\frac{b}{3a}-2\sqrt{\frac{b^2-3ac}{9a^2}}\cos\left(\frac{4\pi}{3}+\psi\right)} \tag{3.24 a-c}$$

where

$$\psi=\frac{1}{3}\cos^{-1}\left[\left(\frac{-27a^2d+9abc-2b^3}{54a^3}\right)\left(\frac{b^2-3ac}{9a^2}\right)^{-3/2}\right] \tag{3.25}$$

Thus, for the case $P<GJ/\left(r_o^2-x_{SC}^2-y_{SC}^2\right)$, the solution takes the form

$$\begin{aligned} \bar{u}(z) = {} & D_1+D_2z+D_7\xi_1\cosh\alpha z+D_8\xi_1\sinh\alpha z+D_9\xi_2\cos\beta z+D_{10}\xi_2\sin\beta z+D_{11}\xi_3\cos\gamma z \\ & +D_{12}\xi_3\sin\gamma z \end{aligned} \tag{3.26}$$

$$\bar{v}(z)=D_3+D_4z+D_7\cosh\alpha z+D_8\sinh\alpha z+D_9\cos\beta z+D_{10}\sin\beta z+D_{11}\cos\gamma z+D_{12}\sin\gamma z \tag{3.27}$$

$$\begin{aligned} \bar{\theta}(z) = {} & D_5+D_6z+D_7\eta_1\cosh\alpha z+D_8\eta_1\sinh\alpha z+D_9\eta_2\cos\beta z+D_{10}\eta_2\sin\beta z+D_{11}\eta_3\cos\gamma z \\ & +D_{12}\eta_3\sin\gamma z \end{aligned} \tag{3.28}$$

where

$$\xi_1 = \frac{P^2 x_{SC}^2 - \left(EI_{xx}\alpha^2 + P\right)\left(EI_{\omega\omega}\alpha^2 + Pr_o^2 - GJ\right)}{P^2 x_{SC} y_{SC} + EI_{xy}\alpha^2\left(EI_{\omega\omega}\alpha^2 + Pr_o^2 - GJ\right)} \qquad \eta_1 = \frac{P\left[E\left(I_{xx}y_{SC} + I_{xy}x_{SC}\right)\alpha^2 + Py_{SC}\right]}{P^2 x_{SC} y_{SC} + EI_{xy}\alpha^2\left(EI_{\omega\omega}\alpha^2 + Pr_o^2 - GJ\right)}$$

$$\xi_2 = \frac{P^2 x_{SC}^2 - \left(EI_{xx}\beta^2 - P\right)\left(EI_{\omega\omega}\beta^2 - Pr_o^2 + GJ\right)}{P^2 x_{SC} y_{SC} + EI_{xy}\beta^2\left(EI_{\omega\omega}\beta^2 - Pr_o^2 + GJ\right)} \qquad \eta_2 = \frac{-P\left[E\left(I_{xx}y_{SC} + I_{xy}x_{SC}\right)\beta^2 - Py_{SC}\right]}{P^2 x_{SC} y_{SC} + EI_{xy}\beta^2\left(EI_{\omega\omega}\beta^2 - Pr_o^2 + GJ\right)}$$

$$\xi_3 = \frac{P^2 x_{SC}^2 - \left(EI_{xx}\gamma^2 - P\right)\left(EI_{\omega\omega}\gamma^2 - Pr_o^2 + GJ\right)}{P^2 x_{SC} y_{SC} + EI_{xy}\gamma^2\left(EI_{\omega\omega}\gamma^2 - Pr_o^2 + GJ\right)} \qquad \eta_3 = \frac{-P\left[E\left(I_{xx}y_{SC} + I_{xy}x_{SC}\right)\gamma^2 - Py_{SC}\right]}{P^2 x_{SC} y_{SC} + EI_{xy}\gamma^2\left(EI_{\omega\omega}\gamma^2 - Pr_o^2 + GJ\right)}$$

It is noted that, numerically, the condition $P < GJ/\left(r_o^2 - x_{SC}^2 - y_{SC}^2\right)$ will be realized in practically all compression members with asymmetric sections and will be investigated in the following sections. In contrast, the cases $P > GJ/\left(r_o^2 - x_{SC}^2 - y_{SC}^2\right)$ and $P = GJ/\left(r_o^2 - x_{SC}^2 - y_{SC}^2\right)$ remain of academic interest and hence are treated separately under Appendix A. For monosymmetric members with end restraints defined along the principal directions, either Eq. (3.15) or (3.16) will be uncoupled from the remaining two differential equations (depending on the axis of symmetry). In such cases, the present solution reverts to the classical solution and Eq. (3.1) becomes applicable.

3.6.3.2. Pure flexural buckling

For doubly symmetric or point symmetric members, where $x_{SC} = y_{SC} = 0$, Eq. (3.17) becomes uncoupled from the remaining governing equations. This leads to a pure coupled flexural buckling mode about both non-principal axes. To obtain the buckling load for this case, Eqs. (3.15) and (3.16) are placed in a matrix form after setting $x_{SC} = y_{SC} = 0$ and assuming an exponential form for the displacement functions, yielding

$$\begin{bmatrix} EI_{yy}m_i^4 + Pm_i^2 & EI_{xy}m_i^4 \\ EI_{xy}m_i^4 & EI_{xx}m_i^4 + Pm_i^2 \end{bmatrix} \begin{Bmatrix} \hat{A} \\ \hat{B} \end{Bmatrix} e^{m_i z} = \begin{Bmatrix} 0 \\ 0 \end{Bmatrix} \tag{3.29}$$

For a non-trivial solution, the determinant of Eq. (3.29) must vanish, leading to

$$m_i^4\left[E^2\left(I_{xx}I_{yy}-I_{xy}^2\right)m_i^4+PE\left(I_{xx}+I_{yy}\right)m_i^2+P^2\right]=0 \tag{3.30}$$

The roots of Eq. (3.30) are $m_{1-4}=0$, $m_{5,6}=\pm i\hat{\alpha}$ and $m_{7,8}=\pm i\hat{\beta}$ where

$$\begin{aligned}\hat{\alpha}&=\sqrt{P\left[\left(I_{xx}+I_{yy}\right)+\sqrt{\left(I_{xx}+I_{yy}\right)^2-4\left(I_{xx}I_{yy}-I_{xy}^2\right)}\right]\Big/2E\left(I_{xx}I_{yy}-I_{xy}^2\right)}\\ \hat{\beta}&=\sqrt{P\left[\left(I_{xx}+I_{yy}\right)-\sqrt{\left(I_{xx}+I_{yy}\right)^2-4\left(I_{xx}I_{yy}-I_{xy}^2\right)}\right]\Big/2E\left(I_{xx}I_{yy}-I_{xy}^2\right)}\end{aligned} \tag{3.31 a,b}$$

The flexural buckling solution in this case takes the form

$$\bar{u}\left(z\right)=D_1+D_2z+D_5\varsigma_1\cos\hat{\alpha}z+D_6\varsigma_1\sin\hat{\alpha}z+D_7\varsigma_2\cos\hat{\beta}z+D_8\varsigma_2\sin\hat{\beta}z \tag{3.32}$$

$$\bar{v}\left(z\right)=D_3+D_4z+D_5\cos\hat{\alpha}z+D_6\sin\hat{\alpha}z+D_7\cos\hat{\beta}z+D_8\sin\hat{\beta}z \tag{3.33}$$

in which, $\varsigma_1=-EI_{xy}\hat{\alpha}^2\big/\left(EI_{yy}\hat{\alpha}^2-P\right)$ and $\varsigma_2=-EI_{xy}\hat{\beta}^2\big/\left(EI_{yy}\hat{\beta}^2-P\right)$ have been defined.

3.7. Boundary conditions

The characteristic equations for determining the buckling loads corresponding to several boundary conditions are developed using the proposed closed-form solutions. Each problem investigated is assigned a designation of the form $x_{n_1n_2}y_{n_3n_4}z_{n_5n_6}$, where n_1,n_2 denote the boundary conditions relative to x axis at the first and second ends of the member, n_3,n_4 denote the boundary conditions relative to y axis at both ends, and n_5,n_6 denote the boundary conditions relative to twist at both ends. A notation $n_i=p$ indicates a pin condition about the relevant axis while $n_i=f$ denotes a fixation. For example, the designation $x_{pp}y_{ff}z_{pp}$ indicates both ends of the member are pinned about x axis, fixed about y axis, and pinned about z axis. For cases of pure flexural buckling, the $z_{\bullet\bullet}$ portion will be omitted from the designation.

3.7.1. Cases involving identical boundary conditions along both directions

For an asymmetric member pinned about both directions and relative to twist at both ends $\left(x_{pp}y_{pp}z_{pp}\right)$, the relevant boundary conditions are

$$\begin{aligned}
&\bar{u}(0)=I_{yy}\bar{u}''(0)+I_{xy}\bar{v}''(0)=0 \qquad \bar{v}(0)=I_{xx}\bar{v}''(0)+I_{xy}\bar{u}''(0)=0 \qquad \bar{\theta}(0)=\bar{\theta}''(0)=0\\
&\bar{u}(L)=I_{yy}\bar{u}''(L)+I_{xy}\bar{v}''(L)=0 \qquad \bar{v}(L)=I_{xx}\bar{v}''(L)+I_{xy}\bar{u}''(L)=0 \qquad \bar{\theta}(L)=\bar{\theta}''(L)=0
\end{aligned} \tag{3.34}$$

From Eqs. (3.26)-(3.28) by substituting into Eq. (3.34), placing the resulting equations into a matrix form, and then setting to zero the determinant of the resulting matrix of coefficients, one recovers the characteristic equation

$$\alpha^2\beta^2\gamma^2\left(I_{xx}I_{yy}-I_{xy}^2\right)\left[\eta_1\left(\xi_2-\xi_3\right)+\eta_2\left(\xi_3-\xi_1\right)+\eta_3\left(\xi_1-\xi_2\right)\right]\sinh\alpha L\sin\beta L\sin\gamma L=0 \tag{3.35}$$

Since α, β and γ are non-zero roots of Eq. (3.22), $\sinh\alpha L$ cannot vanish. Also, we have $I_{xx}I_{yy}-I_{xy}^2=I_{\hat{x}\hat{x}}I_{\hat{y}\hat{y}}>0$ and the term $\left[\eta_1\left(\xi_2-\xi_3\right)+\eta_2\left(\xi_3-\xi_1\right)+\eta_3\left(\xi_1-\xi_2\right)\right]$ vanishes only when $P=0$. One recovers the condition $\sin\beta L\sin\gamma L=0$ leading to either $\beta=\pi/L$ or $\gamma=\pi/L$. Given the values of β and γ, Eqs. (3.24)b-c can be solved to recover the buckling load P. In a similar manner, one can recover the characteristic equations for other cases involving identical boundary conditions along both directions (Table 3.1).

For a given member, it can be verified that the terms $I_{xx}+I_{yy}$, $I_{xx}I_{yy}-I_{xy}^2$, $\left(I_{yy}x_{SC}^2+I_{xx}y_{SC}^2+2I_{xy}x_{SC}y_{SC}\right)$, $I_{\omega\omega}$, J, $\left(x_{SC}^2+y_{SC}^2\right)$ and r_o^2 are invariant quantities that do not depend on the orientation of the axes. Hence, Eqs. (3.23)-(3.25) indicate that α,β,γ depend solely on the buckling load P. Also, Eqs. (3.31) show that $\hat{\alpha}$ and $\hat{\beta}$ depend solely on the buckling load P, and the characteristic equations for $x_{pp}y_{pp}z_{pp}$ $x_{ff}y_{ff}z_{ff}$, $x_{pf}y_{pf}z_{pf}$, $x_{ff}y_{ff}$ and $x_{pf}y_{pf}$ cases in

Table 3.1 indicate that the buckling loads are independent of the orientation of the axes. Physically, this observation is consistent with the fact that, for example, an end pinned about x and y axes, will also be pinned about any other direction within the xy plane. For such cases, the present solution reverts to the classical solution (Eq. (3.1)).

Table 3.1 Boundary conditions and characteristic equations for members with identical end restraints along both directions at one end

Designation: $x_{ff}y_{ff}z_{ff}$						
Boundary conditions	$\bar{u}$ /shear	$\bar{u}'$ /moment	$\bar{v}$ /shear	$\bar{v}'$ /moment	$\bar{\theta}$ /moment	$\bar{\theta}'$ /bimoment
At $z=0$	$\bar{u}=0$	$\bar{u}'=0$	$\bar{v}=0$	$\bar{v}'=0$	$\bar{\theta}=0$	$\bar{\theta}'=0$
At $z=L$	$\bar{u}=0$	$\bar{u}'=0$	$\bar{v}=0$	$\bar{v}'=0$	$\bar{\theta}=0$	$\bar{\theta}'=0$
Characteristic equation	$\left[-\beta L\sin\beta L-2\left(\cos\beta L-1\right)\right]\left[-\gamma L\sin\gamma L-2\left(\cos\gamma L-1\right)\right]=0$					
Designation: $x_{pf}y_{pf}z_{pf}$						
At $z=0$	$\bar{u}=0$	$I_{yy}\bar{u}''+I_{xy}\bar{v}''=0$	$\bar{v}=0$	$I_{xx}\bar{v}''+I_{xy}\bar{u}''=0$	$\bar{\theta}=0$	$\bar{\theta}''=0$
At $z=L$	$\bar{u}=0$	$\bar{u}'=0$	$\bar{v}=0$	$\bar{v}'=0$	$\bar{\theta}=0$	$\bar{\theta}'=0$
Characteristic equation	$\left(\tan\beta L-\beta L\right)\left(\tan\gamma L-\gamma L\right)=0$					
Designation: $x_{pp}y_{pp}$						
At $z=0$	$\bar{u}=0$	$I_{yy}\bar{u}''+I_{xy}\bar{v}''=0$	$\bar{v}=0$	$I_{xx}\bar{v}''+I_{xy}\bar{u}''=0$	NA	NA
At $z=L$	$\bar{u}=0$	$\bar{u}'=0$	$\bar{v}=0$	$\bar{v}'=0$	NA	NA
Characteristic equation	$\sin\hat{\alpha}L\sin\hat{\beta}L=0$					
Designation: $x_{ff}y_{ff}$						
At $z=0$	$\bar{u}=0$	$I_{yy}\bar{u}''+I_{xy}\bar{v}''=0$	$\bar{v}=0$	$I_{xx}\bar{v}''+I_{xy}\bar{u}''=0$	NA	NA
At $z=L$	$\bar{u}=0$	$\bar{u}'=0$	$\bar{v}=0$	$\bar{v}'=0$	NA	NA
Characteristic equation	$\left[-\hat{\alpha}L\sin\hat{\alpha}L-2\left(\cos\hat{\alpha}L-1\right)\right]\left[-\hat{\beta}L\sin\hat{\beta}L-2\left(\cos\hat{\beta}L-1\right)\right]=0$					
Designation: $x_{pf}y_{pf}$						
At $z=0$	$\bar{u}=0$	$I_{yy}\bar{u}''+I_{xy}\bar{v}''=0$	$\bar{v}=0$	$I_{xx}\bar{v}''+I_{xy}\bar{u}''=0$	NA	NA
At $z=L$	$\bar{u}=0$	$\bar{u}'=0$	$\bar{v}=0$	$\bar{v}'=0$	NA	NA
Characteristic equation	$\left(\tan\hat{\alpha}L-\hat{\alpha}L\right)\left(\tan\hat{\beta}L-\hat{\beta}L\right)=0$					
Note: NA= Not Applicable.						

3.7.2. Cases involving different boundary conditions along non-principal directions

For an asymmetric member pinned about the x axis, fixed about y axis and pinned relative to twist at both ends $\left(x_{pp}y_{ff}z_{pp}\right)$, the relevant boundary conditions are

$$\begin{aligned}
&\bar{u}(0)=\bar{u}'(0)=0 \qquad \bar{v}(0)=I_{xx}\bar{v}''(0)+I_{xy}\bar{u}''(0)=0 \qquad \bar{\theta}(0)=\bar{\theta}''(0)=0\\
&\bar{u}(L)=\bar{u}'(L)=0 \qquad \bar{v}(L)=I_{xx}\bar{v}''(L)+I_{xy}\bar{u}''(L)=0 \qquad \bar{\theta}(L)=\bar{\theta}''(L)=0
\end{aligned} \tag{3.36}$$

Again, from Eqs. (3.26)-(3.28) by substituting into Eq. (3.36), arranging the resulting equations in a matrix form and then setting to zero the determinant of the matrix of coefficients, the characteristic equation corresponding to the buckling load is found to take the form

$$\begin{aligned}
&\beta\gamma\xi_1\left[I_{xx}\left(\eta_3-\eta_2\right)+I_{xy}\left(\xi_2\eta_3-\xi_3\eta_2\right)\right]\left(\cosh\alpha L-1\right)\sin\beta L\sin\gamma L\\
&+\alpha\gamma\xi_2\left[I_{xx}\left(\eta_3-\eta_1\right)+I_{xy}\left(\xi_1\eta_3-\xi_3\eta_1\right)\right]\sinh\alpha L\left(\cos\beta L-1\right)\sin\gamma L\\
&+\alpha\beta\xi_3\left[I_{xx}\left(\eta_1-\eta_2\right)+I_{xy}\left(\xi_2\eta_1-\xi_1\eta_2\right)\right]\sinh\alpha L\sin\beta L\left(\cos\gamma L-1\right)=0
\end{aligned} \tag{3.37}$$

Equation (3.37) is iteratively solved for the buckling load P subject to the definitions of α, β and γ as provided in Eqs. (3.24) a-c.

Here, although α, β and γ remain independent from the orientation of x, y axes, the parameters ξ_1, ξ_2, ξ_3, $\left[I_{xx}\left(\eta_3-\eta_2\right)+I_{xy}\left(\xi_2\eta_3-\xi_3\eta_2\right)\right]$, $\left[I_{xx}\left(\eta_3-\eta_1\right)+I_{xy}\left(\xi_1\eta_3-\xi_3\eta_1\right)\right]$ and $\left[I_{xx}\left(\eta_1-\eta_2\right)+I_{xy}\left(\xi_2\eta_1-\xi_1\eta_2\right)\right]$ are clearly dependent on the orientation of the axes, indicating that the buckling load is orientation-dependent. The application of the classical solution (e.g., Eq. (3.1)) in this case would lead to erroneous buckling load predictions. In a similar manner, the characteristic equations can be obtained for $x_{ff}y_{pp}z_{pp}$, $x_{pp}y_{ff}$ and $x_{ff}y_{pp}$, where the boundary conditions along x direction differ from those along y direction (Table 3.2). Here also, the characteristic equations obtained indicate the dependence of the buckling load on the orientation of x, y directions.

Table 3.2 Boundary conditions and characteristic equations for members with different end restraints along non-principal directions at one end

Designation: $x_{ff}y_{pp}z_{pp}$						
Boundary conditions	$\bar{u}$ /shear	$\bar{u}'$ /moment	$\bar{v}$ /shear	$\bar{v}'$ /moment	$\bar{\theta}$ /moment	$\bar{\theta}'$ /bimoment
At $z=0$	$\bar{u}=0$	$I_{yy}\bar{u}''+I_{xy}\bar{v}''=0$	$\bar{v}=0$	$\bar{v}'=0$	$\bar{\theta}=0$	$\bar{\theta}''=0$
At $z=L$	$\bar{u}=0$	$I_{yy}\bar{u}''+I_{xy}\bar{v}''=0$	$\bar{v}=0$	$\bar{v}'=0$	$\bar{\theta}=0$	$\bar{\theta}''=0$
Characteristic equation	$\beta\gamma\left[I_{yy}\left(\xi_3\eta_2-\xi_2\eta_3\right)+I_{xy}\left(\eta_2-\eta_3\right)\right]\left(\cosh\alpha L-1\right)\sin\beta L\sin\gamma L$ $+\alpha\gamma\left[I_{yy}\left(\xi_3\eta_1-\xi_1\eta_3\right)+I_{xy}\left(\eta_1-\eta_3\right)\right]\sinh\alpha L\left(\cos\beta L-1\right)\sin\gamma L$ $+\alpha\beta\left[I_{yy}\left(\xi_1\eta_2-\xi_2\eta_1\right)+I_{xy}\left(\eta_2-\eta_1\right)\right]\sinh\alpha L\sin\beta L\left(\cos\gamma L-1\right)=0$					
Designation: $x_{pp}y_{ff}$						
At $z=0$	$\bar{u}=0$	$\bar{u}'=0$	$\bar{v}=0$	$I_{xx}\bar{v}''+I_{xy}\bar{u}''=0$	NA	NA
At $z=L$	$\bar{u}=0$	$\bar{u}'=0$	$\bar{v}=0$	$I_{xx}\bar{v}''+I_{xy}\bar{u}''=0$	NA	NA
Characteristic equation	$\hat{\alpha}^2\hat{\beta}\varsigma_2\left(I_{xx}+I_{xy}\varsigma_1\right)\sin\hat{\alpha}L\left(\cos\hat{\beta}L-1\right)-\hat{\alpha}\hat{\beta}^2\varsigma_1\left(I_{xx}+I_{xy}\varsigma_2\right)\sin\hat{\beta}L\left(\cos\hat{\alpha}L-1\right)=0$					
Designation: $x_{ff}y_{pp}$						
At $z=0$	$\bar{u}=0$	$I_{yy}\bar{u}''+I_{xy}\bar{v}''=0$	$\bar{v}=0$	$\bar{v}'=0$	NA	NA
At $z=L$	$\bar{u}=0$	$I_{yy}\bar{u}''+I_{xy}\bar{v}''=0$	$\bar{v}=0$	$\bar{v}'=0$	NA	NA
Characteristic equation	$\hat{\alpha}\hat{\beta}^2\left(\varsigma_2 I_{yy}+I_{xy}\right)\sin\hat{\beta}L\left(\cos\hat{\alpha}L-1\right)-\hat{\beta}\hat{\alpha}^2\left(\varsigma_1 I_{yy}+I_{xy}\right)\sin\hat{\alpha}L\left(\cos\hat{\beta}L-1\right)=0$					
Note: NA= Not Applicable.						

3.8. Verification

A compression member with a 4000 mm span has an angle cross-section. Leg dimensions are $b_1=102$ mm and $b_2=152$ mm, and thickness $t=15.9$ mm. Material properties are $E=200,000$ MPa and $G=76,900$ MPa. Four types of boundary conditions are considered: $x_{pp}y_{pp}z_{pp}$, $x_{pp}y_{ff}z_{pp}$, $x_{ff}y_{pp}z_{pp}$ and $x_{ff}y_{ff}z_{ff}$. The orientations of x and y axes are taken parallel to the legs of the angle (Figure 3.3). The predictions based on the present closed-form solution are compared against the predictions of a thin-walled finite element analysis (FEA) beam model based on B31OS

element, and against a FEA shell model based on S4 element, both available in the Abaqus library. Where applicable, predictions based on Eq. (3.1) are provided for comparison.

The B31OS is a two-node thin-walled beam element with seven degrees of freedom (DOFs) per node; three displacements, three rotations and a warping deformation. A mesh sensitivity analysis indicated that convergence is achieved by using 40 elements. The S4 element is a four-node fully integrated shell element with six DOFs per node; three displacements and three rotations. A mesh study indicated that convergence is attained when the mesh consisted of 200 elements along the span, five elements along the short leg and eight elements along the long leg. To simulate the $x_{pp}y_{pp}z_{pp}$ end conditions in the S4 model, the angle of twist and displacements along the x and y directions were restrained for all nodes at the member ends. Two master nodes were defined at the section centroids for both ends. The displacements of the master nodes along the x and y directions were coupled to those of the shear centre at the corner node. The longitudinal displacements of end nodes were related to the longitudinal displacement of the corresponding master node in such a way that the member ends pivot about the centroidal axes of the cross-section. The longitudinal displacement at one of the master nodes was restrained while an axial force was applied at the other master node. Additional restraints were enforced to simulate the $x_{pp}y_{ff}z_{pp}$, $x_{ff}y_{pp}z_{pp}$ and $x_{ff}y_{ff}z_{ff}$ boundary conditions. For $x_{pp}y_{ff}z_{pp}$, the master node rotational DOFs about the y axis were restrained whereas for $x_{ff}y_{pp}z_{pp}$, the master node rotational DOFs about the x axis were restrained. For $x_{ff}y_{ff}z_{ff}$, both rotations about x and y axes were restrained at the master nodes as well as the remaining nodes of the cross-section (in order to restrain local warping).

Table 3.3 shows that the buckling loads predicted by the present solution are nearly identical to those predicted by the B31OS model for all cases. A nearly perfect agreement is also obtained with

the shell S4 model. As expected, when the rotational boundary conditions about the x and y axes are identical (e.g., $x_{pp}y_{pp}\cdots$ or $x_{ff}y_{ff}\cdots$), the buckling loads predicted by the present and the classical solution (Eq. (3.1)) are found to be identical. Also, the normalized mode shapes for $x_{pp}y_{ff}z_{pp}$ as predicted by the present solution are in a close agreement with those based on the B31OS and S4 solutions (Figure 3.3) for displacements $\bar{u},\bar{v}$ and angle of twist $\bar{\theta}$. In the S4 model, the angle of twist for a given section was computed by averaging the angles of twist at the shear centre and at the tip points.

Table 3.3 Buckling load comparison for L152x102x16 member

Boundary Conditions	Buckling load (kN)				Ratios		
	Present	B31OS	S4	Classical solution			
	(1)	(2)	(3)	(4)	(1)/ (2)	(1)/ (3)	(1)/ (4)
$x_{pp}y_{pp}z_{pp}$	218.6	218.6	218.5	218.6	1.00	1.00	1.00
$x_{pp}y_{ff}z_{pp}$	339.7	339.4	338.6	NA	1.00	1.00	NA
$x_{ff}y_{pp}z_{pp}$	749.3	748.9	745.9	NA	1.00	1.00	NA
$x_{ff}y_{ff}z_{ff}$	845.8	845.0	841.9	845.8	1.00	1.00	1.00
Note: NA= Not Applicable.							

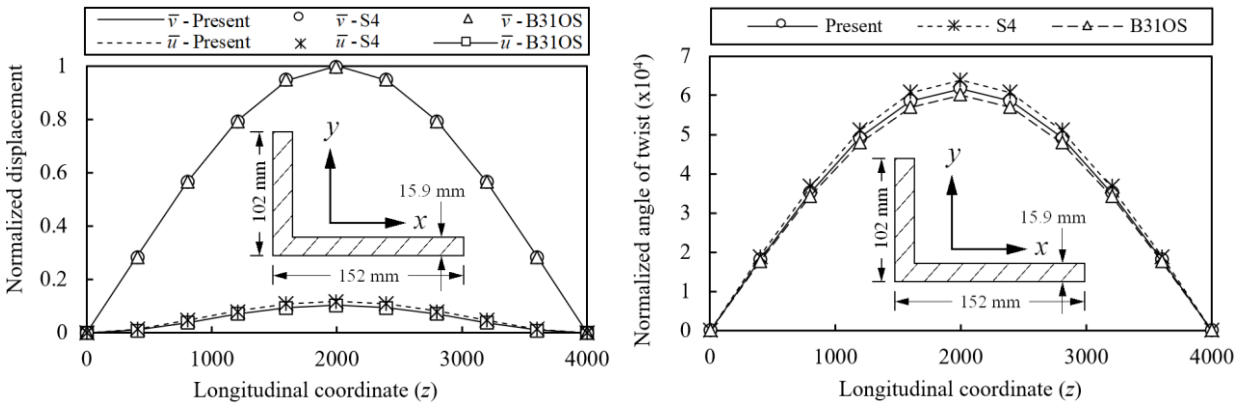

(a) (b)

Figure 3.3 Normalized mode shapes for $x_{pp}y_{ff}z_{pp}$ (a) displacements and (b) angle of twist

3.9. Effect of axes orientation

The present solutions are used to investigate the influence of axes orientation on the buckling loads of members with angle and zed cross-sections subjected to concentric loadings.

3.9.1. Members with single angle cross-section

The buckling loads are investigated for a series of compression members with angle cross-sections and 4000 mm spans. Leg thickness is kept constant at 15.9 mm while legs width b_1 and b_2 are varied from 102 to 203 mm so that $b_1 + b_2 \approx 305$ and the cross-sectional areas of all cross-sections are nearly equal. The leg width ratio b_1/b_2 are varied from 0.5 to 2.0. The boundary conditions considered are $x_{ff}y_{ff}z_{ff}$, $x_{pp}y_{ff}z_{pp}$ and $x_{pp}y_{pp}z_{pp}$, where x and y axes are taken parallel to the angle legs (Figure 3.4a). The buckling load P for a given boundary condition (e.g., $x_{ff}y_{ff}z_{ff}$ or $x_{pp}y_{ff}z_{pp}$) is normalized with respect to the buckling load P_R for $x_{pp}y_{pp}z_{pp}$ of an identical member.

For $x_{ff}y_{ff}z_{ff}$, Figure 3.4a shows that the normalized buckling load P/P_R increases with the legs width ratio b_1/b_2 from 3.58 at $b_1/b_2 = 0.5$ to 4.0 at $b_1/b_2 = 1.0$ where it peaks (as the governing buckling mode transitions from a flexural-torsional when $b_1/b_2 < 1.0$ into a pure flexural at $b_1/b_2 = 1.0$), after which P/P_R reduces with b_1/b_2 and attains a value of 3.58 at $b_1/b_2 = 2.0$ (again corresponding to a flexural torsional when $b_1/b_2 > 1.0$). For $x_{ff}y_{ff}z_{ff}$, Figure 3.4a shows that the effect of b_1/b_2 on the normalized buckling load P/P_R can be characterized as moderate.

The case $x_{pp}y_{ff}z_{pp}$ is of practical importance since it represents the boundary conditions for the commonly used gusset plate end connection details depicted in Figure 3.1a where the gusset plate provides rotational fixity about the y axis with essentially no rotational fixity about the x axis

and will be discussed in the following. For $x_{pp}y_{ff}z_{pp}$, when $b_1/b_2 = 0.5$, the minor principal direction $\hat{x}$ is inclined at 15° from the pinned axis x resulting in a buckling load that is 40% higher than that for $x_{pp}y_{pp}z_{pp}$. The amplitude of displacements $\bar{u}$ and $\bar{v}$ shown in Figure 3.4b indicates that displacement $\bar{v}$, corresponding to the pin boundary condition, dominates the buckling response. As b_1/b_2 increases, the influence of fixity about y axis increases, inducing an increase in P/P_R. Figure 3.4b-f depicts a gradual increase in the amplitude of $\bar{u}$ with b_1/b_2. When $b_1/b_2 = 2.0$, the minor principal direction $\hat{x}$ becomes oriented at 15° from the axis y of rotational fixity leading to a buckling load that is only 3.3% lower than that for $x_{ff}y_{ff}z_{ff}$ Unlike the case $x_{pp}y_{ff}z_{pp}$, Figure 3.4a shows that the effect of b_1/b_2 on the normalized buckling load P/P_R can rather pronounced as it ranges from 1.40 at $b_1/b_2 = 0.5$ to 3.55 at $b_1/b_2 = 2.0$, suggesting the effectiveness of the later design scenario in comparison to the reference pin-ended case $x_{pp}y_{pp}z_{pp}$.

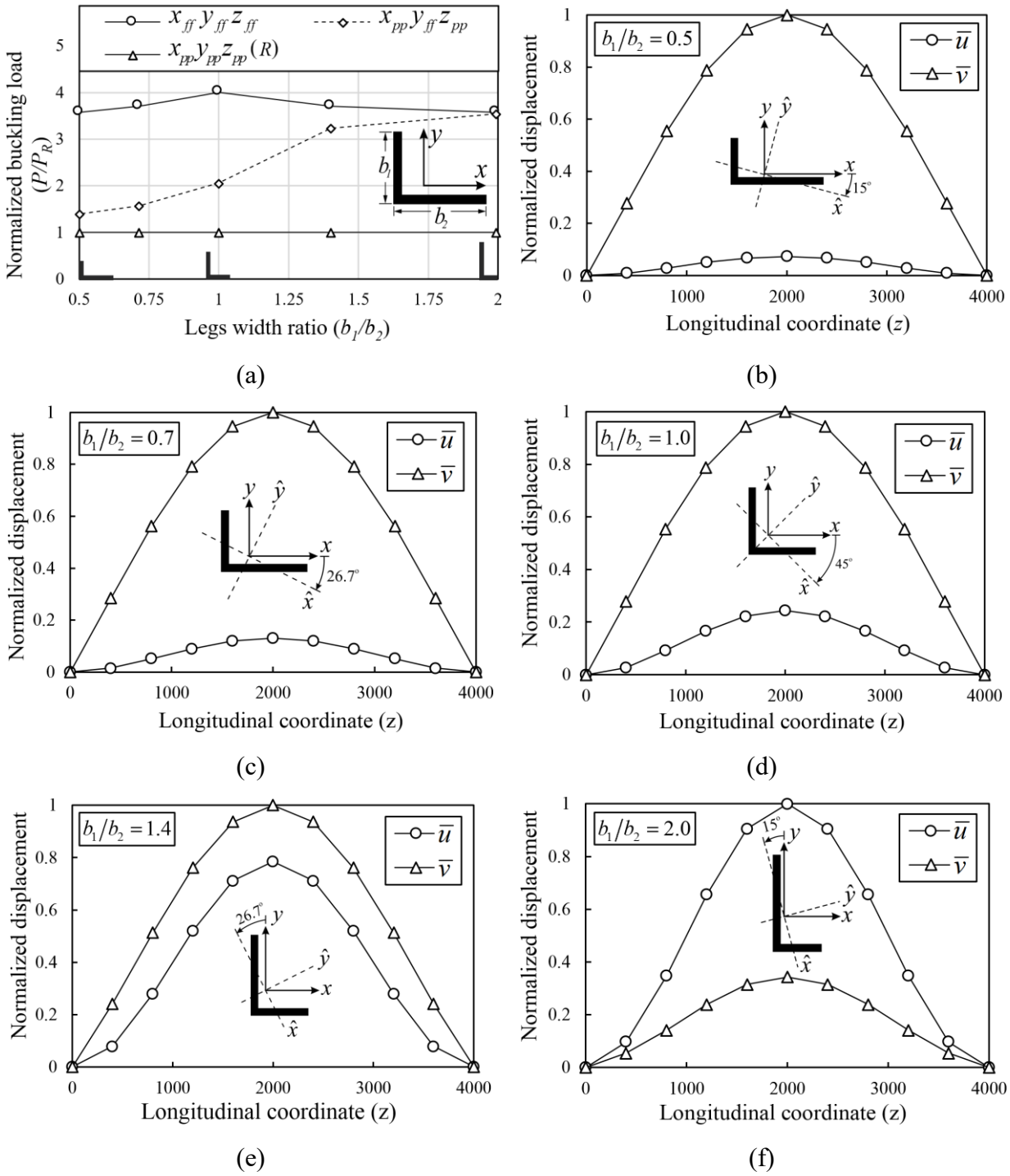

Figure 3.4 Buckling results for angle members (span=4000 mm and thickness=15.9 mm), (a) Normalized buckling load versus leg width ratio, and mode shapes for $x_{pp}y_{ff}z_{pp}$ (b) $b_1/b_2 = 0.5$, (c) $b_1/b_2 = 0.7$, (d) $b_1/b_2 = 1.0$, (e) $b_1/b_2 = 1.4$ and (f) $b_1/b_2 = 2.0$

The orientation of end restraining axes is further investigated by considering two members with L152x152x16 and L203x102x16 cross-sections and 4000 mm spans. For both members, the minor principal direction $\hat{x}$ is oriented at an angle of inclination ϕ ranging from 0 to 180° relative to the x axis. Again, three types of boundary conditions are considered, $x_{pp}y_{pp}z_{pp}$, $x_{pp}y_{ff}z_{pp}$ and $x_{ff}y_{ff}z_{ff}$. For L152x152x16 cases where x, y axes coincide with the principal directions $\hat{x}, \hat{y}$ (i.e., $\phi = 0, 90°, 180°$), Eq. (3.1) is used to calculate the buckling loads.

As expected for $x_{ff}y_{ff}z_{ff}$, Figure 3.5a shows that the normalized buckling load P/P_R has a constant value of 4.00 irrespective of the angle of inclination ϕ. This is the case since (a) an end that is fixed about two perpendicular directions x and y will be also fixed about other directions within the xy plane, and (b) the governing buckling mode is pure flexural. For $x_{pp}y_{ff}z_{pp}$, P/P_R ranges from 1.00 at $\phi = 0$ and peaks to 3.24 at $\phi = 90°$, at which the fixed rotational restraint is provided about an axis coinciding with the minor principal direction. As ϕ increases beyond 90°, P/P_R reduces back to 1.00 at $\phi = 180°$. As expected, for the equal-leg angle member considered, the P/P_R relationship exhibits a symmetric behaviour relative to $\phi = 90°$.

Figure 3.5b shows similar results for the L203x102x16 member, albeit the normalized buckling load P/P_R plot is not symmetric relative to $\phi = 90°$. Also, unlike equal-leg angle member, Figure 3.5b shows that the maximum buckling load for $x_{pp}y_{ff}z_{pp}$ coincides with the buckling load for $x_{ff}y_{ff}z_{ff}$ of an identical cross-section as both cases exhibit flexural-torsional buckling modes.

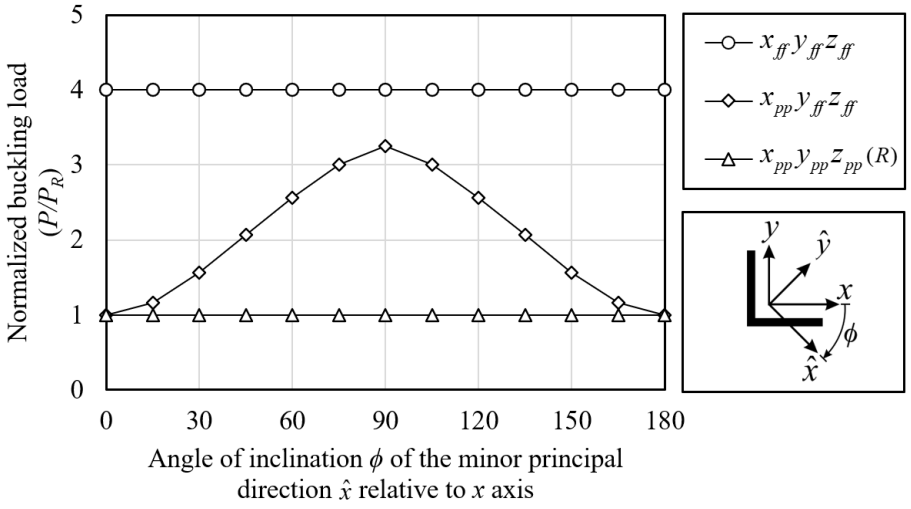

(a)

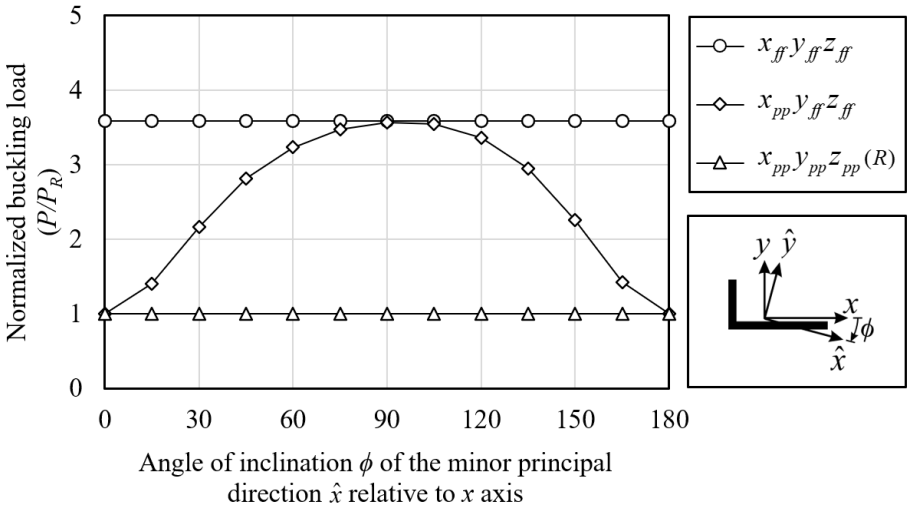

(b)

Figure 3.5 Normalized buckling load versus angle of inclination ϕ of the minor principal direction $\hat{x}$ relative to x axis for members with (a) L152x152x16 (b) L203x102x16 cross-sections (span= 4000 mm)

3.9.2. Members with zed cross-section

The effect of non-principal end restraints on the buckling load for compression members with zed cross-sections is investigated by considering a set of compression members with 4000 mm spans. All thicknesses t were kept constant at 15.9 mm while varying the flange width b_f from 102 to 203 mm and the web height b_w from 254 to 406 mm, under the constraint $\left(2b_f + b_w\right) = 610$ mm

so as to keep the area of the cross-section nearly constant in all runs considered. The corresponding flange width to web height ratios b_f/b_w were thus varied from 0.25 to 1.00. The boundary conditions considered are $x_{pp}y_{pp}$ (which is taken as a reference case), $x_{pp}y_{ff}$, $x_{ff}y_{pp}$ (which would be approached when the web of zed section is connected to gusset plate) and $x_{ff}y_{ff}$, where y axis coincides with the web of the section. Only buckling loads P based on flexural modes are considered. Load P is normalized to the buckling load P_R for identical member with $x_{pp}y_{pp}$ boundary condition.

Figure 3.6 shows that the normalized buckling load P/P_R for $x_{ff}y_{ff}$ is 4.00 irrespective of b_f/b_w since the flexural buckling load for fixed end member is four times that for an identical member with pinned end restraints. For $x_{pp}y_{ff}$, when $b_f/b_w = 0.25$, the minor principal axis is inclined at only $\phi = 8.3°$ relative to the y axis leading to a P/P_R value nearly equal to that of the $x_{ff}y_{ff}$ case. As the b_f/b_w ratio increases, the angle of inclination of the principal axis relative to the fixity axis increases, and thus inducing a gradual reduction in P/P_R which attains a value of 2.88 at $b_f/b_w = 1.00$.

Conversely, for $x_{ff}y_{pp}$, the P/P_R is observed to increase in a nearly linear manner with b_f/b_w. It ranges from 1.58 at $b_f/b_w = 0.25$ to 3.22 at $b_f/b_w = 1.00$. For the case $b_f/b_w = 0.25$, the ratio of moments of inertia is $I_{yy}/I_{xx} \approx 0.05$ and the buckling load is predominantly determined by the fixity conditions about the y axis. As b_f/b_w ratio increases, I_{yy}/I_{xx} ratio increases and the fixity conditions about the x axis gain significance. For a zed section member connected to gusset plates

through the web, it is thus advantageous to maximize the b_f/b_w ratio (while remaining within the classification limits of compactness).

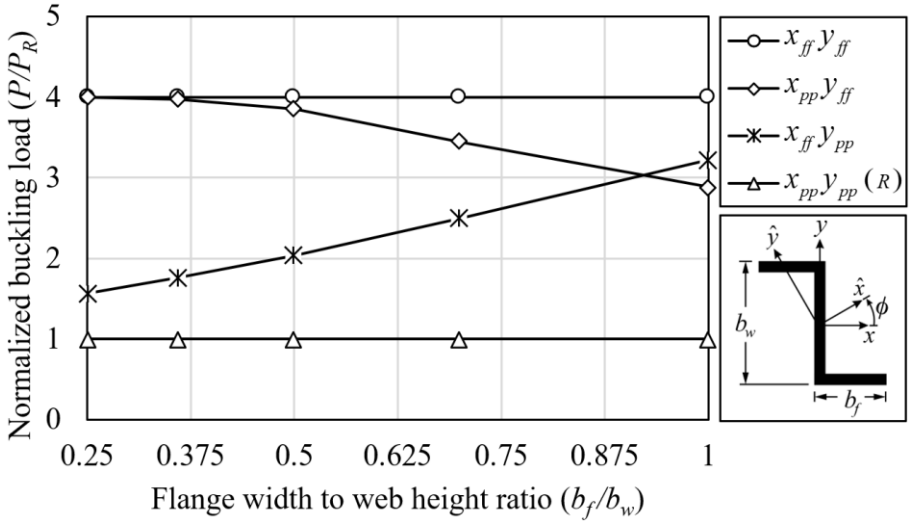

Figure 3.6 Normalized buckling load versus flange width to web height ratio for members with zed cross-sections and 4000 mm spans

3.10. Summary and conclusions

1) The present study developed the variational principle, the governing differential equations and associated boundary conditions for concentrically loaded members with general cross-sections with end restraints defined along non-principal directions.
2) The governing differential equations were analytically solved subject to the boundary conditions to obtain the characteristic equations for several practical design cases.
3) Besides reverting to the classical solution in special cases where the fixity axes coincide with principal directions, the present solution provides insights on the buckling capacity and mode shapes for compression with boundary conditions non-aligned with principal directions.
4) The validity of the solution was verified through comparisons with shell and thin-walled beam finite element buckling models based on Abaqus.
5) As expected, when the boundary conditions of a member at one end were similar along two orthogonal directions (e.g., $x_{pp}y_{pp}z_{pp}$), the buckling loads were found to be independent from the orientation of the axes. Conversely, when the member end restraints about a non-principal

axis differs from that about the orthogonal axis (e.g., $x_{pp}y_{ff}z_{pp}$), the buckling loads is found to largely depend upon the axes' orientation.

6) The normalized buckling load P/P_R for compression angle members connected to end gusset plates (characterized by the boundary condition type $x_{pp}y_{ff}z_{pp}$) was found to highly depend on the leg width ratio b_1/b_2. As the ratio of the outstanding leg to that of the connected leg increases, the buckling load ratio P/P_R was found to increase. In practice, this observation suggests that by connecting unequal leg members to gussets through the shorter leg would result in a higher buckling load resistance. It is recognized here that such a detail would also increase the eccentricity between the centroidal axis of welding (or bolting) and that of the member, inducing higher moments (not accounted for in the present study).
7) For compression member of zed sections connected to end gussets through the web, it was found that the normalized buckling load ratio P/P_R increases as the ratio of flange width to web height b_f/b_w increases. The increase in b_f would need to remain within the compactness of requirements of the cross-section beyond which local buckling (outside the scope of the present study) may govern the design.

Notation

A	Cross-section area;	r_{min}	Minimum radius of gyration;
b_f	Flange height;	$r_{\hat{x}}, r_{\hat{y}}$	Radii of gyration about $\hat{x}, \hat{y}$ axes;
b_w	Web width;	SC	Cross-section shear centre;
b_1, b_2	Legs width;	t	Cross-section thickness;
C	Cross-section centroid;	u	Buckling displacement along x axis;
D_i	Integration constants;	v	Buckling displacement along y axis;
E	Modulus of elasticity;	w_p	Longitudinal pre-buckling displacement;
G	Modulus of rigidity;	x_{SC}, y_{SC}	Shear centre coordinates along x, y axes;
I_{xx}, I_{yy}	Moments of inertia about x, y axes;	$\hat{x}, \hat{y}$	Principal directions;
I_{xy}	Product of inertia about x, y axes;	γ_{sz}	Shear strains;
$I_{\omega\omega}$	Warping constant;	δ	variation of the argument function;
J	Saint-Venant torsional constant;	ε_z	Longitudinal strains;
K_x, K_y, K_z	Effective length factors for buckling about x, y axes and relative to twist;	θ	Angle of twist;
L	Member span;	λ	Multiplier;
m_i	Characteristic equation roots;	Π	Total potential energy;
N_R	Reference load;	σ_z	Longitudinal stresses;
P	Buckling load;	τ_{sz}	Shear stresses;
P_R	Buckling load for a reference case;	ϕ	Angle of inclination;
r_0	Polar radius of gyration;		

References

Ádány, S. and Schafer, B. W. (2006a). "Buckling mode decomposition of single-branched open cross-section members via finite strip method: Derivation." *Thin Wall. Struct*., 44, 563-584.
Ádány, S. and Schafer, B. W. (2006b). "Buckling mode decomposition of single-branched open cross-section members via finite strip method: Application and examples." *Thin Wall. Struct*., 44, 585-600.
Ádány, S. and Schafer, B. W. (2008). "A full modal decomposition of thin-walled, single-branched open cross-section members via the constrained finite strip method." *J. Constr. Steel Res*., 64, 12-29.
AISC (American Institute of Steel Construction). (2016). "Specification for Structural Steel Buildings." *ANSI/AISC 360-16*, Chicago, IL.
Attard, M. M. (1992). "Flexural-torsional buckling of monosymmetric columns." *J. Constr. Steel Res*., 23, 117-126.
Barsoum, R. S. and Gallagher, R. H. (1970). "Finite element analysis of torsional and torsional–flexural stability problems." *Int. J. Numer. Meth. Eng.*, 2(3), 335-352.
Camotim, D., Silvestre, N., Basaglia, C. and Bebiano, R. (2008). "GBT-based buckling analysis of thin-walled members with non-standard support conditions." *Thin Wall. Struct*., 46(7-9), 800-815.
Chan, S. L. and Kitipornchai, S. (1987). "Geometric nonlinear analysis of asymmetric thin-walled beam-columns." *Eng. Struct*., 9(4), 243-254.
CSA (Canadian Standards Association). (2019). "Design of Steel Structures." *CSA S16:19*, Toronto, ON, Canada.
Culver, C. G. (1966). "Exact solution of the biaxial bending equations." *J. Struct. Div.*, 92(2), 63-84.
Davies, J.M., Leach, P. and Heinz, D. (1994). "Second-order generalised beam theory." *J. Constr. Steel Res.*, 31, 221-241.
Dinis, P.B., Camotim, D. and Silvestre, N. (2006). "GBT formulation to analyse the buckling behaviour of thin-walled members with arbitrarily 'branched' open cross-sections." *Thin Wall. Struct*., 44(1), 20-38.
Galambos, T. V. (1968). *Structural Members and Frames*, Prentice-Hall Inc., Englewood Cliffs, NJ.
Gjelsvik, A. (1981). *The theory of thin walled bars*, John Wiley & Sons, New York.
Glauz, R. S. (2017). "Flexural-torsional buckling of general cold-formed steel columns with unequal unbraced lengths." *Thin Wall. Struct*., 119, 946-955.
Goodier, J. N. (1942). "Torsional and flexural buckling of bars of thin-walled open section under compressive and bending loads." *J. Appl. Mech.*, 9(3), 103-107.
He, B., Zhang, Y., Ge, W.Y., An, Y. and Liu, D. (2018). "Buckling analysis of thin-walled members with open-branched cross section via semi-analytical finite strip transfer matrix method." *Thin Wall. Struct*., 124, 20-31.

Hone, C. P. (1967). "Torsional-flexural buckling of axially-loaded, thin-walled, elastic struts of open cross-section." In *Thin Wall. Struct.*, Chatto and Windus, 103–135, London, England.
Kappus, R. (1938). *Twisting Failure of Centrally Loaded Open-Section Columns in The Elastic Range*, National Advisory Committee for Aeronautics. Washington, DC.
Kim, M. Y., Chang, S. P. and Kim, S. B. (1994). "Spatial Stability and Free Vibration of Shear II: Numerical Approach Flexible Thin-Walled Elastic Beams." *Int. J. Numer. Meth. Eng*., 37, 4117-4140.
Kim M. Y., Kim, N. I. and Yun, H. T. (2003). "Exact dynamic and static stiffness matrices of shear deformable thin-walled beam-columns." *J. Sound Vib*., 267, 29-55.
Kim, N. I., Fu, C. C. and Kim M. Y. (2007). "Stiffness matrices for flexural–torsional/lateral buckling and vibration analysis of thin-walled beam." *J. Sound Vib*., 299, 739-756.
Kitipornchai, S. and Chan, S. L. (1987). "Nonlinear finite element analysis of angle and tee beam-columns." *J. Struct. Eng.*, 113(4), 721-739.
Krajcinovic, D. (1969). "A consistent discrete elements technique for thinwalled assemblages." *Int. J. Solids Struct*., 5(7), 639-662.
Lau, S. C. W. and Hancock, G. J. (1986). "Buckling of thin flat-walled structures by a spline finite strip method." *Thin Wall. Struct*., 4(4), 269-294.
Laudiero, F. and Zaccaria, D. (1988). "Finite Element Analysis of Stability of Thin-Walled Beams of Open Section." *Int. J. Mech. Sci.*, 30(8), 543-557.
Li, Z. and Schafer, B.W. (2013). "Constrained finite strip method for thin-walled members with general end boundary conditions." *J. Eng. Mech*., 139(11), 1566-1576.
Liu, S. W., Gao, W. L. and Ziemian, R. D. (2019). "Improved line-element formulations for the stability analysis of arbitrarily-shaped open-section beam-columns." *Thin wall. Struct.,* 144, 106290.
Nickalls, R. W. D. (1993). "A New Approach to Solving the Cubic: Cardan's Solution Revealed." *Math. Gazette*, 77(480), 354-359.
Paavola, J. and Salonen, S. (1992). "Flexural-torsional stability of thin-walled columns." *J. eng. Mech.*, 118(12), 2384-2400.
Papangelis, J. P. and Hancock, G. J. (1995). "Computer analysis of thin-walled structural members*." Comput. Struct*., 56(1), 157-176.
Plank, R. J. and Wittrick, W. H. (1974). "Buckling under combined loading of thin, flat-walled structures by a complex finite strip method." *Int. J. Numer. Meth. Eng.*, 8(2), 323-339.
Rasmussen, K. J. and Trahair, N.S. (2005) "Exact and approximate solutions for the flexural buckling of columns with oblique rotational end restraints." *Thin wall. Struct*., 43(3), 411-426.
Renton, J. D. (1960). "A direct solution of the torsional-flexural buckling of axially loaded thin-walled bars." *Struct. Eng*., 38(9), 273-276.
Sallstrom, J. H. (1996). "Accurate calculation of elastic buckling loads for space frames built up of uniform beams with open thin-walled cross-section." *Int. J. Numer. Meth. Eng*., 38, 2319-2333.

Smith, T. G. and Sridharan, S. (1978). "A finite strip method for the buckling of plate structures under arbitrary loading." *Int. J. Mech. Sci*., 20(10), 685-693.
Timoshenko, S. P. (1945). "Theory of bending, torsion and buckling of thin-walled members of open cross section." *J. Franklin Inst.*, 239(5), 343-361.
Timoshenko, S. P., and Gere, J. M. (1961). *Theory of Elastic Stability*, 2nd Ed., McGraw-Hill, New York, NY.
Trahair, N. S. (1969). "Restrained elastic beam-column." *J. Struct. Div.*, 95(2), 2641-2664.
Trahair, N. S. (1993). *Flexural-Torsional Buckling of Structures*, CRC Press, Boca Raton, FL.
Trahair, N. S., and Rasmussen, K. J. (2005). "Flexural–torsional buckling of columns with oblique eccentric restraints." *J. Struct. Eng.*, 131(11), 1731-1737.
Vlasov V. Z. (1961). *Thin-Walled Elastic Beams*, 2nd Ed., Israel Program for Scientific Translations, Jerusalem.
Wagner, H. (1936). *Torsion and Buckling of Open Sections*, National Advisory Committee for Aeronautics. Washington, DC.
Xiang, Y., Wang, C. M. and Kitipornchai, S. (1992). "Column buckling under general loads with allowances for pre-buckling shortening and shear deformation." *Arch. Appl. Mech*., 62(8), 544-556.

Appendix 3.A. Additional buckling solutions

The solution for the most common case $P < GJ/\left(r_o^2 - x_{SC}^2 - y_{SC}^2\right)$ has been provided in the body of the paper. For completeness, this appendix provides the closed-form solutions for the cases $P > GJ/\left(r_o^2 - x_{SC}^2 - y_{SC}^2\right)$ and $P = GJ/\left(r_o^2 - x_{SC}^2 - y_{SC}^2\right)$

3.A.1 The Case $P > GJ/\left(r_o^2 - x_{SC}^2 - y_{SC}^2\right)$

The roots of the characteristic equation become

$m_{1-6} = 0$, $m_{7,8} = \pm i\tilde{\alpha}$, $m_{9,10} = \pm i\beta$ and $m_{11,12} = \pm i\gamma$, where $\tilde{\alpha} = \sqrt{\frac{b}{3a} - 2\sqrt{\frac{b^2 - 3ac}{9a^2}}\cos(\psi)}$

and the solution takes the form

$$\begin{aligned}\bar{u}(z) = {} & D_1 + D_2 z + D_7\tilde{\xi}_1\cos\tilde{\alpha}z + D_8\tilde{\xi}_1\sin\tilde{\alpha}z + D_9\xi_2\cos\beta z + D_{10}\xi_2\sin\beta z \\ & + D_{11}\xi_3\cos\gamma z + D_{12}\xi_3\sin\gamma z\end{aligned} \tag{3.A.1}$$

$$\bar{v}(z) = D_3 + D_4 z + D_7\cos\tilde{\alpha}z + D_8\sin\tilde{\alpha}z + D_9\cos\beta z + D_{10}\sin\beta z + D_{11}\cos\gamma z + D_{12}\sin\gamma z \tag{3.A.2}$$

$$\begin{aligned}\bar{\theta}(z) = {} & D_5 + D_6 z + D_7\tilde{\eta}_1\cos\tilde{\alpha}z + D_8\tilde{\eta}_1\sin\tilde{\alpha}z + D_9\eta_2\cos\beta z + D_{10}\eta_2\sin\beta z \\ & + D_{11}\eta_3\cos\gamma z + D_{12}\eta_3\sin\gamma z\end{aligned} \tag{3.A.3}$$

in which

$$\tilde{\xi}_1 = \frac{P^2 x_{SC}^2 - \left(EI_{xx}\tilde{\alpha}^2 - P\right)\left(EI_{\omega\omega}\tilde{\alpha}^2 - Pr_o^2 + GJ\right)}{P^2 x_{SC} y_{SC} + EI_{xy}\tilde{\alpha}^2\left(EI_{\omega\omega}\tilde{\alpha}^2 - Pr_o^2 + GJ\right)} \qquad \tilde{\eta}_1 = \frac{-P\left[E\left(I_{xx}y_{SC} + I_{xy}x_{SC}\right)\tilde{\alpha}^2 - Py_{SC}\right]}{P^2 x_{SC} y_{SC} + EI_{xy}\tilde{\alpha}^2\left(EI_{\omega\omega}\tilde{\alpha}^2 - Pr_o^2 + GJ\right)}$$

3.A.2 The Case $P = GJ/\left(r_o^2 - x_{SC}^2 - y_{SC}^2\right)$

The roots of the characteristic equation become

$m_{1-8} = 0$, $m_{9,10} = \pm i\tilde{\beta} = \pm i\sqrt{\frac{b + \sqrt{b^2 - 4ac}}{2a}}$ and $m_{11,12} = \pm i\tilde{\gamma} = \pm i\sqrt{\frac{b - \sqrt{b^2 - 4ac}}{2a}}$

and the solution is expressed as

$$\bar{u}(z) = D_1 + D_2 z - D_7\left(y_{SC}/x_{SC}\right)z^2 - D_8\left(y_{SC}/x_{SC}\right)z^3 + D_9\tilde{\xi}_2\cos\tilde{\beta}z + D_{10}\tilde{\xi}_2\sin\tilde{\beta}z + D_{11}\tilde{\xi}_3\cos\tilde{\gamma}z + D_{12}\tilde{\xi}_3\sin\tilde{\gamma}z \tag{3.A.4}$$

$$\bar{v}(z) = D_3 + D_4 z + D_7 z^2 + D_8 z^3 + D_9\cos\tilde{\beta}z + D_{10}\sin\tilde{\beta}z + D_{11}\cos\tilde{\gamma}z + D_{12}\sin\tilde{\gamma}z \tag{3.A.5}$$

$$\bar{\theta}(z) = D_5 + D_6 z + D_7\left(1/x_{SC}\right)z^2 + D_8\left(1/x_{SC}\right)z^3 + D_9\tilde{\eta}_2\cos\tilde{\beta}z + D_{10}\tilde{\eta}_2\sin\tilde{\beta}z + D_{11}\tilde{\eta}_3\cos\tilde{\gamma}z + D_{12}\tilde{\eta}_3\sin\tilde{\gamma}z \tag{3.A.6}$$

where

$$\tilde{\xi}_2 = \frac{P^2x_{SC}^2 - \left(EI_{xx}\tilde{\beta}^2 - P\right)\left(EI_{\omega\omega}\tilde{\beta}^2 - Pr_o^2 + GJ\right)}{P^2x_{SC}y_{SC} + EI_{xy}\tilde{\beta}^2\left(EI_{\omega\omega}\tilde{\beta}^2 - Pr_o^2 + GJ\right)} \qquad \tilde{\eta}_2 = \frac{-P\left[E\left(I_{xx}y_{SC} + I_{xy}x_{SC}\right)\tilde{\beta}^2 - Py_{SC}\right]}{P^2x_{SC}y_{SC} + EI_{xy}\tilde{\beta}^2\left(EI_{\omega\omega}\tilde{\beta}^2 - Pr_o^2 + GJ\right)}$$

$$\tilde{\xi}_3 = \frac{P^2x_{SC}^2 - \left(EI_{xx}\tilde{\gamma}^2 - P\right)\left(EI_{\omega\omega}\tilde{\gamma}^2 - Pr_o^2 + GJ\right)}{P^2x_{SC}y_{SC} + EI_{xy}\tilde{\gamma}^2\left(EI_{\omega\omega}\tilde{\gamma}^2 - Pr_o^2 + GJ\right)} \qquad \tilde{\eta}_3 = \frac{-P\left[E\left(I_{xx}y_{SC} + I_{xy}x_{SC}\right)\tilde{\gamma}^2 - Py_{SC}\right]}{P^2x_{SC}y_{SC} + EI_{xy}\tilde{\gamma}^2\left(EI_{\omega\omega}\tilde{\gamma}^2 - Pr_o^2 + GJ\right)}$$

Appendix 3.B. Detailed derivation of the buckling solution for asymmetric members when $P < GJ/\left(r_o^2 - x_{SC}^2 - y_{SC}^2\right)$

This appendix provides the steps needed to derive Eqs. (3.26)-(3.28).

When $P < GJ/\left(r_o^2 - x_{SC}^2 - y_{SC}^2\right)$, the constant term in the characteristic equation is negative, i.e.,

$$m_i^6\left[am_i^6 + bm_i^4 + cm_i^2 - d\right] = 0 \tag{3.B.1}$$

and the relevant roots are $m_{1-6} = 0$, $m_{7,8} = \pm\alpha$, $m_{9,10} = \pm i\beta$ and $m_{11,12} = \pm i\gamma$, where

$$\alpha = \sqrt{\frac{-b}{3a} + 2\sqrt{\frac{b^2 - 3ac}{9a^2}}\cos(\psi)} \qquad \beta = \sqrt{\frac{b}{3a} - 2\sqrt{\frac{b^2 - 3ac}{9a^2}}\cos\left(\frac{2\pi}{3} + \psi\right)}$$

$$\gamma = \sqrt{\frac{b}{3a} - 2\sqrt{\frac{b^2 - 3ac}{9a^2}}\cos\left(\frac{4\pi}{3} + \psi\right)}$$

in which,

$$\psi = \frac{1}{3}\cos^{-1}\left[\left(\frac{-27a^2d + 9abc - 2b^3}{54a^3}\right)\left(\frac{b^2 - 3ac}{9a^2}\right)^{-\frac{3}{2}}\right]$$

The corresponding solution takes the form

$$\begin{aligned}\bar{u}(z) = {} & A_1 + A_2 z + A_3 z^2 + A_4 z^3 + A_5 z^4 + A_6 z^5 + A_7\cosh\alpha z + A_8\sinh\alpha z \\ & + A_9\cos\beta z + A_{10}\sin\beta z + A_{11}\cos\gamma z + A_{12}\sin\gamma z\end{aligned} \tag{3.B.2}$$

$$\begin{aligned}\bar{v}(z) = {} & B_1 + B_2 z + B_3 z^2 + B_4 z^3 + B_5 z^4 + B_6 z^5 + B_7\cosh\alpha z + B_8\sinh\alpha z \\ & + B_9\cos\beta z + B_{10}\sin\beta z + B_{11}\cos\gamma z + B_{12}\sin\gamma z\end{aligned} \tag{3.B.3}$$

$$\begin{aligned}\bar{\theta}(z) = {} & C_1 + C_2 z + C_3 z^2 + C_4 z^3 + C_5 z^4 + C_6 z^5 + C_7\cosh\alpha z + C_8\sinh\alpha z \\ & + C_9\cos\beta z + C_{10}\sin\beta z + C_{11}\cos\gamma z + C_{12}\sin\gamma z\end{aligned} \tag{3.B.4}$$

Equations (3.B.2)-(3.B.4) involve 36 constants while the system of equations has only 12 boundary conditions. Therefore, 24 of the 36 constants are redundant and can be related to the other 12

constants. From Eqs. (3.B.2)-(3.B.4), by differentiating and substituting into Eq. (3.15), one obtains

$$\begin{aligned}
&EI_{yy}\bar{u}'''' + EI_{xy}\bar{v}'''' + P\bar{u}'' + Py_{SC}\bar{\theta}'' \\
&\quad = 2\left[12A_5EI_{yy} + 12B_5EI_{xy} + A_3P + C_3Py_{SC}\right] \\
&\quad +6\left[20A_6EI_{yy} + 20B_6EI_{xy} + A_4P + C_4Py_{SC}\right]z \\
&\quad +12\left[A_5P + C_5Py_{SC}\right]z^2 + 20\left[A_6P + C_6Py_{SC}\right]z^3 \\
&\quad +\alpha^2\left[A_7\left(EI_{yy}\alpha^2 + P\right) + B_7EI_{xy}\alpha^2 + C_7Py_{SC}\right]\cosh\alpha z \\
&\quad +\alpha^2\left[A_8\left(EI_{yy}\alpha^2 + P\right) + B_8EI_{xy}\alpha^2 + C_8Py_{SC}\right]\sinh\alpha z \\
&\quad +\beta^2\left[A_9\left(EI_{yy}\beta^2 - P\right) + B_9EI_{xy}\beta^2 - C_9Py_{SC}\right]\cos\beta z \\
&\quad +\beta^2\left[A_{10}\left(EI_{yy}\beta^2 - P\right) + B_{10}EI_{xy}\beta^2 - C_{10}Py_{SC}\right]\sin\beta z \\
&\quad +\gamma^2\left[A_{11}\left(EI_{yy}\gamma^2 - P\right) + B_{11}EI_{xy}\gamma^2 - C_{11}Py_{SC}\right]\cos\gamma z \\
&\quad +\gamma^2\left[A_{12}\left(EI_{yy}\gamma^2 - P\right) + B_{12}EI_{xy}\gamma^2 - C_{12}Py_{SC}\right]\sin\gamma z = 0
\end{aligned} \tag{3.B.5}$$

To satisfy Eq. (3.B.5) for any value of z, the coefficients of $z^0, z, z^2, z^3, z^4, z^5, \cosh\alpha z, \sinh\alpha z, \cos\beta z, \sin\beta z, \cos\gamma z$ and $\sin\gamma z$ must vanish. This leads to

$$A_5P + C_5Py_{SC} = 0 \tag{3.B.6}$$

$$A_6P + C_6Py_{SC} = 0 \tag{3.B.7}$$

$$12A_5EI_{yy} + 12B_5EI_{xy} + A_3P + C_3Py_{SC} = 0 \tag{3.B.8}$$

$$20A_6EI_{yy} + 20B_6EI_{xy} + A_4P + C_4Py_{SC} = 0 \tag{3.B.9}$$

$$A_7\left(EI_{yy}\alpha^2 + P\right) + B_7EI_{xy}\alpha^2 + C_7Py_{SC} = 0 \tag{3.B.10}$$

$$A_8\left(EI_{yy}\alpha^2 + P\right) + B_8EI_{xy}\alpha^2 + C_8Py_{SC} = 0 \tag{3.B.11}$$

$$A_9\left(EI_{yy}\beta^2 - P\right) + B_9EI_{xy}\beta^2 - C_9Py_{SC} = 0 \tag{3.B.12}$$

$$A_{10}\left(EI_{yy}\beta^2 - P\right) + B_{10}EI_{xy}\beta^2 - C_{10}Py_{SC} = 0 \tag{3.B.13}$$

$$A_{11}\left(EI_{yy}\gamma^2 - P\right) + B_{11}EI_{xy}\gamma^2 - C_{11}Py_{SC} = 0 \tag{3.B.14}$$

$$A_{12}\left(EI_{yy}\gamma^2 - P\right) + B_{12}EI_{xy}\gamma^2 - C_{12}Py_{SC} = 0 \tag{3.B.15}$$

In a similar manner, from Eqs. (3.B.2)-(3.B.4) by substituting into Eq. (3.16), one obtains

$$\begin{aligned}
&EI_{xx}\bar{v}'''' + EI_{xy}\bar{u}'''' + P\bar{v}'' - Px_{SC}\bar{\theta}'' \\
&\quad = 2\left[12B_5EI_{xx} + 12A_5EI_{xy} + B_3P - C_3Px_{SC}\right] \\
&\quad +6\left[20B_6EI_{xx} + 20A_6EI_{xy} + B_4P - C_4Px_{SC}\right]z \\
&\quad +12\left[B_5P - C_5Px_{SC}\right]z^2 + 20\left[B_6P - C_6Px_{SC}\right]z^3 \\
&\quad +\alpha^2\left[B_7\left(EI_{xx}\alpha^2 + P\right) + A_7EI_{xy}\alpha^2 - C_7Px_{SC}\right]\cosh\alpha z \\
&\quad +\alpha^2\left[B_8\left(EI_{xx}\alpha^2 + P\right) + A_8EI_{xy}\alpha^2 - C_8Px_{SC}\right]\sinh\alpha z \\
&\quad +\beta^2\left[B_9\left(EI_{xx}\beta^2 - P\right) + A_9EI_{xy}\beta^2 + C_9Px_{SC}\right]\cos\beta z \\
&\quad +\beta^2\left[B_{10}\left(EI_{xx}\beta^2 - P\right) + A_{10}EI_{xy}\beta^2 + C_{10}Px_{SC}\right]\sin\beta z \\
&\quad +\gamma^2\left[B_{11}\left(EI_{xx}\gamma^2 - P\right) + A_{11}EI_{xy}\gamma^2 + C_{11}Px_{SC}\right]\cos\gamma z \\
&\quad +\gamma^2\left[B_{12}\left(EI_{xx}\gamma^2 - P\right) + A_{12}EI_{xy}\gamma^2 + C_{12}Px_{SC}\right]\sin\gamma z = 0
\end{aligned} \tag{3.B.16}$$

Again, the coefficients of z^0, z, z^2, z^3, z^4, z^5, $\cosh\alpha z$, $\sinh\alpha z$, $\cos\beta z$, $\sin\beta z$, $\cos\gamma z$ and $\sin\gamma z$ must vanish, leading to

$$B_5P - C_5Px_{SC} = 0 \tag{3.B.17}$$

$$B_6P - C_6Px_{SC} = 0 \tag{3.B.18}$$

$$12B_5EI_{xx} + 12A_5EI_{xy} + B_3P - C_3Px_{SC} = 0 \tag{3.B.19}$$

$$20B_6EI_{xx} + 20A_6EI_{xy} + B_4P - C_4Px_{SC} = 0 \tag{3.B.20}$$

$$B_7\left(EI_{xx}\alpha^2 + P\right) + A_7EI_{xy}\alpha^2 - C_7Px_{SC} = 0 \tag{3.B.21}$$

$$B_8\left(EI_{xx}\alpha^2 + P\right) + A_8EI_{xy}\alpha^2 - C_8Px_{SC} = 0 \tag{3.B.22}$$

$$B_9\left(EI_{xx}\beta^2 - P\right) + A_9EI_{xy}\beta^2 + C_9Px_{SC} = 0 \tag{3.B.23}$$

$$B_{10}\left(EI_{xx}\beta^2 - P\right) + A_{10}EI_{xy}\beta^2 + C_{10}Px_{SC} = 0 \tag{3.B.24}$$

$$B_{11}\left(EI_{xx}\gamma^2 - P\right) + A_{11}EI_{xy}\gamma^2 + C_{11}Px_{SC} = 0 \tag{3.B.25}$$

$$B_{12}\left(EI_{xx}\gamma^2 - P\right) + A_{12}EI_{xy}\gamma^2 + C_{12}Px_{SC} = 0 \tag{3.B.26}$$

Likewise, from Eqs. (3.B.2)-(3.B.4) by substituting into Eq. (3.17), one obtains

$$\begin{aligned}
&EI_{\omega\omega}\bar{\theta}''' + \left(Pr_0^2 - GJ\right)\bar{\theta}'' + Py_{SC}\bar{u}'' - Px_{SC}\bar{v}'' \\
&\quad = 2\left[12C_5EI_{\omega\omega} + C_3\left(Pr_o^2 - GJ\right) + A_3Py_{SC} - B_3Px_{SC}\right] \\
&\quad +6\left[20C_6EI_{\omega\omega} + C_4\left(Pr_o^2 - GJ\right) + A_4Py_{SC} - B_4Px_{SC}\right]z \\
&\quad +12\left[C_5\left(Pr_o^2 - GJ\right) + A_5Py_{SC} - B_5Px_{SC}\right]z^2 \\
&\quad +20\left[C_6\left(Pr_o^2 - GJ\right) + A_6Py_{SC} - B_6Px_{SC}\right]z^3 \\
&\quad +\alpha^2\left[C_7\left(EI_{\omega\omega}\alpha^2 + Pr_o^2 - GJ\right) + A_7Py_{SC} - B_7Px_{SC}\right]\cosh\alpha z \\
&\quad +\alpha^2\left[C_8\left(EI_{\omega\omega}\alpha^2 + Pr_o^2 - GJ\right) + A_8Py_{SC} - B_8Px_{SC}\right]\sinh\alpha z \\
&\quad +\beta^2\left[C_9\left(EI_{\omega\omega}\beta^2 - Pr_o^2 + GJ\right) - A_9Py_{SC} + B_9Px_{SC}\right]\cos\beta z \\
&\quad +\beta^2\left[C_{10}\left(EI_{\omega\omega}\beta^2 - Pr_o^2 + GJ\right) - A_{10}Py_{SC} + B_{10}Px_{SC}\right]\sin\beta z \\
&\quad +\gamma^2\left[C_{11}\left(EI_{\omega\omega}\gamma^2 - Pr_o^2 + GJ\right) - A_{11}Py_{SC} + B_{11}Px_{SC}\right]\cos\gamma z \\
&\quad +\gamma^2\left[C_{12}\left(EI_{\omega\omega}\gamma^2 - Pr_o^2 + GJ\right) - A_{12}Py_{SC} + B_{12}Px_{SC}\right]\sin\gamma z = 0
\end{aligned} \tag{3.B.27}$$

The coefficients of z^0, z, z^2, z^3, z^4, z^5, $\cosh\alpha z$, $\sinh\alpha z$, $\cos\beta z$, $\sin\beta z$, $\cos\gamma z$ and $\sin\gamma z$ must also vanish, yielding

$$C_5\left(Pr_o^2 - GJ\right) + A_5Py_{SC} - B_5Px_{SC} = 0 \tag{3.B.28}$$

$$C_6\left(Pr_o^2 - GJ\right) + A_6Py_{SC} - B_6Px_{SC} = 0 \tag{3.B.29}$$

$$12C_5EI_{\omega\omega} + C_3\left(Pr_o^2 - GJ\right) + A_3Py_{SC} - B_3Px_{SC} = 0 \tag{3.B.30}$$

$$20C_6EI_{\omega\omega} + C_4\left(Pr_o^2 - GJ\right) + A_4Py_{SC} - B_4Px_{SC} = 0 \tag{3.B.31}$$

$$C_7\left(EI_{\omega\omega}\alpha^2 + Pr_o^2 - GJ\right) + A_7Py_{SC} - B_7Px_{SC} = 0 \tag{3.B.32}$$

$$C_8\left(EI_{\omega\omega}\alpha^2 + Pr_o^2 - GJ\right) + A_8 Py_{SC} - B_8 Px_{SC} = 0 \tag{3.B.33}$$

$$C_9\left(EI_{\omega\omega}\beta^2 - Pr_o^2 + GJ\right) - A_9 Py_{SC} + B_9 Px_{SC} = 0 \tag{3.B.34}$$

$$C_{10}\left(EI_{\omega\omega}\beta^2 - Pr_o^2 + GJ\right) - A_{10} Py_{SC} + B_{10} Px_{SC} = 0 \tag{3.B.35}$$

$$C_{11}\left(EI_{\omega\omega}\gamma^2 - Pr_o^2 + GJ\right) - A_{11} Py_{SC} + B_{11} Px_{SC} = 0 \tag{3.B.36}$$

$$C_{12}\left(EI_{\omega\omega}\gamma^2 - Pr_o^2 + GJ\right) - A_{12} Py_{SC} + B_{12} Px_{SC} = 0 \tag{3.B.37}$$

By placing Eqs. (3.B.6), (3.B.17) and (3.B.28) as well as Eqs. (3.B.7), (3.B.18) and (3.B.29) in a matrix form, one obtains

$$\begin{bmatrix} P & 0 & Py_{SC} \\ 0 & P & -Px_{SC} \\ Py_{SC} & -Px_{SC} & Pr_o^2 - GJ \end{bmatrix} \begin{Bmatrix} A_5 \\ B_5 \\ C_5 \end{Bmatrix} = \begin{Bmatrix} 0 \\ 0 \\ 0 \end{Bmatrix} \qquad \begin{bmatrix} P & 0 & Py_{SC} \\ 0 & P & -Px_{SC} \\ Py_{SC} & -Px_{SC} & Pr_o^2 - GJ \end{bmatrix} \begin{Bmatrix} A_6 \\ B_6 \\ C_6 \end{Bmatrix} = \begin{Bmatrix} 0 \\ 0 \\ 0 \end{Bmatrix} \tag{3.B.38)a,b}$$

The above system leads to one of two possible solutions: Either (1) the determinant of the matrix of coefficients is non-zero leading to the conditions

$$A_5 = B_5 = C_5 = A_6 = B_6 = C_6 = 0 \tag{3.B.39}$$

or (2) the determinant vanishes, i.e.,

$$P = \frac{GJ}{r_0^2 - x_{SC}^2 - y_{SC}^2} \tag{3.B.40}$$

which leads to $A_5 \neq B_5 \neq C_5 \neq A_6 \neq B_6 \neq C_6 \neq 0$. This case is treated separately under Appendix 3.D.

Given the vanishing constant values in Eq. (3.B.39), by substituting into Eqs. (3.B.8), (3.B.19) and (3.B.30), and Eqs. (3.B.9), (3.B.20) and (3.B.31), and putting them in matrix form, one obtains

$$\begin{bmatrix} P & 0 & Py_{SC} \\ 0 & P & -Px_{SC} \\ Py_{SC} & -Px_{SC} & Pr_o^2 - GJ \end{bmatrix} \begin{Bmatrix} A_3 \\ B_3 \\ C_3 \end{Bmatrix} = \begin{Bmatrix} 0 \\ 0 \\ 0 \end{Bmatrix} \qquad \begin{bmatrix} P & 0 & Py_{SC} \\ 0 & P & -Px_{SC} \\ Py_{SC} & -Px_{SC} & Pr_o^2 - GJ \end{bmatrix} \begin{Bmatrix} A_4 \\ B_4 \\ C_4 \end{Bmatrix} = \begin{Bmatrix} 0 \\ 0 \\ 0 \end{Bmatrix} \tag{3.B.41)a,b}$$

Recalling that the condition $A_5 = B_5 = C_5 = A_6 = B_6 = C_6 = 0$ is only valid when $P \neq GJ/\left(r_o^2 - x_{SC}^2 - y_{SC}^2\right)$, the determinant of the matrices of coefficients is non-zero, leading to

$$A_3 = B_3 = C_3 = A_4 = B_4 = C_4 = 0 \tag{3.B.42}$$

Also, by placing Eqs. (3.B.10),(3.B.21) and (3.B.32), and Eqs. (3.B.11), (3.B.22) and (3.B.33) in a matrix form, one obtains

$$\begin{bmatrix} EI_{yy}\alpha^2 + P & EI_{xy}\alpha^2 & Py_{SC} \\ EI_{xy}\alpha^2 & EI_{xx}\alpha^2 + P & -Px_{SC} \\ Py_{SC} & -Px_{SC} & EI_{\omega\omega}\alpha^2 + Pr_o^2 - GJ \end{bmatrix} \begin{Bmatrix} A_7 \\ B_7 \\ C_7 \end{Bmatrix} = \begin{Bmatrix} 0 \\ 0 \\ 0 \end{Bmatrix} \tag{3.B.43}$$

$$\begin{bmatrix} EI_{yy}\alpha^2 + P & EI_{xy}\alpha^2 & Py_{SC} \\ EI_{xy}\alpha^2 & EI_{xx}\alpha^2 + P & -Px_{SC} \\ Py_{SC} & -Px_{SC} & EI_{\omega\omega}\alpha^2 + Pr_o^2 - GJ \end{bmatrix} \begin{Bmatrix} A_8 \\ B_8 \\ C_8 \end{Bmatrix} = \begin{Bmatrix} 0 \\ 0 \\ 0 \end{Bmatrix} \tag{3.B.44}$$

The determinant of the matrices of coefficients in Eqs. (3.B.43) and (3.B.44) can be shown to vanish irrespective of the value of P. This is because the determinant of the matrices of coefficients coincides with the characteristic equation, Eq. (3.22). Hence, one has

$$\begin{aligned} \xi_1 = \frac{A_7}{B_7} = \frac{A_8}{B_8} &= \frac{-Py_{SC} - E\left(I_{xx}y_{SC} + I_{xy}x_{SC}\right)\alpha^2}{Px_{SC} + E\left(I_{yy}x_{SC} + I_{xy}y_{SC}\right)\alpha^2} \\ &= \frac{P^2x_{SC}^2 - \left(EI_{xx}\alpha^2 + P\right)\left(EI_{\omega\omega}\alpha^2 + Pr_o^2 - GJ\right)}{P^2x_{SC}y_{SC} + EI_{xy}\alpha^2\left(EI_{\omega\omega}\alpha^2 + Pr_o^2 - GJ\right)} \\ &= \frac{P^2x_{SC}y_{SC} + EI_{xy}\alpha^2\left(EI_{\omega\omega}\alpha^2 + Pr_o^2 - GJ\right)}{P^2y_{SC}^2 - \left(EI_{yy}\alpha^2 + P\right)\left(EI_{\omega\omega}\alpha^2 + Pr_o^2 - GJ\right)} \end{aligned} \tag{3.B.45}$$

$$\eta_1 = \frac{C_7}{B_7} = \frac{C_8}{B_8} = \frac{P\left[E\left(I_{xx}+I_{yy}\right)\alpha^2+P\right]+E^2\left(I_{yy}I_{xx}-I_{xy}^2\right)\alpha^4}{P\left[E\left(I_{yy}x_{SC}+I_{xy}y_{SC}\right)\alpha^2+Px_{SC}\right]}$$
$$= \frac{P\left[E\left(I_{xy}x_{SC}+I_{xx}y_{SC}\right)\alpha^2+Py_{SC}\right]}{P^2x_{SC}y_{SC}+EI_{xy}\alpha^2\left(EI_{\omega\omega}\alpha^2+Pr_o^2-GJ\right)} \tag{3.B.46}$$
$$= \frac{-P\left[E\left(I_{yy}x_{SC}+I_{xy}y_{SC}\right)\alpha^2+Px_{SC}\right]}{P^2y_{SC}^2-\left(EI_{yy}\alpha^2+P\right)\left(EI_{\omega\omega}\alpha^2+Pr_o^2-GJ\right)}$$

In a similar manner, Eqs. (3.B.12), (3.B.23), (3.B.34), (3.B.13), (3.B.24) and (3.B.35) are placed in the following matrices

$$\begin{bmatrix} EI_{yy}\beta^2-P & EI_{xy}\beta^2 & -Py_{SC} \\ EI_{xy}\beta^2 & EI_{xx}\beta^2-P & Px_{SC} \\ -Py_{SC} & Px_{SC} & EI_{\omega\omega}\beta^2-Pr_o^2+GJ \end{bmatrix}\begin{Bmatrix} A_9 \\ B_9 \\ C_9 \end{Bmatrix} = \begin{Bmatrix} 0 \\ 0 \\ 0 \end{Bmatrix} \tag{3.B.47}$$

$$\begin{bmatrix} EI_{yy}\beta^2-P & EI_{xy}\beta^2 & -Py_{SC} \\ EI_{xy}\beta^2 & EI_{xx}\beta^2-P & Px_{SC} \\ -Py_{SC} & Px_{SC} & EI_{\omega\omega}\beta^2-Pr_o^2+GJ \end{bmatrix}\begin{Bmatrix} A_{10} \\ B_{10} \\ C_{10} \end{Bmatrix} = \begin{Bmatrix} 0 \\ 0 \\ 0 \end{Bmatrix} \tag{3.B.48}$$

Here also, the determinant of the matrices of coefficients in Eqs. (3.B.47) and (3.B.48) vanishes regardless of the value of P, leading to

$$\xi_2 = \frac{A_9}{B_9} = \frac{A_{10}}{B_{10}} = \frac{Py_{SC}-E\left(I_{xx}y_{SC}+I_{xy}x_{SC}\right)\beta^2}{-Px_{SC}+E\left(I_{yy}x_{SC}+I_{xy}y_{SC}\right)\beta^2}$$
$$= \frac{P^2x_{SC}^2-\left(EI_{xx}\beta^2-P\right)\left(EI_{\omega\omega}\beta^2-Pr_o^2+GJ\right)}{P^2x_{SC}y_{SC}+EI_{xy}\beta^2\left(EI_{\omega\omega}\beta^2-Pr_o^2+GJ\right)} \tag{3.B.49}$$
$$= \frac{P^2x_{SC}y_{SC}+EI_{xy}\beta^2\left(EI_{\omega\omega}\beta^2-Pr_o^2+GJ\right)}{P^2y_{SC}^2-\left(EI_{yy}\beta^2-P\right)\left(EI_{\omega\omega}\beta^2-Pr_o^2+GJ\right)}$$

$$\eta_2 = \frac{C_9}{B_9} = \frac{C_{10}}{B_{10}} = \frac{P\left[E\left(I_{xx}+I_{yy}\right)\beta^2 - P\right] - E^2\left(I_{xx}I_{yy} - I_{xy}^2\right)\beta^4}{P\left[E\left(I_{yy}x_{SC} + I_{xy}y_{SC}\right)\beta^2 - Px_{SC}\right]}$$
$$= \frac{-P\left[E\left(I_{xx}y_{SC} + I_{xy}x_{SC}\right)\beta^2 - Py_{SC}\right]}{P^2 x_{SC}y_{SC} + EI_{xy}\beta^2\left(EI_{\omega\omega}\beta^2 - Pr_o^2 + GJ\right)} \tag{3.B.50}$$
$$= \frac{P\left[E\left(I_{yy}x_{SC} + I_{xy}y_{SC}\right)\beta^2 - Px_{SC}\right]}{P^2 y_{SC}^2 - \left(EI_{yy}\beta^2 - P\right)\left(EI_{\omega\omega}\beta^2 - Pr_o^2 + GJ\right)}$$

The last sets of equations, Eqs. (3.B.14), (3.B.25), (3.B.36), (3.B.15), (3.B.26) and (3.B.37), are also grouped in a pair of matrices,

$$\begin{bmatrix} EI_{yy}\gamma^2 - P & EI_{xy}\gamma^2 & -Py_{SC} \\ EI_{xy}\gamma^2 & EI_{xx}\gamma^2 - P & Px_{SC} \\ -Py_{SC} & Px_{SC} & EI_{\omega\omega}\gamma^2 - Pr_o^2 + GJ \end{bmatrix} \begin{Bmatrix} A_{11} \\ B_{11} \\ C_{11} \end{Bmatrix} = \begin{Bmatrix} 0 \\ 0 \\ 0 \end{Bmatrix} \tag{3.B.51}$$

$$\begin{bmatrix} EI_{yy}\gamma^2 - P & EI_{xy}\gamma^2 & -Py_{SC} \\ EI_{xy}\gamma^2 & EI_{xx}\gamma^2 - P & Px_{SC} \\ -Py_{SC} & Px_{SC} & EI_{\omega\omega}\gamma^2 - Pr_o^2 + GJ \end{bmatrix} \begin{Bmatrix} A_{12} \\ B_{12} \\ C_{12} \end{Bmatrix} = \begin{Bmatrix} 0 \\ 0 \\ 0 \end{Bmatrix} \tag{3.B.52}$$

The determinant of the matrices of coefficients in Eqs. (3.B.51) and (3.B.52) is always zero irrespective of the value of P, yielding

$$\xi_3 = \frac{A_{11}}{B_{11}} = \frac{A_{12}}{B_{12}} = \frac{Py_{SC} - E\left(I_{xx}y_{SC} + I_{xy}x_{SC}\right)\gamma^2}{-Px_{SC} + E\left(I_{yy}x_{SC} + I_{xy}y_{SC}\right)\gamma^2}$$
$$= \frac{P^2 x_{SC}^2 - \left(EI_{xx}\gamma^2 - P\right)\left(EI_{\omega\omega}\gamma^2 - Pr_o^2 + GJ\right)}{P^2 x_{SC}y_{SC} + EI_{xy}\gamma^2\left(EI_{\omega\omega}\gamma^2 - Pr_o^2 + GJ\right)} \tag{3.B.53}$$
$$= \frac{P^2 x_{SC}y_{SC} + EI_{xy}\gamma^2\left(EI_{\omega\omega}\gamma^2 - Pr_o^2 + GJ\right)}{P^2 y_{SC}^2 - \left(EI_{yy}\gamma^2 - P\right)\left(EI_{\omega\omega}\gamma^2 - Pr_o^2 + GJ\right)}$$

$$\eta_3 = \frac{C_{11}}{B_{11}} = \frac{C_{12}}{B_{12}} = \frac{P\left[E\left(I_{xx}+I_{yy}\right)\gamma^2 - P\right] - E^2\left(I_{xx}I_{yy} - I_{xy}^2\right)\gamma^4}{P\left[E\left(I_{yy}x_{SC} + I_{xy}y_{SC}\right)\gamma^2 - Px_{SC}\right]}$$
$$= \frac{-P\left[E\left(I_{xx}y_{SC} + I_{xy}x_{SC}\right)\gamma^2 - Py_{SC}\right]}{P^2 x_{SC}y_{SC} + EI_{xy}\gamma^2\left(EI_{\omega\omega}\gamma^2 - Pr_o^2 + GJ\right)} \tag{3.B.54}$$
$$= \frac{P\left[E\left(I_{yy}x_{SC} + I_{xy}y_{SC}\right)\gamma^2 - Px_{SC}\right]}{P^2 y_{SC}^2 - \left(EI_{yy}\gamma^2 - P\right)\left(EI_{\omega\omega}\gamma^2 - Pr_o^2 + GJ\right)}$$

From Eqs. (3.B.39), (3.B.42), (3.B.45), (3.B.46), (3.B.49), (3.B.50), (3.B.53) and (3.B.54), by substituting into Eqs. (3.B.2), (3.B.3) and (3.B.4) yields the solution in terms of twelve independent constants,

$$\bar{u}(z) = A_1 + A_2 z + B_7\xi_1\cosh\alpha z + B_8\xi_1\sinh\alpha z + B_9\xi_2\cos\beta z + B_{10}\xi_2\sin\beta z + B_{11}\xi_3\cos\gamma z + B_{12}\xi_3\sin\gamma z \tag{3.B.55}$$

$$\bar{v}(z) = B_1 + B_2 z + B_7\cosh\alpha z + B_8\sinh\alpha z + B_9\cos\beta z + B_{10}\sin\beta z + B_{11}\cos\gamma z + B_{12}\sin\gamma z \tag{3.B.56}$$

$$\bar{\theta}(z) = C_1 + C_2 z + B_7\eta_1\cosh\alpha z + B_8\eta_1\sinh\alpha z + B_9\eta_2\cos\beta z + B_{10}\eta_2\sin\beta z + B_{11}\eta_3\cos\gamma z + B_{12}\eta_3\sin\gamma z \tag{3.B.57}$$

Appendix 3.C. Detailed derivation of the buckling solution for asymmetric members when $P > GJ/\left(r_o^2 - x_{SC}^2 - y_{SC}^2\right)$

This appendix presents how equations (3.A.1)-(3.A.3) have been developed.

When $P > GJ/\left(r_0^2 - x_{SC}^2 - y_{SC}^2\right)$, the constant term in the characteristic equation is positive, i.e.,

$$m_i^6\left[am_i^6 + bm_i^4 + cm_i^2 + d\right] = 0 \tag{3.C.1}$$

and the relevant roots are

$m_{1-6} = 0$, $m_{7,8} = \pm i\tilde{\alpha}$, $m_{9,10} = \pm i\beta$ and $m_{11,12} = \pm i\gamma$, where $\tilde{\alpha} = \sqrt{\frac{b}{3a} - 2\sqrt{\frac{b^2 - 3ac}{9a^2}}\cos(\psi)}$

As can be noticed, roots $m_{7,8}$ become imaginary while the rest of the roots are identical to those presented in Appendix 3.B. This leads to

$$\begin{aligned} u(z) = {} & A_1 + A_2 z + A_3 z^2 + A_4 z^3 + A_5 z^4 + A_6 z^5 + A_7 \cos\tilde{\alpha}z + A_8 \sin\tilde{\alpha}z \\ & + A_9 \cos\beta z + A_{10} \sin\beta z + A_{11} \cos\gamma z + A_{12} \sin\gamma z \end{aligned} \tag{3.C.2}$$

$$\begin{aligned} v(z) = {} & B_1 + B_2 z + B_3 z^2 + B_4 z^3 + B_5 z^4 + B_6 z^5 + B_7 \cos\tilde{\alpha}z + B_8 \sin\tilde{\alpha}z \\ & + B_9 \cos\beta z + B_{10} \sin\beta z + B_{11} \cos\gamma z + B_{12} \sin\gamma z \end{aligned} \tag{3.C.3}$$

$$\begin{aligned} \theta(z) = {} & C_1 + C_2 z + C_3 z^2 + C_4 z^3 + C_5 z^4 + C_6 z^5 + C_7 \cos\tilde{\alpha}z + C_8 \sin\tilde{\alpha}z \\ & + C_9 \cos\beta z + C_{10} \sin\beta z + C_{11} \cos\gamma z + C_{12} \sin\gamma z \end{aligned} \tag{3.C.4}$$

Only the relations between the coefficients of $\cos\tilde{\alpha}z$ and $\sin\tilde{\alpha}z$ need to be defined as the relations between the other coefficients are previously obtained in Appendix 3.B. Starting from Eqs. (3.C.2) -(3.C.4), by substituting into Eqs. (3.15)-(3.17),

$$
\begin{aligned}
&EI_{yy}\bar{u}'''' + EI_{xy}\bar{v}'''' + P\bar{u}'' + Py_{SC}\bar{\theta}'' \\
&\quad = 2\left[12A_5EI_{yy} + 12B_5EI_{xy} + A_3P + C_3Py_{SCs}\right] \\
&\quad +6\left[20A_6EI_{yy} + 20B_6EI_{xy} + A_4P + C_4Py_{SC}\right]z \\
&\quad +12\left[A_5P + C_5Py_{SC}\right]z^2 + 20\left[A_6P + C_6Py_{SC}\right]z^3 \\
&\quad +\tilde{\alpha}^2\left[A_7\left(EI_{yy}\tilde{\alpha}^2 - P\right) + B_7EI_{xy}\tilde{\alpha}^2 - C_7Py_{SC}\right]\cos\tilde{\alpha}z \\
&\quad +\tilde{\alpha}^2\left[A_8\left(EI_{yy}\tilde{\alpha}^2 - P\right) + B_8EI_{xy}\tilde{\alpha}^2 - C_8Py_{SC}\right]\sin\tilde{\alpha}z \\
&\quad +\beta^2\left[A_9\left(EI_{yy}\beta^2 - P\right) + B_9EI_{xy}\beta^2 - C_9Py_{SC}\right]\cos\beta z \\
&\quad +\beta^2\left[A_{10}\left(EI_{yy}\beta^2 - P\right) + B_{10}EI_{xy}\beta^2 - C_{10}Py_{SC}\right]\sin\beta z \\
&\quad +\gamma^2\left[A_{11}\left(EI_{yy}\gamma^2 - P\right) + B_{11}EI_{xy}\gamma^2 - C_{11}Py_{SC}\right]\cos\gamma z \\
&\quad +\gamma^2\left[A_{12}\left(EI_{yy}\gamma^2 - P\right) + B_{12}EI_{xy}\gamma^2 - C_{12}Py_{SC}\right]\sin\gamma z = 0
\end{aligned}
\tag{3.C.5}
$$

$$
\begin{aligned}
&EI_{xx}\bar{v}'''' + EI_{xy}\bar{u}'''' + P\bar{v}'' - Px_{SC}\bar{\theta}'' \\
&\quad = 2\left[12B_5EI_{xx} + 12A_5EI_{xy} + B_3P - C_3Px_{SC}\right] \\
&\quad +6\left[20B_6EI_{xx} + 20A_6EI_{xy} + B_4P - C_4Px_{SC}\right]z \\
&\quad +12\left[B_5P - C_5Px_{SC}\right]z^2 + 20\left[B_6P - C_6Px_{SC}\right]z^3 \\
&\quad +\tilde{\alpha}^2\left[B_7\left(EI_{xx}\tilde{\alpha}^2 - P\right) + A_7EI_{xy}\tilde{\alpha}^2 + C_7Px_{SC}\right]\cos\tilde{\alpha}z \\
&\quad +\tilde{\alpha}^2\left[B_8\left(EI_{xx}\tilde{\alpha}^2 - P\right) + A_8EI_{xy}\tilde{\alpha}^2 + C_8Px_{SC}\right]\sin\tilde{\alpha}z \\
&\quad +\beta^2\left[B_9\left(EI_{xx}\beta^2 - P\right) + A_9EI_{xy}\beta^2 + C_9Px_{SC}\right]\cos\beta z \\
&\quad +\beta^2\left[B_{10}\left(EI_{xx}\beta^2 - P\right) + A_{10}EI_{xy}\beta^2 + C_{10}Px_{SC}\right]\sin\beta z \\
&\quad +\gamma^2\left[B_{11}\left(EI_{xx}\gamma^2 - P\right) + A_{11}EI_{xy}\gamma^2 + C_{11}Px_{SC}\right]\cos\gamma z \\
&\quad +\gamma^2\left[B_{12}\left(EI_{xx}\gamma^2 - P\right) + A_{12}EI_{xy}\gamma^2 + C_{12}Px_{SC}\right]\sin\gamma z = 0
\end{aligned}
\tag{3.C.6}
$$

and

$$
\begin{aligned}
&EI_{\omega\omega}\bar{\theta}''' + \left(Pr_0^2 - GJ\right)\bar{\theta}'' + Py_{SC}\bar{u}'' - Px_{SC}\bar{v}'' \\
&\quad = 2\left[12C_5EI_{\omega\omega} + C_3\left(Pr_o^2 - GJ\right) + A_3Py_{SC} - B_3Px_{SC}\right] \\
&\quad +6\left[20C_6EI_{\omega\omega} + C_4\left(Pr_o^2 - GJ\right) + A_4Py_{SC} - B_4Px_{SC}\right]z \\
&\quad +12\left[C_5\left(Pr_o^2 - GJ\right) + A_5Py_{SC} - B_5Px_{SC}\right]z^2 \\
&\quad +20\left[C_6\left(Pr_o^2 - GJ\right) + A_6Py_{SC} - B_6Px_{SC}\right]z^3 \\
&\quad +\tilde{\alpha}^2\left[C_7\left(EI_{\omega\omega}\tilde{\alpha}^2 - Pr_o^2 + GJ\right) - A_7Py_{SC} + B_7Px_{SC}\right]\cos\tilde{\alpha}z \\
&\quad +\tilde{\alpha}^2\left[C_8\left(EI_{\omega\omega}\tilde{\alpha}^2 - Pr_o^2 + GJ\right) - A_8Py_{SC} + B_8Px_{SC}\right]\sin\tilde{\alpha}z \\
&\quad +\beta^2\left[C_9\left(EI_{\omega\omega}\beta^2 - Pr_o^2 + GJ\right) - A_9Py_{SC} + B_9Px_{SC}\right]\cos\beta z \\
&\quad +\beta^2\left[C_{10}\left(EI_{\omega\omega}\beta^2 - Pr_o^2 + GJ\right) - A_{10}Py_{SC} + B_{10}Px_{SC}\right]\sin\beta z \\
&\quad +\gamma^2\left[C_{11}\left(EI_{\omega\omega}\gamma^2 - Pr_o^2 + GJ\right) - A_{11}Py_{SC} + B_{11}Px_{SC}\right]\cos\gamma z \\
&\quad +\gamma^2\left[C_{12}\left(EI_{\omega\omega}\gamma^2 - Pr_o^2 + GJ\right) - A_{12}Py_{SC} + B_{12}Px_{SC}\right]\sin\gamma z = 0,
\end{aligned}
\tag{3.C.7}
$$

extracting the coefficients of $\cos\tilde{\alpha}x$ and $\sin\tilde{\alpha}x$ from the three equations,

$$A_7\left(EI_{yy}\tilde{\alpha}^2 - P\right) + B_7EI_{xy}\tilde{\alpha}^2 - C_7Py_{SC} = 0 \tag{3.C.8}$$

$$B_7\left(EI_{xx}\tilde{\alpha}^2 - P\right) + A_7EI_{xy}\tilde{\alpha}^2 + C_7Px_{SC} = 0 \tag{3.C.9}$$

$$C_7\left(EI_{\omega\omega}\tilde{\alpha}^2 - Pr_o^2 + GJ\right) - A_7Py_{SC} + B_7Px_{SC} = 0 \tag{3.C.10}$$

$$A_8\left(EI_{yy}\tilde{\alpha}^2 - P\right) + B_8EI_{xy}\tilde{\alpha}^2 - C_8Py_{SC} = 0 \tag{3.C.11}$$

$$B_8\left(EI_{xx}\tilde{\alpha}^2 - P\right) + A_8EI_{xy}\tilde{\alpha}^2 + C_8Px_{SC} = 0 \tag{3.C.12}$$

$$C_8\left(EI_{\omega\omega}\tilde{\alpha}^2 - Pr_o^2 + GJ\right) - A_8Py_{SC} + B_8Px_{SC} \tag{3.C.13}$$

and then placing Eqs. (3.C.8)-(3.C.13) in a matrix form, one obtains

$$
\begin{bmatrix}
EI_{yy}\tilde{\alpha}^2 - P & EI_{xy}\tilde{\alpha}^2 & -Py_{SC} \\
EI_{xy}\tilde{\alpha}^2 & EI_{xx}\tilde{\alpha}^2 - P & Px_{SC} \\
-Py_{SC} & Px_{SC} & EI_{\omega\omega}\tilde{\alpha}^2 - Pr_o^2 + GJ
\end{bmatrix}
\begin{Bmatrix} A_7 \\ B_7 \\ C_7 \end{Bmatrix} = \begin{Bmatrix} 0 \\ 0 \\ 0 \end{Bmatrix}
\tag{3.C.14}
$$

$$\begin{bmatrix} EI_{yy}\tilde{\alpha}^2 - P & EI_{xy}\tilde{\alpha}^2 & -Py_{SC} \\ EI_{xy}\tilde{\alpha}^2 & EI_{xx}\tilde{\alpha}^2 - P & Px_{SC} \\ -Py_{SC} & Px_{SC} & EI_{\omega\omega}\tilde{\alpha}^2 - Pr_o^2 + GJ \end{bmatrix} \begin{Bmatrix} A_8 \\ B_8 \\ C_8 \end{Bmatrix} = \begin{Bmatrix} 0 \\ 0 \\ 0 \end{Bmatrix} \tag{3.C.15}$$

the determinant of matrices of coefficients in Eqs. (3.C.14) and (3.C.15) is zero irrespective of the value of P yielding

$$\begin{aligned} \tilde{\xi}_1 = \frac{A_7}{B_7} = \frac{A_8}{B_8} &= \frac{Py_{SC} - E\left(I_{xx}y_{SC} + I_{xy}x_{SC}\right)\tilde{\alpha}^2}{-Px_{SC} + E\left(I_{yy}x_{SC} + I_{xy}y_{SC}\right)\tilde{\alpha}^2} \\ &= \frac{P^2x_{SC}^2 - \left(EI_{xx}\tilde{\alpha}^2 - P\right)\left(EI_{\omega\omega}\tilde{\alpha}^2 - Pr_o^2 + GJ\right)}{P^2x_{SC}y_{SC} + EI_{xy}\tilde{\alpha}^2\left(EI_{\omega\omega}\tilde{\alpha}^2 - Pr_o^2 + GJ\right)} \\ &= \frac{P^2x_{SC}y_{SC} + EI_{xy}\tilde{\alpha}^2\left(EI_{\omega\omega}\tilde{\alpha}^2 - Pr_o^2 + GJ\right)}{P^2y_{SC}^2 - \left(EI_{yy}\tilde{\alpha}^2 - P\right)\left(EI_{\omega\omega}\tilde{\alpha}^2 - Pr_o^2 + GJ\right)} \end{aligned} \tag{3.C.16}$$

$$\begin{aligned} \tilde{\eta}_1 = \frac{C_7}{B_7} = \frac{C_8}{B_8} &= \frac{P\left[E\left(I_{xx} + I_{yy}\right)\tilde{\alpha}^2 - P\right] - E^2\left(I_{xx}I_{yy} - I_{xy}^2\right)\tilde{\alpha}^4}{P\left[E\left(I_{yy}x_{SC} + I_{xy}y_{SC}\right)\tilde{\alpha}^2 - Px_{SC}\right]} \\ &= \frac{-P\left[E\left(I_{xx}y_{SC} + I_{xy}x_{SC}\right)\tilde{\alpha}^2 - Py_{SC}\right]}{P^2x_{SC}y_{SC} + EI_{xy}\tilde{\alpha}^2\left(EI_{\omega\omega}\tilde{\alpha}^2 - Pr_o^2 + GJ\right)} \\ &= \frac{P\left[E\left(I_{yy}x_{SC} + I_{xy}y_{SC}\right)\tilde{\alpha}^2 - Px_{SC}\right]}{P^2y_{SC}^2 - \left(EI_{yy}\tilde{\alpha}^2 - P\right)\left(EI_{\omega\omega}\tilde{\alpha}^2 - Pr_o^2 + GJ\right)} \end{aligned} \tag{3.C.17}$$

The solution in terms of twelve independent constants is obtained from Eqs. (3.B.39), (3.B.42), (3.B.49), (3.B.50), (3.B.53), (3.B.54), (3.C.16) and (3.C.17) by substituting into Eqs. (3.C.2), (3.C.3) and (3.C.4) as

$$\begin{aligned} \bar{u}(z) = A_1 + A_2z + B_7\tilde{\xi}_1\cos\tilde{\alpha}z + B_8\tilde{\xi}_1\sin\tilde{\alpha}z + B_9\xi_2\cos\beta z + B_{10}\xi_2\sin\beta z \\ + B_{11}\xi_3\cos\gamma z + B_{12}\xi_3\sin\gamma z \end{aligned} \tag{3.C.18}$$

$$\bar{v}(z) = B_3 + B_4z + B_7\cos\tilde{\alpha}z + B_8\sin\tilde{\alpha}z + B_9\cos\beta z + B_{10}\sin\beta z + B_{11}\cos\gamma z + B_{12}\sin\gamma z \tag{3.C.19}$$

$$\begin{aligned} \bar{\theta}(z) = C_5 + C_6z + B_7\tilde{\eta}_1\cos\tilde{\alpha}z + B_8\eta_4\sin\tilde{\alpha}z + B_9\eta_2\cos\beta z + B_{10}\eta_2\sin\beta z \\ + B_{11}\eta_3\cos\gamma z + B_{12}\eta_3\sin\gamma z \end{aligned} \tag{3.C.20}$$

Appendix 3.D. Detailed derivation of the buckling solution for asymmetric members when $P = GJ/\left(r_o^2 - x_{SC}^2 - y_{SC}^2\right)$

This appendix shows how equations (3.A.4)-(3.A.6) have been derived.

When $P = GJ/\left(r_0^2 - x_{SC}^2 - y_{SC}^2\right)$, the constant term in the characteristic equation vanishes and the equation takes the form

$$m_i^8\left[am_i^4 + bm_i^2 + cm_i\right] = 0 \tag{3.D.1}$$

In which, the roots of the characteristic equation are

$$m_{1-8} = 0,\ m_{9,10} = \pm i\tilde{\beta} = \pm i\sqrt{\frac{b+\sqrt{b^2-4ac}}{2a}} \text{ and } m_{11,12} = \pm i\tilde{\gamma} = \pm i\sqrt{\frac{b-\sqrt{b^2-4ac}}{2a}}$$

Now, we have eight zero roots and four imaginary roots yielding the corresponding solution,

$$\begin{aligned}\bar{u}(z) = {} & A_1 + A_2 z + A_3 z^2 + A_4 z^3 + A_5 z^4 + A_6 z^5 + A_7 z^6 + A_8 z^7 \\ & + A_9 \cos\tilde{\beta}z + A_{10}\sin\tilde{\beta}z + A_{11}\cos\tilde{\gamma}z + A_{12}\sin\tilde{\gamma}z\end{aligned} \tag{3.D.2}$$

$$\begin{aligned}\bar{v}(z) = {} & B_1 + B_2 z + B_3 z^2 + B_4 z^3 + B_5 z^4 + B_6 z^5 + B_7 z^6 + B_8 z^7 \\ & + B_9 \cos\tilde{\beta}z + B_{10}\sin\tilde{\beta}z + B_{11}\cos\tilde{\gamma}z + B_{12}\sin\tilde{\gamma}z\end{aligned} \tag{3.D.3}$$

$$\begin{aligned}\bar{\theta}(z) = {} & C_1 + C_2 z + C_3 z^2 + C_4 z^3 + C_5 z^4 + C_6 z^5 + C_7 z^6 + C_8 z^7 \\ & + C_9 \cos\tilde{\beta}z + C_{10}\sin\tilde{\beta}z + C_{11}\cos\tilde{\gamma}z + C_{12}\sin\tilde{\gamma}z\end{aligned} \tag{3.D.4}$$

From substituting Eqs.(3.D.2)-(3.D.4) and their derivatives into Eqs. (3.15)-(3.17), one obtains

$$
\begin{aligned}
&EI_{yy}\bar{u}'''' + EI_{xy}\bar{v}'''' + P\bar{u}'' + Py_{SC}\bar{\theta}'' \\
&\quad = 2\left[12A_5EI_{yy} + 12B_5EI_{xy} + A_3P + C_3Py_{SC}\right] \\
&\quad +6\left[20A_6EI_{yy} + 20B_6EI_{xy} + A_4P + C_4Py_{SC}\right]z \\
&\quad +12\left[30A_7EI_{yy} + 30B_7EI_{xy} + A_5P + C_5Py_{SC}\right]z^2 \\
&\quad +20\left[42A_8EI_{yy} + 42B_8EI_{xy} + A_6P + C_6Py_{SC}\right]z^3 \\
&\quad +30P\left[A_7 + C_7y_{SC}\right]z^4 + 42P\left[A_8 + C_8y_{SC}\right]z^5 \\
&\quad +\tilde{\beta}^2\left[A_9\left(\tilde{\beta}^2EI_{yy} - P\right) + B_9EI_{xy}\tilde{\beta}^2 - C_9Py_{SC}\right]\cos\tilde{\beta}z \\
&\quad +\tilde{\beta}^2\left[A_{10}\left(\tilde{\beta}^2EI_{yy} - P\right) + B_{10}EI_{xy}\tilde{\beta}^2 - C_{10}Py_{SC}\right]\sin\tilde{\beta}z \\
&\quad +\tilde{\gamma}^2\left[A_{11}\left(\tilde{\gamma}^2EI_{yy} - P\right) + B_{11}EI_{xy}\tilde{\gamma}^2 - C_{11}Py_{SC}\right]\cos\tilde{\gamma}z \\
&\quad +\tilde{\gamma}^2\left[A_{12}\left(\tilde{\gamma}^2EI_{yy} - P\right) + B_{12}EI_{xy}\tilde{\gamma}^2 - C_{12}Py_{SC}\right]\sin\tilde{\gamma}z = 0
\end{aligned}
\tag{3.D.5}
$$

$$
\begin{aligned}
&EI_{xx}\bar{v}'''' + EI_{xy}\bar{u}'''' + P\bar{v}'' - Px_{SC}\bar{\theta}'' \\
&\quad = 2\left[12B_5EI_{xx} + 12A_5EI_{xy} + B_3P - C_3Px_{SC}\right] \\
&\quad +6\left[20B_6EI_{xx} + 20A_6EI_{xy} + B_4P - C_4Px_{SC}\right]z \\
&\quad +12\left[30B_7EI_{xx} + 30A_7EI_{xy} + B_5P - C_5Px_{SC}\right]z^2 \\
&\quad +20\left[42B_8EI_{xx} + 42A_8EI_{xy} + B_6P - C_6Px_{SC}\right]z^3 \\
&\quad +30P\left[B_7 - C_7x_{SC}\right]z^4 + 42P\left[B_8 - C_8x_{SC}\right]z^5 \\
&\quad +\tilde{\beta}^2\left[B_9\left(EI_{xx}\tilde{\beta}^2 - P\right) + A_9EI_{xy}\tilde{\beta}^2 + C_9Px_{SC}\right]\cos\tilde{\beta}z \\
&\quad +\tilde{\beta}^2\left[B_{10}\left(EI_{xx}\tilde{\beta}^2 - P\right) + A_{10}EI_{xy}\tilde{\beta}^2 + C_{10}Px_{SC}\right]\sin\tilde{\beta}z \\
&\quad +\tilde{\gamma}^2\left[B_{11}\left(EI_{xx}\tilde{\gamma}^2 - P\right) + A_{11}EI_{xy}\tilde{\gamma}^2 + C_{11}Px_{SC}\right]\cos\tilde{\gamma}z \\
&\quad +\tilde{\gamma}^2\left[B_{12}\left(EI_{xx}\tilde{\gamma}^2 - P\right) + A_{12}EI_{xy}\tilde{\gamma}^2 + C_{12}Px_{SC}\right]\sin\tilde{\gamma}z = 0
\end{aligned}
\tag{3.D.6}
$$

$$
\begin{aligned}
&EI_{\omega\omega}\bar{\theta}''''+\left(Pr_0^2-GJ\right)\bar{\theta}''+Py_{SC}\bar{u}''-Px_{SC}\bar{v}''\\
&\quad=2\left[12C_5EI_{\omega\omega}+C_3\left(Pr_o^2-GJ\right)+A_3Py_{SC}-B_3Px_{SC}\right]\\
&\quad+6\left[20C_6EI_{\omega\omega}+C_4\left(Pr_o^2-GJ\right)+A_4Py_{SC}-B_4Px_{SC}\right]z\\
&\quad+12\left[30C_7EI_{\omega\omega}+C_5\left(Pr_o^2-GJ\right)+A_5Py_{SC}-B_5Px_{SC}\right]z^2\\
&\quad+20\left[42C_8EI_{\omega\omega}+C_6\left(Pr_o^2-GJ\right)+A_6Py_{SC}-B_6Px_{SC}\right]z^3\\
&\quad+30\left[C_7\left(Pr_o^2-GJ\right)+A_7Py_{SC}-B_7Px_{SC}\right]z^4\\
&\quad+42\left[C_8\left(Pr_o^2-GJ\right)+A_8Py_{SC}-B_8Px_{SC}\right]z^5\\
&\quad+\tilde{\beta}^2\left[C_9\left(EI_{\omega\omega}\tilde{\beta}^2-Pr_o^2+GJ\right)-A_9Py_{SC}+B_9Px_{SC}\right]\cos\tilde{\beta}z\\
&\quad+\tilde{\beta}^2\left[C_{10}\left(EI_{\omega\omega}\tilde{\beta}^2-Pr_o^2+GJ\right)-A_{10}Py_{SC}+B_{10}Px_{SC}\right]\sin\tilde{\beta}z\\
&\quad+\tilde{\gamma}^2\left[C_{11}\left(EI_{\omega\omega}\tilde{\gamma}^2-Pr_o^2+GJ\right)-A_{11}Py_{SC}+B_{11}Px_{SC}\right]\cos\tilde{\gamma}z\\
&\quad+\tilde{\gamma}^2\left[C_{12}\left(EI_{\omega\omega}\tilde{\gamma}^2-Pr_o^2+GJ\right)-A_{12}Py_{SC}+B_{12}Px_{SC}\right]\sin\tilde{\gamma}z=0
\end{aligned}
\tag{3.D.7}
$$

From vanishing the coefficients of z^4 in Eq. (3.D.5) and Eq. (3.D.6), one can obtain

$$A_7=-C_7y_{SC}\qquad B_7=-C_7x_{SC} \tag{3.D.8)a,b}$$

From substituting Eqs. (3.D.8)a,b into the coefficients of z^2 in Eq. (3.D.7) and setting the resulting equation to zero, one has

$$C_5\underbrace{\left[P\left(r_o^2-x_{SC}^2-y_{SC}^2\right)-GJ\right]}_{=0}+30C_7E\underbrace{\left[I_{xx}x_{SC}^2+I_{yy}y_{SC}^2-2I_{xy}x_{SC}y_{SC}+I_{\omega\omega}\right]}_{\neq0}=0 \tag{3.D.9}$$

leading to

$$A_7=B_7=C_7=0 \tag{3.D.10}$$

From substituting Eq. (3.D.10) into the coefficients of z^2 in Eq. (3.D.5) and Eq. (3.D.6) and then setting the resultant to zero, one defines

$$A_5=-C_5y_{SC}\qquad B_5=C_5x_{SC} \tag{3.D.11)a,b}$$

Also, from substituting Eqs. (3.D.11)a,b into the vanishing coefficients of z^0 in Eq. (3.D.5) and Eq. (3.D.6), one can express

$$\begin{aligned} A_3 &= \frac{1}{P}\left[12C_5E\left(I_{yy}y_{SC}-I_{xy}x_{SC}\right)-C_3Py_{SC}\right] \\ B_3 &= \frac{1}{P}\left[-12C_5E\left(x_{SC}I_{xx}-I_{xy}y_{SC}\right)+C_3Px_{SC}\right] \end{aligned} \tag{3.D.12)a,b}$$

From substituting Eqs. (3.D.12)a,b into the vanishing coefficients of z^0 in Eq. (3.D.7), one has

$$C_3\underbrace{\left[P\left(r_o^2-x_{SC}^2-y_{SC}^2\right)-GJ\right]}_{=0}+12C_5E\underbrace{\left[I_{xx}x_{SC}^2+I_{yy}y_{SC}^2-2I_{xy}x_{SC}y_{SC}+I_{\omega\omega}\right]}_{\neq 0}=0 \tag{3.D.13}$$

yielding

$$A_5=B_5=C_5=0 \tag{3.D.14}$$

which in turn leads to

$$A_3/B_3=-y_{SC}/x_{SC} \qquad C_3/B_3=1/x_{SC} \tag{3.D.15)a,b}$$

In a similar manner, it can be shown that

$$A_6=B_6=C_6=A_8=B_8=C_8=0 \tag{3.D.16}$$

and

$$A_4/B_4=-y_{SC}/x_{SC} \qquad C_4/B_4=1/x_{SC} \tag{3.D.17)a,b}$$

From vanishing coefficients of $\cos\tilde{\beta}z$, $\sin\tilde{\beta}z$, $\cos\tilde{\gamma}z$ and $\sin\tilde{\gamma}z$ in Eqs. (3.D.5)-(3.D.7), one obtains

$$\begin{aligned} \tilde{\xi}_2=\frac{A_9}{B_9}=\frac{A_{10}}{B_{10}} &= \frac{Py_{SC}-E\left(I_{xx}y_{SC}+I_{xy}x_{SC}\right)\tilde{\beta}^2}{-Px_{SC}+E\left(I_{yy}x_{SC}+I_{xy}y_{SC}\right)\tilde{\beta}^2} \\ &= \frac{P^2x_{SC}^2-\left(EI_{xx}\tilde{\beta}^2-P\right)\left(EI_{\omega\omega}\tilde{\beta}^2-Pr_o^2+GJ\right)}{P^2x_{SC}y_{SC}+EI_{xy}\tilde{\beta}^2\left(EI_{\omega\omega}\tilde{\beta}^2-Pr_o^2+GJ\right)} \\ &= \frac{P^2x_{SC}y_{SC}+EI_{xy}\tilde{\beta}^2\left(EI_{\omega\omega}\tilde{\beta}^2-Pr_o^2+GJ\right)}{P^2y_{SC}^2-\left(EI_{yy}\tilde{\beta}^2-P\right)\left(EI_{\omega\omega}\tilde{\beta}^2-Pr_o^2+GJ\right)} \end{aligned} \tag{3.D.18}$$

$$\tilde{\eta}_2 = \frac{C_9}{B_9} = \frac{C_{10}}{B_{10}} = \frac{P\left[E\left(I_{xx}+I_{yy}\right)\tilde{\beta}^2 - P\right] - E^2\left(I_{xx}I_{yy}-I_{xy}^2\right)\tilde{\beta}^4}{P\left[E\left(I_{yy}x_{SC}+I_{xy}y_{SC}\right)\tilde{\beta}^2 - Px_{SC}\right]}$$
$$= \frac{-P\left[E\left(I_{xx}y_{SC}+I_{xy}x_{SC}\right)\tilde{\beta}^2 - Py_{SC}\right]}{P^2x_{SC}y_{SC} + EI_{xy}\tilde{\beta}^2\left(EI_{\omega\omega}\tilde{\beta}^2 - Pr_o^2 + GJ\right)}$$
$$= \frac{P\left[E\left(I_{yy}x_{SC}+I_{xy}y_{SC}\right)\tilde{\beta}^2 - Px_{SC}\right]}{P^2y_{SC}^2 - \left(EI_{yy}\tilde{\beta}^2 - P\right)\left(EI_{\omega\omega}\tilde{\beta}^2 - Pr_o^2 + GJ\right)} \tag{3.D.19}$$

$$\tilde{\xi}_3 = \frac{A_{11}}{B_{11}} = \frac{A_{12}}{B_{12}} = \frac{Py_{SC} - E\left(I_{xx}y_{SC}+I_{xy}x_{SC}\right)\tilde{\gamma}^2}{-Px_{SC} + E\left(I_{yy}x_{SC}+I_{xy}y_{SC}\right)\tilde{\gamma}^2}$$
$$= \frac{P^2x_{SC}^2 - \left(EI_{xx}\tilde{\gamma}^2 - P\right)\left(EI_{\omega\omega}\tilde{\gamma}^2 - Pr_o^2 + GJ\right)}{P^2x_{SC}y_{SC} + EI_{xy}\tilde{\gamma}^2\left(EI_{\omega\omega}\tilde{\gamma}^2 - Pr_o^2 + GJ\right)}$$
$$= \frac{P^2x_{SC}y_{SC} + EI_{xy}\tilde{\gamma}^2\left(EI_{\omega\omega}\tilde{\gamma}^2 - Pr_o^2 + GJ\right)}{P^2y_{SC}^2 - \left(EI_{yy}\tilde{\gamma}^2 - P\right)\left(EI_{\omega\omega}\tilde{\gamma}^2 - Pr_o^2 + GJ\right)} \tag{3.D.20}$$

$$\tilde{\eta}_3 = \frac{C_{11}}{B_{11}} = \frac{C_{12}}{B_{12}} = \frac{P\left[E\left(I_{xx}+I_{yy}\right)\tilde{\gamma}^2 - P\right] - E^2\left(I_{xx}I_{yy}-I_{xy}^2\right)\tilde{\gamma}^4}{P\left[E\left(I_{yy}x_{SC}+I_{xy}y_{SC}\right)\tilde{\gamma}^2 - Px_{SC}\right]}$$
$$= \frac{-P\left[E\left(I_{xx}y_{SC}+I_{xy}x_{SC}\right)\tilde{\gamma}^2 - Py_{SC}\right]}{P^2x_{SC}y_{SC} + EI_{xy}\tilde{\gamma}^2\left(EI_{\omega\omega}\tilde{\gamma}^2 - Pr_o^2 + GJ\right)}$$
$$= \frac{P\left[E\left(I_{yy}x_{SC}+I_{xy}y_{SC}\right)\tilde{\gamma}^2 - Px_{SC}\right]}{P^2y_{SC}^2 - \left(EI_{yy}\tilde{\gamma}^2 - P\right)\left(EI_{\omega\omega}\tilde{\gamma}^2 - Pr_o^2 + GJ\right)} \tag{3.D.21}$$

From Eq. (3.D.10) and Eqs. (3.D.14)-(3.D.21), by substituting into Eqs. (3.D.2)-(3.D.4), the solution with twelve independent constants becomes

$$\bar{u}(z) = A_1 + A_2z + B_3\left(y_{SC}/x_{SC}\right)z^2 + B_4\left(y_{SC}/x_{SC}\right)z^3 + A_9\cos\tilde{\beta}z + A_{10}\sin\tilde{\beta}z + A_{11}\cos\tilde{\gamma}z + A_{12}\sin\tilde{\gamma}z \tag{3.D.22}$$

$$\bar{v}(z) = B_1 + B_2z + B_3z^2 + B_4z^3 + B_9\cos\tilde{\beta}z + B_{10}\sin\tilde{\beta}z + B_{11}\cos\tilde{\gamma}z + B_{12}\sin\tilde{\gamma}z \tag{3.D.23}$$

$$\bar{\theta}(z) = C_1 + C_2z + B_3\left(1/x_{SC}\right)z^2 + \left(1/x_{SC}\right)B_4z^3 + B_9\cos\tilde{\beta}z + B_{10}\sin\tilde{\beta}z + B_{11}\cos\tilde{\gamma}z + B_{12}\sin\tilde{\gamma}z \tag{3.D.24}$$

Appendix 3.E. Detailed derivation of the buckling solution for point-symmetric members

This appendix shows the steps for deriving Eqs. (3.32),(3.33).

The characteristic equation

$$m_i^4\left[E^2\left(I_{xx}I_{yy}-I_{xy}^2\right)m_i^4+PE\left(I_{xx}+I_{yy}\right)m_i^2+P^2\right]=0 \tag{3.E.1}$$

has four zero roots, $m_{1-4}=0$, and four imaginary roots, $m_{5,6}=\pm i\hat{\alpha}$ and $m_{7,8}=\pm i\hat{\beta}$ where

$$\begin{aligned}\hat{\alpha}&=\sqrt{P\left[\left(I_{xx}+I_{yy}\right)+\sqrt{\left(I_{xx}+I_{yy}\right)^2-4\left(I_{xx}I_{yy}-I_{xy}^2\right)}\right]\Big/2E\left(I_{xx}I_{yy}-I_{xy}^2\right)}\\ \hat{\beta}&=\sqrt{P\left[\left(I_{xx}+I_{yy}\right)-\sqrt{\left(I_{xx}+I_{yy}\right)^2-4\left(I_{xx}I_{yy}-I_{xy}^2\right)}\right]\Big/2E\left(I_{xx}I_{yy}-I_{xy}^2\right)}\end{aligned} \tag{3.E.2)a,b}$$

The corresponding solution takes the form

$$\bar{u}\left(z\right)=A_1+A_2z+A_3z^2+A_4z^3+A_5\cos\hat{\alpha}z+A_6\sin\hat{\alpha}z+A_7\cos\hat{\beta}z+A_8\sin\hat{\beta}z \tag{3.E.3}$$

$$\bar{v}\left(z\right)=B_1+B_2z+B_3z^2+B_4z^3+B_5\cos\hat{\alpha}z+B_6\sin\hat{\alpha}z+B_7\cos\hat{\beta}z+B_8\sin\hat{\beta}z \tag{3.E.4}$$

From Eqs. (3.E.3), (3.E.4) and their derivatives, by substituting into Eqs. (3.15), (3.16), while setting $x_{SC}=y_{SC}=0$, one has

$$\begin{aligned}&EI_{yy}\bar{u}'''+EI_{xy}\bar{v}'''+P\bar{u}'\\ &\quad=2A_3P+6A_4Pz\\ &\quad+\hat{\alpha}^2\left[A_5\left(EI_{yy}\hat{\alpha}^2-P\right)+B_5EI_{xy}\hat{\alpha}^2\right]\cos\hat{\alpha}z\\ &\quad+\hat{\alpha}^2\left[A_6\left(EI_{yy}\hat{\alpha}^2-P\right)+B_6EI_{xy}\hat{\alpha}^2\right]\sin\hat{\alpha}z\\ &\quad+\hat{\beta}^2\left[A_7\left(EI_{yy}\hat{\beta}^2-P\right)+B_7EI_{xy}\hat{\beta}^2\right]\cos\hat{\beta}z\\ &\quad+\hat{\beta}^2\left[A_8\left(EI_{yy}\hat{\beta}^2-P\right)+B_8EI_{xy}\hat{\beta}^2\right]\sin\hat{\beta}z=0\end{aligned} \tag{3.E.5}$$

$$
\begin{aligned}
&EI_{xx}\bar{v}'''' + EI_{xy}\bar{u}'''' + P\bar{v}'' \\
&\quad = 2B_3P + 6B_4Pz \\
&\quad + \hat{\alpha}^2\left[B_5\left(EI_{xx}\hat{\alpha}^2 - P\right) + A_5EI_{xy}\hat{\alpha}^2\right]\cos\hat{\alpha}z \\
&\quad + \hat{\alpha}^2\left[B_6\left(EI_{xx}\hat{\alpha}^2 - P\right) + A_6EI_{xy}\hat{\alpha}^2\right]\sin\hat{\alpha}z \\
&\quad + \hat{\beta}^2\left[B_7\left(EI_{xx}\hat{\beta}^2 - P\right) + A_7EI_{xy}\hat{\beta}^2\right]\cos\hat{\beta}z \\
&\quad + \hat{\beta}^2\left[B_8\left(EI_{xx}\hat{\beta}^2 - P\right) + A_8EI_{xy}\hat{\beta}^2\right]\sin\hat{\beta}z = 0
\end{aligned}
\tag{3.E.6}
$$

By vanishing the coefficients of z^0 and z in Eqs. (3.E.5) and (3.E.6), one finds

$$A_3 = A_4 = B_3 = B_4 = 0 \tag{3.E.7}$$

Also, by vanishing the coefficients of $\cos\hat{\alpha}z$, $\sin\hat{\alpha}z$, $\cos\hat{\beta}z$ and $\sin\hat{\beta}z$ in Eqs. (3.E.5) and (3.E.6), one obtains

$$
\begin{aligned}
\hat{\xi} &= \frac{A_5}{B_5} = \frac{A_6}{B_6} = \frac{-EI_{xy}\hat{\alpha}^2}{\left(EI_{yy}\hat{\alpha}^2 - P\right)} = \frac{-\left(EI_{xx}\hat{\alpha}^2 - P\right)}{EI_{xy}\hat{\alpha}^2} \\
\hat{\eta} &= \frac{A_7}{B_7} = \frac{A_8}{B_8} = \frac{-EI_{xy}\hat{\beta}^2}{\left(EI_{yy}\hat{\beta}^2 - P\right)} = \frac{-\left(EI_{xx}\hat{\beta}^2 - P\right)}{EI_{xy}\hat{\beta}^2}
\end{aligned}
\tag{3.E.8)a,b}
$$

From Eq. (3.E.7) and Eqs. (3.E.8)a,b, by substituting into Eqs. (3.E.3) and (3.E.4), the solution becomes

$$\bar{u}\left(z\right) = A_1 + A_2z + B_5\hat{\xi}\cos\hat{\alpha}z + B_6\hat{\xi}\sin\hat{\alpha}z + B_7\hat{\eta}\cos\hat{\beta}z + B_8\hat{\eta}\sin\hat{\beta}z \tag{3.E.9}$$

$$\bar{v}\left(z\right) = B_3 + B_4z + B_5\cos\hat{\alpha}z + B_6\sin\hat{\alpha}z + B_7\cos\hat{\beta}z + B_8\sin\hat{\beta}z \tag{3.E.10}$$

Appendix 3.F. Convergence study

This appendix shows the procedure for choosing the appropriate mesh for the 3D shell model used in validating the developed closed-form solution in Section 3.8 for members with pinned end conditions in all directions $x_{pp}y_{pp}z_{pp}$ and fixed end conditions in all directions $x_{ff}y_{ff}z_{ff}$.

The 4m member with L152x102x16 cross-section was discretized into (a) 5 elements along the short leg, 8 elements along the long leg and 200 elements along the span (Mesh 1 in Figure 3.7a), and (b) 10 elements along the short leg, 16 elements along the long leg and 400 elements along the span (Mesh 2 in Figure 3.7b). From the unity ratios in the last column of Table 3.4, it can be concluded that refining the mesh beyond Mesh 1 does not result in an appreciable change and hence Mesh 1 was considered to be suitable for the modeling of the members.

Table 3.4 Results of the mesh study for 3D shell models

Boundary Conditions	Buckling load (kN)		Ratio
	Mesh 1	Mesh 2	Mesh 2/ Mesh 1
$x_{pp}y_{pp}z_{pp}$	218.5	218.3	1.00
$x_{ff}y_{ff}z_{ff}$	841.9	840.4	1.00

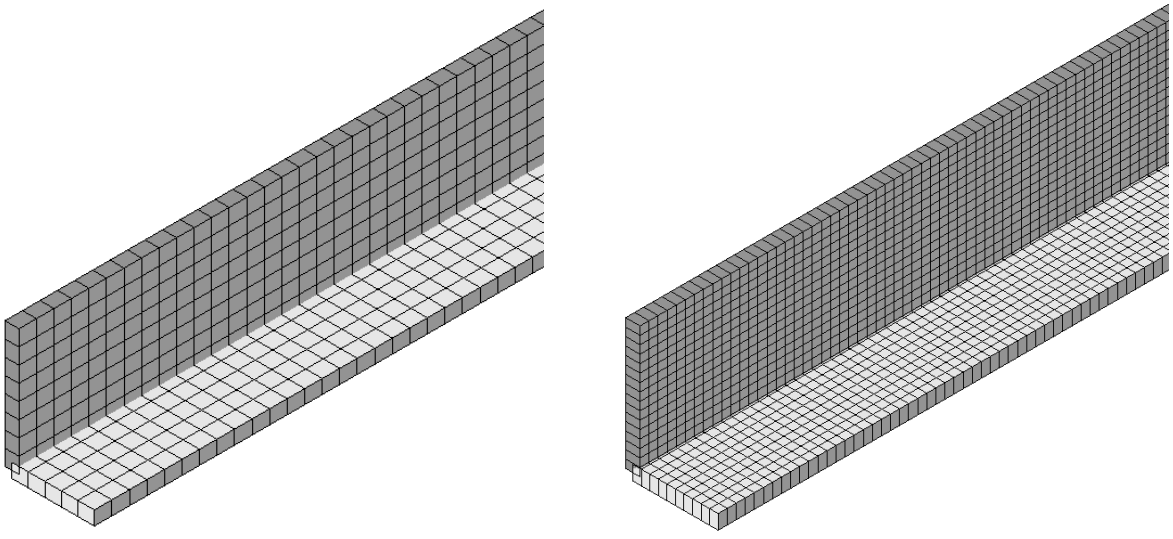

(a) (b)

Figure 3.7 3D view of the angle member with (a) Mesh 1 and (b) Mesh 2

Appendix 3.G. Determining the inelastic compressive resistance

This appendix illustrates the possible means of integrating the elastic buckling load based on the closed-form solutions developed in Chapter 3 into design standards to estimate the inelastic buckling resistance of single angle members under pure compression when the effect of axial load eccentricity from the centroidal axis are negligible.

3.G.1 Illustrative example

A compression member with L152x152x19 cross-section has a 4m span. Steel properties are $E = 200,000$ MPa, $G = 76,900$ MPa and $F_Y = 350$ MPa. The end gusset plate connection can be assumed to restrain the member end rotation about the y axis while providing negligible restraint against rotation about the x axis. Twist end restraint is taken as a pin. Using the elastic buckling closed-form solution derived in Chapter 3 for members with $x_{pp}y_{ff}z_{pp}$,i.e., Eq. (3.37), it is required to estimate the nominal inelastic compressive resistance of the member based on CSA S16-19 provisions.

Solution

The relevant cross-sectional properties are $A = 5415$ mm^2, $I_{xx} = I_{yy} = 11,540,000$ mm^4, $I_{xy} = -6,872,000$ mm^4, $J = 651,600$ mm^4, $I_{\omega\omega} = 1,103,000,000$ mm^6, $x_{SC} = y_{SC} = -35.6$ mm and $r_0 = 82.5$ mm. By substituting into Eqs. (3.23), (3.24), (3.37), and then solving the equations iteratively, one can obtain the elastic buckling load as $P = 1201$ kN. The corresponding elastic buckling stresses is $F_e = 222$ MPa. For a yield strength $F_Y = 350$ Mpa, the nominal inelastic compressive resistance as estimated by the CSA S16-19 equation is $P_n = AF_y\left[1+\left(F_y/F_e\right)^{1.34}\right]^{-1/1.34} = 870$ kN.

For comparison, if, in the absence of Eq. (3.37), the designer opted to conservatively idealize the member as pinned in all directions, the elastic buckling stress would drop to $F_e = 106$ MPa, and the nominal inelastic compressive would drop to $P_n = 500$ kN.

Chapter 4: Inelastic compressive resistance of single angle compression members with gusset plate end connections

4.1. Abstract

The present study investigates the inelastic compressive resistance of eccentrically loaded single angle members by simulating the end conditions of members connected to gusset plates at both ends through one leg. The study develops a series of 3D finite element shell models based on ABAQUS which incorporate material and geometric non-linear effects, initial out-of-straightness, residual stresses, and load eccentricity. The model is validated against published experimental results and then used to carry out a parametric study consisting of more than 900 cases involving multiple cross-sections, spans, and load eccentricities. The results generated are then used to investigate the effect of slenderness ratio, leg width ratio, connected leg width-to-thickness ratio and gusset plate-to-angle thickness ratio on the compressive capacity of eccentrically loaded angle members, and develop a simple design expression for the compressive resistance of the member. The predictions based on the developed design expression are compared against those based on the current Canadian design standard CSA S16-19.

Keywords

Single angle; compression member; angle-gusset plate connection; beam-column; inelastic resistance; finite element method; design equation.

4.2. Introduction and motivation

Members with single angle cross-sections are typically connected at both ends to a gusset plate through one of their legs (Figure 4.1a). The gusset plate is expected to provide a full rotational restraint about the y axis (Figure 4.1b) and a partial rotational restraint about the x axis. The degree of partial fixity would depend on gusset plate dimensions (plate thickness and width, distance between the angle end and plate). Given the complexity of quantifying the degree of partial fixity condition, a practical design approach is to conservatively assume a pin-end condition about the x axis. When detailing the gusset connection at the member end, it is common practice to align the member centerline with the line of action of the expected axial force in the member within the plane of the gusset in a truss-like connection (Figure 4.1a). Such a detail results in a vanishing eccentricity within the plane of the gusset, i.e., $e_x = 0$. Conversely, since the line of action of the internal force within the angle member coincides with its centroidal axis, it is inevitably offset from the middle surface of the gusset by an eccentricity e_y relative to the y axis. A recent study (Alenezi and Mohareb 2021) developed an elastic buckling solution for single angle compression members with end restraints pinned about the x axis and fixed about the y axis and subjected to pure compression. Since the solution in Alenezi and Mohareb (2021) omitted any eccentricity between the line of action of the force P within the gusset and the member centerline, i.e., $e_x = e_y = 0$, the solution was based on an eigenvalue bifurcation type of analysis. In comparison, the connection detail considered in the present study (Figure 4.1a,b) is associated with an additional end moment Pe_y about the x axis . The presence of such end moments transforms the expected member response from a bifurcation type of behaviour into a nonlinear load-deformation response.

The Canadian design standard for steel structures CSA S16 (2019) allows designers to omit the effect of eccentricity in single angle compression members and treat it as a concentrically loaded member when the member is (i) loaded in compression through the same leg at both ends, (ii) connected to the gussets either by welding or a minimum of two-bolt connection, (iii) not subjected to intermediate transverse loads, and (iv) having a long-to-short leg ratio $b_l/b_s < 1.7$. Under these conditions, the standard provides empirical expressions to determine the effective slenderness ratio in individual members and planar trusses. For an angle member with equal-leg or unequal-leg angle connected through the longer leg, the effective slenderness ratio KL/r is given by

$$\frac{KL}{r} = \begin{cases} 72 + 0.75\,L/r_x & 0 \le L/r_x \le 80 \\ 32 + 1.25\,L/r_x \le 200 & L/r_x > 80 \end{cases} \quad \text{(4.1)a,b}$$

where r_x is the radius of gyration about the x axis (Figure 4.1b). For a member with an unequal-leg angle connected through the shorter leg, the effective slenderness ratio is given by

$$\frac{KL}{r} = \begin{cases} 72 + 0.75L/r_x + 4\left[\left(b_l/b_s\right)^2 - 1\right] > 0.95L/r_{min} & 0 \le L/r_x \le 80 \\ 0.95L/r_{min} < 32 + 1.25L/r_x + 4\left[\left(b_l/b_s\right)^2 - 1\right] \le 200 & L/r_x > 80 \end{cases} \quad \text{(4.2)a,b}$$

in which r_{min} is the minimum radius of gyration. The effective slenderness ratio determined is then used to estimate the elastic buckling stress F_e from

$$F_e = \pi^2 E \Big/ \left(KL/r\right)^2 \quad (4.3)$$

where E is the modulus of elasticity. The elastic buckling stress is in turn used to estimate the nominal inelastic compressive resistance for the member from the expression

$$P_n = AF_Y \left[1 + \left(F_Y/F_e\right)^{1.34}\right]^{-1/1.34} \quad (4.4)$$

in which A is the cross-sectional area of the member and F_Y is the yield stress. Equations (4.1)-(4.2) were originally proposed by Lutz (1992) based on regression analysis on limited experimental data. For situations where members do not satisfy the above conditions (e.g., $b_l/b_s > 1.7$) or when the member is part of a bracing system, the effect of eccentricity cannot be ignored, and the compressive resistance of such members needs to be determined based on a beam-column interaction equation. The interaction equation accounts for the reduction in compressive resistance P due to the line of action of the force within the gusset being offset form the member centroidal axis by eccentricities $e_{\hat{x}}$ and $e_{\hat{y}}$ along the principal directions of the member (Figure 4.1c). The equation takes the form

$$\frac{P}{P_n}+\left(\frac{1}{1-P/P_{e\hat{x}}}\right)\frac{Pe_{\hat{y}}}{M_{n\hat{x}-i}}+\left(\frac{1}{1-P/P_{e\hat{y}}}\right)\frac{Pe_{\hat{x}}}{M_{n\hat{y}-i}}\le 1.0 \tag{4.5}$$

where the nominal compressive resistance P_n in the absence of moments is determined from Eq. (4.4) based on the lowest elastic buckling stress F_e obtained from

$$\left(F_e-F_{e\hat{x}}\right)\left(F_e-F_{e\hat{y}}\right)\left(F_e-F_{ez}\right)-F_e^2\left(F_e-F_{e\hat{y}}\right)\left(\hat{x}_S/r_0\right)^2-F_e^2\left(F_e-F_{e\hat{x}}\right)\left(\hat{y}_S/r_0\right)^2=0 \tag{4.6}$$

in which

$$F_{e\hat{x}}=\frac{\pi^2E}{\left(K_{\hat{x}}L_{\hat{x}}/r_{\hat{x}}\right)^2} \qquad F_{e\hat{y}}=\frac{\pi^2E}{\left(K_{\hat{y}}L_{\hat{y}}/r_{\hat{y}}\right)^2} \qquad F_z=\left(\frac{\pi^2EI_{\omega\omega}}{\left(K_zL_z\right)^2}+GJ\right)\frac{1}{Ar_0^2} \tag{4.7a-c}$$

and $\hat{x}_S$ and $\hat{y}_S$ are the coordinates of the shear centre with respect to the centroid of the section, r_0 is the polar radius of gyration about the shear centre given by $r_0=\sqrt{\hat{x}_0^2+\hat{y}_0^2+r_{\hat{x}}^2+r_{\hat{y}}^2}$ where $r_{\hat{x}}, r_{\hat{y}}$ are the radii of gyration about $\hat{x}, \hat{y}$ axes, G is the modulus of rigidity, $I_{\omega\omega}$ is the warping

constant, J is the Saint-Venant torsional constant and $\left(K_{\hat{x}}L_{\hat{x}}/r_{\hat{x}}\right)$, $\left(K_{\hat{y}}L_{\hat{y}}/r_{\hat{y}}\right)$ are the slenderness ratios with respect to the principal directions $\hat{x},\hat{y}$ and K_zL_z is the effective length relative to twist. The bending moments $Pe_{\hat{y}}$ and $Pe_{\hat{x}}$ in Eq. (4.5) are amplified by $1/\left(1-P/P_{e\hat{x}}\right)$ and $1/\left(1-P/P_{e\hat{y}}\right)$ in which, $P_{e\hat{x}}=\pi^2EI_{\hat{x}\hat{x}}/L^2$ and $P_{e\hat{y}}=\pi^2EI_{\hat{y}\hat{y}}/L^2$ are the Euler buckling loads where $I_{\hat{x}\hat{x}}$ and $I_{\hat{y}\hat{y}}$ are the principal moments of inertia, in order to account for the second-order effects. $M_{n\hat{x}-i}=\left(I_{\hat{x}\hat{x}}/\hat{y}_i\right)F_Y$ is the nominal moment resistance of point i on the cross-section about the minor principal axis where $\hat{y}_i$ is the coordinate of point i along the major principal axis. $M_{n\hat{y}-i}$ is the nominal moment resistance of point i about the major principal axis as calculated from

$$M_{n\hat{y}-i}=\begin{cases}\left[0.92-\left(0.17M_{U\hat{y}}/M_{Y\hat{y}-i}\right)\right]M_{U\hat{y}} & M_{U\hat{y}}\le 0.67M_{Y\hat{y}-i}\\ \left(1-0.79M_{Y\hat{y}-i}/M_{U\hat{y}}\right)1.15M_{Y\hat{y}-i}\le M_{Y\hat{y}-i} & M_{U\hat{y}}>0.67M_{Y\hat{y}-i}\end{cases} \tag{4.8}$$

where $M_{Y\hat{y}-i}=\left(I_{\hat{y}\hat{y}}/\hat{x}_i\right)F_Y$ is the elastic yield sectional resistance of point i about the major axis in which, $\hat{x}_i$ is the coordinate of point i along the minor principal axis, and $M_{U\hat{y}}$ is the elastic lateral-torsional buckling moment calculated as

$$M_{U\hat{y}}=\frac{4.9EI_{\hat{x}}}{L^2}\left(\sqrt{\beta_{\hat{y}}^2+0.052\left(\frac{Lt}{r_{\hat{x}}}\right)^2}+\beta_{\hat{y}}\right) \tag{4.9}$$

where t is the cross-sectional thickness and $\beta_{\hat{y}}=\left(1/I_{\hat{y}\hat{y}}\right)\int_A\hat{x}\left(\hat{y}^2+\hat{x}^2\right)dA-2\hat{x}_S$ is the asymmetry parameter which takes a negative value when the shear centre is in tension (Appendix 4.A). Equation (4.5) is to be evaluated at the corner points of the cross-section (Figure 4.1c) and positive stresses denote compression as a sign convention. The resistance of the member is then governed by the lowest P obtained (Appendix 4.B). Although Eq. (4.5) has no limitation regarding the cross-section geometry and load eccentricity, it involves a relatively lengthy procedure.

Within this context, the present study aims to (i) develop a nonlinear finite element model that captures the effects of load eccentricity e_y, geometric and material nonlinearities, and residual stresses to characterize the inelastic buckling resistance of single angle members and assess the validity of the model against documented experimental results, (ii) modify the end conditions of the finite element model to closely idealize end details expected in end gusset connections as depicted in Figure 4.1, (iii) use the modified model to develop a database of runs to quantify the compressive resistance of compression angle members with end gusset details, (iv) assess the validity of present design standard equations against the database of runs generated, and (v) propose an improved design approach.

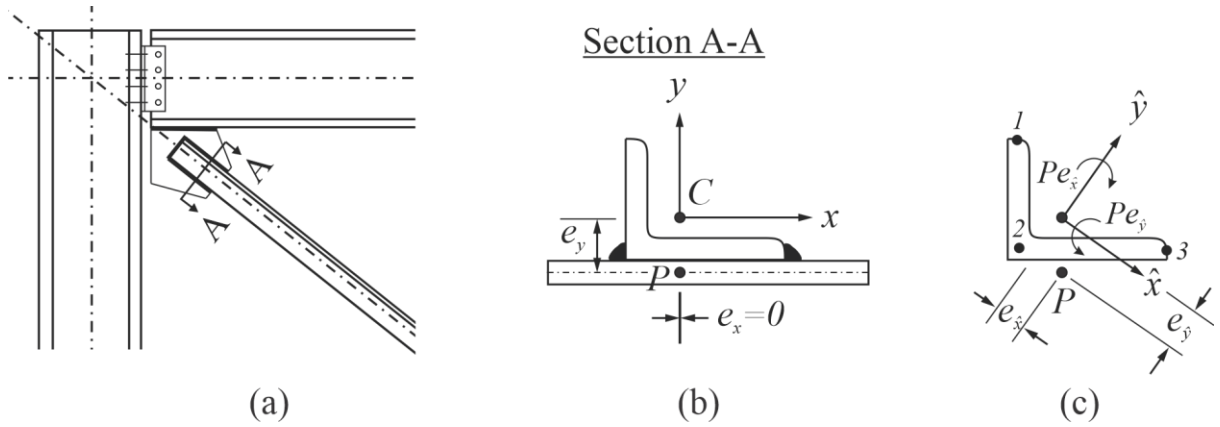

Figure 4.1 (a) typical angle-gusset plate connection in bracing systems, (b) cross-sectional view A-A at the connection and (c) moments induced by an eccentric load P

4.3. Literature review

The earliest investigation on the inelastic compressive resistance of hot-rolled angle members was reported by Stang and Strickenberg (1922) in which, 170 angle members with various end restraints were tested under concentric and eccentric compressive loading. Experimental investigations on eccentrically loaded angle members with pin end conditions, were conducted by Bathon et al. (1993), Liu and Hui (2008), Liu and Chantel (2011) and Spiliopoulos et al. (2018). An experimental study by Bezas et al (2021) tested angle members with fixed end conditions.

Other investigations were conducted on compression members with single leg angles connected at both ends to HSS sections (e.g., Temple et al. 1995), tee sections (e.g., Temple and Sakla 1998a) and gusset plates (e.g., Bhilawe and Gupta 2015, Kettler et al. 2019 and Huang et al. 2021). Experimental studies on eccentrically loaded cold-formed angle members include the work of Popovic et al. (2001), Fasoulakis et al. (2019) and Branquinho and Malite (2021).

Temple and Sakla (1998b) carried out a parametric study using shell models based on ABAQUS to investigate the effects of the distance from the angle end to connection end, the gusset plate thickness and gusset plate width on the inelastic compressive strength of members with L64x64x7.9 cross-sections. The results of the parametric study were then used to develop empirical equations to predict the compressive resistance of the angle members. Another parametric study was conducted by Liu and Hui (2010) using a shell model based on ANSYS to investigate the influence of slenderness ratio, leg width-to-thickness ratio and load eccentricity on the compressive resistance of eccentrically loaded simply supported members with L51x51 cross-sections. The obtained capacities were used to derive a beam-column interaction equation. Kettler et al. (2017) numerically investigated the effect of bolted end connection details on the compressive resistance of angle members using ABAQUS. The model simulated the angle member using shell elements connected to a gusset plate modelled using solid elements through one or two bolts modelled using solid elements. A parametric study was conducted on members with L60x60x6, L80x80x8 and 120x120x12 cross-sections and considered three types of boundary conditions; (i) pinned in all directions, (ii) fixed in all directions, and (iii) pinned about one direction, and fixed about the orthogonal direction. Hussain et al. (2018) developed a shell model based on ABAQUS to study the response of eccentrically loaded angle members with pin-end restraints in all directions. The study consisted of members with L100x100x10 and L150x100x12

cross-sections. The study resulted in beam-column plastic interaction equations that account for the eccentricity of the loads. Most recently, Kettler et al. (2021) developed design solution to predict the compressive resistance of eccentrically loaded hot-rolled bolted angles with end-connection details consisting of (a) gusset plates and (b) web/flange of I sections. The solution was based on elastic second order analysis and incorporated the effect of the end restraints as rotational spring stiffness.

A number of design solutions were proposed to predict the compressive resistance of concentrically loaded hot-rolled angle members (e.g., Cao et al. 2015, Sarquis et al. 2020, Sun et al. 2021, and Behzadi-Sofiani et al. 2021a,b). While these studies have focused on hot-rolled members, multiple design solutions were also proposed for cold-formed compression angle members (e.g., Rasmussen 2005, 2006, Dinis and Camotim 2015, Camotim et al. 2020, Dinis et al. 2021, and Branquinho and Malite 2021).

Table 4.1 summarizes the geometric and material parameters considered in the parametric studies that are most relevant to the present study along with the boundary conditions and the type of design aids proposed. It is noted that Sakla (1998b) and Liu and Hui (2010) considered only equal-leg angle cross-sections. The studies by Liu and Hui (2010) and Hussain et al. (2018) were limited to members with pinned end conditions in all directions. In contrast, the present study intends to cover both equal- and unequal-leg angle cross-sections while focusing on members with end restraints pinned about x axis and fixed about y axis (Figure 4.1b).

Table 4.1 Summary of the parameters considered in most relevant studies

Study	Temple and Sakla (1998b)	Liu and Hui (2010)	Kettler et al (2017)	Hussain et al. (2018)	Present
Slenderness ratio	80 to 300	20 to 180	48.7 to 223	50 to 200	25 to 200
Leg width ratio	1.0	1.0	1.0	0.5 and 1.0	0.5 to 2.0
Long leg to thickness ratio	8.1	5.3 to 16	10	10 and 12.5	8 to 14
Load eccentricity	$y_S + 0.5\left(t + t_g\right)$	0 to $2\hat{y}_S$	$y_S + 0.5\left(t + t_g\right)$	$-3.0\hat{y}_S$ to $+3.0\hat{y}_S$	$y_S + 0.5\left(t + t_g\right)$
Initial imperfections	$L/1000$	$L/1000$	$L/300, L/200$	$L/1000$	$L/1000$
End connection	Tee section	NA	Gusset plate	NA	NA
Boundary conditions	Fixed in all directions	Pinned in all directions	-Pinned in all directions -Fixed in all directions -Pinned about x axis, fixed about y axis	Pinned in all directions	Pinned about x axis and fixed about y axis
Design aids obtained	Empirical equation	Beam-column interaction equation	NA	Beam-column interaction equation	Reduction factor

Note: NA= Not applicable; t = angle thickness; t_g = gusset plate thickness; $\hat{y}$ = major principal axis; y = vertical non-principal axis; y_S = shear centre coordinate along y axis.

4.4. Model description

A shell finite element model is developed using ABAQUS to simulate the test set-up used by Liu and Hui (2008) and Liu and Chantel (2011). In both studies, the specimens had pin end conditions about both principal axes, and the load was eccentrically applied along either the minor or the major principal directions (Figure 4.2). The model is based on the S4 shell element, a four-node fully integrated element with finite membrane strain capabilities with six degrees of freedom per node, three displacements and three rotations. At each end of the member, a master node is defined at $x = e_x$ and $y = e_y$ where e_x and e_y are measured from the centroid of the angle (Figure 4.1b). Each master node is rigidly linked to all the nodes of the cross-section through the multiple point constraint feature in Abaqus *MPC type BEAM. This BEAM type constraint provides a rigid link

between two nodes to constrain all degrees of freedom of the first node to those of the second node. The displacements along the x and y directions for the master nodes are then restrained along with the angle of twist. The angle steel is modelled as an elastic-perfectly plastic material with a modulus of elasticity E and yield strengths F_Y equal to the average values reported by Liu and Hui (2008) and Liu and Chantel (2011) as listed in Table 4.2 and Table 4.3, and Poisson's ratio is taken as $\mu = 0.3$.

The model incorporates initial out-of-straightness where the imperfect geometry is taken to match the first mode as predicted by a linearized buckling analysis of an identical perfectly straight member subjected to a concentric compressive load. The resultant of the displacements along the x and y directions of the corner node (shear centre) based on the first buckling mode at member mid-span is scaled to $\alpha = L/2100$ for equal-leg angles and $\alpha = L/1607$ for unequal-leg angles to match the average values reported in Liu and Hui (2008) and Liu and Chantel (2011). The initial out-of-straightness is then applied to the non-linear model using the *IMPERFECTION keyword. The model also incorporates residual stresses as initial stresses based on the residual stress pattern shown in Figure 4.3a in which the residual stress amplitudes at the three corner points are $\beta_i F_y$, with $i = 1, 2, 3$. Moŝe et al. (2014) found that residual stresses in angles do not generally exceed $0.2F_y$, and hence the values $-\beta_1 = +\beta_2 = -\beta_3 = 0.2$ were taken in the present model, in which positive signs denote tension. In order to ensure a close approximation of the linear residual stress distribution, the three-point pattern was converted into a step pattern where the number of steps matched the number of elements along each leg (Figure 4.3b) so that each element has a uniform stress field. Each uniform stress is then applied to a strip of elements along the span by using the *INITIAL CONDITIONS, TYPE=STRESS keyword. Twenty shell elements were taken along the

width of each leg to accurately represent the initial residual stress pattern. Both end master nodes were incrementally subjected to equal and opposite longitudinal displacements and the nonlinear load deformation response was determined by the Newton-Raphson iterative scheme by incorporating the geometric and material nonlinear effects.

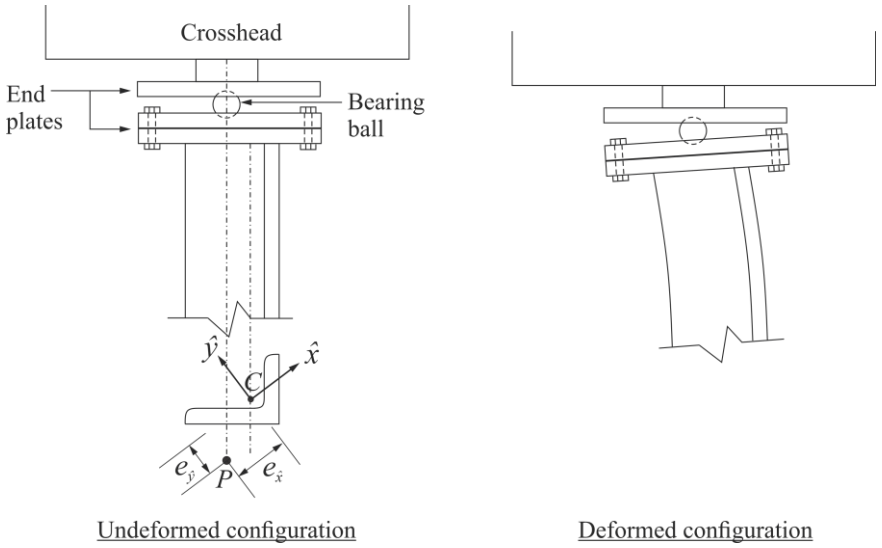

Figure 4.2 End details in the experimental study by Liu and Hui (2008) and Liu and Chantel (2011)

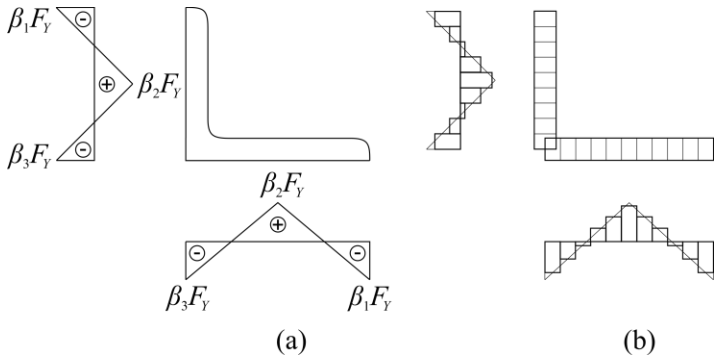

Figure 4.3 (a) three-point residual stress pattern (b) idealized step residual stress pattern

4.4.1. Assessment of model validity

As shown in Table 4.2, ratios P_p/P_t of the compressive capacities for the equal-leg angles based on the finite element model predictions to those of test results reported in Liu and Hui (2008) were found to range from 0.89 to 1.10 with a mean value of 1.00, a standard deviation of 0.050 and a corresponding coefficient of variation of 5.0%. For the unequal-leg angles members, Table 4.3

shows that the P_p/P_t ranges from 0.89 to 1.09 with a mean value of 1.01, a standard deviation of 0.057 and a coefficient of variation of 5.7%. The differences between the experimental and numerical results are partially attributed to the fact that the assumed amplitudes for the initial out-of-straightness were based on the average measured values and the residual stresses were based on idealized distribution as no specific values were reported for each member. Also, the moduli of elasticity and yield strengths were based on average values. The comparison suggests that the finite element model reliably predicts the compressive resistance of eccentrically loaded single angles.

Table 4.2 Compressive capacities comparison for L51x51x6.4 (Liu and Hui 2008)

L/r_{min}	F_Y (MPa)	E (MPa)	$e_{\hat{x}}$ (mm)	$e_{\hat{y}}$ (mm)	P_t (kN)	P_p (kN)	P_e/P_t
96.0	330	199900	0	4.2	110.9	114.2	1.03
96.3	330	199900	0	10	105.3	109.3	1.04
95.5	330	199900	0	16.8	84.5	80.4	0.95
95.5	330	199900	0	29.4	59.0	58.3	0.99
95.5	330	199900	0	50.4	46.1	40.9	0.89
95.4	348	202500	8.4	0	65.6	62.5	0.95
95.4	348	202500	16.8	0	46.4	45.9	0.99
95.9	348	202500	29.4	0	34.4	33.3	0.97
95.9	348	202500	50.4	0	23.3	23.1	0.99
126.2	330	199900	0	4.2	68.1	69.8	1.02
126.2	330	199900	0	10	66.7	68.7	1.03
126.2	348	202500	0	16.8	66.4	67.7	1.02
126.3	330	199900	0	29.4	57.0	58.6	1.03
126.5	348	202500	0	50.4	42.5	40	0.94
157.0	348	202500	0	8.4	42.9	46.5	1.08
157.0	348	202500	0	16.8	41.3	45.5	1.10
157.0	348	202500	0	29.4	40.1	42.7	1.06
156.8	348	202500	0	50.4	37.0	35.8	0.97
156.8	348	202500	8.4	0	35.2	35	0.99
157.6	348	202500	16.8	0	27.8	28.3	1.02
157.4	348	202500	29.4	0	23.4	22.3	0.95
156.8	348	202500	50.4	0	18.0	17	0.94
						Mean =	1.00
						Standard Deviation =	0.050
						Coefficient of Variation (%) =	5.0

Table 4.3 Compressive capacities comparison for L76x51x6.4 (Liu and Chantel 2011)

L/r_{min}	F_Y (MPa)	E (MPa)	$e_{\hat{x}}$ (mm)	$e_{\hat{y}}$ (mm)	P_t (kN)	P_p (kN)	P_e/P_t
112.8	356	203164	0	8.8	97.8	101.3	1.04
112.9	356	203164	0	17.5	92.0	94.2	1.02
112.9	356	203164	0	26.3	84.4	85.9	1.02
112.4	356	203164	0	35	78.0	78.6	1.01
112.8	356	203164	0	-8.8	120.9	108	0.89
112.9	356	203164	0	-17.5	118.4	106.1	0.90
112.9	356	203164	0	-26.3	109.7	101.1	0.92
112.3	356	203164	0	-35	98.4	95.5	0.97
112.8	356	203164	17.5	0	49.3	46.9	0.95
112.9	356	203164	-17.5	0	49.9	50.3	1.01
112.8	356	203164	-26.3	0	41.4	41.0	0.99
168.5	356	203164	0	8.8	46.6	49.7	1.07
168.5	356	203164	0	17.5	45.2	47.8	1.06
168.6	356	203164	0	26.3	42.1	45.6	1.08
168.6	356	203164	0	-8.8	49.1	51.7	1.05
168.5	356	203164	0	-17.5	48.8	51.7	1.06
168.6	356	203164	0	-26.3	46.8	51.1	1.09
168.6	356	203164	17.5	0	32.1	31.1	0.97
168.7	356	203164	-17.5	0	30.8	32.1	1.04
168.5	356	203164	-26.3	0	26.6	27.6	1.04
						Mean =	1.01
						Standard Deviation =	0.057
						Coefficient of Variation (%) =	5.7

4.4.2. Model modification to simulate gusset plate end connections

As discussed in Section 4.2, the gusset plate details of typical field conditions (Figure 4.1b) can be assumed to provide a fixity end restraint about the y axis and a pin end restraint about an axis parallel to the x axis passing through the gusset plate middle surface. The eccentric load P acts at eccentricities $e_x = 0$ and $e_y = y_S - 0.5\left(t + t_g\right)$ where y_S is the shear centre coordinate relative to the angle centroid, t is the angle thickness and t_g is the gusset plate thickness. The pin end condition in the finite element model described previously is modified to simulate the gusset plate end connection shown in Figure 4.1b. This includes restraining the angle of rotation about the y

axis at the master nodes, while enabling the rotation about the x axis and providing a restrain relative to twist. An initial out-of-straightness was applied based on the first buckling mode for an identical concentrically loaded straight member.

4.5. Preliminary investigation

This section investigates the effect of end conditions on the compressive resistance of eccentrically loaded angle members by comparing the compressive resistance of a member with a pinned end condition in all directions to that of identical member with a gusset end condition. It also evaluates the effect of residual stresses and initial out-of-straightness on the compressive resistance. For all runs, the yield strength is taken as $F_Y = 350$ MPa and the modulus of elasticity is taken as $E = 200,000$ MPa.

4.5.1. Effect of end conditions

A set of runs of compression members with L152x152x16, L178x127x16 and L203x102x16 cross-sections was conducted to investigate the effect of end details. For the unequal leg angle, two scenarios were considered; (i) the shorter leg is connected to the gusset plate and (ii) the long leg is connected to the gusset plate, so as to vary the leg width ratio b_y/b_x from 0.5 to 2.0 . Two types of end conditions are considered: (i) pinned in all directions (Figure 4.2) (ii) pinned about an axis parallel to the x axis and fixed about the y axis to emulate typical end gusset plate connections (Figure 4.1b). The slenderness ratios L/r_{min} based on the minimum radius of gyration were varied within the range 50 to 200. The compressive load is applied at eccentricities $e_x = 0$ and $e_y = y_S - t$. All members were subjected to a three-point residual stress pattern (Figure 4.3a) with $-\beta_1 = +\beta_2 = -\beta_3 = 0.2$ and an initial out-of-straightness with $\alpha = L/1000$. The compressive

resistance P_e of a member with a gusset plate end connection is normalized to that of an identical member with a pinned connection P_p.

The normalized compressive resistance P_e/P_p depicted in Figure 4.4a is observed to range from 1.13 to 2.78. and is found to be sensitive to the leg width ratio b_y/b_x. The influence of b_y/b_x on P_e/P_p gains significance as the slenderness ratio L/r_{min} increases. Figure 4.4b-f depicts the load versus the midspan resultant displacement for members with $L/r_{min} = 200$ and $b_y/b_x = 0.5 - 2.0$. For these members, the normalized compressive resistance P_e/P_p is only 1.18 when $b_y/b_x = 0.5$ but remarkably increases to 2.78 when $b_y/b_x = 2.0$. The considerable variation in the range in P_e/P_p reflects the sensitivity of results on the fixity restraint about the y axis, provided by the gusset plate. The degree of fixity provided by the gusset primarily depends on the angle of inclination of the fixity axis normal to the gusset middle surface relative to the minor principal axis of the angle. For the member with $b_y/b_x = 0.5$, the fixity axis y is inclined at 75 degrees from the minor principal axis and hence the member is mildly influenced by the fixity restraint leading to buckling predominantly about the x axis (Figure 4.5a) which corresponds to a low buckling load ratio P_e/P_p. On the other hand, the influence of the fixity restraint in the member with $b_y/b_x = 2.0$ is significant since the fixity axis y is inclined at 15 degrees from the minor principal axis of the angle. This causes a considerable increase in P_e/P_p as the member primarily buckles about the y axis (Figure 4.5b). This implies that a member with an unequal-leg angle connected to the gusset by the shorter leg has a higher compressive resistance. This observation holds true for all slenderness ratios. It is also consistent with the elastic critical loads obtained in

Alenezi and Mohareb (2021) for concentrically loaded angle compression members pinned about the x axis and fixed about the y axis.

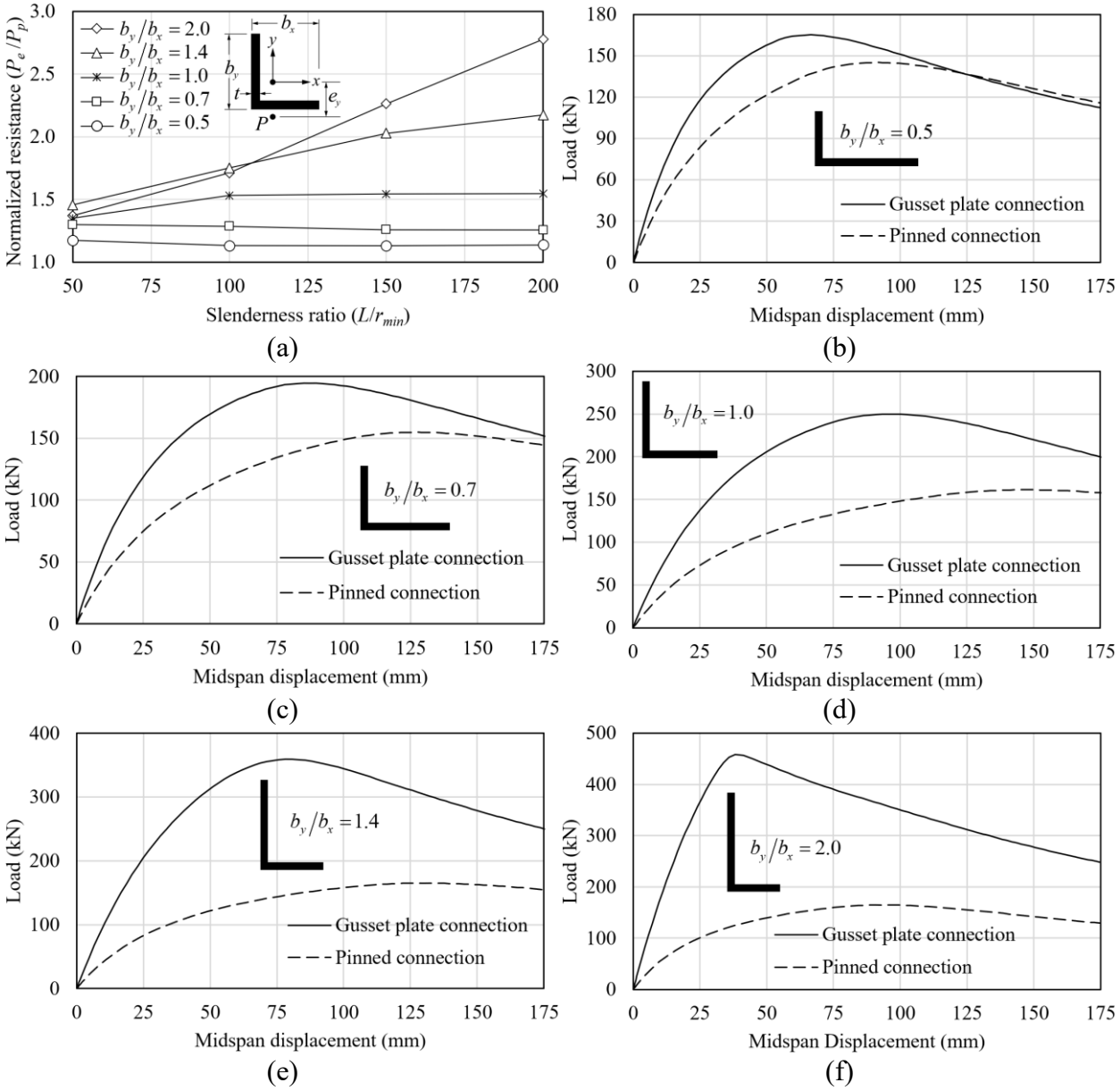

Figure 4.4 (a) Normalized compressive resistance P_e/P_p versus slenderness ratio L/r_{min} and Load versus the midspan resultant displacements for members with $L/r_{min} = 200$ and (b) $b_y/b_x = 0.5$, (c) $b_y/b_x = 0.7$, (d) $b_y/b_x = 1.0$, (e) $b_y/b_x = 1.4$ and (f) $b_y/b_x = 2.0$

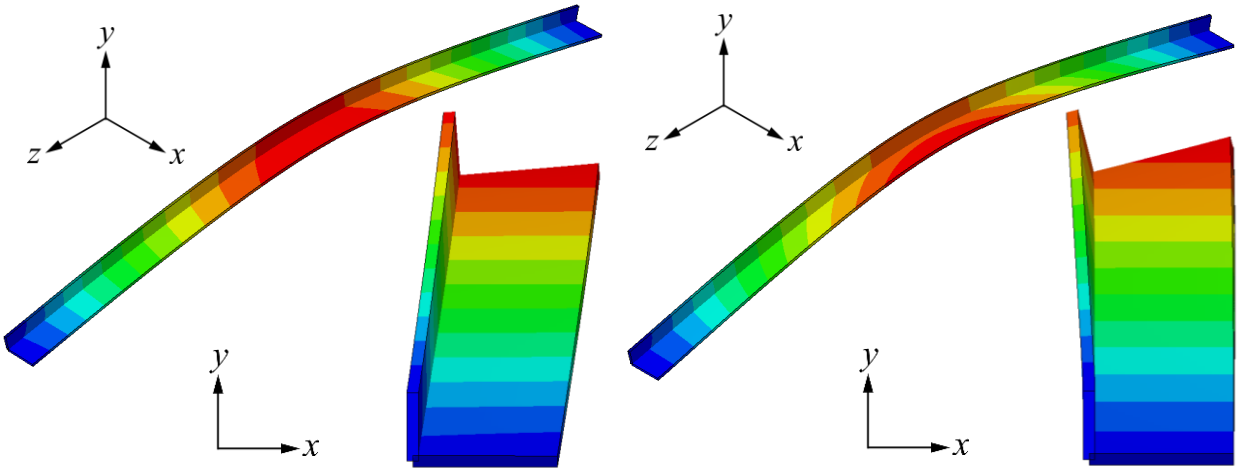

Pinned connection Gusset plate connection

(a)

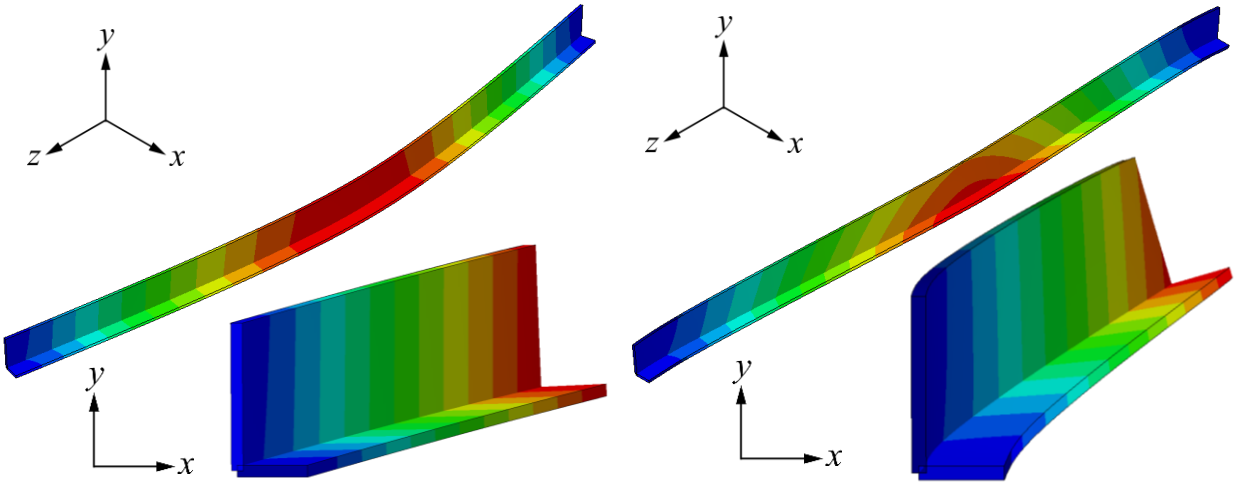

Pinned connection Gusset plate connection

(b)

Figure 4.5 Deformed configurations (magnification factor=2.0) for members with (a) $b_y/b_x = 0.5$ and (b) $b_y/b_x = 2.0$

4.5.2. Effect of residual stresses

The effect of residual stresses on the compressive resistance of eccentrically loaded angle members is investigated by varying the amplitude $-\beta_1 = +\beta_2 = -\beta_3$ of the three-point residual stress pattern depicted in Figure 4.3a from 0.05 to 0.30. The member modelled have a L152x152x16 cross-section and is connected to a gusset plate with $t_g = 15.9$ mm at both ends. The slenderness ratios L/r_x considered range from 50 to 200. The members are subjected to eccentric loads acting at

$e_x = 0$ and $e_y = y_S - 0.5\left(t + t_g\right)$.The compressive resistance P_r of a member with initial residual stresses is normalized relative to the compressive resistance P_{nr} of an identical member with no residual stresses.

The normalized compressive resistance P_r/P_{nr} shown Figure 4.6a negligibly reduces as the amplitude β of the residual stress increases. The reduction becomes more pronounced for members with lower slenderness L/r_x. The lowest normalized compressive resistance $P_r/P_{nr} \approx 0.98$ corresponds to a member with a $L/r_x = 50$ with a peak residual stress value of $0.3F_y$ while members with $L/r_x = 200$ show no reduction in resistance due to residual stresses. Because of the insignificant effect of residual stresses, they will be omitted from the remaining part of the study. It was also found that the omission of residual stresses from the analysis enables the use of a coarser finite element mesh, as each leg can be modelled with only seven elements along the width (as opposed to twenty elements) with no loss in accuracy.

4.5.3. Effect of initial out-of-straightness

The members defined in Section 4.5.2 are investigated to determine the effect of initial out-of-straightness on the compressive resistance of eccentrically loaded angle members. The initial out-of-straightness amplitude α is varied from $L/2000$ to $L/250$. The compressive resistance P_i of an imperfect member is normalized to the compressive resistance P_{ni} of an identical perfectly straight member.

Figure 4.6b shows that the normalized compressive resistance P_i/P_{ni} decreases as the amplitude of initial out-of-straightness α increases. The lowest $P_i/P_{ni} = 0.81$ corresponds to a member with $L/r_x = 50$ and $\alpha = L/250$. For a member with an identical level of initial out-of-straightness

amplitude but with $L/r_x = 200$, P_i/P_{ni} slightly increases to 0.84. The effect of slenderness ratio L/r_x on the normalized compressive resistance strength P_i/P_{ni}, however, seems to fade away as α reduces. For members with $\alpha = L/1000$, P_i/P_{ni} is nearly 0.95 for all slenderness ratios. The initial out-of-straightness amplitude $\alpha = L/1000$, is the maximum allowed amplitude in typical steel members according to CSA S16-19 and will therefore be considered in the remaining part of the analysis.

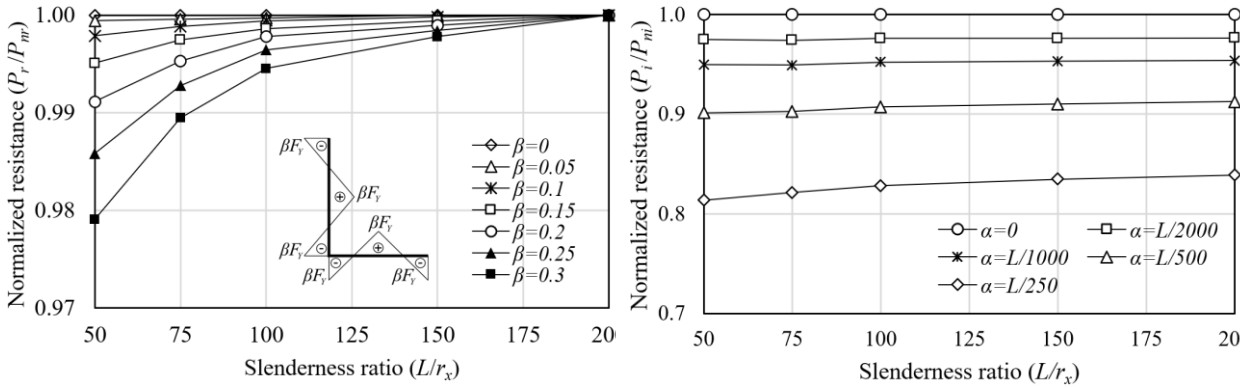

(a) (b)

Figure 4.6 (a) Effect of residual stresses amplitude β on the normalized compressive resistance P_r/P_{nr} and (b) Effect of initial out-of-straightness amplitude α on the normalized compressive resistance P_i/P_{ni}.

4.6. Parametric study

The model developed is used to generate a database of the compressive resistance for over 900 members with end gusset plate details. The database covers slenderness ratios L/r_x ranging from 25 to 200, leg width ratios b_y/b_x ranging from 0.5 to 2.0, connected leg width-to-thickness ratios b_x/t ranging from 4.5 to 14.0 and gusset plate-to-angle thickness ratios t_g/t ranging from 1.0 to 2.0. The members are subjected to an eccentric load acting at $e_x = 0$ and $e_y = y_S - 0.5\left(t + t_g\right)$. For all members, an initial out-of-straightness amplitude $\alpha = L/1000$ is taken based on the fundamental buckling mode of an identical member under pure compression. Steel is assumed to

be elastic perfectly plastic with $F_Y = 350$ MPa, $E = 200,000$ MPa and $\mu = 0.3$. The compressive resistance of an eccentrically loaded member P_e is normalized relative to its yield strength of the cross-section $P_Y = F_Y A$. The results are summarized in Appendix 4.C.

The database is used to (i) investigate the effect of L/r_x, b_y/b_x, b_x/t and t_g/t parameters on the compressive resistance of angle members, (ii) develop a design expression to adequately predict the compressive resistance of such members, and (iii) compare the predictions of the proposed design expressions against available solutions in CSA S16-19 for eccentrically loaded single angle members.

4.6.1. Effect of the geometric parameters

Three sets of runs were selected from the database with the input parameters summarized in Table 4.4. The normalized compressive resistance P_e/P_Y versus slenderness ratio L/r_x is depicted in Figure 4.7a-c. Figure 4.7a shows that P_e/P_Y increases as b_y/b_x increases from 0.5 to 1.0 whereas it decreases when b_y/b_x increases from 1.0 to 2.0. For members with $L/r_x = 200$, the P_e/P_Y ratio for a member with $b_y/b_x = 1.0$ to that for a member with $b_y/b_x = 0.5$ is 1.03. This ratio increases to 1.20 when the slenderness ratio of the members reduces to 50. Conversely, the P_e/P_Y for a member with $L/r_x = 200$ and $b_y/b_x = 1.0$ to that for an equivalent member with $b_y/b_x = 2.0$ is 1.50 . The ratio reduces to 1.18 for $L/r_x = 50$.

An insignificant change in P_e/P_Y is observed when b_x/t is varied (Figure 4.7b). The effect of b_x/t on P_e/P_Y is directly influenced by L/r_x. As b_x/t decreases, P_e/P_Y was found to decrease when $L/r_x = 50$ but increase when $L/r_x = 200$.

Figure 4.7c depicts a decrease in P_e/P_Y as t_g/t increases. This is expected since the increase in t_g/t leads to an increase in the load eccentricity e_y. The influence of t_g/t (i.e., e_y) is more pronounce in short members (i.e., $L/r_x = 50$). The P_e/P_Y ratio for a member with $t_g/t = 1.0$ to that for an identical member with $t_g/t = 2.0$ ranges from 1.03 to 1.09.

In conclusion, the normalized compressive resistance is highly dependent on the b_y/b_x ratio. The second most influential parameter is the gusset plate-to-angle thickness ratio t_g/t and the least influential parameter is the width-to-thickness ratio b_x/t.

Table 4.4 Geometrical parameters for the considered members

run series	Sectional dimensions (mm)					Dimensionless parameters			
	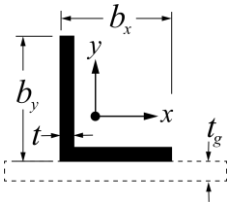					Slenderness	Leg width	Connected leg width-to- thickness	Gusset plate-to-angle thickness
	b_y	b_x	t	t_g	L	L/r_x	b_y/b_x	b_x/t	t_g/t
1	102	203	15.9	15.9	1360-5438	50-200	0.5	12.8	1.0
	127	178	15.9	15.9	1842-7367		0.7	11.2	
	152	152	15.9	15.9	2330-9321		1.0	9.6	
	178	127	15.9	15.9	2818-11273		1.4	8.0	
	203	102	15.9	15.9	3253-13013		2.0	6.4	
2	152	152	12.7	12.7	2354-9416	50-200	1.0	12.0	1.0
	152	152	15.9	15.9	2330-9321			9.6	
	152	152	19.0	19.0	2308-9231			8.0	
	152	152	22.2	22.2	2285-9140			6.8	
3	152	152	15.9	15.9	2330-9321	50-200	1.0	9.6	1.0
	152	152	15.9	19.0					1.2
	152	152	15.9	22.2					1.4
	152	152	15.9	25.4					1.6
	152	152	15.9	28.6					1.8
	152	152	15.9	31.8					2.0

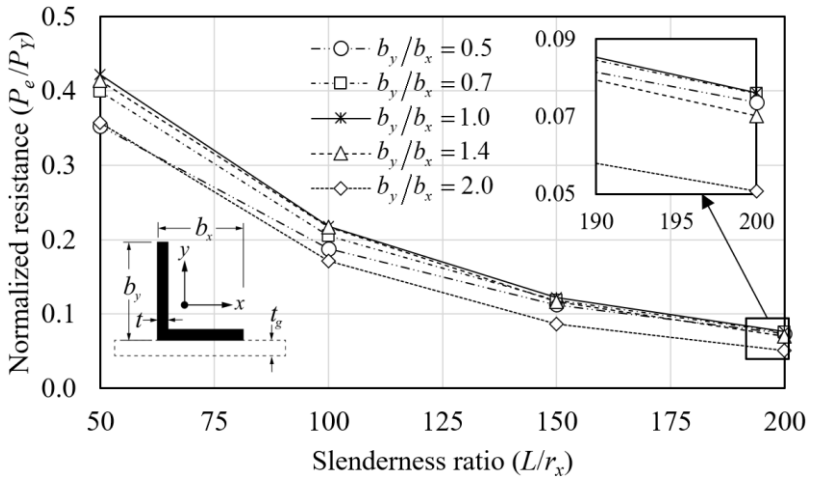

(a)

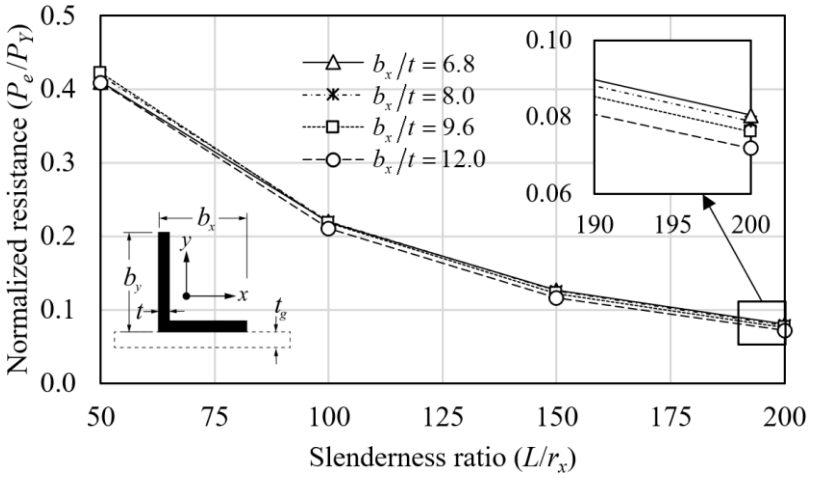

(b)

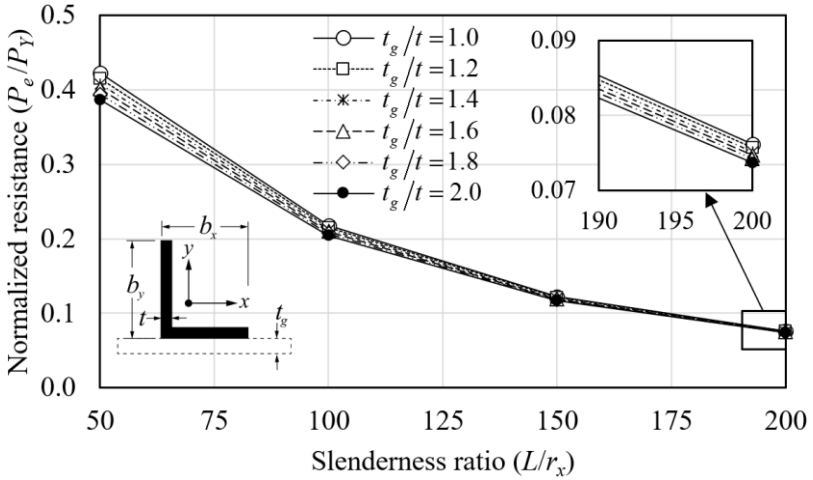

(c)

Figure 4.7 Normalized compressive resistance P_e/P_Y versus slenderness ratio L/r_x for members with (a) leg width ratios $b_y/b_x = 0.5-2.0$ (b) connected leg width-to-thickness ratios $b_x/t = 6.8-12.0$ and (c) gusset plate-to-angle thickness ratios $t_g/t = 1.0-2.0$

4.6.2. Proposed design expressions

The design expression sought herein is in a form of a reduction factor Ω that is to be applied to the yield load P_Y, i.e.,

$$P_d = \Omega P_Y \tag{4.10}$$

Since the reduction factor Ω is developed based on the generated database using the developed finite element shell model, it captures material nonlinear effects and geometric non-linear effects (and hence the slenderness), non-principal end restraints and load eccentricity.

4.6.2.1. Reduction factor

The normalized compressive resistance P_e/P_Y of 936 cases (Appendix 4.C) with $L/r_x = 25-200$, $b_y/b_x = 0.5-2.0$, $b_x/t = 4.5-14.0$ and $t_g/t = 1.0-2.0$ are used to fit a regression function $\Omega\left(L/r_x, b_y/b_x, b_x/t, t_g/t\right)$ to approximately predict P_e/P_Y. A non-linear regression analysis is performed by the symbolic regression analysis software TuringBot (2020). In line with the conclusion reached in Section 4.6.1, regression results suggested that b_x/t parameter has an insignificant influence on the reduction factor Ω function sought in comparison to the three parameters $b_r = b_y/b_x, l_r = L/r_x, t_r = t_g/t$, and thus was omitted for the regression for simplicity. The function Ω obtained can be expressed as:

$$\Omega = 1.0 - \begin{cases} \dfrac{\left(199-103b_r\right)\left(t_r/l_r+0.050\right)+l_r}{0.88l_r+46.8} & b_r \le 1.0 \\ \dfrac{\left(53.6b_r-2.35\right)\left(t_r/l_r+0.12\right)+l_r}{0.83l_r+56.9} & b_r > 1.0 \end{cases} \tag{4.11)a,b}$$

Equation (4.11)a has a coefficient of determination of 0.99 and ensures that $\Omega P_Y/P_e$ has a mean value of 1.00 with a standard deviation of 0.062, and a corresponding coefficient of variation of

6.16%. Equation (4.11)b has a coefficient of determination of 0.99, and ensures that $\Omega P_Y / P_e$ has a mean value of 1.00, a standard deviation of 0.080 and a coefficient of variation of 7.96%. Both equations overestimate the FEA predicted compressive strength nearly 54% of the time. For a design-oriented lower bound solution, function Ω can be multiplied by a resistance factor. For example, the resistance

$$P_{dr} = 0.88\Omega P_Y \tag{4.12}$$

would overpredict the resistance estimated by the FEA for 0.75% of the cases when $b_r \le 1.0$ and for 3.2% of the cases when $b_r > 1.0$. It is noted that Eqs. (4.11) and (4.12) are limited to members with end restraints pinned about the x axis and fixed about the y axis and relative to twist with $L/r_x = 25-200$, $b_y/b_x = 0.5-2.0$, $b_x/t = 4.5-14.0$ and $t_g/t = 1.0-2.0$.

4.6.2.2. Illustrative design example

A diagonal bracing system has a 5m diagonal member with L203x152x19 cross-section. The member is made of CSA G40.21 grade 350W steel ($F_Y = 350$ MPa). Using the design expressions developed in the present study, it is required to calculate the compressive resistance of the member when connected to a 22.2 mm thick gusset plate at both ends (a) through the longer leg, and (b) through the shorter leg.

Solution:

The yield strength of the cross-section is determined as $P_Y = F_Y A = 350 \times 6384 \times 10^{-3} = 2234$ kN.

(a) For the case where the member is connected to a gusset plate by the longer leg, Ω is calculated based on Eq. (4.11)a. The relevant dimensionless parameters $l_r = L/r_x = 112.5$, $b_r = b_y/b_x = 0.75$ and $t_r = t_g/t = 1.17$ are determined from Eq. (4.11)a yielding a value of $\Omega = 0.178$. The corresponding best estimate of the compressive resistance of the member is

$P_d = 0.178 \times 2234 = 397$ kN. It is associated with a probability of about 50% of being exceeded by the FEA model prediction. The more conservative estimate $P_{dr} = 0.88 \times 397 = 350$ kN would be associate with a 0.75% probability of being exceeded by the FEA model prediction. In comparison, the compressive resistance of the member as determined from the finite element model is $P_e = 395$, i.e., in this case, $P_d / P_e = 1.005$.

(b) For the case where the member is connected to a gusset plate by the shorter leg, Ω is determined from Eq. (4.11)b. The relevant parameters $l_r = L/r_x = 78.1$, $b_r = b_y / b_x = 1.34$ and $t_r = t_g / t = 1.17$ are substituted into Eq. (4.11)b yielding $\Omega = 0.281$. The corresponding compressive resistance of the member associated with a probability of about 50% of being exceeded by the FEA model prediction is $P_d = 0.284 \times 2234 = 628.5$ kN whereas the conservative estimate associated with 3.2% probability of being exceeded by the FEA model prediction is $P_{dr} = 0.88 \times 628.5 = 553$ kN. The compressive resistance of the member as estimated from the finite element model is $P_e = 651$ kN leading to $P_d / P_e = 0.965$.

4.6.3. Comparison against present standard solutions

The compressive resistance predicted by the design expression proposed herein is evaluated against available solutions in CSA S16-19 for select cases (Table 4.5). The comparison involves: (a) The resistance P_{dr} predicted by the proposed design expression (Eq. (4.12)), (b) The resistance P_s predicted by the effective slenderness ratio expression (Eqs.(4.1)-(4.4)) , (c) The resistance P_b predicted by the beam-column interaction equation (Eqs.(4.5)-(4.9)), and (d) The resistance P_e predicted by ABAQUS based on the developed finite element model. The compressive resistance P_d, P_s or P_b is normalized to the FEA-predicted resistance P_e .

It is noted that the effective slenderness method is inapplicable for members with L203x102x22 cross-sections (i.e., $b_l/b_s > 1.7$) and for the member with a slenderness $L/r_{min} = 200$ and a L178x127x22 cross-section connected to a gusset plate by the shorter leg for which, the calculated effective slenderness ratio KL/r is larger than 200. For these cases, the compressive resistance P_s is thus not provided in Table 4.5. For the remaining cases, the normalized compressive resistance ratio P_s/P_e ranges from 0.64 to 1.19, with an average value of 0.94 and a standard deviation of 0.14. The effective slenderness method for these cases is found to overestimate the member resistance for 25% of the cases. It is also realized that the method does not incorporate the effect of various load eccentricities. This is reflected in Table 4.5 by providing identical compressive resistance P_s for identical members with different load eccentricities (i.e., $t_g/t = 1.0$ and 2.0).

Unlike the effective slenderness method, the resistance P_b based on the beam-column interaction equation is applicable to all cases. The normalized compressive resistance P_b/P_e ranges from 0.20 to 0.85 with an average value of 0.49 and a standard deviation of 0.22. It is found that P_b/P_e grossly decreases as the leg width ratio b_y/b_x increases. The average P_b/P_e ratio for members with L152x152x22 is 0.50. The ratio further reduces to 0.29 for L178x127x22 and 0.22 for L203x102x22 members, both connected to gusset plates by their shorter legs. The underprediction of the resistance is attributed, for the most part, to the pin-end boundary condition assumed when determine the elastic buckling load and critical moments induced by the eccentricity, whereas the true end restraints are pinned about the x axis and fixed about the y axis. Also, the amplification factors based on Euler buckling loads for pin-end conditions may inaccurately capture the actual second-order effect arising from the angle-gusset plate end connection as the member is not

expected to buckle in a pure sinusoidal wave about the principal axes, as is the case for pin-end condition.

Table 4.5 Geometric parameters and compressive resistance

Cross-section	Geometric parameters [1]			Compressive resistance (kN)				Ratios		
	b_y/b_x	L/r_{min}	t_g/t	P_s [2]	P_b [3]	P_{dr} [4]	P_e [5]	P_s/P_e	P_b/P_e	P_{dr}/P_e
L152x152x22	1.0	100	1.0	713	378	615	763	0.93	0.50	0.81
			2.0	713	347	587	684	1.04	0.51	0.86
		150	1.0	484	249	435	507	0.95	0.49	0.86
			2.0	484	233	420	465	1.04	0.50	0.90
		200	1.0	318	171	315	350	0.91	0.49	0.90
			2.0	318	162	306	327	0.97	0.50	0.94
L178x127x22	0.7	100	1.0	647	402	516	622	0.99	0.65	0.83
			2.0	647	365	487	542	1.19	0.67	0.90
		150	1.0	391	252	347	398	0.98	0.63	0.87
			2.0	391	233	332	360	1.09	0.65	0.92
		200	1.0	NA	173	238	272	NA	0.64	0.88
			2.0	NA	163	229	252	NA	0.65	0.91
	1.4	100	1.0	793	277	767	883	0.90	0.31	0.87
			2.0	793	254	737	815	0.97	0.31	0.90
		150	1.0	539	186	576	682	0.79	0.27	0.84
			2.0	539	173	560	633	0.85	0.27	0.88
		200	1.0	323	144	438	503	0.64	0.29	0.87
			2.0	323	136	427	473	0.76	0.29	0.90
L203x102x22	0.5	100	1.0	NA	386	460	507	NA	0.76	0.91
			2.0	NA	340	430	428	NA	0.79	1.00
		150	1.0	NA	255	300	330	NA	0.77	0.91
			2.0	NA	233	285	291	NA	0.80	0.98
		200	1.0	NA	187	198	229	NA	0.82	0.86
			2.0	NA	176	188	207	NA	0.85	0.91
	2.0	100	1.0	NA	224	815	901	NA	0.25	0.90
			2.0	NA	207	743	845	NA	0.24	0.88
		150	1.0	NA	166	666	764	NA	0.22	0.87
			2.0	NA	155	625	720	NA	0.22	0.87
		200	1.0	NA	122	544	623	NA	0.20	0.87
			2.0	NA	116	517	594	NA	0.20	0.87
							Mean =	0.94	0.49	0.89
							Standard Deviation =	0.14	0.22	0.04
							Coefficient of Variation (%) =	14.8	44.0	4.35

[1] L/r_{min} = slenderness ratio relative to the minor axis; b_y/b_x =Leg width ratio; t_g/t = Gusset plate-to-angle thickness ratio.

[2] P_s = Compressive resistance based on the effective slenderness method.

[3] P_b = Compressive resistance based on the beam-column interaction equation.

[4] P_{dr} =Compressive resistance based on the developed design expressions.

[5] P_e =Compressive resistance based on the shell finite element model.

NA= The effective slenderness method is not applicable for members with $b_l/b_s > 1.7$ and $KL/r > 200$

The resistance P_{dr} based on the proposed methodology correspond to a ratio P_{dr}/P_e ranging from 0.80 to 1.00 with an average value of 0.90 and a standard deviation of 0.05. The method is found to slightly err on the conservative side for all cases considered in Table 4.5. The method also offers an advantage in terms of simplicity when compared to the interaction relation method. However, while the beam-column solution is applicable to all angle member geometries and load eccentricities, the present method is limited to angle members with $L/r_x = 25-200$, $b_x/t = 4.5-14.0$ and load eccentricities $e_x = 0$ and $e_y = y_S - 0.5\left(t + t_g\right)$ in which, $t_g/t = 1.0-2.0$.

4.7. Summary and conclusions

The present study developed a 3D shell-based finite element model to predict the compressive resistance of eccentrically loaded single angle members with gusset plate end connections. The model incorporated geometric and material non-linear effects. The model was validated against reported experimental results and used to investigate the effects of non-principal end restraints, initial out-of-straightness, and residual stresses. The model was then used to generate a database of over 900 cases with slenderness ratios ranging from 25 to 200, leg width ratios ranging from 0.5 to 2.0, connected leg width-to-thickness ratios ranging from 4.5 to 14.0 and gusset plate-to-angle thickness ratios ranging from 1.0 to 2.0. The database was used to investigate the effects of these parameters on the compressive resistance of the members. The database was subsequently used to develop an empirical design equation. The predictions of the design equation were then compared with those based on the available solutions in CSA S16-19. The following conclusions can be drawn from the study

1. Members with end gusset plate connections possess a significantly larger compressive resistance compared to the idealized case of pin-end restraints. The resistance gain peaks in

members with larger slenderness $L/r_x = 200$ and with an unconnected-to-connected leg ratio of $b_y/b_x = 2.0$

2. While the magnitude of initial out-of-straightness can significantly affect the angle members, the influence of residual stresses was shown to be insignificant.
3. The normalized compressive resistance P_e/P_Y is highly influenced by the slenderness ratio L/r_x , followed by the leg width ratio b_y/b_x and to a lesser extent by the gusset plate-to-angle thickness ratio t_g/t while the effect of the connected leg width-to-thickness ratio b_x/t is negligible.
4. The proposed design method based on the developed reduction factor Ω provides a simple determination of the compressive resistance of the angles while maintaining an adequate level of accuracy.
5. The effective slenderness method implemented in CSA S16-19 does not incorporate the effect of various load eccentricities and can overestimate the compressive resistance of angles.
6. The beam-column interaction method in CSA S16-19 underestimates the compressive resistance of single angle members. The underestimation of the resistance grossly grows with the leg width ratio.

Notation

A	Cross-sectional area	P_d, P_{dr}	Compressive resistance based on the proposed design method
b_l, b_s	Long and short leg width	P_e	Compressive resistance based on the developed finite element model
b_x, b_y	Leg width along x, y axes	$P_{e\hat{x}}, P_{e\hat{y}}$	Euler buckling loads with respect to the principal axes
E	Modulus of elasticity	P_i, P_{ni}	Compressive resistance for members with and without initial out-of-straightness, respectively
e_x, e_y	Load eccentricities along the non-principal axes x, y	P_n	Nominal compressive resistance
$e_{\hat{x}}, e_{\hat{y}}$	Load eccentricities along the principal axes $\hat{x}, \hat{y}$	P_p	Compressive resistance for pin-ended members
F_e	Elastic stress	P_r, P_{nr}	Compressive resistance for members with and without residual stresses, respectively
F_Y	Yield stress	P_s	Compressive resistance based on the effective slenderness method
$I_{\hat{x}\hat{x}}, I_{\hat{y}\hat{y}}$	Principal moments of inertia	P_t	Compressive resistance based on test results
(KL/r)	Effective slenderness ratio	P_Y	Yield load
$(K_{\hat{x}}L/r_{\hat{x}})$	Slenderness ratio about $\hat{x}$ axis	t	Angle thickness
L	Span	t_g	Gusset plate thickness
(L/r_x)	Slenderness ratio about x axis	x, y	Non-principal axes
(L/r_{min})	Minimum slenderness ratio	$\hat{x}, \hat{y}$	Principal axes
$M_{n\hat{x}-i}$	Nominal moment resistance about the minor principal axis $\hat{x}$ at point i	$\hat{x}_i, \hat{y}_i$	Principal coordinates for point i
$M_{n\hat{y}-i}$	Nominal moment resistance about the major principal axis $\hat{x}$ at point i	$y_S, \hat{y}_S$	Shear centre coordinates along $y, \hat{y}$ axes
$M_{U\hat{y}}$	elastic lateral-torsional buckling moment	α	Initial out-of-straightness amplitude
$M_{Y\hat{y}-i}$	elastic yield sectional resistance of point i about the major axis	β_i	Residual stress amplitude at point $i(i=1,2,3)$
P	Applied load	$\beta_{\hat{y}}$	The symmetry parameter
P_b	Compressive resistance based on beam-column interaction equation	μ	Poisson's ratio
P_c	Compressive resistance for concentrically loaded members	Ω	Reduction factor

References

Alenezi, A. M. and Mohareb, M. (2021). "Buckling solutions for compression members with end restraints defined along non-principal directions." *J. Constr. Steel Res.*, 181, 106505.

Bathon, L., Mueller III, W. H. and Kempner Jr, L. (1993). "Ultimate load capacity of single steel angles." *J. Struct. Eng*., 119(1), 279-300.

Behzadi-Sofiani, B., Gardner, L., Wadee, M. A., Dinis, P. B. and Camotim, D. (2021a). "Behaviour and design of fixed-ended steel equal-leg angle section columns." *J. Constr. Steel Res.*, 182, 106649.

Behzadi-Sofiani, B., Gardner, L. and Wadee, M. A. (2021b). "Stability and design of fixed-ended stainless steel equal-leg angle section compression members." *Eng. Struct.*, 249, 113281.

Bezas, M. Z., Demonceau, J. F., Vayas, I. and Jaspart, J. P. (2021). "Experimental and numerical investigations on large angle high strength steel columns." *Thin Wall. Struct.*, 159, 107287.

Bhilawe, J. V. and Gupta, L. M. (2015). "Experimental investigation of steel equal angle subjected to compression." *Eng. Struct. Tech*., 7(2), 55-66.

Branquinho, M. Á. and Malite, M. (2021). "Effective slenderness ratio approach for thin-walled angle columns connected by the leg." *J. Constr. Steel Res.*, 176, 106434.

Cao, K., Guo, Y. J. and Zeng, D. W. (2015). "Buckling behavior of large-section and 420 MPa high-strength angle steel columns." *J. Constr. Steel Res.*, 111, 11-20.

Dinis, P. B. and Camotim, D. (2015). "A novel DSM-based approach for the rational design of fixed-ended and pin-ended short-to-intermediate thin-walled angle columns." *Thin Wall. Struct.*, 87, 158-182.

Dinis, P. B., Santana, K. G., Landesmann, A. and Camotim, D. (2021). "Numerical and experimental study on CFS spherically-hinged equal-leg angle columns: stability, strength and DSM design." *Thin Wall. Struct.*, 161, 106862.

Fasoulakis, Z. C., Lignos, X. A., Avraam, T. P. and Katsatsidis, S. P. (2019). "Investigation on single-bolted cold-formed steel angles with geometric imperfections under compression." *J. Constr. Steel Res.*, 162, 105733.

Huang, Z., Liu, H., Liu, H. and Li, Z. (2021). "Experimental study on stability behavior of equal-leg angle steel columns. *Thin Wall. Struct.*, 166, 108042.

Hussain A., Liu Y. P. and Chan S. L. (2018). "Finite Element Modeling and Design of Single Angle Member Under Bi-axial Bending." *Struct.*, 16, 373-389.

Kettler, M., Taras, A. and Unterweger, H. (2017). "Member capacity of bolted steel angles in compression–Influence of realistic end supports." *J. Constr. Steel Res.*, 130, 22-35.

Kettler, M., Lichtl, G. and Unterweger, H. (2019). "Experimental tests on bolted steel angles in compression with varying end supports." *J. Constr. Steel Res.*, 155, 301-315.

Kettler, M., Unterweger, H. and Zauchner, P. (2021). "Design model for bolted angle members in compression including joint stiffness." *J. Constr. Steel Res.*, 184, 106778.

Liu, Y. and Chantel, S. (2011). "Experimental study of steel single unequal-leg angles under eccentric compression." *J. Constr. Steel Res.*, 67(**6**), 919-928.

Liu, Y. and Hui, L. (2008). "Experimental study of beam–column behaviour of steel single angles." *J. Constr. Steel Res.*, 64(**5**), 505-514.
Liu Y. and Hui L. (2010b). "Finite element study of steel single angle beam-columns." *Eng. Struct.*, 32, 2087-2095.
Liu Y. and Chantel S. (2011). "Experimental study of steel single unequal-leg angles under eccentric compression." *Can. J. Eng.*, 67, 919-928.
Lutz, L. A. (1992). "Critical slenderness of compression members with effective Lengths about non-principal axes." In *Proc. Annual Technical Session and Meeting of the Structural Stability Research Council*, Bethlehem, PA, 107-116.
Može, P., Cajot, L. G., Sinur, F., Rejec, K. and Beg, D. (2014). "Residual stress distribution of large steel equal leg angles." *Eng. Struct.*, 71, 35-47.
Popovic, D., Hancock, G. J. and Rasmussen, K. J. (2001). "Compression tests on cold-formed angles loaded parallel with a leg." *J. Struct. Eng.*, 127(**6**), 600-607.
Rasmussen, K. J. (2005). "Design of angle columns with locally unstable legs." *J. Struct. Eng.*, 131(**10**), 1553-1560.
Rasmussen, K. J. (2006). "Design of slender angle section beam-columns by the direct strength method." *J. Struct. Eng.*, 132(**2**), 204-211.
Sarquis, F. R., de Lima, L. R. O., da S Vellasco, P. C. G. and Rodrigues, M. C. (2020). "Experimental and numerical investigation of hot-rolled stainless steel equal leg angles under compression." *Thin Wall. Struct.*, 151, 106742.
Silvestre, N., Dinis, P. B. and Camotim, D. (2013). "Developments on the design of cold-formed steel angles." *J. Struct. Eng.*, 139(**5**), 680-694.
Spiliopoulos, A., Dasiou, M. E., Thanopoulos, P. and Vayas, I. (2018). "Experimental tests on members made from rolled angle sections." *Steel Constr.*, 11(**1**), 84-93.
Stang, A. H. and Strickenberg, L. R. (1922). "Results of some compression tests of structural steel angles.", *No. 218*. US Government Printing Office.
Temple, M. C., Petretta, D. M. and Morand, C. (1995). "Influence of the assumed effective length factor on the load carrying capacity of steel angles in compression." *Can. J. Civ. Eng.,* 22, 1171-1177.
Temple, M. C. and Sakla, S. S. S. (1998a). "Single-angle compression members welded by one leg to a gusset plate. I. Experimental study." *Can. J. Civ. Eng.,* 25, 569-584.
Temple, M. C. and Sakla, S. S. S. (1998b). "Single-angle compression members welded by one leg to a gusset plate. II. A parametric study and design equation." *Can. J. Civ. Eng.,* 25, 585-594.
TuringBot. (2020). "Symbolic regression software-TuringBot", < https://turingbotsoftware.com> (accessed Feb. 2, 2022)

Appendix 4.A. Asymmetry parameter calculation for angle cross-sections

This appendix provides an expression to calculate the asymmetry parameter for unequal-leg angles.

The asymmetric parameter $\beta_{\hat{y}}$ relative to the major principal axis $\hat{y}$ is calculated from

$$\beta_{\hat{y}} = \frac{1}{I_{\hat{y}\hat{y}}}\int_A \hat{x}\left(\hat{x}^2+\hat{y}^2\right)dA - 2\hat{x}_S = \frac{t}{I_{\hat{y}\hat{y}}}\left(H_1\sin\phi + H_2\cos\phi\right) - 2\hat{x}_S \tag{4.A.1}$$

where

$$H_1 = \frac{1}{2}\tilde{b}_y^2\left(x_S^2+3y_S^2\right)+\left(\tilde{b}_y+\tilde{b}_x\right)\left(x_S^2+y_S^2\right)y_S+\tilde{b}_x^2\left(\frac{1}{3}\tilde{b}_x+x_S\right)y_S+\tilde{b}_y^3\left(\frac{1}{4}\tilde{b}_y+y_S\right)$$
$$H_2 = \frac{1}{2}\tilde{b}_x^2\left(y_S^2+3x_S^2\right)+\left(\tilde{b}_y+\tilde{b}_x\right)\left(y_S^2+x_S^2\right)x_S+\tilde{b}_y^2\left(\frac{1}{3}\tilde{b}_y+y_S\right)x_S+\tilde{b}_x^3\left(\frac{1}{4}\tilde{b}_x+x_S\right) \tag{4.A.2)a,b}$$

in which, x_S and y_S are the shear centre coordinates along the x and y axes, $\tilde{b}_x$ and $\tilde{b}_y$ are the centre line leg width along the x and y axes, and t is the angle thickness (Figure 4.8).

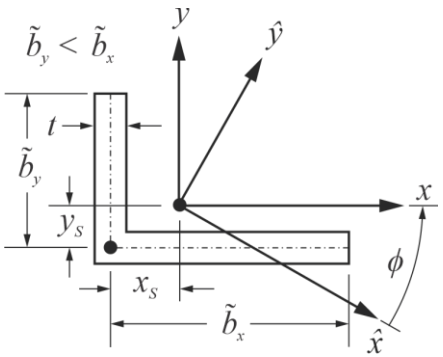

Figure 4.8 unequal-leg angle cross-sections

Appendix 4.B. Sample Calculation for compressive member capacity based on the beam-column interaction equation

This appendix shows how to estimate the compressive resistance of eccentrically loaded angle members using the beam-column interaction equation in accordance with CSA S16-19.

4.B.1 Illustrative example

A compression member with L203x102x22 and a 4m span is connected to a 44.4 mm thick gusset plate through the longer leg. The member is subjected to a compressive load acting at $e_x = 0$ and $e_y = y_S - 0.5(t + t_g) = -47.9$ mm . The member is made of steel with a yield stress $F_Y = 350$ MPa and a modulus of elasticity $E = 200,000$ MPa. It is required to calculate the compressive resistance of the member based on CSA S16-19 requirements.

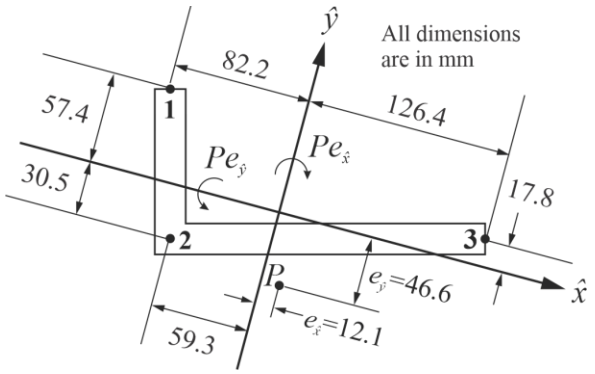

Figure 4.9 Load and critical points coordinates

Solution

Since the long-to-short leg ratio of the angle is larger than 1.7, the effective slenderness method is not applicable. Thus, the nominal compressive resistance of the member is obtained from satisfying the interaction equation, Eq. (4.5). The equation is based on the principal axes $\hat{x}, \hat{y}$ and hence the load eccentricities in Figure 4.9 are expressed relative to the $\hat{x}, \hat{y}$ axes leading to $e_{\hat{x}} = 12.1$ mm and $e_{\hat{y}} = 46.6$ mm .

The Euler buckling loads about the principal axes are calculated as

$$P_{e\hat{x}} = \frac{\pi^2 E I_{\hat{x}\hat{x}}}{L^2} = \frac{\pi^2 (200{,}000)(2{,}838{,}000)}{(4000)^2} = 350 \text{ kN} \tag{4.B.1}$$

$$P_{e\hat{y}} = \frac{\pi^2 E I_{\hat{y}\hat{y}}}{L^2} = \frac{\pi^2 (200{,}000)(27{,}320{,}000)}{(4000)^2} = 3{,}370 \text{ kN} \tag{4.B.2}$$

The nominal compressive resistance P_n in the absence of moments is calculated from Eq. (4.4) based on the lowest elastic buckling stress F_e obtained from Eq. (4.6), i.e.,

$$P_n = 6278 \times 350 \left[1 + (350/54.9)^{1.34} \right]^{-1/1.34} = 325 \text{ kN} \tag{4.B.3}$$

The lateral tortional moment $M_{U\hat{y}}$ is calculated from Eq. (4.9) as

$$\begin{aligned} M_{U\hat{y}} &= \frac{4.9 E I_{\hat{x}}}{L^2} \left(\sqrt{\beta_{\hat{y}}^2 + 0.052 \left(\frac{Lt}{r_{\hat{x}}} \right)^2} + \beta_{\hat{y}} \right) \\ &= \frac{4.9 \times 200{,}000 \times 2{,}838{,}000}{(4{,}000)^2} \left(\sqrt{(-137.8)^2 + 0.052 \left(\frac{4{,}000 \times 22.2}{21.3} \right)^2} - 137.8 \right) \\ &= 141{,}300 \text{ kNmm} \end{aligned} \tag{4.B.4}$$

The nominal moments resistance about the minor and major principal axes $M_{n\hat{x}-i}, M_{n\hat{y}-i}$, respectively, are calculated at the points 1-3 shown in Figure 4.9, i.e.,

Point	$\hat{y}_i$ (mm)	$\hat{x}_i$ (mm)	$M_{n\hat{x}-i} = (I_{\hat{x}\hat{x}} / \hat{y}_i) F_Y$ (kNmm)	$M_{Y\hat{y}-i} = (I_{\hat{y}\hat{y}} / \hat{x}_i) F_Y$ (kNmm)	$M_{n\hat{y}-i} = \left(1 - 0.79 \frac{M_{Y\hat{y}-i}}{M_{U\hat{y}}} \right) 1.15 M_{Y\hat{y}-i}$ (kNmm)
1	57.4	82.2	17,300	116,300	46,780
2	30.5	59.3	32,570	161,200	18,300
3	17.8	126.4	55,800	75,650	50,200

By substituting P_n, $P_{e\hat{x}}$, $P_{e\hat{y}}$, $e_{\hat{x}}$, $e_{\hat{y}}$, $M_{n\hat{x}-i}$, $M_{n\hat{y}-i}$ into Eq. (4.5) and taking into consideration the appropriate sign of stresses at each point (positive sign for compression and negative sign for tension), one obtains

Point	Interaction equation	P (kN)
1	$\frac{P}{325}-\left(\frac{1}{1-P/350}\right)\frac{46.6P}{17,300}-\left(\frac{1}{1-P/3,370}\right)\frac{12.1P}{46,780}\le 1.0$	222
2	$\frac{P}{325}+\left(\frac{1}{1-P/350}\right)\frac{46.6P}{32,570}-\left(\frac{1}{1-P/3,370}\right)\frac{12.1P}{18,300}\le 1.0$	185
3	$\frac{P}{325}-\left(\frac{1}{1-P/350}\right)\frac{46.6P}{55,800}+\left(\frac{1}{1-P/3,370}\right)\frac{12.1P}{50,200}\le 1.0$	306

Thus, the governing nominal compressive resistance P is 185 kN.

Appendix 4.C. Database of inelastic Resistances for eccentrically loaded single angle members

This appendix summarizes the compressive resistance values generated for eccentrically loaded single angle members. The results for members with equal-leg angles are presented in Table 4.6 while those for members with unequal-leg angle are presented in Table 4.7 when connected to gusset plate through the longer legs and Table 4.8 when connected through the shorter legs.

Table 4.6 Inelastic compressive resistance database for members with equal-leg angles

Run #	Geometric properties (mm)						Dimensionless parameters				Compressive resistance			
											kN		Ratio	
	b_y	b_x	t	r_x	L	t_g	b_y/b_x	b_x/t	L/r_x	t_g/t	P_e	P_Y	P_e/P_Y	Ω
1	152	152	12.7	47.1	1177	12.7	1.00	12.0	25.0	1.0	604	1295	0.466	0.511
2	152	152	12.7	47.1	1177	19.0	1.00	12.0	25.0	1.5	584	1295	0.451	0.483
3	152	152	12.7	47.1	1177	25.4	1.00	12.0	25.0	2.0	565	1295	0.437	0.455
4	152	152	15.9	46.6	1165	15.9	1.00	9.6	25.0	1.0	801	1603	0.500	0.511
5	152	152	15.9	46.6	1165	25.4	1.00	9.6	25.0	1.6	763	1603	0.476	0.478
6	152	152	15.9	46.6	1165	31.8	1.00	9.6	25.0	2.0	739	1603	0.461	0.455
7	152	152	19.0	46.2	1154	19.0	1.00	8.0	25.0	1.0	953	1895	0.503	0.511
8	152	152	19.0	46.2	1154	28.6	1.00	8.0	25.0	1.5	908	1895	0.479	0.483
9	152	152	19.0	46.2	1154	38.1	1.00	8.0	25.0	2.0	866	1895	0.457	0.455
10	152	152	22.2	45.7	1143	22.2	1.00	6.8	25.0	1.0	1086	2190	0.496	0.511
11	152	152	22.2	45.7	1143	31.8	1.00	6.8	25.0	1.4	1036	2190	0.473	0.487
12	152	152	22.2	45.7	1143	44.4	1.00	6.8	25.0	2.0	974	2190	0.445	0.455
13	152	152	25.4	45.3	1131	25.4	1.00	6.0	25.0	1.0	1194	2477	0.482	0.511
14	152	152	25.4	45.3	1131	38.1	1.00	6.0	25.0	1.5	1128	2477	0.456	0.483
15	152	152	25.4	45.3	1131	50.8	1.00	6.0	25.0	2.0	1062	2477	0.429	0.455
16	152	152	12.7	47.1	2354	12.7	1.00	12.0	50.0	1.0	529	1295	0.409	0.375
17	152	152	12.7	47.1	2354	19.0	1.00	12.0	50.0	1.5	512	1295	0.395	0.365
18	152	152	12.7	47.1	2354	25.4	1.00	12.0	50.0	2.0	494	1295	0.382	0.354
19	152	152	15.9	46.6	2330	15.9	1.00	9.6	50.0	1.0	677	1603	0.422	0.375
20	152	152	15.9	46.6	2330	19.0	1.00	9.6	50.0	1.2	666	1603	0.415	0.371
21	152	152	15.9	46.6	2330	22.2	1.00	9.6	50.0	1.4	654	1603	0.408	0.367
22	152	152	15.9	46.6	2330	25.4	1.00	9.6	50.0	1.6	643	1603	0.401	0.363

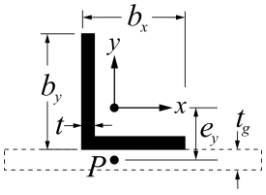

P_e = Compressive resistance based on 3D shell model

$P_Y = F_Y A = 350 \times A$

$$\Omega = 1.0 - \left(\frac{\left[199 - 103\left(b_y/b_x\right)\right]\left[\left(t_g/t\right)/\left(L/r_x\right) + 0.050\right] + \left(L/r_x\right)}{0.88\left(L/r_x\right) + 46.8} \right)$$

Run #	b_y	b_x	t	r_x	L	t_g	b_y/b_x	b_x/t	L/r_x	t_g/t	P_e	P_Y	P_e/P_Y	Ω
23	152	152	15.9	46.6	2330	28.6	1.00	9.6	50.0	1.8	632	1603	0.394	0.358
24	152	152	15.9	46.6	2330	31.8	1.00	9.6	50.0	2.0	620	1603	0.387	0.354
25	152	152	19.0	46.2	2308	19.0	1.00	8.0	50.0	1.0	794	1895	0.419	0.375
26	152	152	19.0	46.2	2308	28.6	1.00	8.0	50.0	1.5	754	1895	0.398	0.365
27	152	152	19.0	46.2	2308	38.1	1.00	8.0	50.0	2.0	719	1895	0.379	0.354
28	152	152	22.2	45.7	2285	22.2	1.00	6.8	50.0	1.0	897	2190	0.410	0.375
29	152	152	22.2	45.7	2285	31.8	1.00	6.8	50.0	1.4	853	2190	0.390	0.366
30	152	152	22.2	45.7	2285	38.1	1.00	6.8	50.0	1.7	826	2190	0.377	0.360
31	152	152	22.2	45.7	2285	44.4	1.00	6.8	50.0	2.0	801	2190	0.366	0.354
32	152	152	25.4	45.3	2263	25.4	1.00	6.0	50.0	1.0	986	2477	0.398	0.375
33	152	152	25.4	45.3	2263	38.1	1.00	6.0	50.0	1.5	924	2477	0.373	0.365
34	152	152	25.4	45.3	2263	50.8	1.00	6.0	50.0	2.0	867	2477	0.350	0.354
35	152	152	12.7	47.1	3531	12.7	1.00	12.0	75.0	1.0	384	1295	0.297	0.281
36	152	152	12.7	47.1	3531	19.0	1.00	12.0	75.0	1.5	373	1295	0.288	0.276
37	152	152	12.7	47.1	3531	25.4	1.00	12.0	75.0	2.0	361	1295	0.279	0.270
38	152	152	15.9	46.6	3495	15.9	1.00	9.6	75.0	1.0	489	1603	0.305	0.281
39	152	152	15.9	46.6	3495	25.4	1.00	9.6	75.0	1.6	466	1603	0.291	0.274
40	152	152	15.9	46.6	3495	31.8	1.00	9.6	75.0	2.0	453	1603	0.282	0.270
41	152	152	19.0	46.2	3462	19.0	1.00	8.0	75.0	1.0	578	1895	0.305	0.281
42	152	152	19.0	46.2	3462	28.6	1.00	8.0	75.0	1.5	552	1895	0.291	0.275
43	152	152	19.0	46.2	3462	38.1	1.00	8.0	75.0	2.0	528	1895	0.279	0.270
44	152	152	22.2	45.7	3428	22.2	1.00	6.8	75.0	1.0	660	2190	0.301	0.281
45	152	152	22.2	45.7	3428	31.8	1.00	6.8	75.0	1.4	631	2190	0.288	0.276
46	152	152	22.2	45.7	3428	44.4	1.00	6.8	75.0	2.0	596	2190	0.272	0.270
47	152	152	25.4	45.3	3394	25.4	1.00	6.0	75.0	1.0	732	2477	0.296	0.281
48	152	152	25.4	45.3	3394	38.1	1.00	6.0	75.0	1.5	691	2477	0.279	0.276
49	152	152	25.4	45.3	3394	50.8	1.00	6.0	75.0	2.0	653	2477	0.264	0.270
50	152	152	12.7	47.1	4708	12.7	1.00	12.0	100.0	1.0	272	1295	0.210	0.215
51	152	152	12.7	47.1	4708	19.0	1.00	12.0	100.0	1.5	265	1295	0.205	0.212
52	152	152	12.7	47.1	4708	25.4	1.00	12.0	100.0	2.0	259	1295	0.200	0.208
53	152	152	15.9	46.6	4661	15.9	1.00	9.6	100.0	1.0	349	1603	0.218	0.215
54	152	152	15.9	46.6	4661	19.0	1.00	9.6	100.0	1.2	345	1603	0.215	0.214
55	152	152	15.9	46.6	4661	22.2	1.00	9.6	100.0	1.4	341	1603	0.212	0.213
56	152	152	15.9	46.6	4661	25.4	1.00	9.6	100.0	1.6	336	1603	0.210	0.211
57	152	152	15.9	46.6	4661	28.6	1.00	9.6	100.0	1.8	332	1603	0.207	0.210
58	152	152	15.9	46.6	4661	31.8	1.00	9.6	100.0	2.0	328	1603	0.205	0.208
59	152	152	19.0	46.2	4615	19.0	1.00	8.0	100.0	1.0	417	1895	0.220	0.215
60	152	152	19.0	46.2	4615	28.6	1.00	8.0	100.0	1.5	401	1895	0.212	0.212
61	152	152	19.0	46.2	4615	38.1	1.00	8.0	100.0	2.0	387	1895	0.204	0.208
62	152	152	22.2	45.7	4570	22.2	1.00	6.8	100.0	1.0	481	2190	0.219	0.215
63	152	152	22.2	45.7	4570	31.8	1.00	6.8	100.0	1.4	463	2190	0.211	0.212
64	152	152	22.2	45.7	4570	38.1	1.00	6.8	100.0	1.7	452	2190	0.206	0.210

Run #	b_y	b_x	t	r_x	L	t_g	b_y/b_x	b_x/t	L/r_x	t_g/t	P_e	P_Y	P_e/P_Y	Ω
65	152	152	22.2	45.7	4570	44.4	1.00	6.8	100.0	2.0	442	2190	0.202	0.208
66	152	152	25.4	45.3	4526	25.4	1.00	6.0	100.0	1.0	538	2477	0.217	0.215
67	152	152	25.4	45.3	4526	38.1	1.00	6.0	100.0	1.5	513	2477	0.207	0.212
68	152	152	25.4	45.3	4526	50.8	1.00	6.0	100.0	2.0	490	2477	0.198	0.208
69	152	152	12.7	47.1	5885	12.7	1.00	12.0	125.0	1.0	199	1295	0.154	0.167
70	152	152	12.7	47.1	5885	19.0	1.00	12.0	125.0	1.5	195	1295	0.151	0.165
71	152	152	12.7	47.1	5885	25.4	1.00	12.0	125.0	2.0	191	1295	0.147	0.162
72	152	152	15.9	46.6	5826	15.9	1.00	9.6	125.0	1.0	257	1603	0.160	0.167
73	152	152	15.9	46.6	5826	25.4	1.00	9.6	125.0	1.6	249	1603	0.156	0.164
74	152	152	15.9	46.6	5826	31.8	1.00	9.6	125.0	2.0	244	1603	0.152	0.162
75	152	152	19.0	46.2	5769	19.0	1.00	8.0	125.0	1.0	310	1895	0.163	0.167
76	152	152	19.0	46.2	5769	28.6	1.00	8.0	125.0	1.5	300	1895	0.159	0.165
77	152	152	19.0	46.2	5769	38.1	1.00	8.0	125.0	2.0	292	1895	0.154	0.162
78	152	152	22.2	45.7	5713	22.2	1.00	6.8	125.0	1.0	360	2190	0.164	0.167
79	152	152	22.2	45.7	5713	31.8	1.00	6.8	125.0	1.4	349	2190	0.159	0.165
80	152	152	22.2	45.7	5713	44.4	1.00	6.8	125.0	2.0	336	2190	0.153	0.162
81	152	152	25.4	45.3	5657	25.4	1.00	6.0	125.0	1.0	406	2477	0.164	0.167
82	152	152	25.4	45.3	5657	38.1	1.00	6.0	125.0	1.5	390	2477	0.157	0.165
83	152	152	25.4	45.3	5657	50.8	1.00	6.0	125.0	2.0	375	2477	0.152	0.162
84	152	152	12.7	47.1	7062	12.7	1.00	12.0	150.0	1.0	150	1295	0.116	0.131
85	152	152	12.7	47.1	7062	19.0	1.00	12.0	150.0	1.5	148	1295	0.114	0.129
86	152	152	12.7	47.1	7062	25.4	1.00	12.0	150.0	2.0	145	1295	0.112	0.127
87	152	152	15.9	46.6	6991	15.9	1.00	9.6	150.0	1.0	196	1603	0.122	0.131
88	152	152	15.9	46.6	6991	19.0	1.00	9.6	150.0	1.2	194	1603	0.121	0.130
89	152	152	15.9	46.6	6991	22.2	1.00	9.6	150.0	1.4	192	1603	0.120	0.129
90	152	152	15.9	46.6	6991	25.4	1.00	9.6	150.0	1.6	191	1603	0.119	0.129
91	152	152	15.9	46.6	6991	28.6	1.00	9.6	150.0	1.8	189	1603	0.118	0.128
92	152	152	15.9	46.6	6991	31.8	1.00	9.6	150.0	2.0	188	1603	0.117	0.127
93	152	152	19.0	46.2	6923	19.0	1.00	8.0	150.0	1.0	237	1895	0.125	0.131
94	152	152	19.0	46.2	6923	28.6	1.00	8.0	150.0	1.5	231	1895	0.122	0.129
95	152	152	19.0	46.2	6923	38.1	1.00	8.0	150.0	2.0	229	1895	0.121	0.127
96	152	152	22.2	45.7	6855	22.2	1.00	6.8	150.0	1.0	277	2190	0.127	0.131
97	152	152	22.2	45.7	6855	31.8	1.00	6.8	150.0	1.4	270	2190	0.123	0.129
98	152	152	22.2	45.7	6855	38.1	1.00	6.8	150.0	1.7	266	2190	0.121	0.128
99	152	152	22.2	45.7	6855	44.4	1.00	6.8	150.0	2.0	262	2190	0.119	0.127
100	152	152	25.4	45.3	6789	25.4	1.00	6.0	150.0	1.0	314	2477	0.127	0.131
101	152	152	25.4	45.3	6789	38.1	1.00	6.0	150.0	1.5	304	2477	0.123	0.129
102	152	152	25.4	45.3	6789	50.8	1.00	6.0	150.0	2.0	295	2477	0.119	0.127
103	152	152	12.7	47.1	8239	12.7	1.00	12.0	175.0	1.0	117	1295	0.090	0.102
104	152	152	12.7	47.1	8239	19.0	1.00	12.0	175.0	1.5	115	1295	0.089	0.100
105	152	152	12.7	47.1	8239	25.4	1.00	12.0	175.0	2.0	113	1295	0.088	0.099
106	152	152	15.9	46.6	8156	15.9	1.00	9.6	175.0	1.0	153	1603	0.095	0.102

Run #	b_y	b_x	t	r_x	L	t_g	b_y/b_x	b_x/t	L/r_x	t_g/t	P_e	P_Y	P_e/P_Y	Ω
107	152	152	15.9	46.6	8156	25.4	1.00	9.6	175.0	1.6	150	1603	0.093	0.100
108	152	152	15.9	46.6	8156	31.8	1.00	9.6	175.0	2.0	147	1603	0.092	0.099
109	152	152	19.0	46.2	8077	19.0	1.00	8.0	175.0	1.0	186	1895	0.098	0.102
110	152	152	19.0	46.2	8077	28.6	1.00	8.0	175.0	1.5	182	1895	0.096	0.100
111	152	152	19.0	46.2	8077	38.1	1.00	8.0	175.0	2.0	178	1895	0.094	0.099
112	152	152	22.2	45.7	7998	22.2	1.00	6.8	175.0	1.0	219	2190	0.100	0.102
113	152	152	22.2	45.7	7998	31.8	1.00	6.8	175.0	1.4	214	2190	0.098	0.101
114	152	152	22.2	45.7	7998	44.4	1.00	6.8	175.0	2.0	208	2190	0.095	0.099
115	152	152	25.4	45.3	7920	25.4	1.00	6.0	175.0	1.0	249	2477	0.101	0.102
116	152	152	25.4	45.3	7920	38.1	1.00	6.0	175.0	1.5	242	2477	0.098	0.100
117	152	152	25.4	45.3	7920	50.8	1.00	6.0	175.0	2.0	236	2477	0.095	0.099
118	152	152	12.7	47.1	9416	12.7	1.00	12.0	200.0	1.0	93	1295	0.072	0.079
119	152	152	12.7	47.1	9416	19.0	1.00	12.0	200.0	1.5	92	1295	0.071	0.078
120	152	152	12.7	47.1	9416	25.4	1.00	12.0	200.0	2.0	90	1295	0.070	0.076
121	152	152	15.9	46.6	9321	15.9	1.00	9.6	200.0	1.0	122	1603	0.076	0.079
122	152	152	15.9	46.6	9321	19.0	1.00	9.6	200.0	1.2	121	1603	0.076	0.078
123	152	152	15.9	46.6	9321	22.2	1.00	9.6	200.0	1.4	121	1603	0.075	0.078
124	152	152	15.9	46.6	9321	25.4	1.00	9.6	200.0	1.6	120	1603	0.075	0.077
125	152	152	15.9	46.6	9321	28.6	1.00	9.6	200.0	1.8	119	1603	0.074	0.077
126	152	152	15.9	46.6	9321	31.8	1.00	9.6	200.0	2.0	118	1603	0.074	0.076
127	152	152	19.0	46.2	9231	19.0	1.00	8.0	200.0	1.0	149	1895	0.079	0.079
128	152	152	19.0	46.2	9231	28.6	1.00	8.0	200.0	1.5	147	1895	0.077	0.078
129	152	152	19.0	46.2	9231	38.1	1.00	8.0	200.0	2.0	144	1895	0.076	0.076
130	152	152	22.2	45.7	9140	22.2	1.00	6.8	200.0	1.0	176	2190	0.080	0.079
131	152	152	22.2	45.7	9140	31.8	1.00	6.8	200.0	1.4	173	2190	0.079	0.078
132	152	152	22.2	45.7	9140	38.1	1.00	6.8	200.0	1.7	171	2190	0.078	0.077
133	152	152	22.2	45.7	9140	44.4	1.00	6.8	200.0	2.0	169	2190	0.077	0.076
134	152	152	25.4	45.3	9051	25.4	1.00	6.0	200.0	1.0	202	2477	0.081	0.079
135	152	152	25.4	45.3	9051	38.1	1.00	6.0	200.0	1.5	197	2477	0.079	0.078
136	152	152	25.4	45.3	9051	50.8	1.00	6.0	200.0	2.0	192	2477	0.078	0.076

Table 4.7 Inelastic compressive resistance database for members with unequal-leg angles connected to gusset plates through the longer legs

Run #	Geometric properties (mm)						Dimensionless parameters				Compressive resistance			
											kN		Ratio	
	b_y	b_x	t	r_x	L	t_g	b_y/b_x	b_x/t	L/r_x	t_g/t	P_e	P_Y	P_e/P_Y	Ω
137	102	203	15.9	27.2	680	15.9	0.50	12.8	25	1.0	754	1609	0.468	0.444
138	102	203	15.9	27.2	680	25.4	0.50	12.8	25	1.6	679	1609	0.422	0.393
139	102	203	15.9	27.2	680	31.8	0.50	12.8	25	2.0	634	1609	0.394	0.358
140	102	203	22.2	26.5	661	22.2	0.50	9.1	25	1.0	970	2197	0.441	0.444
141	102	203	22.2	26.5	661	31.8	0.50	9.1	25	1.4	868	2197	0.395	0.407
142	102	203	22.2	26.5	661	44.4	0.50	9.1	25	2.0	757	2197	0.345	0.358
143	102	203	15.9	27.2	1360	15.9	0.50	12.8	50	1.0	568	1609	0.353	0.336
144	102	203	15.9	27.2	1360	25.4	0.50	12.8	50	1.6	513	1609	0.319	0.316
145	102	203	15.9	27.2	1360	31.8	0.50	12.8	50	2.0	481	1609	0.299	0.303
146	102	203	19.0	26.8	1341	19.0	0.50	10.7	50	1.0	662	1902	0.348	0.336
147	102	203	19.0	26.8	1341	28.6	0.50	10.7	50	1.5	598	1902	0.314	0.319
148	102	203	19.0	26.8	1341	38.1	0.50	10.7	50	2.0	544	1902	0.286	0.303
149	102	203	22.2	26.5	1323	22.2	0.50	9.1	50	1.0	736	2197	0.335	0.336
150	102	203	22.2	26.5	1323	31.8	0.50	9.1	50	1.4	667	2197	0.303	0.322
151	102	203	22.2	26.5	1323	38.1	0.50	9.1	50	1.7	627	2197	0.286	0.313
152	102	203	22.2	26.5	1323	44.4	0.50	9.1	50	2.0	593	2197	0.270	0.303
153	102	203	25.4	26.1	1306	25.4	0.50	8.0	50	1.0	793	2486	0.319	0.336
154	102	203	25.4	26.1	1306	38.1	0.50	8.0	50	1.5	701	2486	0.282	0.320
155	102	203	25.4	26.1	1306	50.8	0.50	8.0	50	2.0	629	2486	0.253	0.303
156	102	203	15.9	27.2	2039	15.9	0.50	12.8	75	1.0	408	1609	0.254	0.252
157	102	203	15.9	27.2	2039	25.4	0.50	12.8	75	1.6	375	1609	0.233	0.242
158	102	203	15.9	27.2	2039	31.8	0.50	12.8	75	2.0	355	1609	0.221	0.235
159	102	203	22.2	26.5	1984	22.2	0.50	9.1	75	1.0	541	2197	0.246	0.252
160	102	203	22.2	26.5	1984	31.8	0.50	9.1	75	1.4	499	2197	0.227	0.245
161	102	203	22.2	26.5	1984	44.4	0.50	9.1	75	2.0	453	2197	0.206	0.235
162	102	203	15.9	27.2	2719	15.9	0.50	12.8	100	1.0	302	1609	0.188	0.193
163	102	203	15.9	27.2	2719	25.4	0.50	12.8	100	1.6	282	1609	0.175	0.186
164	102	203	15.9	27.2	2719	31.8	0.50	12.8	100	2.0	270	1609	0.168	0.182
165	102	203	19.0	26.8	2681	19.0	0.50	10.7	100	1.0	358	1902	0.188	0.193
166	102	203	19.0	26.8	2681	28.6	0.50	10.7	100	1.5	334	1902	0.176	0.187
167	102	203	19.0	26.8	2681	38.1	0.50	10.7	100	2.0	313	1902	0.165	0.182
168	102	203	22.2	26.5	2645	22.2	0.50	9.1	100	1.0	408	2197	0.186	0.193

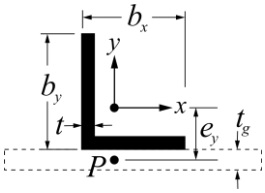

P_e = Compressive resistance based on 3D shell model

$P_Y = F_Y A = 350 \times A$

$$\Omega = 1.0 - \left(\frac{\left[199 - 103\left(b_y/b_x\right) \right] \left[\left(t_g/t\right)/\left(L/r_x\right) + 0.050 \right] + \left(L/r_x\right)}{0.88\left(L/r_x\right) + 46.8} \right)$$

Run #	b_y	b_x	t	r_x	L	t_g	b_y/b_x	b_x/t	L/r_x	t_g/t	P_e	P_Y	P_e/P_Y	Ω
169	102	203	22.2	26.5	2645	31.8	0.50	9.1	100	1.4	381	2197	0.174	0.188
170	102	203	22.2	26.5	2645	38.1	0.50	9.1	100	1.7	366	2197	0.166	0.185
171	102	203	22.2	26.5	2645	44.4	0.50	9.1	100	2.0	351	2197	0.160	0.182
172	102	203	25.4	26.1	2612	25.4	0.50	8.0	100	1.0	452	2486	0.182	0.193
173	102	203	25.4	26.1	2612	38.1	0.50	8.0	100	1.5	415	2486	0.167	0.187
174	102	203	25.4	26.1	2612	50.8	0.50	8.0	100	2.0	384	2486	0.154	0.182
175	102	203	15.9	27.2	3399	15.9	0.50	12.8	125	1.0	231	1609	0.144	0.148
176	102	203	15.9	27.2	3399	25.4	0.50	12.8	125	1.6	218	1609	0.135	0.144
177	102	203	15.9	27.2	3399	31.8	0.50	12.8	125	2.0	210	1609	0.131	0.141
178	102	203	22.2	26.5	3307	22.2	0.50	9.1	125	1.0	316	2197	0.144	0.148
179	102	203	22.2	26.5	3307	31.8	0.50	9.1	125	1.4	299	2197	0.136	0.145
180	102	203	22.2	26.5	3307	44.4	0.50	9.1	125	2.0	279	2197	0.127	0.141
181	102	203	15.9	27.2	4079	15.9	0.50	12.8	150	1.0	181	1609	0.113	0.114
182	102	203	15.9	27.2	4079	25.4	0.50	12.8	150	1.6	173	1609	0.107	0.111
183	102	203	15.9	27.2	4079	31.8	0.50	12.8	150	2.0	167	1609	0.104	0.109
184	102	203	19.0	26.8	4022	19.0	0.50	10.7	150	1.0	217	1902	0.114	0.114
185	102	203	19.0	26.8	4022	28.6	0.50	10.7	150	1.5	207	1902	0.109	0.112
186	102	203	19.0	26.8	4022	38.1	0.50	10.7	150	2.0	198	1902	0.104	0.109
187	102	203	22.2	26.5	3968	22.2	0.50	9.1	150	1.0	251	2197	0.114	0.114
188	102	203	22.2	26.5	3968	31.8	0.50	9.1	150	1.4	239	2197	0.109	0.112
189	102	203	22.2	26.5	3968	38.1	0.50	9.1	150	1.7	232	2197	0.106	0.110
190	102	203	22.2	26.5	3968	44.4	0.50	9.1	150	2.0	226	2197	0.103	0.109
191	102	203	25.4	26.1	3918	25.4	0.50	8.0	150	1.0	282	2486	0.113	0.114
192	102	203	25.4	26.1	3918	38.1	0.50	8.0	150	1.5	265	2486	0.107	0.112
193	102	203	25.4	26.1	3918	50.8	0.50	8.0	150	2.0	251	2486	0.101	0.109
194	102	203	15.9	27.2	4759	15.9	0.50	12.8	175	1.0	145	1609	0.090	0.088
195	102	203	15.9	27.2	4759	25.4	0.50	12.8	175	1.6	139	1609	0.087	0.085
196	102	203	15.9	27.2	4759	31.8	0.50	12.8	175	2.0	136	1609	0.084	0.083
197	102	203	22.2	26.5	4629	22.2	0.50	9.1	175	1.0	204	2197	0.093	0.088
198	102	203	22.2	26.5	4629	31.8	0.50	9.1	175	1.4	195	2197	0.089	0.086
199	102	203	22.2	26.5	4629	44.4	0.50	9.1	175	2.0	186	2197	0.084	0.083
200	102	203	15.9	27.2	5438	15.9	0.50	12.8	200	1.0	119	1609	0.074	0.066
201	102	203	15.9	27.2	5438	25.4	0.50	12.8	200	1.6	114	1609	0.071	0.064
202	102	203	15.9	27.2	5438	31.8	0.50	12.8	200	2.0	112	1609	0.069	0.063
203	102	203	19.0	26.8	5363	19.0	0.50	10.7	200	1.0	143	1902	0.075	0.066
204	102	203	19.0	26.8	5363	28.6	0.50	10.7	200	1.5	138	1902	0.073	0.064
205	102	203	19.0	26.8	5363	38.1	0.50	10.7	200	2.0	134	1902	0.070	0.063
206	102	203	22.2	26.5	5291	22.2	0.50	9.1	200	1.0	167	2197	0.076	0.066
207	102	203	22.2	26.5	5291	31.8	0.50	9.1	200	1.4	162	2197	0.073	0.065
208	102	203	22.2	26.5	5291	38.1	0.50	9.1	200	1.7	158	2197	0.072	0.064
209	102	203	22.2	26.5	5291	44.4	0.50	9.1	200	2.0	155	2197	0.070	0.063
210	102	203	25.4	26.1	5224	25.4	0.50	8.0	200	1.0	190	2486	0.076	0.066

Run #	b_y	b_x	t	r_x	L	t_g	b_y/b_x	b_x/t	L/r_x	t_g/t	P_e	P_Y	P_e/P_Y	Ω
211	102	203	25.4	26.1	5224	38.1	0.50	8.0	200	1.5	181	2486	0.073	0.064
212	102	203	25.4	26.1	5224	50.8	0.50	8.0	200	2.0	174	2486	0.070	0.063
213	102	178	15.9	28.0	700	15.9	0.57	11.2	25	1.0	714	1470	0.486	0.454
214	102	178	15.9	28.0	700	25.4	0.57	11.2	25	1.6	648	1470	0.441	0.405
215	102	178	15.9	28.0	700	31.8	0.57	11.2	25	2.0	606	1470	0.413	0.372
216	102	178	22.2	27.2	680	22.2	0.57	8.0	25	1.0	908	2003	0.453	0.454
217	102	178	22.2	27.2	680	31.8	0.57	8.0	25	1.4	821	2003	0.410	0.418
218	102	178	22.2	27.2	680	44.4	0.57	8.0	25	2.0	722	2003	0.360	0.372
219	102	178	15.9	28.0	1399	15.9	0.57	11.2	50	1.0	546	1470	0.371	0.341
220	102	178	15.9	28.0	1399	25.4	0.57	11.2	50	1.6	495	1470	0.337	0.323
221	102	178	15.9	28.0	1399	31.8	0.57	11.2	50	2.0	465	1470	0.317	0.311
222	102	178	22.2	27.2	1361	22.2	0.57	8.0	50	1.0	696	2003	0.347	0.341
223	102	178	22.2	27.2	1361	31.8	0.57	8.0	50	1.4	633	2003	0.316	0.328
224	102	178	22.2	27.2	1361	44.4	0.57	8.0	50	2.0	565	2003	0.282	0.311
225	102	178	15.9	28.0	2099	15.9	0.57	11.2	75	1.0	392	1470	0.266	0.257
226	102	178	15.9	28.0	2099	25.4	0.57	11.2	75	1.6	361	1470	0.245	0.247
227	102	178	15.9	28.0	2099	31.8	0.57	11.2	75	2.0	342	1470	0.233	0.240
228	102	178	22.2	27.2	2041	22.2	0.57	8.0	75	1.0	512	2003	0.255	0.257
229	102	178	22.2	27.2	2041	31.8	0.57	8.0	75	1.4	473	2003	0.236	0.249
230	102	178	22.2	27.2	2041	44.4	0.57	8.0	75	2.0	431	2003	0.215	0.240
231	102	178	15.9	28.0	2798	15.9	0.57	11.2	100	1.0	288	1470	0.196	0.196
232	102	178	15.9	28.0	2798	25.4	0.57	11.2	100	1.6	269	1470	0.183	0.190
233	102	178	15.9	28.0	2798	31.8	0.57	11.2	100	2.0	258	1470	0.176	0.185
234	102	178	22.2	27.2	2722	22.2	0.57	8.0	100	1.0	385	2003	0.192	0.196
235	102	178	22.2	27.2	2722	31.8	0.57	8.0	100	1.4	361	2003	0.180	0.191
236	102	178	22.2	27.2	2722	44.4	0.57	8.0	100	2.0	333	2003	0.166	0.185
237	102	178	15.9	28.0	3498	15.9	0.57	11.2	125	1.0	219	1470	0.149	0.151
238	102	178	15.9	28.0	3498	25.4	0.57	11.2	125	1.6	207	1470	0.141	0.147
239	102	178	15.9	28.0	3498	31.8	0.57	11.2	125	2.0	200	1470	0.136	0.144
240	102	178	22.2	27.2	3402	22.2	0.57	8.0	125	1.0	297	2003	0.148	0.151
241	102	178	22.2	27.2	3402	31.8	0.57	8.0	125	1.4	282	2003	0.141	0.148
242	102	178	22.2	27.2	3402	44.4	0.57	8.0	125	2.0	264	2003	0.132	0.144
243	102	178	15.9	28.0	4198	15.9	0.57	11.2	150	1.0	171	1470	0.116	0.117
244	102	178	15.9	28.0	4198	25.4	0.57	11.2	150	1.6	163	1470	0.111	0.114
245	102	178	15.9	28.0	4198	31.8	0.57	11.2	150	2.0	159	1470	0.108	0.111
246	102	178	22.2	27.2	4083	22.2	0.57	8.0	150	1.0	235	2003	0.117	0.117
247	102	178	22.2	27.2	4083	31.8	0.57	8.0	150	1.4	225	2003	0.112	0.114
248	102	178	22.2	27.2	4083	44.4	0.57	8.0	150	2.0	212	2003	0.106	0.111
249	102	178	15.9	28.0	4897	15.9	0.57	11.2	175	1.0	137	1470	0.093	0.090
250	102	178	15.9	28.0	4897	25.4	0.57	11.2	175	1.6	131	1470	0.089	0.087
251	102	178	15.9	28.0	4897	31.8	0.57	11.2	175	2.0	128	1470	0.087	0.086
252	102	178	22.2	27.2	4763	22.2	0.57	8.0	175	1.0	190	2003	0.095	0.090

Run #	b_y	b_x	t	r_x	L	t_g	b_y/b_x	b_x/t	L/r_x	t_g/t	P_e	P_Y	P_e/P_Y	Ω
253	102	178	22.2	27.2	4763	31.8	0.57	8.0	175	1.4	183	2003	0.091	0.088
254	102	178	22.2	27.2	4763	44.4	0.57	8.0	175	2.0	174	2003	0.087	0.086
255	102	178	15.9	28.0	5597	15.9	0.57	11.2	200	1.0	111	1470	0.076	0.068
256	102	178	15.9	28.0	5597	25.4	0.57	11.2	200	1.6	108	1470	0.073	0.066
257	102	178	15.9	28.0	5597	31.8	0.57	11.2	200	2.0	105	1470	0.072	0.065
258	102	178	22.2	27.2	5444	22.2	0.57	8.0	200	1.0	156	2003	0.078	0.068
259	102	178	22.2	27.2	5444	31.8	0.57	8.0	200	1.4	151	2003	0.075	0.066
260	102	178	22.2	27.2	5444	44.4	0.57	8.0	200	2.0	145	2003	0.072	0.065
261	76.2	127	9.5	21.4	535	9.5	0.60	13.3	25	1.0	307	646	0.475	0.457
262	76.2	127	9.5	21.4	535	14.3	0.60	13.3	25	1.5	289	646	0.447	0.417
263	76.2	127	9.5	21.4	535	19.0	0.60	13.3	25	2.0	273	646	0.422	0.378
264	76.2	127	12.7	21.0	525	12.7	0.60	10.0	25	1.0	416	847	0.491	0.457
265	76.2	127	12.7	21.0	525	19.0	0.60	10.0	25	1.5	382	847	0.451	0.418
266	76.2	127	12.7	21.0	525	25.4	0.60	10.0	25	2.0	349	847	0.412	0.377
267	76.2	127	9.5	21.4	1071	9.5	0.60	13.3	50	1.0	242	646	0.374	0.344
268	76.2	127	9.5	21.4	1071	14.3	0.60	13.3	50	1.5	227	646	0.352	0.328
269	76.2	127	9.5	21.4	1071	19.0	0.60	13.3	50	2.0	213	646	0.330	0.314
270	76.2	127	12.7	21.0	1050	12.7	0.60	10.0	50	1.0	319	847	0.377	0.344
271	76.2	127	12.7	21.0	1050	19.0	0.60	10.0	50	1.5	293	847	0.346	0.329
272	76.2	127	12.7	21.0	1050	25.4	0.60	10.0	50	2.0	269	847	0.318	0.313
273	76.2	127	9.5	21.4	1606	9.5	0.60	13.3	75	1.0	173	646	0.268	0.258
274	76.2	127	9.5	21.4	1606	14.3	0.60	13.3	75	1.5	163	646	0.253	0.250
275	76.2	127	9.5	21.4	1606	19.0	0.60	13.3	75	2.0	155	646	0.240	0.242
276	76.2	127	12.7	21.0	1575	12.7	0.60	10.0	75	1.0	229	847	0.270	0.258
277	76.2	127	12.7	21.0	1575	19.0	0.60	10.0	75	1.5	213	847	0.252	0.250
278	76.2	127	12.7	21.0	1575	25.4	0.60	10.0	75	2.0	199	847	0.235	0.242
279	76.2	127	9.5	21.4	2142	9.5	0.60	13.3	100	1.0	126	646	0.194	0.197
280	76.2	127	9.5	21.4	2142	14.3	0.60	13.3	100	1.5	120	646	0.186	0.192
281	76.2	127	9.5	21.4	2142	19.0	0.60	13.3	100	2.0	116	646	0.179	0.187
282	76.2	127	12.7	21.0	2100	12.7	0.60	10.0	100	1.0	169	847	0.199	0.197
283	76.2	127	12.7	21.0	2100	19.0	0.60	10.0	100	1.5	159	847	0.188	0.192
284	76.2	127	12.7	21.0	2100	25.4	0.60	10.0	100	2.0	150	847	0.178	0.187
285	76.2	127	9.5	21.4	2677	9.5	0.60	13.3	125	1.0	95	646	0.147	0.152
286	76.2	127	9.5	21.4	2677	14.3	0.60	13.3	125	1.5	91	646	0.141	0.149
287	76.2	127	9.5	21.4	2677	19.0	0.60	13.3	125	2.0	88	646	0.137	0.145
288	76.2	127	12.7	21.0	2625	12.7	0.60	10.0	125	1.0	128	847	0.151	0.152
289	76.2	127	12.7	21.0	2625	19.0	0.60	10.0	125	1.5	122	847	0.144	0.149
290	76.2	127	12.7	21.0	2625	25.4	0.60	10.0	125	2.0	117	847	0.138	0.145
291	76.2	127	9.5	21.4	3212	9.5	0.60	13.3	150	1.0	74	646	0.114	0.118
292	76.2	127	9.5	21.4	3212	14.3	0.60	13.3	150	1.5	71	646	0.111	0.115
293	76.2	127	9.5	21.4	3212	19.0	0.60	13.3	150	2.0	69	646	0.107	0.113
294	76.2	127	12.7	21.0	3149	12.7	0.60	10.0	150	1.0	100	847	0.118	0.118

Run #	b_y	b_x	t	r_x	L	t_g	b_y/b_x	b_x/t	L/r_x	t_g/t	P_e	P_Y	P_e/P_Y	Ω
295	76.2	127	12.7	21.0	3149	19.0	0.60	10.0	150	1.5	96	847	0.113	0.115
296	76.2	127	12.7	21.0	3149	25.4	0.60	10.0	150	2.0	92	847	0.109	0.112
297	76.2	127	9.5	21.4	3748	9.5	0.60	13.3	175	1.0	59	646	0.091	0.090
298	76.2	127	9.5	21.4	3748	14.3	0.60	13.3	175	1.5	57	646	0.089	0.088
299	76.2	127	9.5	21.4	3748	19.0	0.60	13.3	175	2.0	56	646	0.086	0.087
300	76.2	127	12.7	21.0	3674	12.7	0.60	10.0	175	1.0	80	847	0.095	0.090
301	76.2	127	12.7	21.0	3674	19.0	0.60	10.0	175	1.5	77	847	0.091	0.088
302	76.2	127	12.7	21.0	3674	25.4	0.60	10.0	175	2.0	75	847	0.088	0.087
303	76.2	127	9.5	21.4	4283	9.5	0.60	13.3	200	1.0	48	646	0.074	0.068
304	76.2	127	9.5	21.4	4283	14.3	0.60	13.3	200	1.5	47	646	0.072	0.067
305	76.2	127	9.5	21.4	4283	19.0	0.60	13.3	200	2.0	46	646	0.070	0.065
306	76.2	127	12.7	21.0	4199	12.7	0.60	10.0	200	1.0	66	847	0.077	0.068
307	76.2	127	12.7	21.0	4199	19.0	0.60	10.0	200	1.5	64	847	0.075	0.067
308	76.2	127	12.7	21.0	4199	25.4	0.60	10.0	200	2.0	62	847	0.073	0.065
309	102	152	15.9	28.9	721	15.9	0.67	9.6	25	1.0	665	1325	0.502	0.467
310	102	152	15.9	28.9	721	25.4	0.67	9.6	25	1.6	608	1325	0.459	0.422
311	102	152	15.9	28.9	721	31.8	0.67	9.6	25	2.0	572	1325	0.432	0.391
312	102	152	22.2	28.1	702	22.2	0.67	6.8	25	1.0	833	1801	0.463	0.467
313	102	152	22.2	28.1	702	31.8	0.67	6.8	25	1.4	759	1801	0.422	0.434
314	102	152	22.2	28.1	702	44.4	0.67	6.8	25	2.0	677	1801	0.376	0.391
315	102	152	15.9	28.9	1443	15.9	0.67	9.6	50	1.0	518	1325	0.391	0.349
316	102	152	15.9	28.9	1443	25.4	0.67	9.6	50	1.6	472	1325	0.356	0.332
317	102	152	15.9	28.9	1443	31.8	0.67	9.6	50	2.0	445	1325	0.336	0.321
318	102	152	22.2	28.1	1403	22.2	0.67	6.8	50	1.0	646	1801	0.359	0.349
319	102	152	22.2	28.1	1403	31.8	0.67	6.8	50	1.4	592	1801	0.329	0.337
320	102	152	22.2	28.1	1403	44.4	0.67	6.8	50	2.0	532	1801	0.296	0.321
321	102	152	15.9	28.9	2164	15.9	0.67	9.6	75	1.0	371	1325	0.280	0.262
322	102	152	15.9	28.9	2164	25.4	0.67	9.6	75	1.6	343	1325	0.259	0.253
323	102	152	15.9	28.9	2164	31.8	0.67	9.6	75	2.0	326	1325	0.246	0.247
324	102	152	22.2	28.1	2105	22.2	0.67	6.8	75	1.0	478	1801	0.265	0.262
325	102	152	22.2	28.1	2105	31.8	0.67	6.8	75	1.4	444	1801	0.246	0.256
326	102	152	22.2	28.1	2105	44.4	0.67	6.8	75	2.0	406	1801	0.225	0.247
327	102	152	15.9	28.9	2885	15.9	0.67	9.6	100	1.0	271	1325	0.205	0.200
328	102	152	15.9	28.9	2885	25.4	0.67	9.6	100	1.6	255	1325	0.192	0.195
329	102	152	15.9	28.9	2885	31.8	0.67	9.6	100	2.0	245	1325	0.185	0.191
330	102	152	22.2	28.1	2806	22.2	0.67	6.8	100	1.0	358	1801	0.199	0.200
331	102	152	22.2	28.1	2806	31.8	0.67	6.8	100	1.4	337	1801	0.187	0.196
332	102	152	22.2	28.1	2806	44.4	0.67	6.8	100	2.0	313	1801	0.174	0.191
333	102	152	15.9	28.9	3606	15.9	0.67	9.6	125	1.0	205	1325	0.155	0.155
334	102	152	15.9	28.9	3606	25.4	0.67	9.6	125	1.6	195	1325	0.147	0.151
335	102	152	15.9	28.9	3606	31.8	0.67	9.6	125	2.0	188	1325	0.142	0.148
336	102	152	22.2	28.1	3508	22.2	0.67	6.8	125	1.0	276	1801	0.153	0.155

Run #	b_y	b_x	t	r_x	L	t_g	b_y/b_x	b_x/t	L/r_x	t_g/t	P_e	P_Y	P_e/P_Y	Ω
337	102	152	22.2	28.1	3508	31.8	0.67	6.8	125	1.4	262	1801	0.145	0.152
338	102	152	22.2	28.1	3508	44.4	0.67	6.8	125	2.0	246	1801	0.137	0.148
339	102	152	15.9	28.9	4328	15.9	0.67	9.6	150	1.0	160	1325	0.121	0.120
340	102	152	15.9	28.9	4328	25.4	0.67	9.6	150	1.6	153	1325	0.115	0.117
341	102	152	15.9	28.9	4328	31.8	0.67	9.6	150	2.0	149	1325	0.112	0.115
342	102	152	22.2	28.1	4209	22.2	0.67	6.8	150	1.0	217	1801	0.121	0.120
343	102	152	22.2	28.1	4209	31.8	0.67	6.8	150	1.4	208	1801	0.116	0.118
344	102	152	22.2	28.1	4209	44.4	0.67	6.8	150	2.0	198	1801	0.110	0.115
345	102	152	15.9	28.9	5049	15.9	0.67	9.6	175	1.0	127	1325	0.096	0.092
346	102	152	15.9	28.9	5049	25.4	0.67	9.6	175	1.6	122	1325	0.092	0.090
347	102	152	15.9	28.9	5049	31.8	0.67	9.6	175	2.0	120	1325	0.090	0.089
348	102	152	22.2	28.1	4911	22.2	0.67	6.8	175	1.0	175	1801	0.097	0.092
349	102	152	22.2	28.1	4911	31.8	0.67	6.8	175	1.4	169	1801	0.094	0.091
350	102	152	22.2	28.1	4911	44.4	0.67	6.8	175	2.0	161	1801	0.090	0.089
351	102	152	15.9	28.9	5770	15.9	0.67	9.6	200	1.0	103	1325	0.078	0.070
352	102	152	15.9	28.9	5770	25.4	0.67	9.6	200	1.6	100	1325	0.075	0.069
353	102	152	15.9	28.9	5770	31.8	0.67	9.6	200	2.0	98	1325	0.074	0.067
354	102	152	22.2	28.1	5612	22.2	0.67	6.8	200	1.0	143	1801	0.080	0.070
355	102	152	22.2	28.1	5612	31.8	0.67	6.8	200	1.4	139	1801	0.077	0.069
356	102	152	22.2	28.1	5612	44.4	0.67	6.8	200	2.0	134	1801	0.074	0.067
357	127	178	15.9	36.8	921	15.9	0.71	11.2	25	1.0	803	1609	0.499	0.472
358	127	178	15.9	36.8	921	25.4	0.71	11.2	25	1.6	750	1609	0.466	0.429
359	127	178	15.9	36.8	921	31.8	0.71	11.2	25	2.0	717	1609	0.446	0.399
360	127	178	22.2	36.0	900	22.2	0.71	8.0	25	1.0	1091	2197	0.496	0.472
361	127	178	22.2	36.0	900	31.8	0.71	8.0	25	1.4	1017	2197	0.463	0.441
362	127	178	22.2	36.0	900	44.4	0.71	8.0	25	2.0	926	2197	0.421	0.399
363	127	178	12.7	37.3	1865	12.7	0.71	14.0	50	1.0	498	1299	0.383	0.353
364	127	178	12.7	37.3	1865	19.0	0.71	14.0	50	1.5	475	1299	0.366	0.339
365	127	178	12.7	37.3	1865	25.4	0.71	14.0	50	2.0	453	1299	0.349	0.325
366	127	178	15.9	36.8	1842	15.9	0.71	11.2	50	1.0	643	1609	0.399	0.353
367	127	178	15.9	36.8	1842	25.4	0.71	11.2	50	1.6	598	1609	0.372	0.336
368	127	178	15.9	36.8	1842	31.8	0.71	11.2	50	2.0	571	1609	0.355	0.325
369	127	178	19.0	36.4	1821	19.0	0.71	9.4	50	1.0	757	1902	0.398	0.353
370	127	178	19.0	36.4	1821	28.6	0.71	9.4	50	1.5	704	1902	0.370	0.339
371	127	178	19.0	36.4	1821	38.1	0.71	9.4	50	2.0	656	1902	0.345	0.325
372	127	178	22.2	36.0	1799	22.2	0.71	8.0	50	1.0	852	2197	0.388	0.353
373	127	178	22.2	36.0	1799	31.8	0.71	8.0	50	1.4	792	2197	0.360	0.341
374	127	178	22.2	36.0	1799	44.4	0.71	8.0	50	2.0	724	2197	0.330	0.325
375	127	178	25.4	35.6	1779	25.4	0.71	7.0	50	1.0	927	2486	0.373	0.353
376	127	178	25.4	35.6	1779	38.1	0.71	7.0	50	1.5	884	2486	0.356	0.339
377	127	178	25.4	35.6	1779	50.8	0.71	7.0	50	2.0	776	2486	0.312	0.325
378	127	178	15.9	36.8	2763	15.9	0.71	11.2	75	1.0	457	1609	0.284	0.265

Run #	b_y	b_x	t	r_x	L	t_g	b_y/b_x	b_x/t	L/r_x	t_g/t	P_e	P_Y	P_e/P_Y	Ω
379	127	178	15.9	36.8	2763	25.4	0.71	11.2	75	1.6	429	1609	0.267	0.256
380	127	178	15.9	36.8	2763	31.8	0.71	11.2	75	2.0	412	1609	0.256	0.250
381	127	178	22.2	36.0	2699	22.2	0.71	8.0	75	1.0	616	2197	0.280	0.265
382	127	178	22.2	36.0	2699	31.8	0.71	8.0	75	1.4	580	2197	0.264	0.258
383	127	178	22.2	36.0	2699	44.4	0.71	8.0	75	2.0	538	2197	0.245	0.250
384	127	178	12.7	37.3	3729	12.7	0.71	14.0	100	1.0	257	1299	0.198	0.202
385	127	178	12.7	37.3	3729	19.0	0.71	14.0	100	1.5	249	1299	0.191	0.198
386	127	178	12.7	37.3	3729	25.4	0.71	14.0	100	2.0	241	1299	0.185	0.193
387	127	178	15.9	36.8	3684	15.9	0.71	11.2	100	1.0	331	1609	0.206	0.202
388	127	178	15.9	36.8	3684	25.4	0.71	11.2	100	1.6	314	1609	0.195	0.197
389	127	178	15.9	36.8	3684	31.8	0.71	11.2	100	2.0	304	1609	0.189	0.193
390	127	178	19.0	36.4	3641	19.0	0.71	9.4	100	1.0	395	1902	0.207	0.202
391	127	178	19.0	36.4	3641	28.6	0.71	9.4	100	1.5	375	1902	0.197	0.198
392	127	178	19.0	36.4	3641	38.1	0.71	9.4	100	2.0	357	1902	0.188	0.193
393	127	178	22.2	36.0	3599	22.2	0.71	8.0	100	1.0	453	2197	0.206	0.202
394	127	178	22.2	36.0	3599	31.8	0.71	8.0	100	1.4	431	2197	0.196	0.198
395	127	178	22.2	36.0	3599	44.4	0.71	8.0	100	2.0	405	2197	0.184	0.193
396	127	178	25.4	35.6	3558	25.4	0.71	7.0	100	1.0	505	2486	0.203	0.202
397	127	178	25.4	35.6	3558	38.1	0.71	7.0	100	1.5	474	2486	0.191	0.198
398	127	178	25.4	35.6	3558	50.8	0.71	7.0	100	2.0	447	2486	0.180	0.193
399	127	178	15.9	36.8	4605	15.9	0.71	11.2	125	1.0	248	1609	0.154	0.156
400	127	178	15.9	36.8	4605	25.4	0.71	11.2	125	1.6	238	1609	0.148	0.153
401	127	178	15.9	36.8	4605	31.8	0.71	11.2	125	2.0	231	1609	0.144	0.150
402	127	178	22.2	36.0	4499	22.2	0.71	8.0	125	1.0	344	2197	0.157	0.156
403	127	178	22.2	36.0	4499	31.8	0.71	8.0	125	1.4	331	2197	0.150	0.154
404	127	178	22.2	36.0	4499	44.4	0.71	8.0	125	2.0	314	2197	0.143	0.150
405	127	178	12.7	37.3	5594	12.7	0.71	14.0	150	1.0	147	1299	0.113	0.121
406	127	178	12.7	37.3	5594	19.0	0.71	14.0	150	1.5	144	1299	0.111	0.119
407	127	178	12.7	37.3	5594	25.4	0.71	14.0	150	2.0	141	1299	0.108	0.117
408	127	178	15.9	36.8	5526	15.9	0.71	11.2	150	1.0	191	1609	0.119	0.121
409	127	178	15.9	36.8	5526	25.4	0.71	11.2	150	1.6	185	1609	0.115	0.118
410	127	178	15.9	36.8	5526	31.8	0.71	11.2	150	2.0	181	1609	0.112	0.117
411	127	178	19.0	36.4	5462	19.0	0.71	9.4	150	1.0	231	1902	0.122	0.121
412	127	178	19.0	36.4	5462	28.6	0.71	9.4	150	1.5	223	1902	0.117	0.119
413	127	178	19.0	36.4	5462	38.1	0.71	9.4	150	2.0	216	1902	0.113	0.117
414	127	178	22.2	36.0	5398	22.2	0.71	8.0	150	1.0	269	2197	0.122	0.121
415	127	178	22.2	36.0	5398	31.8	0.71	8.0	150	1.4	260	2197	0.118	0.119
416	127	178	22.2	36.0	5398	44.4	0.71	8.0	150	2.0	249	2197	0.113	0.117
417	127	178	25.4	35.6	5338	25.4	0.71	7.0	150	1.0	304	2486	0.122	0.121
418	127	178	25.4	35.6	5338	38.1	0.71	7.0	150	1.5	290	2486	0.117	0.119
419	127	178	25.4	35.6	5338	50.8	0.71	7.0	150	2.0	279	2486	0.112	0.117
420	127	178	15.9	36.8	6447	15.9	0.71	11.2	175	1.0	151	1609	0.094	0.094

Run #	b_y	b_x	t	r_x	L	t_g	b_y/b_x	b_x/t	L/r_x	t_g/t	P_e	P_Y	P_e/P_Y	Ω
421	127	178	15.9	36.8	6447	25.4	0.71	11.2	175	1.6	147	1609	0.091	0.092
422	127	178	15.9	36.8	6447	31.8	0.71	11.2	175	2.0	144	1609	0.089	0.090
423	127	178	22.2	36.0	6298	22.2	0.71	8.0	175	1.0	215	2197	0.098	0.094
424	127	178	22.2	36.0	6298	31.8	0.71	8.0	175	1.4	209	2197	0.095	0.092
425	127	178	22.2	36.0	6298	44.4	0.71	8.0	175	2.0	201	2197	0.091	0.090
426	127	178	12.7	37.3	7458	12.7	0.71	14.0	200	1.0	94	1299	0.072	0.071
427	127	178	12.7	37.3	7458	19.0	0.71	14.0	200	1.5	92	1299	0.071	0.070
428	127	178	12.7	37.3	7458	25.4	0.71	14.0	200	2.0	90	1299	0.070	0.069
429	127	178	15.9	36.8	7367	15.9	0.71	11.2	200	1.0	122	1609	0.076	0.071
430	127	178	15.9	36.8	7367	25.4	0.71	11.2	200	1.6	119	1609	0.074	0.070
431	127	178	15.9	36.8	7367	31.8	0.71	11.2	200	2.0	117	1609	0.073	0.069
432	127	178	19.0	36.4	7282	19.0	0.71	9.4	200	1.0	149	1902	0.078	0.071
433	127	178	19.0	36.4	7282	28.6	0.71	9.4	200	1.5	145	1902	0.076	0.070
434	127	178	19.0	36.4	7282	38.1	0.71	9.4	200	2.0	141	1902	0.074	0.069
435	127	178	22.2	36.0	7198	22.2	0.71	8.0	200	1.0	175	2197	0.079	0.071
436	127	178	22.2	36.0	7198	31.8	0.71	8.0	200	1.4	170	2197	0.077	0.070
437	127	178	22.2	36.0	7198	44.4	0.71	8.0	200	2.0	165	2197	0.075	0.069
438	127	178	25.4	35.6	7117	25.4	0.71	7.0	200	1.0	199	2486	0.080	0.071
439	127	178	25.4	35.6	7117	38.1	0.71	7.0	200	1.5	193	2486	0.077	0.070
440	127	178	25.4	35.6	7117	50.8	0.71	7.0	200	2.0	187	2486	0.075	0.069
441	152	203	15.9	44.9	1122	15.9	0.75	12.8	25	1.0	902	1887	0.478	0.477
442	152	203	15.9	44.9	1122	25.4	0.75	12.8	25	1.6	855	1887	0.453	0.435
443	152	203	15.9	44.9	1122	31.8	0.75	12.8	25	2.0	825	1887	0.437	0.406
444	152	203	22.2	44.0	1100	22.2	0.75	9.1	25	1.0	1315	2586	0.508	0.477
445	152	203	22.2	44.0	1100	31.8	0.75	9.1	25	1.4	1243	2586	0.481	0.447
446	152	203	22.2	44.0	1100	44.4	0.75	9.1	25	2.0	1153	2586	0.446	0.406
447	152	203	15.9	44.9	2244	15.9	0.75	12.8	50	1.0	746	1887	0.395	0.355
448	152	203	15.9	44.9	2244	25.4	0.75	12.8	50	1.6	704	1887	0.373	0.339
449	152	203	15.9	44.9	2244	31.8	0.75	12.8	50	2.0	678	1887	0.359	0.329
450	152	203	22.2	44.0	2200	22.2	0.75	9.1	50	1.0	1041	2586	0.403	0.355
451	152	203	22.2	44.0	2200	31.8	0.75	9.1	50	1.4	980	2586	0.379	0.344
452	152	203	22.2	44.0	2200	44.4	0.75	9.1	50	2.0	909	2586	0.351	0.329
453	152	203	15.9	44.9	3366	15.9	0.75	12.8	75	1.0	532	1887	0.282	0.267
454	152	203	15.9	44.9	3366	25.4	0.75	12.8	75	1.6	506	1887	0.268	0.258
455	152	203	15.9	44.9	3366	31.8	0.75	12.8	75	2.0	490	1887	0.259	0.252
456	152	203	22.2	44.0	3300	22.2	0.75	9.1	75	1.0	746	2586	0.288	0.267
457	152	203	22.2	44.0	3300	31.8	0.75	9.1	75	1.4	708	2586	0.274	0.260
458	152	203	22.2	44.0	3300	44.4	0.75	9.1	75	2.0	664	2586	0.257	0.252
459	152	203	15.9	44.9	4488	15.9	0.75	12.8	100	1.0	383	1887	0.203	0.204
460	152	203	15.9	44.9	4488	25.4	0.75	12.8	100	1.6	367	1887	0.195	0.199
461	152	203	15.9	44.9	4488	31.8	0.75	12.8	100	2.0	357	1887	0.189	0.195
462	152	203	22.2	44.0	4400	22.2	0.75	9.1	100	1.0	542	2586	0.209	0.204

Run #	b_y	b_x	t	r_x	L	t_g	b_y/b_x	b_x/t	L/r_x	t_g/t	P_e	P_Y	P_e/P_Y	Ω
463	152	203	22.2	44.0	4400	31.8	0.75	9.1	100	1.4	519	2586	0.201	0.200
464	152	203	22.2	44.0	4400	44.4	0.75	9.1	100	2.0	493	2586	0.191	0.195
465	152	203	15.9	44.9	5610	15.9	0.75	12.8	125	1.0	285	1887	0.151	0.158
466	152	203	15.9	44.9	5610	25.4	0.75	12.8	125	1.6	276	1887	0.146	0.154
467	152	203	15.9	44.9	5610	31.8	0.75	12.8	125	2.0	269	1887	0.143	0.152
468	152	203	22.2	44.0	5500	22.2	0.75	9.1	125	1.0	408	2586	0.158	0.158
469	152	203	22.2	44.0	5500	31.8	0.75	9.1	125	1.4	394	2586	0.152	0.155
470	152	203	22.2	44.0	5500	44.4	0.75	9.1	125	2.0	377	2586	0.146	0.152
471	152	203	15.9	44.9	6732	15.9	0.75	12.8	150	1.0	219	1887	0.116	0.122
472	152	203	15.9	44.9	6732	25.4	0.75	12.8	150	1.6	213	1887	0.113	0.120
473	152	203	15.9	44.9	6732	31.8	0.75	12.8	150	2.0	209	1887	0.111	0.118
474	152	203	22.2	44.0	6600	22.2	0.75	9.1	150	1.0	316	2586	0.122	0.122
475	152	203	22.2	44.0	6600	31.8	0.75	9.1	150	1.4	307	2586	0.119	0.120
476	152	203	22.2	44.0	6600	44.4	0.75	9.1	150	2.0	296	2586	0.114	0.118
477	152	203	15.9	44.9	7854	15.9	0.75	12.8	175	1.0	173	1887	0.091	0.095
478	152	203	15.9	44.9	7854	25.4	0.75	12.8	175	1.6	168	1887	0.089	0.093
479	152	203	15.9	44.9	7854	31.8	0.75	12.8	175	2.0	165	1887	0.088	0.091
480	152	203	22.2	44.0	7700	22.2	0.75	9.1	175	1.0	251	2586	0.097	0.095
481	152	203	22.2	44.0	7700	31.8	0.75	9.1	175	1.4	245	2586	0.095	0.093
482	152	203	22.2	44.0	7700	44.4	0.75	9.1	175	2.0	237	2586	0.092	0.091
483	152	203	15.9	44.9	8976	15.9	0.75	12.8	200	1.0	139	1887	0.074	0.072
484	152	203	15.9	44.9	8976	25.4	0.75	12.8	200	1.6	136	1887	0.072	0.071
485	152	203	15.9	44.9	8976	31.8	0.75	12.8	200	2.0	134	1887	0.071	0.070
486	152	203	22.2	44.0	8799	22.2	0.75	9.1	200	1.0	203	2586	0.078	0.072
487	152	203	22.2	44.0	8799	31.8	0.75	9.1	200	1.4	199	2586	0.077	0.071
488	152	203	22.2	44.0	8799	44.4	0.75	9.1	200	2.0	193	2586	0.075	0.070
489	88.9	102	7.9	27.0	676	7.9	0.87	12.8	25	1.0	239	508	0.470	0.494
490	88.9	102	7.9	27.0	676	12.7	0.87	12.8	25	1.6	229	508	0.450	0.456
491	88.9	102	7.9	27.0	676	15.9	0.87	12.8	25	2.0	222	508	0.437	0.430
492	88.9	102	9.5	26.8	670	9.5	0.87	10.7	25	1.0	304	605	0.502	0.494
493	88.9	102	9.5	26.8	670	14.3	0.87	10.7	25	1.5	291	605	0.480	0.462
494	88.9	102	9.5	26.8	670	19.0	0.87	10.7	25	2.0	278	605	0.460	0.431
495	88.9	102	7.9	27.0	1351	7.9	0.87	12.8	50	1.0	204	508	0.402	0.365
496	88.9	102	7.9	27.0	1351	12.7	0.87	12.8	50	1.6	195	508	0.384	0.351
497	88.9	102	7.9	27.0	1351	15.9	0.87	12.8	50	2.0	190	508	0.373	0.341
498	88.9	102	9.5	26.8	1340	9.5	0.87	10.7	50	1.0	252	605	0.416	0.365
499	88.9	102	9.5	26.8	1340	14.3	0.87	10.7	50	1.5	241	605	0.399	0.353
500	88.9	102	9.5	26.8	1340	19.0	0.87	10.7	50	2.0	230	605	0.381	0.341
501	88.9	102	7.9	27.0	2027	7.9	0.87	12.8	75	1.0	147	508	0.290	0.274
502	88.9	102	7.9	27.0	2027	12.7	0.87	12.8	75	1.6	141	508	0.278	0.266
503	88.9	102	7.9	27.0	2027	15.9	0.87	12.8	75	2.0	138	508	0.270	0.261
504	88.9	102	9.5	26.8	2009	9.5	0.87	10.7	75	1.0	180	605	0.298	0.274

Run #	b_y	b_x	t	r_x	L	t_g	b_y/b_x	b_x/t	L/r_x	t_g/t	P_e	P_Y	P_e/P_Y	Ω
505	88.9	102	9.5	26.8	2009	14.3	0.87	10.7	75	1.5	173	605	0.286	0.267
506	88.9	102	9.5	26.8	2009	19.0	0.87	10.7	75	2.0	166	605	0.275	0.261
507	88.9	102	7.9	27.0	2702	7.9	0.87	12.8	100	1.0	105	508	0.206	0.210
508	88.9	102	7.9	27.0	2702	12.7	0.87	12.8	100	1.6	101	508	0.199	0.205
509	88.9	102	7.9	27.0	2702	15.9	0.87	12.8	100	2.0	99	508	0.194	0.201
510	88.9	102	9.5	26.8	2679	9.5	0.87	10.7	100	1.0	129	605	0.213	0.210
511	88.9	102	9.5	26.8	2679	14.3	0.87	10.7	100	1.5	124	605	0.205	0.205
512	88.9	102	9.5	26.8	2679	19.0	0.87	10.7	100	2.0	120	605	0.199	0.201
513	88.9	102	7.9	27.0	3378	7.9	0.87	12.8	125	1.0	77	508	0.152	0.162
514	88.9	102	7.9	27.0	3378	12.7	0.87	12.8	125	1.6	75	508	0.148	0.159
515	88.9	102	7.9	27.0	3378	15.9	0.87	12.8	125	2.0	74	508	0.145	0.157
516	88.9	102	9.5	26.8	3349	9.5	0.87	10.7	125	1.0	95	605	0.157	0.162
517	88.9	102	9.5	26.8	3349	14.3	0.87	10.7	125	1.5	93	605	0.153	0.160
518	88.9	102	9.5	26.8	3349	19.0	0.87	10.7	125	2.0	90	605	0.149	0.157
519	88.9	102	7.9	27.0	4054	7.9	0.87	12.8	150	1.0	59	508	0.116	0.126
520	88.9	102	7.9	27.0	4054	12.7	0.87	12.8	150	1.6	58	508	0.113	0.124
521	88.9	102	7.9	27.0	4054	15.9	0.87	12.8	150	2.0	57	508	0.112	0.122
522	88.9	102	9.5	26.8	4019	9.5	0.87	10.7	150	1.0	73	605	0.121	0.126
523	88.9	102	9.5	26.8	4019	14.3	0.87	10.7	150	1.5	71	605	0.118	0.124
524	88.9	102	9.5	26.8	4019	19.0	0.87	10.7	150	2.0	70	605	0.115	0.122
525	88.9	102	7.9	27.0	4729	7.9	0.87	12.8	175	1.0	46	508	0.091	0.098
526	88.9	102	7.9	27.0	4729	12.7	0.87	12.8	175	1.6	45	508	0.089	0.096
527	88.9	102	7.9	27.0	4729	15.9	0.87	12.8	175	2.0	45	508	0.088	0.095
528	88.9	102	9.5	26.8	4689	9.5	0.87	10.7	175	1.0	57	605	0.095	0.098
529	88.9	102	9.5	26.8	4689	14.3	0.87	10.7	175	1.5	56	605	0.093	0.097
530	88.9	102	9.5	26.8	4689	19.0	0.87	10.7	175	2.0	55	605	0.091	0.095
531	88.9	102	7.9	27.0	5405	7.9	0.87	12.8	200	1.0	37	508	0.072	0.075
532	88.9	102	7.9	27.0	5405	12.7	0.87	12.8	200	1.6	36	508	0.071	0.074
533	88.9	102	7.9	27.0	5405	15.9	0.87	12.8	200	2.0	36	508	0.070	0.073
534	88.9	102	9.5	26.8	5358	9.5	0.87	10.7	200	1.0	46	605	0.076	0.075
535	88.9	102	9.5	26.8	5358	14.3	0.87	10.7	200	1.5	45	605	0.075	0.074
536	88.9	102	9.5	26.8	5358	19.0	0.87	10.7	200	2.0	44	605	0.073	0.073

Table 4.8 Inelastic compressive resistance database for members with unequal-leg angles connected to gusset plates through the shorter legs

Run #	Geometric properties (mm)						Dimensionless parameters				Compressive resistance			
											kN		Ratio	
	b_y	b_x	t	r_x	L	t_g	b_y/b_x	b_x/t	L/r_x	t_g/t	P_e	P_Y	P_e/P_Y	Ω
537	203	102	15.9	65.1	1627	15.9	1.99	6.4	25	1.0	742	1609	0.461	0.463
538	203	102	15.9	65.1	1627	25.4	1.99	6.4	25	1.6	721	1609	0.448	0.431
539	203	102	15.9	65.1	1627	31.8	1.99	6.4	25	2.0	707	1609	0.439	0.409
540	203	102	22.2	64.1	1601	22.2	1.99	4.6	25	1.0	976	2197	0.444	0.463
541	203	102	22.2	64.1	1601	31.8	1.99	4.6	25	1.4	947	2197	0.431	0.440
542	203	102	22.2	64.1	1601	44.4	1.99	4.6	25	2.0	912	2197	0.415	0.409
543	203	102	15.9	65.1	3253	15.9	1.99	6.4	50	1.0	576	1609	0.358	0.343
544	203	102	15.9	65.1	3253	25.4	1.99	6.4	50	1.6	561	1609	0.349	0.331
545	203	102	15.9	65.1	3253	31.8	1.99	6.4	50	2.0	551	1609	0.342	0.322
546	203	102	19.0	64.6	3228	19.0	1.99	5.4	50	1.0	670	1902	0.352	0.343
547	203	102	19.0	64.6	3228	28.6	1.99	5.4	50	1.5	652	1902	0.343	0.333
548	203	102	19.0	64.6	3228	38.1	1.99	5.4	50	2.0	636	1902	0.334	0.322
549	203	102	22.2	64.1	3203	22.2	1.99	4.6	50	1.0	762	2197	0.347	0.343
550	203	102	22.2	64.1	3203	31.8	1.99	4.6	50	1.4	742	2197	0.338	0.334
551	203	102	22.2	64.1	3203	38.1	1.99	4.6	50	1.7	730	2197	0.332	0.328
552	203	102	22.2	64.1	3203	44.4	1.99	4.6	50	2.0	718	2197	0.327	0.322
553	203	102	25.4	63.6	3178	25.4	1.99	4.0	50	1.0	849	2486	0.342	0.343
554	203	102	25.4	63.6	3178	38.1	1.99	4.0	50	1.5	821	2486	0.330	0.333
555	203	102	25.4	63.6	3178	50.8	1.99	4.0	50	2.0	795	2486	0.320	0.322
556	203	102	15.9	65.1	4880	15.9	1.99	6.4	75	1.0	408	1609	0.254	0.254
557	203	102	15.9	65.1	4880	25.4	1.99	6.4	75	1.6	400	1609	0.249	0.247
558	203	102	15.9	65.1	4880	31.8	1.99	6.4	75	2.0	395	1609	0.245	0.242
559	203	102	22.2	64.1	4804	22.2	1.99	4.6	75	1.0	551	2197	0.251	0.254
560	203	102	22.2	64.1	4804	31.8	1.99	4.6	75	1.4	542	2197	0.246	0.249
561	203	102	22.2	64.1	4804	44.4	1.99	4.6	75	2.0	528	2197	0.240	0.242
562	203	102	15.9	65.1	6506	15.9	1.99	6.4	100	1.0	276	1609	0.172	0.188
563	203	102	15.9	65.1	6506	25.4	1.99	6.4	100	1.6	272	1609	0.169	0.184
564	203	102	15.9	65.1	6506	31.8	1.99	6.4	100	2.0	269	1609	0.167	0.181
565	203	102	19.0	64.6	6457	19.0	1.99	5.4	100	1.0	328	1902	0.172	0.188
566	203	102	19.0	64.6	6457	28.6	1.99	5.4	100	1.5	323	1902	0.170	0.184
567	203	102	19.0	64.6	6457	38.1	1.99	5.4	100	2.0	319	1902	0.168	0.181
568	203	102	22.2	64.1	6406	22.2	1.99	4.6	100	1.0	379	2197	0.173	0.188

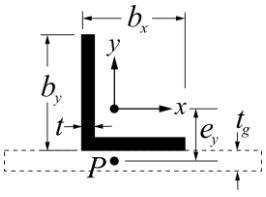

P_e = Compressive resistance based on 3D shell model

$$P_Y = F_Y A = 350 \times A$$

$$\Omega = 1.0 - \left(\frac{\left[53.6\left(b_y/b_x\right) - 2.35 \right]\left[\left(t_g/t\right)/\left(L/r_x\right) + 0.12 \right] + \left(L/r_x\right)}{0.83\left(L/r_x\right) + 56.9} \right)$$

Run #	b_y	b_x	t	r_x	L	t_g	b_y/b_x	b_x/t	L/r_x	t_g/t	P_e	P_Y	P_e/P_Y	Ω
569	203	102	22.2	64.1	6406	31.8	1.99	4.6	100	1.4	374	2197	0.170	0.185
570	203	102	22.2	64.1	6406	38.1	1.99	4.6	100	1.7	371	2197	0.169	0.183
571	203	102	22.2	64.1	6406	44.4	1.99	4.6	100	2.0	368	2197	0.167	0.181
572	203	102	25.4	63.6	6355	25.4	1.99	4.0	100	1.0	430	2486	0.173	0.188
573	203	102	25.4	63.6	6355	38.1	1.99	4.0	100	1.5	422	2486	0.170	0.185
574	203	102	25.4	63.6	6355	50.8	1.99	4.0	100	2.0	415	2486	0.167	0.181
575	203	102	15.9	65.1	8133	15.9	1.99	6.4	125	1.0	192	1609	0.119	0.139
576	203	102	15.9	65.1	8133	25.4	1.99	6.4	125	1.6	190	1609	0.118	0.136
577	203	102	15.9	65.1	8133	31.8	1.99	6.4	125	2.0	188	1609	0.117	0.134
578	203	102	22.2	64.1	8007	22.2	1.99	4.6	125	1.0	267	2197	0.121	0.139
579	203	102	22.2	64.1	8007	31.8	1.99	4.6	125	1.4	264	2197	0.120	0.137
580	203	102	22.2	64.1	8007	44.4	1.99	4.6	125	2.0	260	2197	0.118	0.134
581	203	102	15.9	65.1	9760	15.9	1.99	6.4	150	1.0	139	1609	0.087	0.100
582	203	102	15.9	65.1	9760	25.4	1.99	6.4	150	1.6	138	1609	0.086	0.098
583	203	102	15.9	65.1	9760	31.8	1.99	6.4	150	2.0	137	1609	0.085	0.096
584	203	102	19.0	64.6	9685	19.0	1.99	5.4	150	1.0	167	1902	0.088	0.100
585	203	102	19.0	64.6	9685	28.6	1.99	5.4	150	1.5	165	1902	0.087	0.098
586	203	102	19.0	64.6	9685	38.1	1.99	5.4	150	2.0	165	1902	0.087	0.096
587	203	102	22.2	64.1	9609	22.2	1.99	4.6	150	1.0	195	2197	0.089	0.100
588	203	102	22.2	64.1	9609	31.8	1.99	4.6	150	1.4	193	2197	0.088	0.099
589	203	102	22.2	64.1	9609	38.1	1.99	4.6	150	1.7	192	2197	0.087	0.098
590	203	102	22.2	64.1	9609	44.4	1.99	4.6	150	2.0	191	2197	0.087	0.096
591	203	102	25.4	63.6	9533	25.4	1.99	4.0	150	1.0	222	2486	0.089	0.100
592	203	102	25.4	63.6	9533	38.1	1.99	4.0	150	1.5	219	2486	0.088	0.098
593	203	102	25.4	63.6	9533	50.8	1.99	4.0	150	2.0	217	2486	0.087	0.096
594	203	102	15.9	65.1	11386	15.9	1.99	6.4	175	1.0	105	1609	0.065	0.069
595	203	102	15.9	65.1	11386	25.4	1.99	6.4	175	1.6	104	1609	0.065	0.068
596	203	102	15.9	65.1	11386	31.8	1.99	6.4	175	2.0	103	1609	0.064	0.066
597	203	102	22.2	64.1	11210	22.2	1.99	4.6	175	1.0	147	2197	0.067	0.069
598	203	102	22.2	64.1	11210	31.8	1.99	4.6	175	1.4	146	2197	0.067	0.068
599	203	102	22.2	64.1	11210	44.4	1.99	4.6	175	2.0	145	2197	0.066	0.066
600	203	102	15.9	65.1	13013	15.9	1.99	6.4	200	1.0	82	1609	0.051	0.044
601	203	102	15.9	65.1	13013	25.4	1.99	6.4	200	1.6	81	1609	0.050	0.043
602	203	102	15.9	65.1	13013	31.8	1.99	6.4	200	2.0	80	1609	0.050	0.042
603	203	102	19.0	64.6	12914	19.0	1.99	5.4	200	1.0	98	1902	0.052	0.044
604	203	102	19.0	64.6	12914	28.6	1.99	5.4	200	1.5	98	1902	0.051	0.043
605	203	102	19.0	64.6	12914	38.1	1.99	5.4	200	2.0	97	1902	0.051	0.042
606	203	102	22.2	64.1	12812	22.2	1.99	4.6	200	1.0	115	2197	0.052	0.044
607	203	102	22.2	64.1	12812	31.8	1.99	4.6	200	1.4	114	2197	0.052	0.043
608	203	102	22.2	64.1	12812	38.1	1.99	4.6	200	1.7	114	2197	0.052	0.043
609	203	102	22.2	64.1	12812	44.4	1.99	4.6	200	2.0	113	2197	0.052	0.042
610	203	102	25.4	63.6	12711	25.4	1.99	4.0	200	1.0	131	2486	0.053	0.044

Run #	b_y	b_x	t	r_x	L	t_g	b_y/b_x	b_x/t	L/r_x	t_g/t	P_e	P_Y	P_e/P_Y	Ω
611	203	102	25.4	63.6	12711	38.1	1.99	4.0	200	1.5	130	2486	0.052	0.043
612	203	102	25.4	63.6	12711	50.8	1.99	4.0	200	2.0	129	2486	0.052	0.042
613	178	102	15.9	56.7	1418	15.9	1.75	6.4	25	1.0	705	1470	0.479	0.490
614	178	102	15.9	56.7	1418	25.4	1.75	6.4	25	1.6	681	1470	0.463	0.462
615	178	102	15.9	56.7	1418	31.8	1.75	6.4	25	2.0	666	1470	0.453	0.443
616	178	102	22.2	55.7	1394	22.2	1.75	4.6	25	1.0	913	2003	0.456	0.490
617	178	102	22.2	55.7	1394	31.8	1.75	4.6	25	1.4	882	2003	0.440	0.470
618	178	102	22.2	55.7	1394	44.4	1.75	4.6	25	2.0	843	2003	0.421	0.443
619	178	102	15.9	56.7	2836	15.9	1.75	6.4	50	1.0	557	1470	0.379	0.362
620	178	102	15.9	56.7	2836	25.4	1.75	6.4	50	1.6	540	1470	0.367	0.351
621	178	102	15.9	56.7	2836	31.8	1.75	6.4	50	2.0	529	1470	0.360	0.344
622	178	102	22.2	55.7	2787	22.2	1.75	4.6	50	1.0	731	2003	0.365	0.362
623	178	102	22.2	55.7	2787	31.8	1.75	4.6	50	1.4	709	2003	0.354	0.354
624	178	102	22.2	55.7	2787	44.4	1.75	4.6	50	2.0	681	2003	0.340	0.344
625	178	102	15.9	56.7	4254	15.9	1.75	6.4	75	1.0	412	1470	0.280	0.268
626	178	102	15.9	56.7	4254	25.4	1.75	6.4	75	1.6	401	1470	0.273	0.262
627	178	102	15.9	56.7	4254	31.8	1.75	6.4	75	2.0	394	1470	0.268	0.258
628	178	102	22.2	55.7	4181	22.2	1.75	4.6	75	1.0	551	2003	0.275	0.268
629	178	102	22.2	55.7	4181	31.8	1.75	4.6	75	1.4	537	2003	0.268	0.264
630	178	102	22.2	55.7	4181	44.4	1.75	4.6	75	2.0	520	2003	0.259	0.258
631	178	102	15.9	56.7	5672	15.9	1.75	6.4	100	1.0	289	1470	0.197	0.200
632	178	102	15.9	56.7	5672	25.4	1.75	6.4	100	1.6	283	1470	0.193	0.197
633	178	102	15.9	56.7	5672	31.8	1.75	6.4	100	2.0	279	1470	0.190	0.194
634	178	102	22.2	55.7	5574	22.2	1.75	4.6	100	1.0	395	2003	0.197	0.200
635	178	102	22.2	55.7	5574	31.8	1.75	4.6	100	1.4	388	2003	0.194	0.198
636	178	102	22.2	55.7	5574	44.4	1.75	4.6	100	2.0	378	2003	0.189	0.194
637	178	102	15.9	56.7	7090	15.9	1.75	6.4	125	1.0	205	1470	0.140	0.149
638	178	102	15.9	56.7	7090	25.4	1.75	6.4	125	1.6	202	1470	0.137	0.147
639	178	102	15.9	56.7	7090	31.8	1.75	6.4	125	2.0	200	1470	0.136	0.145
640	178	102	22.2	55.7	6968	22.2	1.75	4.6	125	1.0	286	2003	0.143	0.149
641	178	102	22.2	55.7	6968	31.8	1.75	4.6	125	1.4	282	2003	0.141	0.147
642	178	102	22.2	55.7	6968	44.4	1.75	4.6	125	2.0	276	2003	0.138	0.145
643	178	102	15.9	56.7	8507	15.9	1.75	6.4	150	1.0	151	1470	0.102	0.109
644	178	102	15.9	56.7	8507	25.4	1.75	6.4	150	1.6	149	1470	0.101	0.107
645	178	102	15.9	56.7	8507	31.8	1.75	6.4	150	2.0	147	1470	0.100	0.106
646	178	102	22.2	55.7	8361	22.2	1.75	4.6	150	1.0	212	2003	0.106	0.109
647	178	102	22.2	55.7	8361	31.8	1.75	4.6	150	1.4	209	2003	0.105	0.108
648	178	102	22.2	55.7	8361	44.4	1.75	4.6	150	2.0	206	2003	0.103	0.106
649	178	102	15.9	56.7	9925	15.9	1.75	6.4	175	1.0	114	1470	0.078	0.078
650	178	102	15.9	56.7	9925	25.4	1.75	6.4	175	1.6	113	1470	0.077	0.076
651	178	102	15.9	56.7	9925	31.8	1.75	6.4	175	2.0	112	1470	0.076	0.075
652	178	102	22.2	55.7	9755	22.2	1.75	4.6	175	1.0	162	2003	0.081	0.078

Run #	b_y	b_x	t	r_x	L	t_g	b_y/b_x	b_x/t	L/r_x	t_g/t	P_e	P_Y	P_e/P_Y	Ω
653	178	102	22.2	55.7	9755	31.8	1.75	4.6	175	1.4	160	2003	0.080	0.076
654	178	102	22.2	55.7	9755	44.4	1.75	4.6	175	2.0	158	2003	0.079	0.075
655	178	102	15.9	56.7	11343	15.9	1.75	6.4	200	1.0	89	1470	0.061	0.052
656	178	102	15.9	56.7	11343	25.4	1.75	6.4	200	1.6	88	1470	0.060	0.050
657	178	102	15.9	56.7	11343	31.8	1.75	6.4	200	2.0	88	1470	0.060	0.050
658	178	102	22.2	55.7	11148	22.2	1.75	4.6	200	1.0	127	2003	0.063	0.052
659	178	102	22.2	55.7	11148	31.8	1.75	4.6	200	1.4	126	2003	0.063	0.051
660	178	102	22.2	55.7	11148	44.4	1.75	4.6	200	2.0	124	2003	0.062	0.050
661	127	76.2	9.5	40.7	1018	9.5	1.67	8.0	25	1.0	323	646	0.501	0.499
662	127	76.2	9.5	40.7	1018	14.3	1.67	8.0	25	1.5	316	646	0.489	0.476
663	127	76.2	9.5	40.7	1018	19.0	1.67	8.0	25	2.0	308	646	0.477	0.454
664	127	76.2	12.7	40.2	1006	12.7	1.67	6.0	25	1.0	407	847	0.481	0.499
665	127	76.2	12.7	40.2	1006	19.0	1.67	6.0	25	1.5	394	847	0.466	0.477
666	127	76.2	12.7	40.2	1006	25.4	1.67	6.0	25	2.0	382	847	0.451	0.454
667	127	76.2	9.5	40.7	2036	9.5	1.67	8.0	50	1.0	255	646	0.394	0.368
668	127	76.2	9.5	40.7	2036	14.3	1.67	8.0	50	1.5	249	646	0.386	0.359
669	127	76.2	9.5	40.7	2036	19.0	1.67	8.0	50	2.0	243	646	0.376	0.351
670	127	76.2	12.7	40.2	2011	12.7	1.67	6.0	50	1.0	324	847	0.383	0.368
671	127	76.2	12.7	40.2	2011	19.0	1.67	6.0	50	1.5	314	847	0.370	0.359
672	127	76.2	12.7	40.2	2011	25.4	1.67	6.0	50	2.0	306	847	0.361	0.350
673	127	76.2	9.5	40.7	3054	9.5	1.67	8.0	75	1.0	186	646	0.288	0.273
674	127	76.2	9.5	40.7	3054	14.3	1.67	8.0	75	1.5	182	646	0.282	0.268
675	127	76.2	9.5	40.7	3054	19.0	1.67	8.0	75	2.0	179	646	0.277	0.264
676	127	76.2	12.7	40.2	3017	12.7	1.67	6.0	75	1.0	243	847	0.286	0.273
677	127	76.2	12.7	40.2	3017	19.0	1.67	6.0	75	1.5	236	847	0.279	0.268
678	127	76.2	12.7	40.2	3017	25.4	1.67	6.0	75	2.0	231	847	0.272	0.263
679	127	76.2	9.5	40.7	4072	9.5	1.67	8.0	100	1.0	130	646	0.201	0.204
680	127	76.2	9.5	40.7	4072	14.3	1.67	8.0	100	1.5	128	646	0.198	0.201
681	127	76.2	9.5	40.7	4072	19.0	1.67	8.0	100	2.0	126	646	0.195	0.198
682	127	76.2	12.7	40.2	4023	12.7	1.67	6.0	100	1.0	173	847	0.204	0.204
683	127	76.2	12.7	40.2	4023	19.0	1.67	6.0	100	1.5	170	847	0.200	0.201
684	127	76.2	12.7	40.2	4023	25.4	1.67	6.0	100	2.0	166	847	0.196	0.198
685	127	76.2	9.5	40.7	5090	9.5	1.67	8.0	125	1.0	92	646	0.142	0.153
686	127	76.2	9.5	40.7	5090	14.3	1.67	8.0	125	1.5	90	646	0.140	0.150
687	127	76.2	9.5	40.7	5090	19.0	1.67	8.0	125	2.0	89	646	0.138	0.148
688	127	76.2	12.7	40.2	5028	12.7	1.67	6.0	125	1.0	124	847	0.147	0.153
689	127	76.2	12.7	40.2	5028	19.0	1.67	6.0	125	1.5	122	847	0.145	0.150
690	127	76.2	12.7	40.2	5028	25.4	1.67	6.0	125	2.0	121	847	0.142	0.148
691	127	76.2	9.5	40.7	6108	9.5	1.67	8.0	150	1.0	67	646	0.103	0.112
692	127	76.2	9.5	40.7	6108	14.3	1.67	8.0	150	1.5	66	646	0.102	0.111
693	127	76.2	9.5	40.7	6108	19.0	1.67	8.0	150	2.0	65	646	0.101	0.109
694	127	76.2	12.7	40.2	6034	12.7	1.67	6.0	150	1.0	92	847	0.109	0.112

Run #	b_y	b_x	t	r_x	L	t_g	b_y/b_x	b_x/t	L/r_x	t_g/t	P_e	P_Y	P_e/P_Y	Ω
695	127	76.2	12.7	40.2	6034	19.0	1.67	6.0	150	1.5	91	847	0.107	0.111
696	127	76.2	12.7	40.2	6034	25.4	1.67	6.0	150	2.0	89	847	0.106	0.109
697	127	76.2	9.5	40.7	7126	9.5	1.67	8.0	175	1.0	51	646	0.078	0.080
698	127	76.2	9.5	40.7	7126	14.3	1.67	8.0	175	1.5	50	646	0.078	0.079
699	127	76.2	9.5	40.7	7126	19.0	1.67	8.0	175	2.0	50	646	0.077	0.078
700	127	76.2	12.7	40.2	7040	12.7	1.67	6.0	175	1.0	70	847	0.083	0.080
701	127	76.2	12.7	40.2	7040	19.0	1.67	6.0	175	1.5	69	847	0.082	0.079
702	127	76.2	12.7	40.2	7040	25.4	1.67	6.0	175	2.0	68	847	0.081	0.078
703	127	76.2	9.5	40.7	8144	9.5	1.67	8.0	200	1.0	40	646	0.061	0.054
704	127	76.2	9.5	40.7	8144	14.3	1.67	8.0	200	1.5	39	646	0.061	0.053
705	127	76.2	9.5	40.7	8144	19.0	1.67	8.0	200	2.0	39	646	0.060	0.052
706	127	76.2	12.7	40.2	8046	12.7	1.67	6.0	200	1.0	55	847	0.065	0.054
707	127	76.2	12.7	40.2	8046	19.0	1.67	6.0	200	1.5	54	847	0.064	0.053
708	127	76.2	12.7	40.2	8046	25.4	1.67	6.0	200	2.0	54	847	0.063	0.052
709	152	102	15.9	47.9	1197	15.9	1.49	6.4	25	1.0	660	1325	0.498	0.518
710	152	102	15.9	47.9	1197	25.4	1.49	6.4	25	1.6	634	1325	0.478	0.494
711	152	102	15.9	47.9	1197	31.8	1.49	6.4	25	2.0	617	1325	0.465	0.478
712	152	102	22.2	47.0	1174	22.2	1.49	4.6	25	1.0	837	1801	0.465	0.518
713	152	102	22.2	47.0	1174	31.8	1.49	4.6	25	1.4	802	1801	0.445	0.501
714	152	102	22.2	47.0	1174	44.4	1.49	4.6	25	2.0	760	1801	0.422	0.478
715	152	102	15.9	47.9	2395	15.9	1.49	6.4	50	1.0	527	1325	0.398	0.382
716	152	102	15.9	47.9	2395	25.4	1.49	6.4	50	1.6	507	1325	0.382	0.372
717	152	102	15.9	47.9	2395	31.8	1.49	6.4	50	2.0	494	1325	0.373	0.366
718	152	102	22.2	47.0	2348	22.2	1.49	4.6	50	1.0	682	1801	0.379	0.382
719	152	102	22.2	47.0	2348	31.8	1.49	4.6	50	1.4	656	1801	0.364	0.375
720	152	102	22.2	47.0	2348	44.4	1.49	4.6	50	2.0	624	1801	0.346	0.366
721	152	102	15.9	47.9	3592	15.9	1.49	6.4	75	1.0	396	1325	0.299	0.284
722	152	102	15.9	47.9	3592	25.4	1.49	6.4	75	1.6	382	1325	0.289	0.279
723	152	102	15.9	47.9	3592	31.8	1.49	6.4	75	2.0	374	1325	0.282	0.275
724	152	102	22.2	47.0	3522	22.2	1.49	4.6	75	1.0	523	1801	0.291	0.284
725	152	102	22.2	47.0	3522	31.8	1.49	4.6	75	1.4	505	1801	0.280	0.280
726	152	102	22.2	47.0	3522	44.4	1.49	4.6	75	2.0	483	1801	0.268	0.275
727	152	102	15.9	47.9	4790	15.9	1.49	6.4	100	1.0	286	1325	0.216	0.213
728	152	102	15.9	47.9	4790	25.4	1.49	6.4	100	1.6	278	1325	0.210	0.210
729	152	102	15.9	47.9	4790	31.8	1.49	6.4	100	2.0	272	1325	0.206	0.208
730	152	102	22.2	47.0	4696	22.2	1.49	4.6	100	1.0	386	1801	0.214	0.213
731	152	102	22.2	47.0	4696	31.8	1.49	4.6	100	1.4	375	1801	0.208	0.211
732	152	102	22.2	47.0	4696	44.4	1.49	4.6	100	2.0	362	1801	0.201	0.208
733	152	102	15.9	47.9	5987	15.9	1.49	6.4	125	1.0	208	1325	0.157	0.160
734	152	102	15.9	47.9	5987	25.4	1.49	6.4	125	1.6	203	1325	0.153	0.158
735	152	102	15.9	47.9	5987	31.8	1.49	6.4	125	2.0	200	1325	0.151	0.156
736	152	102	22.2	47.0	5869	22.2	1.49	4.6	125	1.0	287	1801	0.159	0.160

Run #	b_y	b_x	t	r_x	L	t_g	b_y/b_x	b_x/t	L/r_x	t_g/t	P_e	P_Y	P_e/P_Y	Ω
737	152	102	22.2	47.0	5869	31.8	1.49	4.6	125	1.4	280	1801	0.156	0.158
738	152	102	22.2	47.0	5869	44.4	1.49	4.6	125	2.0	272	1801	0.151	0.156
739	152	102	15.9	47.9	7185	15.9	1.49	6.4	150	1.0	155	1325	0.117	0.119
740	152	102	15.9	47.9	7185	25.4	1.49	6.4	150	1.6	152	1325	0.115	0.117
741	152	102	15.9	47.9	7185	31.8	1.49	6.4	150	2.0	150	1325	0.113	0.116
742	152	102	22.2	47.0	7043	22.2	1.49	4.6	150	1.0	218	1801	0.121	0.119
743	152	102	22.2	47.0	7043	31.8	1.49	4.6	150	1.4	214	1801	0.119	0.118
744	152	102	22.2	47.0	7043	44.4	1.49	4.6	150	2.0	208	1801	0.116	0.116
745	152	102	15.9	47.9	8382	15.9	1.49	6.4	175	1.0	119	1325	0.090	0.086
746	152	102	15.9	47.9	8382	25.4	1.49	6.4	175	1.6	117	1325	0.088	0.085
747	152	102	15.9	47.9	8382	31.8	1.49	6.4	175	2.0	116	1325	0.087	0.084
748	152	102	22.2	47.0	8217	22.2	1.49	4.6	175	1.0	169	1801	0.094	0.086
749	152	102	22.2	47.0	8217	31.8	1.49	4.6	175	1.4	166	1801	0.092	0.085
750	152	102	22.2	47.0	8217	44.4	1.49	4.6	175	2.0	163	1801	0.091	0.084
751	152	102	15.9	47.9	9580	15.9	1.49	6.4	200	1.0	93	1325	0.070	0.059
752	152	102	15.9	47.9	9580	25.4	1.49	6.4	200	1.6	92	1325	0.069	0.058
753	152	102	15.9	47.9	9580	31.8	1.49	6.4	200	2.0	91	1325	0.069	0.058
754	152	102	22.2	47.0	9391	22.2	1.49	4.6	200	1.0	134	1801	0.074	0.059
755	152	102	22.2	47.0	9391	31.8	1.49	4.6	200	1.4	132	1801	0.073	0.059
756	152	102	22.2	47.0	9391	44.4	1.49	4.6	200	2.0	130	1801	0.072	0.058
757	178	127	15.9	56.4	1409	15.9	1.40	8.0	25	1.0	848	1609	0.527	0.528
758	178	127	15.9	56.4	1409	25.4	1.40	8.0	25	1.6	822	1609	0.511	0.506
759	178	127	15.9	56.4	1409	31.8	1.40	8.0	25	2.0	802	1609	0.498	0.491
760	178	127	22.2	55.4	1385	22.2	1.40	5.7	25	1.0	1083	2197	0.493	0.528
761	178	127	22.2	55.4	1385	31.8	1.40	5.7	25	1.4	1044	2197	0.475	0.512
762	178	127	22.2	55.4	1385	44.4	1.40	5.7	25	2.0	996	2197	0.453	0.491
763	178	127	12.7	56.9	2843	12.7	1.40	10.0	50	1.0	562	1299	0.433	0.388
764	178	127	12.7	56.9	2843	19.0	1.40	10.0	50	1.5	549	1299	0.423	0.381
765	178	127	12.7	56.9	2843	25.4	1.40	10.0	50	2.0	536	1299	0.413	0.374
766	178	127	15.9	56.4	2818	15.9	1.40	8.0	50	1.0	666	1609	0.414	0.388
767	178	127	15.9	56.4	2818	25.4	1.40	8.0	50	1.6	643	1609	0.400	0.379
768	178	127	15.9	56.4	2818	31.8	1.40	8.0	50	2.0	628	1609	0.391	0.374
769	178	127	19.0	55.9	2795	19.0	1.40	6.7	50	1.0	769	1902	0.404	0.388
770	178	127	19.0	55.9	2795	28.6	1.40	6.7	50	1.5	742	1902	0.390	0.381
771	178	127	19.0	55.9	2795	38.1	1.40	6.7	50	2.0	733	1902	0.386	0.373
772	178	127	22.2	55.4	2771	22.2	1.40	5.7	50	1.0	870	2197	0.396	0.388
773	178	127	22.2	55.4	2771	31.8	1.40	5.7	50	1.4	840	2197	0.382	0.382
774	178	127	22.2	55.4	2771	44.4	1.40	5.7	50	2.0	803	2197	0.365	0.374
775	178	127	25.4	54.9	2747	25.4	1.40	5.0	50	1.0	963	2486	0.387	0.388
776	178	127	25.4	54.9	2747	38.1	1.40	5.0	50	1.5	919	2486	0.370	0.381
777	178	127	25.4	54.9	2747	50.8	1.40	5.0	50	2.0	879	2486	0.354	0.374
778	178	127	15.9	56.4	4227	15.9	1.40	8.0	75	1.0	491	1609	0.305	0.289

Run #	b_y	b_x	t	r_x	L	t_g	b_y/b_x	b_x/t	L/r_x	t_g/t	P_e	P_Y	P_e/P_Y	Ω
779	178	127	15.9	56.4	4227	25.4	1.40	8.0	75	1.6	475	1609	0.295	0.284
780	178	127	15.9	56.4	4227	31.8	1.40	8.0	75	2.0	465	1609	0.289	0.281
781	178	127	22.2	55.4	4156	22.2	1.40	5.7	75	1.0	660	2197	0.300	0.289
782	178	127	22.2	55.4	4156	31.8	1.40	5.7	75	1.4	639	2197	0.291	0.286
783	178	127	22.2	55.4	4156	44.4	1.40	5.7	75	2.0	613	2197	0.279	0.281
784	178	127	12.7	56.9	5686	12.7	1.40	10.0	100	1.0	274	1299	0.211	0.218
785	178	127	12.7	56.9	5686	19.0	1.40	10.0	100	1.5	269	1299	0.207	0.215
786	178	127	12.7	56.9	5686	25.4	1.40	10.0	100	2.0	264	1299	0.203	0.212
787	178	127	15.9	56.4	5637	15.9	1.40	8.0	100	1.0	349	1609	0.217	0.218
788	178	127	15.9	56.4	5637	25.4	1.40	8.0	100	1.6	340	1609	0.211	0.214
789	178	127	15.9	56.4	5637	31.8	1.40	8.0	100	2.0	334	1609	0.207	0.212
790	178	127	19.0	55.9	5590	19.0	1.40	6.7	100	1.0	417	1902	0.219	0.218
791	178	127	19.0	55.9	5590	28.6	1.40	6.7	100	1.5	406	1902	0.213	0.215
792	178	127	19.0	55.9	5590	38.1	1.40	6.7	100	2.0	395	1902	0.208	0.212
793	178	127	22.2	55.4	5542	22.2	1.40	5.7	100	1.0	482	2197	0.219	0.218
794	178	127	22.2	55.4	5542	31.8	1.40	5.7	100	1.4	469	2197	0.213	0.215
795	178	127	22.2	55.4	5542	44.4	1.40	5.7	100	2.0	453	2197	0.206	0.212
796	178	127	25.4	54.9	5495	25.4	1.40	5.0	100	1.0	542	2486	0.218	0.218
797	178	127	25.4	54.9	5495	38.1	1.40	5.0	100	1.5	523	2486	0.210	0.215
798	178	127	25.4	54.9	5495	50.8	1.40	5.0	100	2.0	506	2486	0.203	0.212
799	178	127	15.9	56.4	7046	15.9	1.40	8.0	125	1.0	252	1609	0.157	0.164
800	178	127	15.9	56.4	7046	25.4	1.40	8.0	125	1.6	247	1609	0.153	0.162
801	178	127	15.9	56.4	7046	31.8	1.40	8.0	125	2.0	243	1609	0.151	0.160
802	178	127	22.2	55.4	6927	22.2	1.40	5.7	125	1.0	356	2197	0.162	0.164
803	178	127	22.2	55.4	6927	31.8	1.40	5.7	125	1.4	348	2197	0.158	0.162
804	178	127	22.2	55.4	6927	44.4	1.40	5.7	125	2.0	338	2197	0.154	0.160
805	178	127	12.7	56.9	8529	12.7	1.40	10.0	150	1.0	143	1299	0.110	0.122
806	178	127	12.7	56.9	8529	19.0	1.40	10.0	150	1.5	142	1299	0.109	0.121
807	178	127	12.7	56.9	8529	25.4	1.40	10.0	150	2.0	140	1299	0.107	0.120
808	178	127	15.9	56.4	8455	15.9	1.40	8.0	150	1.0	187	1609	0.116	0.122
809	178	127	15.9	56.4	8455	25.4	1.40	8.0	150	1.6	184	1609	0.114	0.121
810	178	127	15.9	56.4	8455	31.8	1.40	8.0	150	2.0	182	1609	0.113	0.120
811	178	127	19.0	55.9	8384	19.0	1.40	6.7	150	1.0	229	1902	0.120	0.122
812	178	127	19.0	55.9	8384	28.6	1.40	6.7	150	1.5	224	1902	0.118	0.121
813	178	127	19.0	55.9	8384	38.1	1.40	6.7	150	2.0	220	1902	0.116	0.120
814	178	127	22.2	55.4	8313	22.2	1.40	5.7	150	1.0	269	2197	0.122	0.122
815	178	127	22.2	55.4	8313	31.8	1.40	5.7	150	1.4	264	2197	0.120	0.121
816	178	127	22.2	55.4	8313	44.4	1.40	5.7	150	2.0	258	2197	0.117	0.120
817	178	127	25.4	54.9	8242	25.4	1.40	5.0	150	1.0	307	2486	0.123	0.122
818	178	127	25.4	54.9	8242	38.1	1.40	5.0	150	1.5	300	2486	0.121	0.121
819	178	127	25.4	54.9	8242	50.8	1.40	5.0	150	2.0	293	2486	0.118	0.120
820	178	127	15.9	56.4	9864	15.9	1.40	8.0	175	1.0	143	1609	0.089	0.089

Run #	b_y	b_x	t	r_x	L	t_g	b_y/b_x	b_x/t	L/r_x	t_g/t	P_e	P_Y	P_e/P_Y	Ω
821	178	127	15.9	56.4	9864	25.4	1.40	8.0	175	1.6	141	1609	0.088	0.088
822	178	127	15.9	56.4	9864	31.8	1.40	8.0	175	2.0	140	1609	0.087	0.087
823	178	127	22.2	55.4	9698	22.2	1.40	5.7	175	1.0	208	2197	0.095	0.089
824	178	127	22.2	55.4	9698	31.8	1.40	5.7	175	1.4	205	2197	0.093	0.088
825	178	127	22.2	55.4	9698	44.4	1.40	5.7	175	2.0	201	2197	0.091	0.087
826	178	127	12.7	56.9	11372	12.7	1.40	10.0	200	1.0	87	1299	0.067	0.062
827	178	127	12.7	56.9	11372	19.0	1.40	10.0	200	1.5	86	1299	0.066	0.061
828	178	127	12.7	56.9	11372	25.4	1.40	10.0	200	2.0	85	1299	0.065	0.060
829	178	127	15.9	56.4	11273	15.9	1.40	8.0	200	1.0	113	1609	0.070	0.062
830	178	127	15.9	56.4	11273	25.4	1.40	8.0	200	1.6	111	1609	0.069	0.061
831	178	127	15.9	56.4	11273	31.8	1.40	8.0	200	2.0	110	1609	0.068	0.060
832	178	127	19.0	55.9	11179	19.0	1.40	6.7	200	1.0	139	1902	0.073	0.062
833	178	127	19.0	55.9	11179	28.6	1.40	6.7	200	1.5	137	1902	0.072	0.061
834	178	127	19.0	55.9	11179	38.1	1.40	6.7	200	2.0	135	1902	0.071	0.060
835	178	127	22.2	55.4	11084	22.2	1.40	5.7	200	1.0	165	2197	0.075	0.062
836	178	127	22.2	55.4	11084	31.8	1.40	5.7	200	1.4	162	2197	0.074	0.061
837	178	127	22.2	55.4	11084	44.4	1.40	5.7	200	2.0	160	2197	0.073	0.060
838	178	127	25.4	54.9	10989	25.4	1.40	5.0	200	1.0	190	2486	0.076	0.062
839	178	127	25.4	54.9	10989	38.1	1.40	5.0	200	1.5	187	2486	0.075	0.061
840	178	127	25.4	54.9	10989	50.8	1.40	5.0	200	2.0	184	2486	0.074	0.060
841	203	152	15.9	64.5	1612	15.9	1.34	9.6	25	1.0	1041	1887	0.551	0.535
842	203	152	15.9	64.5	1612	25.4	1.34	9.6	25	1.6	1006	1887	0.533	0.514
843	203	152	15.9	64.5	1612	31.8	1.34	9.6	25	2.0	981	1887	0.520	0.500
844	203	152	22.2	63.5	1588	22.2	1.34	6.8	25	1.0	1341	2586	0.518	0.535
845	203	152	22.2	63.5	1588	31.8	1.34	6.8	25	1.4	1305	2586	0.505	0.520
846	203	152	22.2	63.5	1588	44.4	1.34	6.8	25	2.0	1249	2586	0.483	0.500
847	203	152	15.9	64.5	3224	15.9	1.34	9.6	50	1.0	830	1887	0.440	0.393
848	203	152	15.9	64.5	3224	25.4	1.34	9.6	50	1.6	805	1887	0.427	0.385
849	203	152	15.9	64.5	3224	31.8	1.34	9.6	50	2.0	789	1887	0.418	0.379
850	203	152	22.2	63.5	3176	22.2	1.34	6.8	50	1.0	1055	2586	0.408	0.393
851	203	152	22.2	63.5	3176	31.8	1.34	6.8	50	1.4	1023	2586	0.395	0.387
852	203	152	22.2	63.5	3176	44.4	1.34	6.8	50	2.0	981	2586	0.379	0.379
853	203	152	15.9	64.5	4835	15.9	1.34	9.6	75	1.0	576	1887	0.305	0.293
854	203	152	15.9	64.5	4835	25.4	1.34	9.6	75	1.6	559	1887	0.296	0.288
855	203	152	15.9	64.5	4835	31.8	1.34	9.6	75	2.0	547	1887	0.290	0.285
856	203	152	22.2	63.5	4764	22.2	1.34	6.8	75	1.0	790	2586	0.306	0.293
857	203	152	22.2	63.5	4764	31.8	1.34	6.8	75	1.4	767	2586	0.297	0.290
858	203	152	22.2	63.5	4764	44.4	1.34	6.8	75	2.0	739	2586	0.286	0.285
859	203	152	15.9	64.5	6447	15.9	1.34	9.6	100	1.0	405	1887	0.215	0.221
860	203	152	15.9	64.5	6447	25.4	1.34	9.6	100	1.6	395	1887	0.209	0.218
861	203	152	15.9	64.5	6447	31.8	1.34	9.6	100	2.0	388	1887	0.206	0.216
862	203	152	22.2	63.5	6352	22.2	1.34	6.8	100	1.0	571	2586	0.221	0.221

Run #	b_y	b_x	t	r_x	L	t_g	b_y/b_x	b_x/t	L/r_x	t_g/t	P_e	P_Y	P_e/P_Y	Ω
863	203	152	22.2	63.5	6352	31.8	1.34	6.8	100	1.4	557	2586	0.215	0.219
864	203	152	22.2	63.5	6352	44.4	1.34	6.8	100	2.0	539	2586	0.209	0.216
865	203	152	15.9	64.5	8059	15.9	1.34	9.6	125	1.0	291	1887	0.154	0.167
866	203	152	15.9	64.5	8059	25.4	1.34	9.6	125	1.6	285	1887	0.151	0.165
867	203	152	15.9	64.5	8059	31.8	1.34	9.6	125	2.0	281	1887	0.149	0.163
868	203	152	22.2	63.5	7940	22.2	1.34	6.8	125	1.0	419	2586	0.162	0.167
869	203	152	22.2	63.5	7940	31.8	1.34	6.8	125	1.4	410	2586	0.159	0.165
870	203	152	22.2	63.5	7940	44.4	1.34	6.8	125	2.0	400	2586	0.155	0.163
871	203	152	15.9	64.5	9671	15.9	1.34	9.6	150	1.0	216	1887	0.114	0.125
872	203	152	15.9	64.5	9671	25.4	1.34	9.6	150	1.6	212	1887	0.112	0.123
873	203	152	15.9	64.5	9671	31.8	1.34	9.6	150	2.0	209	1887	0.111	0.122
874	203	152	22.2	63.5	9528	22.2	1.34	6.8	150	1.0	315	2586	0.122	0.125
875	203	152	22.2	63.5	9528	31.8	1.34	6.8	150	1.4	310	2586	0.120	0.124
876	203	152	22.2	63.5	9528	44.4	1.34	6.8	150	2.0	303	2586	0.117	0.122
877	203	152	15.9	64.5	11282	15.9	1.34	9.6	175	1.0	165	1887	0.087	0.091
878	203	152	15.9	64.5	11282	25.4	1.34	9.6	175	1.6	163	1887	0.086	0.090
879	203	152	15.9	64.5	11282	31.8	1.34	9.6	175	2.0	161	1887	0.085	0.089
880	203	152	22.2	63.5	11116	22.2	1.34	6.8	175	1.0	243	2586	0.094	0.091
881	203	152	22.2	63.5	11116	31.8	1.34	6.8	175	1.4	240	2586	0.093	0.090
882	203	152	22.2	63.5	11116	44.4	1.34	6.8	175	2.0	236	2586	0.091	0.089
883	203	152	15.9	64.5	12894	15.9	1.34	9.6	200	1.0	131	1887	0.069	0.064
884	203	152	15.9	64.5	12894	25.4	1.34	9.6	200	1.6	129	1887	0.068	0.063
885	203	152	15.9	64.5	12894	31.8	1.34	9.6	200	2.0	127	1887	0.067	0.062
886	203	152	22.2	63.5	12704	22.2	1.34	6.8	200	1.0	193	2586	0.074	0.064
887	203	152	22.2	63.5	12704	31.8	1.34	6.8	200	1.4	190	2586	0.074	0.063
888	203	152	22.2	63.5	12704	44.4	1.34	6.8	200	2.0	187	2586	0.072	0.062
889	102	88.9	7.9	32.1	802	7.9	1.15	11.2	25	1.0	294	508	0.579	0.556
890	102	88.9	7.9	32.1	802	12.7	1.15	11.2	25	1.6	285	508	0.560	0.538
891	102	88.9	7.9	32.1	802	15.9	1.15	11.2	25	2.0	279	508	0.548	0.526
892	102	88.9	9.5	31.8	796	9.5	1.15	9.3	25	1.0	343	605	0.567	0.556
893	102	88.9	9.5	31.8	796	14.3	1.15	9.3	25	1.5	331	605	0.548	0.541
894	102	88.9	9.5	31.8	796	19.0	1.15	9.3	25	2.0	320	605	0.530	0.526
895	102	88.9	7.9	32.1	1604	7.9	1.15	11.2	50	1.0	207	508	0.408	0.408
896	102	88.9	7.9	32.1	1604	12.7	1.15	11.2	50	1.6	200	508	0.393	0.401
897	102	88.9	7.9	32.1	1604	15.9	1.15	11.2	50	2.0	195	508	0.384	0.396
898	102	88.9	9.5	31.8	1592	9.5	1.15	9.3	50	1.0	255	605	0.421	0.408
899	102	88.9	9.5	31.8	1592	14.3	1.15	9.3	50	1.5	246	605	0.406	0.402
900	102	88.9	9.5	31.8	1592	19.0	1.15	9.3	50	2.0	238	605	0.393	0.396
901	102	88.9	7.9	32.1	2406	7.9	1.15	11.2	75	1.0	153	508	0.302	0.304
902	102	88.9	7.9	32.1	2406	12.7	1.15	11.2	75	1.6	149	508	0.292	0.300
903	102	88.9	7.9	32.1	2406	15.9	1.15	11.2	75	2.0	146	508	0.286	0.298
904	102	88.9	9.5	31.8	2388	9.5	1.15	9.3	75	1.0	186	605	0.308	0.304

Run #	b_y	b_x	t	r_x	L	t_g	b_y/b_x	b_x/t	L/r_x	t_g/t	P_e	P_Y	P_e/P_Y	Ω
905	102	88.9	9.5	31.8	2388	14.3	1.15	9.3	75	1.5	181	605	0.298	0.301
906	102	88.9	9.5	31.8	2388	19.0	1.15	9.3	75	2.0	175	605	0.289	0.298
907	102	88.9	7.9	32.1	3208	7.9	1.15	11.2	100	1.0	108	508	0.213	0.230
908	102	88.9	7.9	32.1	3208	12.7	1.15	11.2	100	1.6	105	508	0.207	0.228
909	102	88.9	7.9	32.1	3208	15.9	1.15	11.2	100	2.0	103	508	0.203	0.226
910	102	88.9	9.5	31.8	3184	9.5	1.15	9.3	100	1.0	133	605	0.219	0.230
911	102	88.9	9.5	31.8	3184	14.3	1.15	9.3	100	1.5	129	605	0.214	0.228
912	102	88.9	9.5	31.8	3184	19.0	1.15	9.3	100	2.0	126	605	0.208	0.226
913	102	88.9	7.9	32.1	4010	7.9	1.15	11.2	125	1.0	78	508	0.154	0.175
914	102	88.9	7.9	32.1	4010	12.7	1.15	11.2	125	1.6	77	508	0.151	0.173
915	102	88.9	7.9	32.1	4010	15.9	1.15	11.2	125	2.0	76	508	0.148	0.172
916	102	88.9	9.5	31.8	3980	9.5	1.15	9.3	125	1.0	97	605	0.160	0.175
917	102	88.9	9.5	31.8	3980	14.3	1.15	9.3	125	1.5	95	605	0.156	0.173
918	102	88.9	9.5	31.8	3980	19.0	1.15	9.3	125	2.0	93	605	0.153	0.172
919	102	88.9	7.9	32.1	4812	7.9	1.15	11.2	150	1.0	59	508	0.116	0.132
920	102	88.9	7.9	32.1	4812	12.7	1.15	11.2	150	1.6	58	508	0.113	0.130
921	102	88.9	7.9	32.1	4812	15.9	1.15	11.2	150	2.0	57	508	0.112	0.130
922	102	88.9	9.5	31.8	4776	9.5	1.15	9.3	150	1.0	73	605	0.121	0.132
923	102	88.9	9.5	31.8	4776	14.3	1.15	9.3	150	1.5	72	605	0.119	0.131
924	102	88.9	9.5	31.8	4776	19.0	1.15	9.3	150	2.0	70	605	0.116	0.130
925	102	88.9	7.9	32.1	5614	7.9	1.15	11.2	175	1.0	45	508	0.089	0.098
926	102	88.9	7.9	32.1	5614	12.7	1.15	11.2	175	1.6	45	508	0.088	0.097
927	102	88.9	7.9	32.1	5614	15.9	1.15	11.2	175	2.0	44	508	0.087	0.096
928	102	88.9	9.5	31.8	5572	9.5	1.15	9.3	175	1.0	57	605	0.094	0.098
929	102	88.9	9.5	31.8	5572	14.3	1.15	9.3	175	1.5	56	605	0.092	0.097
930	102	88.9	9.5	31.8	5572	19.0	1.15	9.3	175	2.0	55	605	0.091	0.096
931	102	88.9	7.9	32.1	6416	7.9	1.15	11.2	200	1.0	36	508	0.071	0.070
932	102	88.9	7.9	32.1	6416	12.7	1.15	11.2	200	1.6	35	508	0.070	0.069
933	102	88.9	7.9	32.1	6416	15.9	1.15	11.2	200	2.0	35	508	0.069	0.068
934	102	88.9	9.5	31.8	6368	9.5	1.15	9.3	200	1.0	45	605	0.074	0.070
935	102	88.9	9.5	31.8	6368	14.3	1.15	9.3	200	1.5	44	605	0.073	0.069
936	102	88.9	9.5	31.8	6368	19.0	1.15	9.3	200	2.0	44	605	0.072	0.068

Appendix 4.D. Regression analysis

This appendix provides a description of the software TuringBot (2020) along with the procedures for developing Eqs. (4.11)a,b based on nonlinear regression.

4.D.1 TuringBot

TuringBot is a symbolic regression software developed based on the simulated annealing technique. The software uses artificial intelligence (AI) to search through a set of data to find mathematical expressions that describe the relationships between the input variables. The expressions are obtained from combining common functions such as arithmetic, trigonometric, hyperbolic, exponential functions and others. The software can also determine the numerical constants associated with known functions. Several search merits are available in the program including root mean square error, mean error, mean relative error, maximum error, maximum relative error, classification accuracy, F1 score, correlation coefficient and Nash-Sutcliffe efficiency.

4.D.2 Choosing the appropriate function

When fitting a data set, it is desirable to obtain the simplest possible expression while maintaining a sufficient level of accuracy. The accuracy of the fitting is mostly determined from the coefficient of determination $\left(r^2\right)$. Other statistical parameters such as the mean value, standard deviation and coefficient of variation also play an important role in choosing the appropriate function.

The data obtained from the parametric study (Appendix 4.C) was sorted and divided into two sets of data. The first data set represents the normalized compressive resistances for members with equal-leg angles and unequal-leg angles connected by the longer leg to a gusset plate at both ends whereas the second set of data consists of the normalized compressive resistances for members with unequal-leg angles connected by the shorter leg to a gusset plate at both ends.

By using the advanced option in TuringBot (2020), the potential family of functions representing the first set of data was set to take the form $\Omega = 1.0 - f\left[\left(L/r_x\right),\left(b_y/b_x\right),\left(t_g/t\right),\left(b_x/t\right)\right]$. The software then provided several candidate functions. Some of them are presented in Table 4.9 along with the relevant coefficient of determination $\left(r^2\right)$ in each case. Equation 3 in Table 4.9 (or Eq. (4.11)a in Chapter 4) was selected because it provides, based on the author's judgment, the right balance between simplicity and accuracy. Equation (4.11)b was obtained by forcing the second data set to fit a function that has the same structure as Eq. (4.11)a and then using TuringBot (2020) to determine the numerical constants.

Table 4.9 Potential functions fit the first data set

Eq. #	$1.0 - f\left[\left(L/r_x\right),\left(b_y/b_x\right),\left(t_g/t\right),\left(b_x/t\right)\right]$	r^2
1	$1.0 - \left(\dfrac{\left(L/r_x\right)}{\left(L/r_x\right)+23.3}\right)$	0.933
2	$1.0 - \left(\dfrac{\left(L/r_x\right)+12.9}{14.3\left(b_y/b_x\right)+0.91\left(L/r_x\right)+38.9}\right)$	0.971
3	$1.0 - \left(\dfrac{\left[199-103\left(b_y/b_x\right)\right]\left[\left(t_g/t\right)/\left(L/r_x\right)+0.050\right]+\left(L/r_x\right)}{0.88\left(L/r_x\right)+46.8}\right)$	0.987
4	$1.0 - \left(\dfrac{\dfrac{16.0}{\left(L/r_x\right)-22.1}+\left(L/r_x\right)+\dfrac{\left(t_g/t\right)}{\left[5.22-\left(b_x/t\right)\right]\left(b_y/b_x\right)}+2.58\left(t_g/t\right)-1.67}{0.90\left(L/r_x\right)+11.9\left(b_x/t\right)+29.3}\right)$	0.991
5	$1.0 - \left(\dfrac{\dfrac{16.2}{\left(L/r_x\right)-22.0}+\left(L/r_x\right)-\dfrac{\left(t_g/t\right)}{\left[4.70-\left(b_x/t\right)\right]\left[\left(b_y/b_x\right)-0.389\right]}+2.16\left(t_g/t\right)-1.94}{0.90\left(L/r_x\right)+8.95\left(b_y/b_x\right)+31.0}\right)$	0.993

Chapter 5: Elastic Compressive Buckling Resistance for Back-to-Back Double Angle Assemblies[2]

5.1. Abstract

The present study investigates the elastic buckling resistance of compression members consisting of non-slender hot-rolled double angles connected back-to-back with discrete interconnectors. Towards this goal, the study (a) formulates a thin-walled beam finite element buckling solution that treats both angles as independent members away from the intermediate connector locations while constraining the displacements for both angles at interconnector locations, and (b) develops an extension of the Vlasov thin-walled beam theory, originally intended for monolithic members, to determine the effective torsional/warping sectional properties for back-to-back double angle members. The validity of the thin-walled beam finite element model is then verified against experimental results and shell finite element models and its predictions are shown to asymptotically converge to the Vlasov theory extension developed in the present study as the number of interconnectors is increased. A systematic parametric study consisting of 1250 finite element runs is then conducted and the database of results generated is used to propose a simple equation to predict the elastic compressive buckling resistance of double angle compression members.

Keywords

Elastic Buckling; Flexural-torsional buckling; compression member; back-to-back; double angle; built-up member; assembly; interconnectors; thin-walled; finite element method.

[2]Alenezi, A. M. and Mohareb, M. (2022) "Elastic Compressive Buckling Resistance for Back-to-Back Double Angle Assemblies", submitted to an international journal.

5.2. Introduction and motivation

Long span compression members subjected to relatively high compressive forces in structural steel bracing systems and trusses frequently consist of back-to-back hot-rolled double angles connected at intermediate points along the span to form a built-up member (Figure 5.1a). In such members, the gusset plate details at the member end provide a fixity restraint about the X axis and a pin restraint about the Y axis. While the X and Y axes are aligned with the principal directions of the assembly, they are inclined relative to the principal axes of each individual angle ($\hat{x}_{1,2}$ and $\hat{y}_{1,2}$ axes in Figure 5.1c). Also, while interconnectors between the connected legs of both angle members provide inter-element simple constraints when displacements are expressed along the principal directions of the assembly, they result into more complex relations when expressed in terms of the displacements along the principal directions of the individual angles.

When predicting the elastic buckling stresses for built-up members, design standards (e.g., ANSI/AISC 360 2016, CSA S16 2019) adopt the classical buckling solution for monolithic members as a starting point. For a monolithic member with a monosymmetric section with an axis of symmetry aligned with the Y axis (i.e., coordinate of the shear centre S relative to the section centroid along the X axis is $X_S = 0$), the buckling stress F_X associated with pure flexure about the X axis is given by

$$F_X = \pi^2 E \Big/ \left(K_X L / r_X \right)^2 \tag{5.1}$$

while the buckling stress associated with the flexural-torsional mode F_{YZ} characterized by the combined torsion and flexure about the Y axis is determined from

$$F_{YZ} = \frac{F_Y + F_Z}{2\left[1 - \left(Y_S^2 / r_0^2\right)\right]} \left(1 - \sqrt{1 - \frac{4 F_Y F_Z \left[1 - \left(Y_S^2 / r_0^2\right)\right]}{\left(F_Y + F_Z\right)^2}} \right) \tag{5.2}$$

in which,

$$F_Y = \pi^2 E \Big/ \left(K_Y L_Y / r_Y\right)^2 \qquad F_Z = \left(\left[\pi^2 E I_{\omega\omega} \Big/ \left(K_Z L_Z\right)^2\right] + GJ\right) \Big/ A r_0^2 \tag{5.3)a,b}$$

and E is the modulus of elasticity, G is the modulus of rigidity, $I_{\omega\omega}$ is the warping constant, J is the Saint-Venant torsional constant, A is the sectional area, Y_S is the coordinates of the shear centre S relative to the section centroid along the Y axis, and

$$r_X = \sqrt{I_{XX}/A},\ r_Y = \sqrt{I_{YY}/A} \text{ and } r_0 = \sqrt{Y_S^2 + r_X^2 + r_X^2} \tag{5.4)a-c}$$

are the radii of gyration about the X and Y axes, and the polar radius of gyration about the shear centre, respectively, in which I_{XX} and I_{YY} are the principal moments of inertia, $\left(K_X L_X / r_X\right)$ and $\left(K_Y L_Y / r_Y\right)$ are the slenderness ratios along the principal directions of the member and $K_Z L_Z$ is the effective length relative to twist.

For built-up members consisting of back-to-back double angles, the effective slenderness ratio of the assembly in ANSI/AISC 360-16 for cases where the buckling mode induces shear stresses within the interconnectors (i.e., the combined buckling mode involving torsion and flexure about the axis of symmetry Y) is modified based on the type of intermediate connections between the individual members. For bolted connections with snug-tightened bolts, the modified slenderness ratio relative to the Y axis .$\left(K_Y L_Y / r_Y\right)_m$. for the member is

$$\left(K_Y L_Y / r_Y\right)_m = \sqrt{\left(K_Y L_Y / r_Y\right)^2 + \left(a / r_{min}\right)^2} \tag{5.5}$$

while for welded or bolted connections with pre-tensioned bolts, the modified slenderness ratio takes the form

$$\left(K_Y L_Y / r_Y\right)_m = \begin{cases} K_Y L_Y / r_Y & a/r_{min} \le 40 \\ \sqrt{\left(K_Y L_Y / r_Y\right)^2 + \left(0.5a / r_{min}\right)^2} & a/r_{min} > 40 \end{cases} \tag{5.6)a,b}$$

in which a is the distance between interconnectors along the span and r_{min} is the minimum radius of gyration of the individual angle. The modified slenderness ratio expressions are based on the work of Bleich (1952) whose formulation was intended for assemblies consisting of two chord members battened to form, essentially, a doubly symmetric arrangement (Figure 5.2). Consequently, Bleich (1952) considered only pure flexural buckling about the principal axis Y in formulating his solution. In contrast, back-to-back double angle assemblies forming a monosymmetric entity are expected to buckle into a flexural-torsional buckling mode (Figure 5.1) rather than a pure flexural mode about the Y axis. Hence, the use of the effective slenderness equations available in standards such as Eq. (5.6) based on Bleich's solution, or a modified version thereof, (e.g., Zahn and Haaijer 1987, Duan and Chen 1988, Aslani and Goel 1991, Sato and Uang 2007) is questionable and has implications on the estimated elastic buckling stresses based on Eqs. (5.2) and (5.3).

Furthermore, existing elastic buckling solutions for monosymmetric cross-sections (e.g., Eq. (5.2)) are intended for monolithic sections that act as a rigid disk in their own plane, i.e., they do not capture, for example, the difference in angles of twist $\theta_1(z) \neq \theta_2(z)$ (Figure 5.1c) expected to take place in both members away from the interconnector locations, as the assembly undergoes buckling.

Within the above context, the present study develops an elastic buckling finite element solution that captures the separation between both angle members away from the intermediate connector locations (Figure 5.1c) owing to their different buckling displacements, e.g., angles of twist $\theta_1(z) \neq \theta_2(z)$, while constraining both members at the locations of the interconnectors (Figure 5.1b), e.g., both angles would have the same angle of twist $\theta_1(z) = \theta_2(z)$. The model sought thus provides a mechanistic basis to quantify the elastic buckling stress associated with the flexural-

torsional buckling mode of back-to-back double angle assemblies while capturing the beneficial effect of interconnectors. Also, for the case where enough interconnectors are provided between both angle members, both angle sections would approach a condition similar, but not identical, to the monolithic condition. Towards developing an elastic buckling analytical solution for this limiting case, the Vlasov thin-walled theory, originally intended for monolithic sections, is extended for back-to-back double angle assemblies, yielding novel analytical expressions for the torsional/warping properties of the assembly.

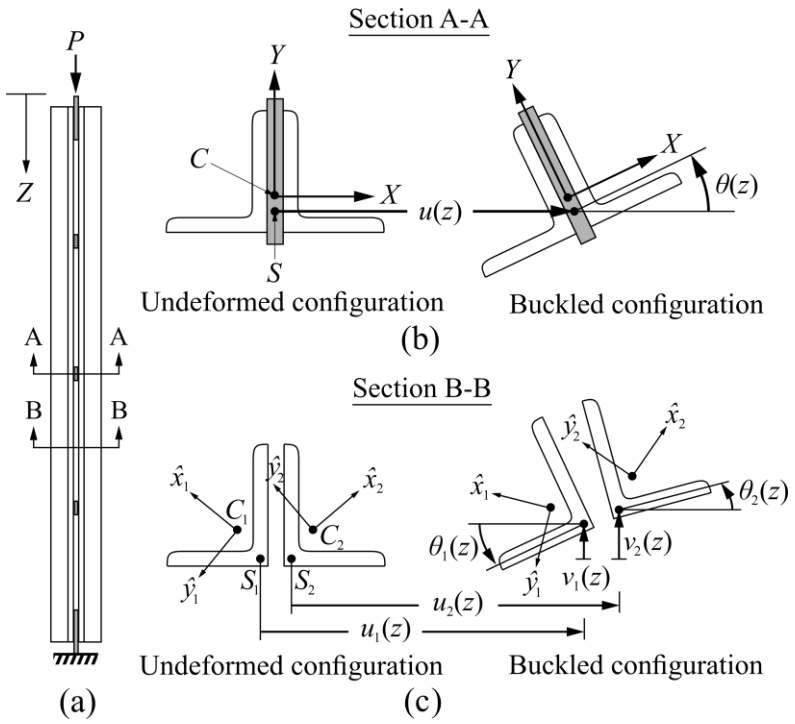

Figure 5.1 Compression assembly made of closely spaced back-to-back double angles with interconnectors (a) Elevation view, (b) Cross-sectional view A-A at interconnector, (c) Cross-sectional view B-B away from interconnectors.

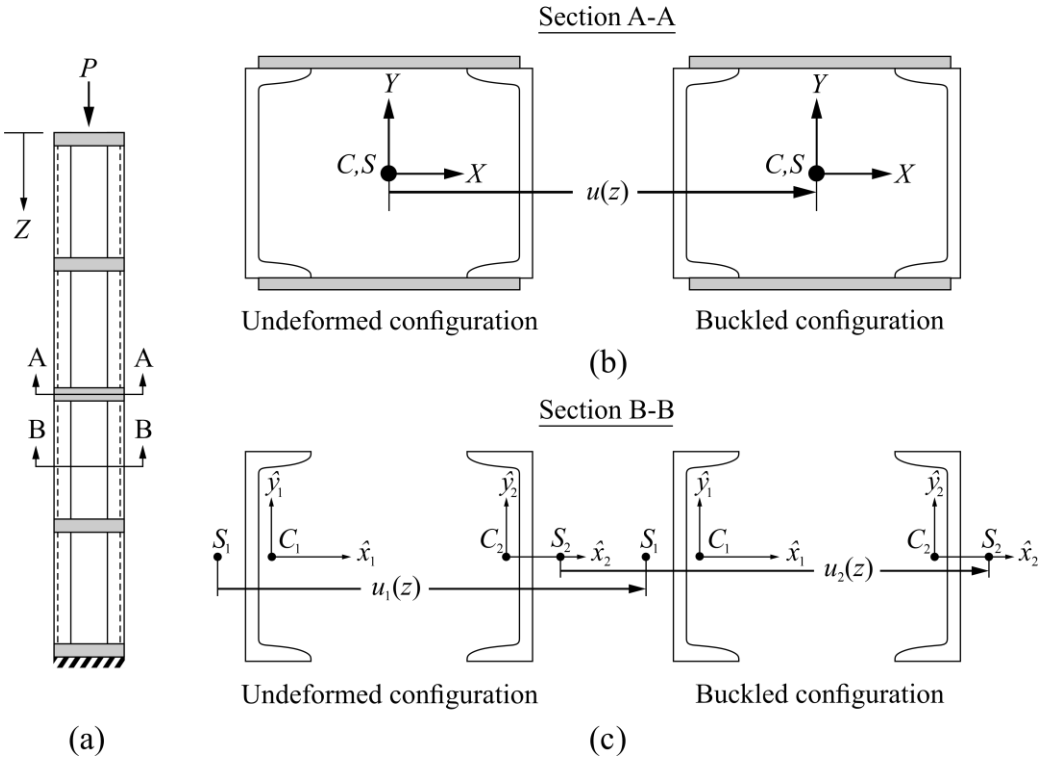

Figure 5.2 Compression assembly made of widely spaced double channels with battens (a) Elevation view (b) Cross-sectional view A-A at battens, and (c) Cross-sectional view B-B away from battens.

5.3. Literature review

Kennedy and Murty (1972) experimentally investigated the inelastic buckling resistance of pin-ended and fix-ended hot-rolled double equal-leg angle struts bolt-connected back-to-back at midspan and both ends under the action of monotonic compressive loading. It was observed that pin-ended members globally buckled either in a pure flexural or flexural-torsional mode while fix-ended members buckled globally only in a flexural-torsional mode. For pin-ended struts with double unequal-leg angles connected back-to-back by weld through the longer legs at both ends along with two intermediate weld connections, Kitipornchai and Lee (1986a,b) reported that such members bucked in a flexural-torsional mode. A similar observation was reported by Astaneh-Asl et al. (1985) and Aslani and Goel (1991) for double unequal-leg angles connected back-to-back through the longer legs to gusset plates at both ends under the effect of cyclic loading. Another

experimental and numerical study by Temple et al. (1986) investigating the effect of interconnectors on the buckling strength of starred angles under the effect of monotonically increasing compressive loading revealed that two interconnectors were enough for star-shaped assemblies to reach the buckling load of an equivalent monolithic member. A similar conclusion was reached for boxed angles in an experimental study by Temple et al. (1987). Another experimental investigation by Temple and Tan (1988) on widely spaced back-to-back double angle members under compressive loading reported that forces and moments in the interconnectors are negligible. Unlike the results reported by Astaneh-Asl et al. (1985) where an assembly with intermediate pretensioned bolts showed significant increase in the inelastic buckling resistance compared to an identical assembly with snug-tightened bolts, Sherman and Yura (1998) experimentally showed that both types of bolted interconnectors yield nearly identical elastic buckling resistances. It was concluded that, however, the use of pretensioned bolts at the end connections significantly increased the compressive resistance of the assembly. Other experimental investigations on closely spaced back-to-back hot-rolled channels include the work of Zandonini (1985), Lue et al. (2006) and Liu et al. (2009).

As an alternative to experimental investigations, the buckling behaviour of members can be effectively studied by numerical techniques such as the finite element method. Finite element buckling solutions for monolithic members with general open-cross sections include the work of Xiang et al. (1992) who developed a formulation for the buckling of members subjected to concentric end loading with a trapezoidal-shaped distribution of the axial loading along the span. Trahair and Rasmussen (2005) developed a formulation for monolithic compressive members with elastic end restraints defined along non-principal axes and offset from the shear centre. More general finite element buckling formulations for monolithic members with general open cross-

sections under combined compression and bending include the work of Krajcinovic (1969) and Barsoum and Gallagher (1970) who developed solutions for Vlasov type elements and Bradford and Trahair (1982) who developed a distortional buckling solution. Chan and Kitipornchai (1987) and Laudiero and Zaccaria (1988) developed buckling solutions by incorporating second order effects and Chin et al. (1993) developed a thin-plate element formulation. Kim et al. (1994) developed shear deformable buckling solutions. Papangelis et al. (1998) developed a finite element buckling program (PRFELB) for beam-columns and plane frames. Liu et al. (2019) developed a buckling solution that automates the calculation of section properties based on orthogonal axes. Other numerical buckling solutions for monolithic members under combined compression and bending involve the finite strip method (e.g., Plank and Wittrick 1974, Smith and Sridharan 1978, Lau and Hancock 1986, Papangelis and Hancock 1995, Naderian and Ronagh 2015 and He et al. 2018), the constrained finite strip method (e. g., Ádány and Schafer 2006a,b Ádány and Schafer 2008, Li and Schafer 2013 and Ádány and Schafer 2014) and the generalized beam theory (GBT) method (e.g., Davies et al. 1994, Silvestre and Camotim 2002, Dinis et al. 2006, and Camotim et al. 2008). A common theme among the previous solutions is that they are geared towards monolithic members and hence they are not intended for assemblies with multiple members connected at discrete locations. Numerical buckling solutions for compression cold-formed built-up members with discrete fasteners were developed by Abbasi et al. (2018) based on the compound strip method and by Mahar and Jayachandran (2021) based on compound spline finite strip method. Pure flexural buckling solutions were developed analytically by Zhou et al. (2020) for cold-formed assemblies with back-to-back cross-sections and by Rasmussen et al. (2020) for cold-formed assemblies with general cross-sections.

Approximate solutions for back-to-back double angle compression assemblies were developed by Marsh (1997) and Chen and Su (2003). Recent research on hot-rolled angle assemblies (e.g., Haifeng et al. 2016, Han et al. 2017, Hu et al. 2019, Qu et al. 2020 and Botelho et al. 2021) focused on star-shaped arrangements of double angles which tend to buckle either in a pure flexural or pure torsional mode (as opposed to a combined flexural-torsional buckling mode in the case of back-to-back double angles). Recent studies on cold-formed built-up members with angle cross-sections include the work of Maia et al. (2016), Ananthi et al. (2019a,b) and (2021) and Anbarasu and Dar (2020), and those with channel cross-sections include the work of Zhang and Young (2015), Dobrić et al. (2018a,b), Fratamico et al. (2018), Ting et al. (2018), Roy at al. (2018, 2019 and 2020), Chen at al. (2020), Dar et al. (2020 and 2021), Li et al. (2021), Mahar et al. (2021), Phan et al. (2021), Selvaraj and Madhavan (2021) Zhou et al (2021) and Li and Young (2022).

Within the context of understanding the buckling behaviour of built-up members and developing buckling solutions, the present study focuses on the elastic buckling resistance of back-to-back double angles by (i) developing a thin-walled finite element formulation for the buckling analysis of axially loaded members featuring non-principal end restraints and multi-point constraints and (ii) developing an extension of the Vlasov theory, originally intended for monolithic sections, to assemblies consisting of back-to-back double angles subjected to axial loads. Both solutions are verified against 3D shell-based finite element model predictions and subsequently used to (a) investigate the influence of interconnectors on the buckling load of back-to-back double angle assemblies, (b) assess the validity of the relevant design provisions in current standards and (c) develop an improved elastic buckling equation that capture the effect of the number of interconnectors on the elastic buckling resistance.

5.4. Formulation I: Thin-walled members with discrete interconnectors

5.4.1. Idealization

Each of the back-to-back double angles forming the assembly is idealized as a separate thin-walled member. Prior to buckling, each member is subjected to half of the pre-buckling compressive load at one end and is restrained longitudinally at the other end. The gusset plates ensure that the ends of both members pivot about the Y axis of the assembly, a condition that will be enforced through kinematic constraints in the finite element model sought herein. The end detail is such that the member ends are restrained from rotating about the X axis and relative to twist. The no-slip condition at the interface of the interconnectors is to be simulated by another set of kinematic constraints at each interconnector.

5.4.2. Assumptions

The thin-walled element formulation is based the following assumptions:

1. Each angle cross-section moves as a rigid disk in its own plane throughout buckling deformation, i.e., the section does not distort, in line with the first Vlasov's assumption (Vlasov 1961).
2. Shear strains vanish at the middle surface of the cross-section, in line with the second Vlasov's assumption.
3. The normal to the middle surface of the cross-section remains normal during deformation, in line with the Kirchhoff plate assumption (e.g., Gjelsvik 1981).

In addition, the formulation is restricted to prismatic members. Material is assumed to be linearly elastic isotropic homogeneous. The formulation is based on the assumptions that strains are small, but rotations are moderate.

5.4.3. Coordinate systems and orthogonality conditions

The treatment of the present section follows, for the most part, the work of Vlasov (1961) and Gjelsvik (1981) while introducing modifications that are deemed necessary for treating double angle members within the context of the finite element formulation sought. A right-handed Cartesian coordinate system (x_i, y_i, z_i) is adopted for each angle, where $i = 1, 2$, respectively, denote the left and right angle sections in Figure 5.1, with an origin C_i, satisfying the conditions $\int_{A_i} x_i dA_i = 0$, $\int_{A_i} y_i dA_i = 0$. The centroidal axes x_i, y_i are taken along the principal directions of the assembly to facilitate the imposition of kinematic constraints between the two angles at the locations of the interconnectors and hence are not aligned with the principal directions of the individual angles, i.e., $I_{xy,i} = \int_{A_i} x_i y_i dA_i \neq 0$, in contrast to the classical treatment in Vlasov (1961).

Additional right-handed coordinate systems (s_i, n_i, z_i) are adopted where s_i is a tangential coordinate along the middle surface of angle i, and n_i is a coordinate normal to the contour of the angle (Figure 5.3a). The sectorial origin B_i is chosen to be principal, thus, satisfying the condition $\int_{A_i} \omega_i dA_i = 0$ where the total warping function is $\omega_i = \bar{\omega}_i + \bar{\bar{\omega}}_i$ and $\bar{\omega}_i, \bar{\bar{\omega}}_i$ are the global and local sectorial coordinates, respectively. As a matter of notation, all single bars denote global coordinates while double bars denote local coordinates. The global sectorial coordinate $\bar{\omega}_i$ results from satisfying the zero-shear strain assumption at the middle surface of the cross-section (Assumption 2) and characterizes the longitudinal displacement distribution for points on the middle surface of the member. The value of $\bar{\omega}_i = \bar{\omega}_i(s_i, B_i, R_i)$ for a point s_i on the middle surface of angle i depends on (i) the coordinates of point s_i (ii) the sectorial origin B_i located on middle surface of the angle and (iii) the chosen pole R_i of the angle. It is numerically equal to twice the

area enclosed between the fixed radius R_iB_i, the mobile radius R_is_i and the sector B_is_i along the middle surface (Figure 5.3a). In the present formulation, pole R_i is taken to coincide with the shear centre S_i of the angle by satisfying the orthogonality conditions $\int_{A_i} \omega_i x_i dA_i = 0$ and $\int_{A_i} \omega_i y_i dA_i = 0$. For angle sections, the shear centre S_i is located at the point of intersection of the two legs (Figure 5.3) and the corresponding global sectorial coordinate $\bar{\omega}_i = \bar{\omega}_i\left(s_i, B_i, R_i = S_i\right)$ vanishes at all points on the middle surface of the section. The local sectorial coordinate $\bar{\bar{\omega}}_i = \bar{\bar{\omega}}_i\left(s_i, n_i, S_i\right)$ is obtained by applying the normality condition (Gjelsvik 1981) based on the Kirchhoff assumption (Assumption 3) and characterizes the distribution of the additional longitudinal displacement relative to a point on the middle surface, for a point that is offset from the middle surface by a distance n_i. The local sectorial coordinate $\bar{\bar{\omega}}_i\left(s_i, n_i, S_i\right) = -n_i q_i\left(s_i, S_i\right)$ where $q_i\left(s_i\right)$ is a tangential distance along the middle surface measured from the shear centre S_i (Figure 5.3b). Under the previous relationships, it can be shown that the orthogonality condition $\int_{A_i} \omega_i dA_i = 0$ is satisfied when the sectorial coordinate B_i is taken to coincide with the shear centre S_i (Figure 5.3b).

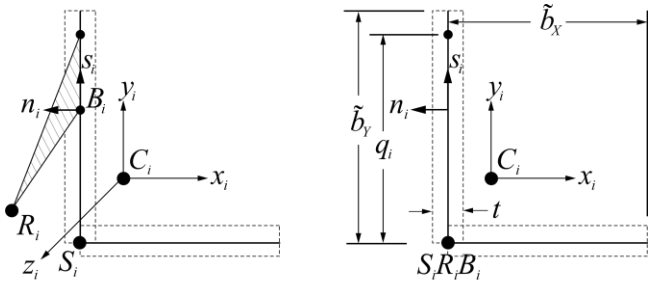

(a) (b)

Figure 5.3 Angle cross-section with (a) arbitrary pole R_i and sectorial origin B_i (b) pole R_i and sectorial origin B_i taken to coincide with the shear centre S_i

5.4.4. Deformation stages for flexural-torsional buckling

A back-to-back double angle assembly is shown in Figure 5.4 in the undeformed configuration. Under a compressive load N_p, the assembly displaces longitudinally from the undeformed to the deformed configuration by a pre-buckling displacement $w_p(z)$. As a matter of notation, a subscript p to a field denotes that the field pertains to pre-buckling stage whereas fields with no subscripts pertain to the buckling stage. The load N_p is then increased to λN_p, to reach the onset of buckling configuration. Under load λN_p, the pre-buckling longitudinal displacement increases proportionally to $\lambda w_p(z)$. At the onset of buckling, the member tends to buckle (by going from the onset of buckling configuration to the final buckled configuration) into a flexural-torsional mode. During buckling, load λN_p for the entire assembly is assumed to remain constant while angles i $(i=1,2)$ undergo additional longitudinal buckling displacements $w_i(z_i)$ at their centroidal axes, in addition to shear centre displacements $u_i(z_i)$ and $v_i(z_i)$ along the x_i and y_i directions, and twisting angles $\theta_i(z_i)$. It is noted that the present analysis deviates from the conventional treatment of monolithic members undergoing flexural-torsional buckling in which the longitudinal displacement $w(z)$ throughout buckling is taken to vanish at the centroidal axis of the monolithic member (e.g., Trahair 1993, Alenezi and Mohareb 2021). In contrast, in the back-to-back double angle assembly considered in the present study, the centroidal axis of each angle member undergoes a longitudinal displacement throughout buckling while that of the centroidal axis of the assembly vanishes, in a manner similar to monolithic members.

For a point on cross-section i with coordinates $x_i(s_i,n_i)$, $y_i(s_i,n_i)$ and $\omega_i(s_i,n_i)$, the buckling displacements $\tilde{u}_i(s_i,n_i,z_i)$ and $\tilde{v}_i(s_i,n_i,z_i)$ along x and y axes after enforcing the rigid body deformation (Assumption 1) are given by (e.g., Gjelsvik 1981, Trahair 1993)

$$\tilde{u}_i(s_i,n_i,z_i) = u_i(z_i) - \left[y_i(s_i,n_i) - y_{S_i}\right]\theta_i(z_i) \tag{5.7}$$

$$\tilde{v}_i(s_i,n_i,z_i) = v_i(z_i) + \left[x_i(s_i,n_i) - x_{S_i}\right]\theta_i(z_i) \tag{5.8}$$

and the longitudinal displacement including the effect of moderate rotations (e.g., Trahair 1993) is given by

$$\begin{aligned}\tilde{w}_i(s_i,n_i,z_i) = {} & \lambda w_{pi}(z_i) + w_i(z_i) - x_i(s_i,n_i)u_i'(z_i) - y_i(s_i,n_i)v_i'(z_i) + \omega_i(s_i,n_i)\theta_i'(z_i) \\ & + y_i(s_i,n_i)u_i'(z_i)_i\,\theta_i(z_i) - x_i(s_i,n_i)v_i'(z_i)\theta_i(z_i)\end{aligned} \tag{5.9}$$

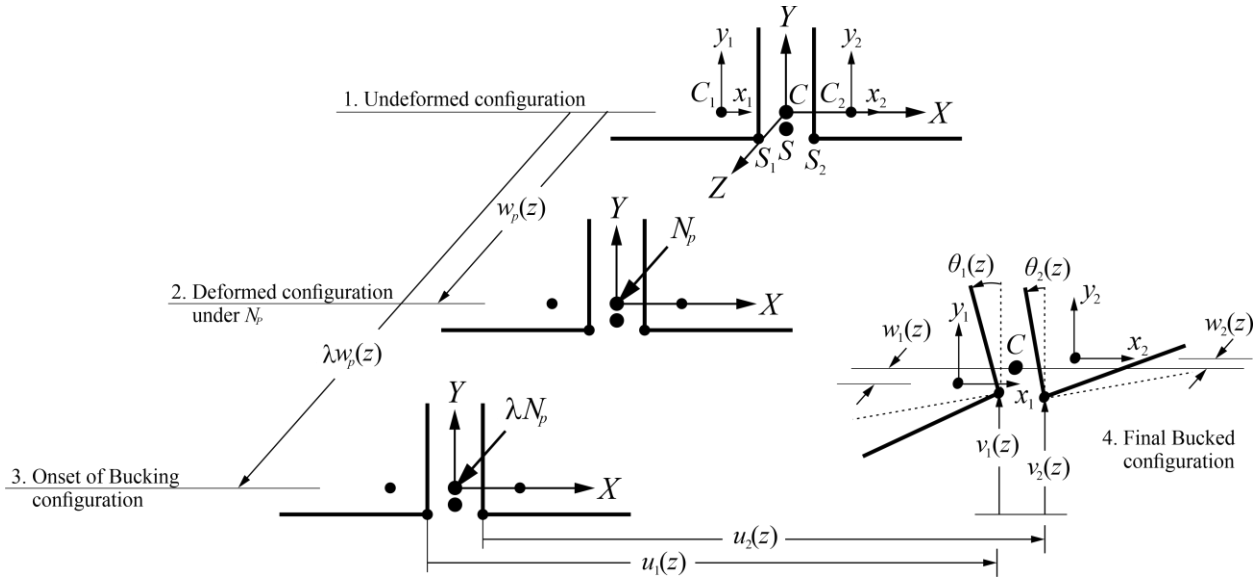

Figure 5.4. Stages of deformation throughout flexural-torsional buckling

5.4.5. Variational principle

At the final buckled configuration (Figure 5.4), the total potential energy Π_i for element i ($i=1$ for the left member and $i=2$ for the right member) of length l arises from the internal strain energy due to longitudinal and shear strains (e.g., Trahair 1993) and is given by

$$\Pi_i = \frac{1}{2}\int_0^l \left[\int_{A_i} \left(\sigma_i + \lambda\sigma_{pi}\right)\left(\varepsilon_i + \lambda\varepsilon_{pi}\right) + \left(\tau_i + \lambda\tau_{pi}\right)\left(\gamma_i + \lambda\gamma_{pi}\right) \right] dA_i dz_i \tag{5.10}$$

in which, $\left(\sigma_i + \lambda\sigma_{pi}\right)$ is the total longitudinal stress for element i and $\left(\varepsilon_i + \lambda\varepsilon_{pi}\right)$ is the corresponding strain. Also, $\left(\tau_i + \lambda\tau_{pi}\right)$ is the total shear stress and $\left(\gamma_i + \lambda\gamma_{pi}\right)$ is the corresponding strain. By noting that the pre-buckling shear stress and strain vanish for members under pure compression (i.e., $\lambda\tau_{pi} = \lambda\gamma_{pi} = 0$), and taking the second variation of Eq. (5.10), one obtains

$$\frac{1}{2}\delta^2\Pi_i = \frac{1}{2}\int_0^l \int_{A_i} \left[E\left(\delta\varepsilon_i\right)^2 + \lambda\sigma_{pi}\delta^2\varepsilon_i + G\left(\delta\gamma_i\right)^2 \right] dA_i dz_i \tag{5.11}$$

in which δ denotes the first variation of the argument function and δ^2 denotes the second variation of the argument function/functional. The longitudinal buckling strain ε_i for element i is given by

$$\begin{aligned}\varepsilon_i\left(s_i, n_i, z_i\right) \approx \tilde{w}_i' + \frac{1}{2}\left(\tilde{u}_i'^2 + \tilde{v}_i'^2\right) &= \lambda w_{pi}' + w_i' - x_i u_i'' - y_i v_i'' + \omega_i\theta_i'' + y_i\left(u_i'\theta_i' + \theta_i u_i''\right) - x_i\left(v_i'\theta_i' + \theta_i v_i''\right) \\ &\quad + \frac{1}{2}\left[u_i' - \left(y_i - y_{S_i}\right)\theta_i'\right]^2 + \frac{1}{2}\left[v_i' + \left(x_i - x_{S_i}\right)\theta_i'\right]^2\end{aligned} \tag{5.12}$$

By omitting the second-order terms of the shear strain (e.g., Gjelsvik 1981), one obtains

$$\gamma_i = 2n_i\theta_i' \tag{5.13}$$

By taking the first and second variations of Eq. (5.12), and the first variation of Eq. (5.13), and recalling that the buckling displacements u_i, v_i, w_i and θ_i vanish at the onset of buckling, one obtains

$$\begin{aligned}\delta\varepsilon_i &= \delta w_i' - x_i\delta u_i'' - y_i\delta v_i'' + \omega_i\delta\theta_i'' \\ \delta^2\varepsilon_i &= \delta u_i'^2 + \delta v_i'^2 + 2y_i\left(\delta u_i'\delta\theta_i' + \delta u_i''\delta\theta_i\right) - 2x_i\left(\delta v_i'\delta\theta_i' + \delta v_i''\delta\theta_i\right) \\ &\quad -2\left(y_i - y_{S_i}\right)\delta u_i'\delta\theta_i' + 2\left(x_i - x_{S_i}\right)\delta v_i'\delta\theta_i' + \left[\left(y_i - y_{S_i}\right)^2 + \left(x_i - x_{S_i}\right)^2\right]\delta\theta_i'^2\end{aligned} \tag{5.14}a,b$$

$$\delta\gamma_i = 2n_i\delta\theta_i' \tag{5.15}$$

As discussed under Section 5.4.3, by adopting centroidal axes for angle i, taking the pole at the shear centre of the angle and adopting a principal sectorial origin, one obtains the orthogonality conditions,

$$\int_{A_i} x_i dA_i = \int_{A_i} y_i dA_i = \int_{A_i} \omega_i dA_i = \int_{A_i} \omega_i x_i dA_i = \int_{A_i} \omega_i y_i dA_i = 0 \tag{5.16}$$

We also recall that, unlike conventional solutions, the present treatment considers the x_i, y_i axes to be aligned with the principal directions of the assembly as opposed to those of the angles, i.e., $I_{x_i y_i} = \int_{A_i} x_i y_i dA_i \neq 0$. From Eqs. (5.14) and (5.15), by substituting into Eq. (5.11), integrating over area A_i of angle i and then applying the orthogonality conditions in Eq. (5.16), the second variation of the total potential energy can be expressed as

$$\begin{aligned}\frac{1}{2}\delta^2\Pi_i = \frac{1}{2}\int_0^l \Big[&\underline{EA_i\delta w_i'^2} + EI_{y_i y_i}\delta u_i''^2 + EI_{x_i x_i}\delta v_i''^2 + \underline{2EI_{x_i y_i}\delta u_i''\delta v_i''} + EI_{\omega_i\omega_i}\delta\theta_i''^2 + GJ_i\delta\theta_i'^2 \\ &-\lambda\left(N_p/2\right)\left(\delta u_i'^2 + \delta v_i'^2 + r_{0_i}^2\delta\theta_i'^2 + 2y_{S_i}\delta u_i'\delta\theta_i' - 2x_{S_i}\delta v_i'\delta\theta_i'\right)\Big] dz_i\end{aligned} \tag{5.17}$$

in which, the sectional properties for angles $i = 1, 2$ are given by

$$A_i = t\left(\tilde{b}_X + \tilde{b}_Y\right) \qquad x_{S_i} = \frac{(-1)^{i+1}\tilde{b}_X^2}{2\left(\tilde{b}_X + \tilde{b}_Y\right)} \qquad y_{S_i} = \frac{-\tilde{b}_Y^2}{2\left(\tilde{b}_X + \tilde{b}_Y\right)}$$

$$I_{y_i y_i} = \frac{t}{12}\left(t^2\tilde{b}_Y + 4\tilde{b}_X^3 - \frac{3\tilde{b}_X^4}{\tilde{b}_X + \tilde{b}_Y}\right) \qquad I_{x_i x_i} = \frac{t}{12}\left(4\tilde{b}_Y^3 + t^2\tilde{b}_X - \frac{3\tilde{b}_Y^4}{\tilde{b}_X + \tilde{b}_Y}\right) \tag{5.18a-i}$$

$$I_{x_i y_i} = \frac{(-1)^{i+1} t\tilde{b}_Y^2\tilde{b}_X^2}{4\left(\tilde{b}_X + \tilde{b}_Y\right)} \qquad I_{\omega_i\omega_i} = \frac{t^3}{36}\left(\tilde{b}_X^3 + \tilde{b}_Y^3\right) \qquad J_i = \frac{t^3}{3}\left(\tilde{b}_X + \tilde{b}_Y\right) \qquad r_{0_i}^2 = \frac{\tilde{b}_X^3 + \tilde{b}_Y^3}{3\left(\tilde{b}_X + \tilde{b}_Y\right)} + \frac{t^2}{12}$$

where $\tilde{b}_X$ and $\tilde{b}_Y$ are the centreline dimensions of the angle legs along X and Y directions and t is the thickness (Figure 5.3b). We note that the present formulation gives rise to the underlined

two terms in Eq. (5.17) which do not appear in the classical buckling formulation for monolithic sections.

5.4.6. Finite element formulation

5.4.6.1. Interpolation scheme

A two-node thin-walled beam element is developed based on the non-principal axes (as depicted in Figure 5.5). The element is intended to model one of the two angles forming the assembly. It has seven degrees of freedom per node to characterize the buckling response of the member, three displacements u_N, v_N, w_N , three rotations u'_N, v'_N, θ_N and a warping deformation θ'_N (Figure 5.5) where subscripts $N = 1, 2$, respectively, denote the first and second nodes of the element.

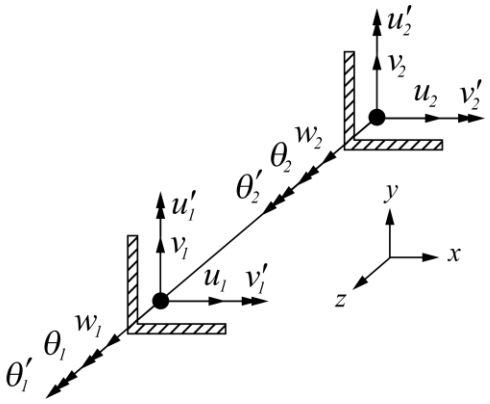

Figure 5.5 Flexural-torsional buckling element with 14 degrees of freedom

The variation of the longitudinal buckling displacement δw is related to the nodal displacement vector $\mathbf{d}_{\mathbf{w}i}^{\mathrm{T}} = \langle w_1 \quad w_2 \rangle$ through

$$\delta w(z) = \mathbf{S}(z)_{1\times 2}\, \mathbf{d}_{\mathbf{w}i(2\times 1)} \tag{5.19}$$

where $\mathbf{S}(z) = \langle 1 - z/l \quad z/l \rangle$ is the vector of linear shape functions. The variations of lateral displacements $\delta u, \delta v$ and angle of twist $\delta\theta$ are related to the nodal displacement vectors $\mathbf{d}_{\mathbf{u}i}$, $\mathbf{d}_{\mathbf{v}i}$ and $\mathbf{d}_{\boldsymbol{\theta}i}$ defined by

$$\mathbf{d}_{\mathbf{u}i}^{\mathbf{T}} = \langle u_1 \quad u_1' \quad u_2 \quad u_2' \rangle \qquad \mathbf{d}_{\mathbf{v}i}^{\mathbf{T}} = \langle v_1 \quad v_1' \quad v_2 \quad v_2' \rangle \qquad \mathbf{d}_{\boldsymbol{\theta}i}^{\mathbf{T}} = \langle \theta_1 \quad \theta_1' \quad \theta_2 \quad \theta_2' \rangle \qquad (5.20)\text{a-c}$$

through Hermitian polynomials, i.e.,

$$\delta u(z) = \mathbf{H_1}(z)_{1\times 4}\,\mathbf{d}_{\mathbf{u}i(4\times 1)} \qquad \delta v(z) = \mathbf{H_2}(z)_{1\times 4}\,\mathbf{d}_{\mathbf{v}i(4\times 1)} \qquad \delta\theta(z) = \mathbf{H_1}(z)_{1\times 4}\,\mathbf{d}_{\boldsymbol{\theta}i(4\times 1)} \qquad (5.21)\text{a-c}$$

in which, $\mathbf{H_1}(z)$ and $\mathbf{H_2}(z)$ are the vectors of Hermitian shape functions defined as

$$\mathbf{H_1}(z) = \frac{1}{l^3}\left\langle \left(2z^3 - 3z^2 l + l^3\right) \quad \left(z^3 l - 2z^2 l^2 + z l^3\right) \quad \left(-2z^3 + 3z^2 l\right) \quad \left(z^3 l - z^2 l^2\right) \right\rangle \qquad (5.22)$$

$$\mathbf{H_2}(z) = \frac{1}{l^3}\left\langle \left(2z^3 - 3z^2 l + l^3\right) \quad -\left(z^3 l - 2z^2 l^2 + z l^3\right) \quad \left(-2z^3 + 3z^2 l\right) \quad -\left(z^3 l - z^2 l^2\right) \right\rangle \qquad (5.23)$$

From Eqs. (5.19) and (5.21)a-c by substituting into Eq. (5.17), the second variation of the total potential energy is expressed as

$$\delta^2 \Pi_i / 2 = (1/2)\,\mathbf{d}_i^{\mathrm{T}} \left(\mathbf{k}_{\mathbf{E}i} - \lambda \mathbf{k}_{\mathbf{G}i}\right)\mathbf{d}_i \qquad (5.24)$$

where $\mathbf{k}_{\mathbf{E}i}$ is the element stiffness matrix, $\mathbf{k}_{\mathbf{G}i}$ is the element geometric matrix and $\mathbf{d}_i$ is the element nodal displacements vector defined by

$$\mathbf{k}_{\mathbf{E}i} = \begin{bmatrix} \mathbf{k}_{\mathbf{E}\mathbf{w}\mathbf{w}i} & \mathbf{0} & \mathbf{0} & \mathbf{0} \\ \mathbf{0} & \mathbf{k}_{\mathbf{E}\mathbf{u}\mathbf{u}i} & \mathbf{k}_{\mathbf{E}\mathbf{u}\mathbf{v}i} & \mathbf{0} \\ \mathbf{0} & \mathbf{k}_{\mathbf{E}\mathbf{u}\mathbf{v}i}^{\mathbf{T}} & \mathbf{k}_{\mathbf{E}\mathbf{v}\mathbf{v}i} & \mathbf{0} \\ \mathbf{0} & \mathbf{0} & \mathbf{0} & \mathbf{k}_{\mathbf{E}\boldsymbol{\omega}\boldsymbol{\omega}i} + \mathbf{k}_{\mathbf{E}\mathbf{s}\mathbf{v}i} \end{bmatrix},\ \mathbf{k}_{\mathbf{G}i} = \begin{bmatrix} \mathbf{0} & \mathbf{0} & \mathbf{0} & \mathbf{0} \\ \mathbf{0} & \mathbf{k}_{\mathbf{G}\mathbf{u}\mathbf{u}i} & \mathbf{0} & \mathbf{k}_{\mathbf{G}\mathbf{u}\boldsymbol{\theta}i} \\ \mathbf{0} & \mathbf{0} & \mathbf{k}_{\mathbf{G}\mathbf{v}\mathbf{v}i} & \mathbf{k}_{\mathbf{G}\mathbf{v}\boldsymbol{\theta}i} \\ \mathbf{0} & \mathbf{k}_{\mathbf{G}\mathbf{u}\boldsymbol{\theta}i}^{\mathbf{T}} & \mathbf{k}_{\mathbf{G}\mathbf{v}\boldsymbol{\theta}i}^{\mathbf{T}} & \mathbf{k}_{\mathbf{G}\boldsymbol{\theta}\boldsymbol{\theta}i} \end{bmatrix},\ \mathbf{d}_i = \begin{Bmatrix} \mathbf{d}_{\mathbf{w}i} \\ \mathbf{d}_{\mathbf{u}i} \\ \mathbf{d}_{\mathbf{v}i} \\ \mathbf{d}_{\boldsymbol{\theta}i} \end{Bmatrix} \qquad (5.25)\text{a-c}$$

The elastic stiffness submatrices arising in Eq. (5.25) are defined as

$$\mathbf{k}_{\mathbf{E}\mathbf{w}\mathbf{w}i} = EA_i \int_0^l \mathbf{S}'(z)_{2\times 1}\,\mathbf{S}'(z)_{1\times 2}^{\mathbf{T}}\,dz \qquad \mathbf{k}_{\mathbf{E}\mathbf{u}\mathbf{u}i} = EI_{y_i y_i} \int_0^l \mathbf{H_1}''(z)_{4\times 1}\,\mathbf{H_1}''(z)_{1\times 4}^{\mathbf{T}}\,dz$$

$$\mathbf{k}_{\mathbf{E}\mathbf{v}\mathbf{v}i} = EI_{x_i x_i} \int_0^l \mathbf{H_2}''(z)_{4\times 1}\,\mathbf{H_2}''(z)_{1\times 4}^{\mathbf{T}}\,dz \qquad \mathbf{k}_{\mathbf{E}\mathbf{u}\mathbf{v}i} = EI_{x_i y_i} \int_0^l \mathbf{H_1}''(z)_{4\times 1}\,\mathbf{H_2}''(z)_{1\times 4}^{\mathbf{T}}\,dz \qquad (5.26)\text{a-f}$$

$$\mathbf{k}_{\mathbf{E}\boldsymbol{\omega}\boldsymbol{\omega}i} = EI_{\omega_i \omega_i} \int_0^l \mathbf{H_1}''(z)_{4\times 1}\,\mathbf{H_1}''(z)_{1\times 4}^{\mathbf{T}}\,dz \qquad \mathbf{k}_{\mathbf{E}\mathbf{s}\mathbf{v}i} = GJ_i \int_0^l \mathbf{H_1}'(z)_{4\times 1}\,\mathbf{H_1}'(z)_{1\times 4}^{\mathbf{T}}\,dz$$

and the geometric submatrices are defined as

$$\mathbf{k}_{\mathbf{Guu}i} = \left(N_p/2\right)\int_0^l \mathbf{H}_\mathbf{1}'\left(z\right)_{4\times1}\mathbf{H}_\mathbf{1}'\left(z\right)_{1\times4}^{\mathbf{T}}dz \qquad \mathbf{k}_{\mathbf{Gvv}i} = \left(N_p/2\right)\int_0^l \mathbf{H}_\mathbf{2}'\left(z\right)_{4\times1}\mathbf{H}_\mathbf{2}'\left(z\right)_{1\times4}^{\mathbf{T}}dz$$
$$\mathbf{k}_{\mathbf{G}\theta\theta i} = \left(N_p/2\right)r_{0_i}^2\int_0^l \mathbf{H}_\mathbf{1}'\left(z\right)_{4\times1}\mathbf{H}_\mathbf{1}'\left(z\right)_{1\times4}^{\mathbf{T}}dz \qquad \mathbf{k}_{\mathbf{Gu}\theta i} = \left(N_p/2\right)y_{S_i}\int_0^l \mathbf{H}_\mathbf{1}'\left(z\right)_{4\times1}\mathbf{H}_\mathbf{1}'\left(z\right)_{1\times4}^{\mathbf{T}}dz \quad (5.27)\text{a-e}$$
$$\mathbf{k}_{\mathbf{Gv}\theta i} = -\left(N_p/2\right)x_{S_i}\int_0^l \mathbf{H}_\mathbf{2}'\left(z\right)_{4\times1}\mathbf{H}_\mathbf{1}'\left(z\right)_{1\times4}^{\mathbf{T}}dz$$

5.4.6.2. Variational formulation for the assembly

The elastic stiffness matrix $\mathbf{K}_{\mathbf{E}(n\times n)}$ and geometric matrix $\mathbf{K}_{\mathbf{G}(n\times n)}$ for a structure consisting of two lines of elements (to simulate both angles), where subscript n denotes the total number of degrees of freedom in the structure, are then formed from the element stiffness and geometric matrices using the conventional assembly technique. The second variation of the total potential energy of the structure prior to applying any constraints arising from the interconnectors or gusset plates takes the form

$$\delta^2\Pi/2 = \left(1/2\right)\mathbf{D}_{(1\times n)}^{\mathbf{T}}\left(\mathbf{K}_{\mathbf{E}(n\times n)} - \lambda\mathbf{K}_{\mathbf{G}(n\times n)}\right)\mathbf{D}_{(n\times1)} \tag{5.28}$$

5.4.6.3. Kinematic constraints

The kinematic constrains defined herein are intended to characterize the effect of interconnectors between the two angle members. From Figure 5.6a,b, the bending rotation v_i' and angle of twist θ_i of both members are set equal at the locations of the intermediate connectors, i.e.,

$$u_1' - u_2' = 0 \qquad \theta_1 - \theta_2 = 0 \tag{5.29}\text{a-b}$$

where we recall that subscripts 1 and 2 represent the left and right angle members, respectively, as shown in Figure 5.6. Unlike the rotations about y and z axes, the rotations about the x axis for both angles are kept independent so that the angle members can warp independently form one another at the interconnector locations. In cases where the global warping is to be restrained at the interconnector, the rotations about the x axis for both angles would need be set equal i.e.,

$$v_1' - v_2' = 0 \tag{5.30}$$

From Figure 5.6a, the total lateral displacements u_i and v_i along the x_i and y_i axes of the left angle are related to those of the right angle through

$$u_1 - u_2 = 0 \qquad v_1 - v_2 + \Delta_S \theta_2 = 0 \tag{5.31)a,b}$$

in which Δ_S is the distance between the shear centres of the angles. Also, from Figure 5.6b, the total longitudinal displacement of the left angle is related to the total longitudinal displacement of the right angle as

$$w_1 - w_2 + \Delta_C u_2' = 0 \tag{5.32}$$

in which Δ_C is the distance between the centroids of the angles. In order to restrain the longitudinal displacement of the assembly while allowing both angles to pivot about the Y axis (e.g., at the supports), Eqs. (5.29)a and (5.32) are applied in addition to the constraint

$$w_1 + w_2 = 0 \tag{5.33}$$

The above kinematic constraints are consolidated into a matrix form as

$$\mathbf{C}_{(m\times n)}\mathbf{D}_{(n\times 1)} = \mathbf{0}_{(m\times 1)} \tag{5.34}$$

where $\mathbf{C}$ is a matrix of coefficients of m linear equations, m being the total number of constraints in the problem, that define the above buckling constraints at specific nodes.

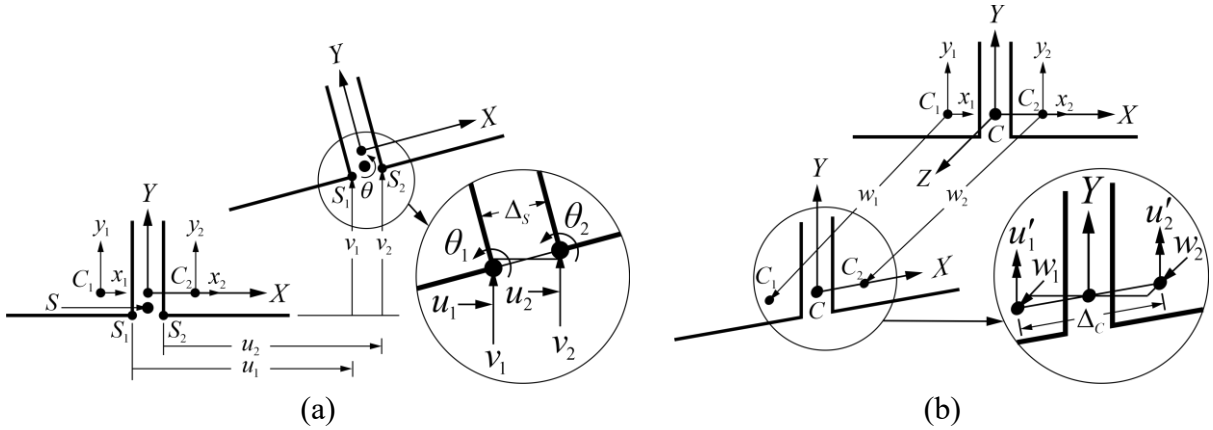

Figure 5.6 (a) Lateral and (b) longitudinal buckling displacements for back-to-back double angle assembly at interconnectors.

5.4.6.4. Modification of variational formulation to accommodate kinematic constraints

In order to evoke the stationarity condition of the second variation of the total potential energy in Eq. (5.28) subject to the constraints in Eq.(5.34), an auxiliary functional $\delta^2\Pi^*/2$ is constructed by augmenting Eq. (5.28) by a term arising from pre-multiplying Eq.(5.34) by a vector of Lagrange multipliers $\boldsymbol{\lambda}_{\mathbf{L}(m\times 1)}$ i.e.,

$$\delta^2\Pi^*/2 = (1/2)\,\mathbf{D}^{\mathbf{T}}_{(1\times n)}\left(\mathbf{K}_{\mathbf{E}(n\times n)} - \lambda\mathbf{K}_{\mathbf{G}(n\times n)}\right)\mathbf{D}_{(n\times 1)} + \boldsymbol{\lambda}^{\mathbf{T}}_{\mathbf{L}(1\times m)}\mathbf{C}_{(m\times n)}\mathbf{D}_{(n\times 1)} \tag{5.35}$$

The stationarity conditions of $\delta^2\Pi^*/2$ with respect to $\mathbf{D}$ and $\boldsymbol{\lambda}_{\mathbf{L}}$, i.e., $\partial\left(\delta^2\Pi^*/2\right)/\partial\mathbf{D} = \mathbf{0}$ and $\partial\left(\delta^2\Pi^*/2\right)/\partial\boldsymbol{\lambda}_{\mathbf{L}} = \mathbf{0}$, are enforced and consolidated into a matrix form as

$$\left(\left[\begin{array}{c|c} \mathbf{K}_{\mathbf{E}(n\times n)} & \mathbf{C}^{\mathbf{T}}_{(n\times m)} \\ \hline \mathbf{C}_{(m\times n)} & \mathbf{0}_{(m\times m)} \end{array}\right] - \lambda\left[\begin{array}{c|c} \mathbf{K}_{\mathbf{G}(n\times n)} & \mathbf{0}_{(n\times m)} \\ \hline \mathbf{0}_{(m\times n)} & \mathbf{0}_{(m\times m)} \end{array}\right]\right)\left\{\begin{array}{c} \mathbf{D}_{(n\times 1)} \\ \hline \boldsymbol{\lambda}_{\mathbf{L}(m\times 1)} \end{array}\right\} = \left\{\begin{array}{c} \mathbf{0}_{(n\times 1)} \\ \hline \mathbf{0}_{(m\times 1)} \end{array}\right\} \tag{5.36}$$

After enforcing the boundary conditions, the eigenvalue problem in Eq. (5.36) is solved for the load multipliers λ and associated eigenvectors. The buckling load for the structure as determined from the preceding formulation will be subsequently denoted as $P_T = \lambda N_p$.

5.5. Formulation II: Monolithic solution

As the number of interconnectors in back-to-back double angles increases, the assembly is expected to reach a state where it deforms essentially as a single monolithic member. Under the no-slip assumption between the cross-sections that form a built-up member, Pezeshky et al. (2020) extended the Vlasov theory for the lateral torsional buckling analysis of flexural members made of monosymmetric assemblies, in which the axis of symmetry of the assembly passes through the centroids of all sections forming the assembly. The present study further extends the Generalized Vlasov thin-walled beam theory to the flexural-torsional buckling analysis of built-up columns

consisting of double angle sections. Unlike Pezeshky et al. (2020), the built-up assembly herein consists of angle members with centroids that do not intercept the axis of symmetry of the assembly, leading to different mathematical expressions.

5.5.1. Assumptions

In addition to the assumptions in Section 5.4.2, the present extension of the Vlasov theory is based on the following assumptions:

1. The entire double angle assembly moves as a rigid disc in the plane of the cross-section throughout deformation (i.e., no relative slip/separation takes place between the angles)
2. In a manner similar to Pezeshky et al. (2020), the assembly has a single shear centre S located along the axis of symmetry Y of the assembly at a distance Y_S from the centroid C as shown in Figure 5.7.
3. Also, in a manner similar to Pezeshky et al. (2020), each angle member i has its own sectorial origin B_i $\left(i=1,2\right)$, each lying on the contour of the angle i (Figure 5.7).

5.5.2. Coordinate systems and orthogonality conditions

This section provides a generalization of the classical thin-walled beam theory, originally devised for single sections, to extend its applicability to double angle back-to-back assemblies that are constrained to move together by providing enough interconnectors. The extension provides a formal methodology to determine the torsional properties of the assembly. A right-handed Cartesian coordinate system $\left(X,Y,Z\right)$ is defined for an assembly consisting of a pair of unequal-leg angles connected back-to-back (Figure 5.7). The origin is taken at the centroid C of the assembly, thus satisfying the conditions $\sum_{i=1}^{2}\int_{A_i} XdA_i = 0$ and $\sum_{i=1}^{2}\int_{A_i} YdA_i = 0$, in which, $i=1,2$ denote the left and right angles. The centroidal axes are oriented along the principal directions of

the assembly, i.e., they satisfy the condition $\sum_{i=1}^{2}\int_{A_i} XYdA_i = 0$. Another right-handed local coordinate system $\left(s_i, n_i, Z\right)$ is defined for each angle i. Since the sectorial origins must lie on the middle surface of each angle, they are offset from the axis of symmetry of the assembly. The location of the principal sectorial origins B_i are determined from the orthogonality conditions

$$\int_{A_i} \omega_i dA_i = \int_{A_i} \left(\bar{\omega}_i + \bar{\bar{\omega}}_i\right) dA_i = 0, \quad i = 1,2 \tag{5.37}$$

Unlike Section 5.4.3, in which the pole for each angle was taken to coincide with the shear centre of the angle, both global and local sectorial coordinates for the assembly depend on the location of shear centre S of the assembly which coincides neither with S_1 nor S_2. Coordinates $\left(X_S, Y_S\right)$ of the shear centre of the assembly are determined by satisfying the orthogonality conditions

$$\sum_{i=1}^{2}\int_{A_i} \omega_i X dA_i = 0 \qquad \sum_{i=1}^{2}\int_{A_i} \omega_i Y dA_i = 0 \tag{5.38)a,b}$$

Since the shear centre of the assembly is located on the axis of symmetry Y, one has $X_S = 0$ and Eq. (5.38)b is identically satisfied. The total warping constant $I_{\omega\omega}$ for the assembly is then defined from the expression

$$I_{\omega\omega} = \sum_{i=1}^{2}\int_{A_i} \omega_i^2 dA_i = \sum_{i=1}^{2}\int_{A_i} \left(\bar{\omega}_i + \bar{\bar{\omega}}_i\right)^2 dA_i = I_{\bar{\omega}\bar{\omega}} + I_{\bar{\bar{\omega}}\bar{\bar{\omega}}} \tag{5.39}$$

in which, $I_{\bar{\omega}\bar{\omega}}$ and $I_{\bar{\bar{\omega}}\bar{\bar{\omega}}}$ are the global and local warping constants for the assembly defined as

$$I_{\bar{\omega}\bar{\omega}} = 2\int_{A_i} \bar{\omega}_i^2 dA_i \qquad I_{\bar{\bar{\omega}}\bar{\bar{\omega}}} = \frac{t^3}{6}\int_{S_i} q_i^{\,2} ds_i \tag{5.40)a,b}$$

5.5.3. Sectional properties

The coordinates of the shear centre and principal sectorial origins of the back-to-back double angle assembly are determined by enforcing Eqs. (5.37) and (5.38). In this case, the area A, coordinates

of the shear center X_S and Y_S, principal moments of inertia I_{YY} and I_{XX}, product of inertia I_{XY}, total warping constant $I_{\omega\omega}$, Saint-Venant torsional constant J and polar radius of gyration r_0 for the assembly are given by

$$A = 2t\left(\tilde{b}_X + \tilde{b}_Y\right) \qquad X_S = 0 \qquad Y_S = \frac{3\tilde{d}\tilde{b}_Y^2}{\left(8\tilde{b}_Y + 2\tilde{b}_X\right)\tilde{b}_X} - \frac{\tilde{b}_Y^2}{2\left(\tilde{b}_Y + \tilde{b}_X\right)}$$

$$I_{YY} = \frac{t}{6}\left(t^2\tilde{b}_Y + 4\tilde{b}_X^3 + 6\tilde{d}\tilde{b}_X^2 + 3\left(\tilde{b}_X + \tilde{b}_Y\right)\tilde{d}^2\right) \quad I_{XX} = \frac{t}{6}\left(4\tilde{b}_Y^3 + t^2\tilde{b}_X - \frac{3\tilde{b}_Y^4}{\tilde{b}_X + \tilde{b}_Y}\right) \qquad I_{XY} = 0$$

$$I_{\omega\omega} = I_{\bar{\omega}\bar{\omega}} + I_{\bar{\bar{\omega}}\bar{\bar{\omega}}} = \frac{t\tilde{d}^2\tilde{b}_Y^3\left(\tilde{b}_Y + \tilde{b}_X\right)}{6\left(4\tilde{b}_Y + \tilde{b}_X\right)} + \frac{t^3}{18}\left(\tilde{b}_Y^3 + \tilde{b}_X^3 + \frac{3}{4}\tilde{b}_X\tilde{d}\left(2\tilde{b}_X + \tilde{d}\right) - \frac{9\tilde{d}\tilde{b}_Y^4\left[\left(8\tilde{b}_Y + 2\tilde{b}_X\right)\tilde{b}_X - 3\tilde{d}\tilde{b}_Y\right]}{\left(8\tilde{b}_Y + 2\tilde{b}_X\right)^2\tilde{b}_X^2}\right)$$

$$J = \frac{2t^3}{3}\left(\tilde{b}_X + \tilde{b}_Y\right) \qquad r_0^2 = \frac{t^2 + 3\tilde{d}^2}{12} + \frac{2\tilde{b}_X^3 + 2\tilde{b}_Y^3 + 3\tilde{d}\tilde{b}_X^2}{6\left(\tilde{b}_X + \tilde{b}_Y\right)} + \frac{9\tilde{d}^2\tilde{b}_Y^5 + 3\tilde{d}\tilde{b}_Y^4\tilde{b}_X\left(3\tilde{d} - 8\tilde{b}_Y - 2\tilde{b}_X\right)}{\left(8\tilde{b}_Y + 2\tilde{b}_X\right)^2\tilde{b}_X^2\left(\tilde{b}_Y + \tilde{b}_X\right)}$$

(5.41)a-i

where $\tilde{b}_X, \tilde{b}_Y$ are the centreline dimensions for the legs along the X and Y axes, t is the thickness of the angles and $\tilde{d}$ is the centreline distance (spacing) between the outstanding legs as shown Figure 5.7. Interestingly, unlike single angles or tee sections in which the global warping constant vanishes, the present extension of the Vlasov theory predicts a non-vanishing global warping constant that depends on the distance $\tilde{d}$ separating the centrelines of back-to-back legs. Hence, the warping constant of the assembly is more than twice the local warping constant of a single angle. In contrast, Equation (5.41), indicates that the Saint-Venant torsional constant for the assembly is exactly twice that of a single angle. For an assembly consisting of equal-leg angles (i.e., $\tilde{b}_X = \tilde{b}_Y$), Eqs. (5.41)a-i simplify to

$$A = 4t\tilde{b}_X \qquad X_S = 0 \qquad Y_S = \frac{6\tilde{d} - 5\tilde{b}_X}{20} \qquad I_{YY} = \frac{t\tilde{b}_X}{6}\left(t^2 + 6\tilde{d}^2 + 6\tilde{d}\tilde{b}_X + 4\tilde{b}_X^2\right)$$

$$I_{XX} = \frac{t}{6}\left(t^2\tilde{b}_X + \frac{5\tilde{b}_X^3}{2}\right) \qquad I_{\omega\omega} = I_{\bar{\omega}\bar{\omega}} + I_{\bar{\bar{\omega}}\bar{\bar{\omega}}} = \frac{t\tilde{d}^2\tilde{b}_X^3}{15} + \frac{t^3}{9}\left[\tilde{b}_X^3 + \frac{\tilde{d}\tilde{b}_X}{100}\left(30\tilde{b}_X + 51\tilde{d}\right)\right] \qquad \text{(5.42)a-i}$$

$$I_{XY} = 0 \qquad J = \frac{4}{3}t^3\tilde{b}_X \qquad r_0^2 = \frac{1}{300}\left(25t^2 + 102\tilde{d}^2 + 100\tilde{b}_X^2 + 30\tilde{d}\tilde{b}_X\right)$$

The sectional properties derived in Eqs. (5.41) and (5.42) enable the prediction of the buckling load P_M by treating the assembly as a monolithic member using the buckling classical solution in Eq. (5.2).

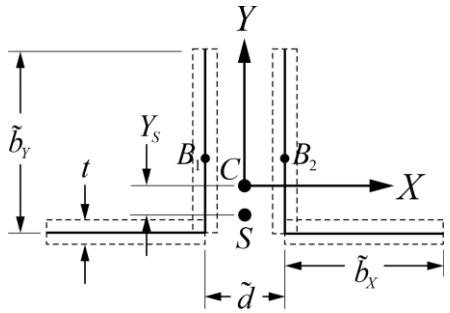

Figure 5.7 Geometric parameters defined for back-to-back unequal-leg angle assemblies

5.6. Verification

5.6.1. Comparison against shell finite element analysis

A set of compression assemblies spanning 5 m consists of back-to-back double angle cross-sections. Three cross-sections are considered: 2L152x152x16, 2L178x127x16 and 2L203x102x16. For the unequal-leg angle cross-sections, two arrangements are considered: (i) short legs are back-to-back and (ii) long legs are back-to-back, resulting in a total of five assemblies. The angles are spaced 15.9 mm apart to accommodate a gusset plate of common thickness. The gusset plate at each end of the assembly is assumed to restrain the rotation of the assembly about the X axis while enabling its rotation about the Y axis. The end connection is assumed to restrain both twisting and warping. Members are longitudinally restrained at one end

and subjected to a compressive force at the other end. For all assemblies, the angles are connected at three equally spaced locations along the span $\left(z/L = 0.25, 0.5, 0.75\right)$. The modulus of elasticity is taken as $200,000$ MPa and the modulus of rigidity is $76,900$ MPa. The assembly is modeled using the thin-walled member formulation developed in Section 5.4.6 and a three-dimensional shell model based on the commercial software package ABAQUS.

An elastic eigenvalue buckling analysis is developed based on the S4 shell element. The S4 is a four-node fully integrated shell element with three displacements and three rotations per node. The zero-twist boundary conditions at the member ends are modeled by restraining the displacements along the X and Y axes as well as the rotation about the Z axis of all nodes at the member ends (Figure 5.8a-c). The bending fixity condition is modelled by restraining the rotations about the X axis for all nodes at the ends of the angles (Figure 5.8d) while the rotations about the Y axis were kept free (Figure 5.8e). A master node is defined at the centroid of the assembly at each end. At one end of the assembly, the longitudinal displacement of the master node is restrained while at the other end, the master node is subjected to a compressive force. At each end, the longitudinal displacements of all nodes for the angle ends are linked to the longitudinal displacement of the master node and its rotation about the Y axis in such a way that both angles pivot about the master node (Figure 5.8f), using the *EQUATION keyword in Abaqus. Interconnectors are modeled by defining a master node at the centroid of each angle. The nodes along the angle cross-section are then linked to the corresponding master node in such a way that the angle cross-section pivots about its centroidal axes x_i, y_i (Figure 5.9a,b). The rotation of the master node of the left angle about the y_1 axis is constrained to be equal to the rotation of the master node of the right angle about the y_2 axis. Also, the longitudinal displacement of the master node of left angle is linked to that of the master node of the right angle so that both angles pivot about the axis of symmetry of

the assembly (Figure 5.9c). Another master node is defined at the shear centre of the assembly. The twisting degrees of freedom of the nodes at the shear centres of the angles (corner nodes) are then constrained to be equal to that of the shear centre of the assembly. The in-plane displacements of the corner nodes are then related to the in-plane displacements u_S, v_S and angle of twist θ_Z of the master node (Figure 5.9d-f) in such a way that both angles revolve around the shear centre of the assembly. A mesh study indicated that convergence is achieved for the assembly with 2L152x152x16 when the span is discretized into 200 elements and each leg is discretized into seven elements.

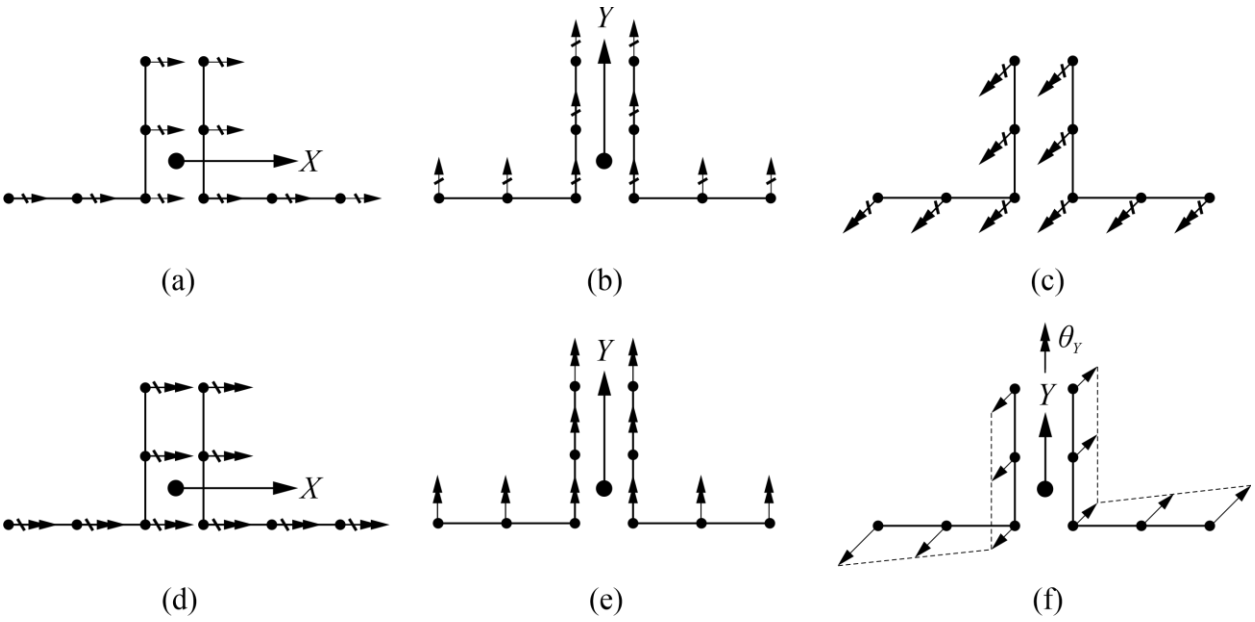

Figure 5.8 Modelling end conditions (double headed arrows denote rotation about the direction of the arrow, crossed arrows denote restraints): (a) restraints of displacement along X direction, (b) restraints of displacements along Y direction, (c) angle of twist restraints, (d) restraints of rotations about X axis, (e) free rotations along Y direction and (f) longitudinal displacements of all nodes due to rotation θ_Y

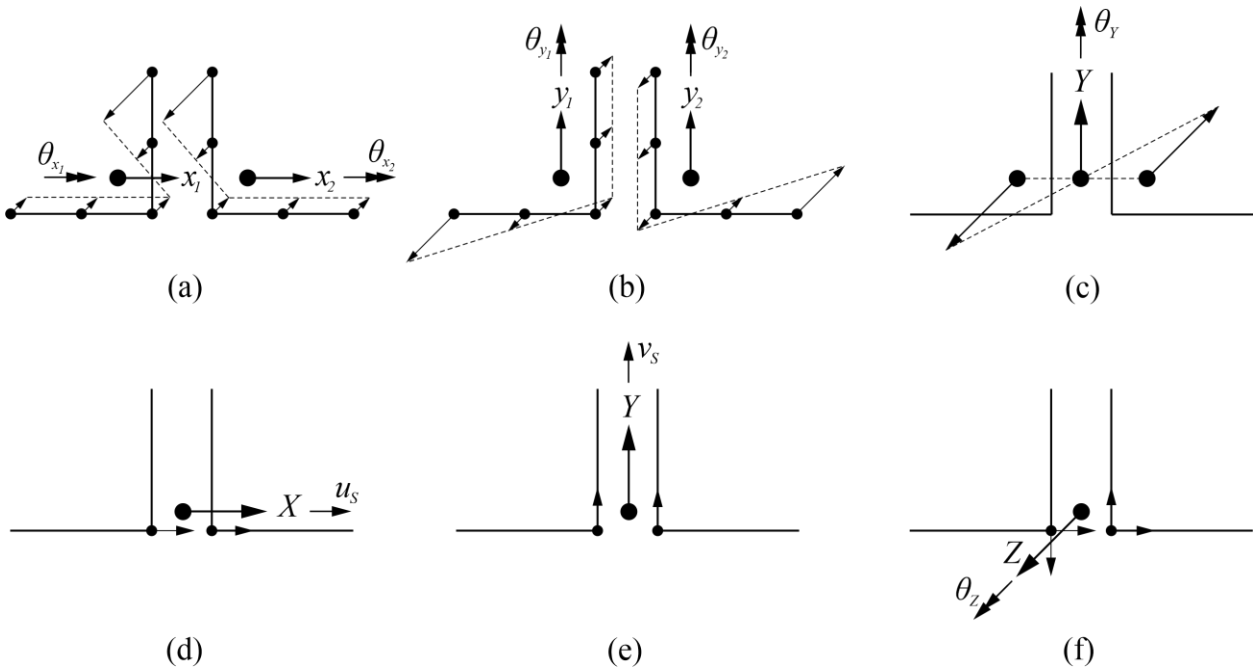

Figure 5.9 Displacements associated with each degree of freedom at the interconnectors: (a) longitudinal displacements of all nodes due to rotations $\theta_{x_1}, \theta_{x_2}$ (b) longitudinal displacements of all nodes due to rotations $\theta_{y_1}, \theta_{y_2}$, (c) longitudinal displacement of the master nodes due to rotation θ_Y. In-plane displacements of the shear centres for both angles due to master node (d) displacement u_S, (e) displacement v_S and (f) and angle of θ_Z.

For the thin-walled member model developed in the present study, the sectional properties for each angle are calculated from Eqs. (5.18)a-i. At each end of the assembly, the degrees of freedom associated with the lateral displacements, rotations about the X axis, angles of twist and warping deformations are restrained. Also, Eqs. (5.29)a and (5.32) are applied to the angles nodes to constrain both angle ends to pivot about the axis of symmetry Y. One of the assembly ends is then restrained longitudinally by applying Eq. (5.33) to the angles nodes while the other end is subjected to a compressive force. The interconnectors are modeled by applying Eqs. (5.29)a,b, (5.31)a,b and (5.32) to the nodes located at the interconnector locations. A mesh study indicated that convergence was achieved when ten elements were used per angle. However, the number of

elements was increased to forty per angle to provide a smoother representation of buckling mode shapes.

The buckling load predictions based on the 3D shell and present models for the built-up members are compared in Table 5.1. Very close agreement is observed in all five cases with a percentage difference ranging from 1.0 to 2.2%. The normalized mode shapes predicted by both models for the 2L152x152x16 assembly (Figure 5.10) are also in a very close agreement. In Figure 5.10, the longitudinal displacement and angle of twist of the 3D shell model were determined based on the average values of the longitudinal displacements and angles of twist of all nodes on the angle cross-sections.

Table 5.1 Buckling load predictions based on the present finite element solution and 3D shell models for multiple members

Cross-section	Arrangement	Buckling load (kN)			Buckling mode
		P_T	P_{3D}	P_T/P_{3D}	
2L152x152x16		3052	3008	1.015	Flexural-torsional
2L178x127x16		3765	3684	1.022	Pure flexural
	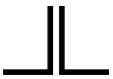	1900	1877	1.012	Flexural-torsional
2L203x102x16		2073	2040	1.016	Pure flexural
		1094	1083	1.010	Flexural-torsional
Notes: P_T = Elastic buckling loads based on the present finite element solution P_{3D} = Elastic buckling loads based on 3D shell model					

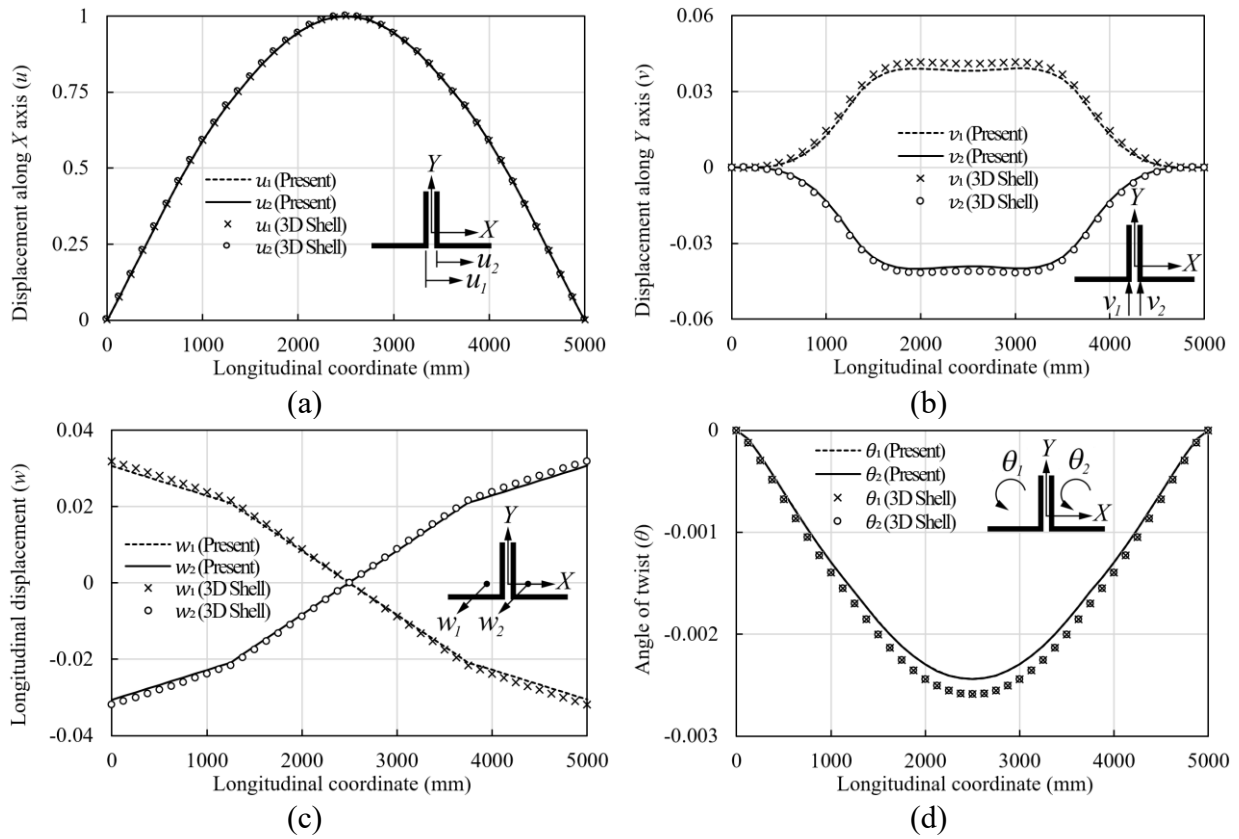

Figure 5.10 Normalized mode shapes for back-to-back double angles with 2L152x152x16 and 5000 mm span, (a) lateral displacement along the *X* axis (b) lateral displacement along the *Y* axis (c) longitudinal displacement and (d) angle of twist

5.6.2. Comparison against experimental results

The validity of the present finite element formulation is further assessed against test results by Sherman and Yura (1998). All assemblies had a 3810mm span and 2L127x76x6.4 cross-sections connected back-to-back through the longer legs to a 9.53mm thick gusset plate at each end. The gusset plates were then connected to knife edge supports that allow rotations about the axis of symmetry. The individual angle members were also connected at intermediate locations along the span either by snug-tightened or pre-tensioned bolts.

The thin-walled finite element model described in Section 5.1 was used to estimate the buckling loads for the assemblies considered. The elastic buckling loads P_T predicted by the present finite element model and the elastic buckling loads P_{SY} reported by Sherman and Yura (1998) based on

the Southwell plot technique are presented in Table 5.2. Close agreement is obtained between the numerical predictions and experimental results as the ratio of the elastic buckling load P_T/P_{SY} ranged from 0.98 to 1.06 with a mean value of 1.01, a standard deviation of 0.031 and a coefficient of variation of 3.1%. Also, all tested specimens and model simulations buckled in a flexural-torsional mode.

Table 5.2 Buckling load predictions based on the present finite element solution and those reported by Sherman and Yura (1998) for multiple members

Intermediate connection		End connection type	Buckling load (kN)		Ratio
Number	Type		P_T	P_{SY}	P_T/P_{SY}
1	Snug-tightened	Plates	238	244	0.98
1	Pre-tensioned	Plates	238	243	0.98
2	Snug-tightened	Plates	255	257	0.99
2	Pre-tensioned	Plates	255	259	0.98
5	Snug-tightened	Plates	268	258	1.04
5	Pre-tensioned	Plates	268	264	1.02
5	Snug-tightened	Washers	268	252	1.06
				Mean =	1.01
				Standard Deviation =	0.031
				Coefficient of Variation =	3.08%
Notes: P_T = Elastic buckling loads based on the present finite element model P_{SY} = Elastic buckling loads reported by Sherman and Yura (1998)					

5.7. Parametric investigations

5.7.1. Effect of torsional property approximations on the predicted buckling resistance

When determining the elastic buckling resistance for a back-to-back double angle assembly, designers may opt, as an approximation, to consider the coordinate Y_S of the shear centre for the assembly to be equal to the coordinate of the shear centres of the individual angles, i.e., $Y_S \approx y_{S_i}$. Also, in the absence of more accurate solution intended to tackle double angles, designers may resort to take the warping constant $I_{\omega\omega}$ for the assembly as twice as the warping constant of an

individual angle, i.e., $I_{\omega\omega} \approx 2I_{\omega_i\omega_i}$, in which $I_{\omega_i\omega_i}$ is provided typically in tables of sectional properties for individual angles, and are based on local warping alone, as the global warping contribution vanishes/nearly vanishes for a single angle under the classical thin-walled beam theory. The classical solution in Eq. (5.2) is used to determine the flexural-torsional buckling loads for a series of back-to-back double angle assemblies with $K_Y L_Y / r_Y = 50$. Cross-sections 2L152x152x16, 2L178x127x16, 2L203x102x16 are considered, with b_Y / b_X ranging from 0.5 to 2.0, and spacing d ranging from 9.53 to 22.2 mm. Member ends in the study are fixed about the X axis and relative to twist, and pinned about the Y axis. For each member, Y_S and $I_{\omega\omega}$ are determined from Eqs. (5.41)c and (5.41)f, respectively. Assemblies with spacing $d = 22.2$ mm are also modeled using ABAQUS based on the S4 element (dotted lines in Figure 5.11), in which, the model consists of 24 elements along the span and three elements along each leg. At all cross-sectional nodes along the span, a set of kinematic constraints are applied by using the *EQUATION keyword to replicate the monolithic behaviour. This includes constraining the corner nodes of the angles to revolve around the shear center of the assembly and relating the longitudinal displacements of all nodes to the longitudinal displacement of the centroid of the assembly and the additional longitudinal displacements due to bending the angles about the X and Y axes and warping. The predicted buckling load P_M of an assembly based on the monolithic treatment or that P_{3D} based on the 3D shell model are normalized with respect to the buckling load P_C of an identical assembly with the shear center assumed at $\left(X_S = 0, Y_S = y_{S_i}\right)$, and an approximate warping constant value taken as twice the warping constant of a single angle $\left(I_{\omega\omega} = 2I_{\omega_i\omega_i}\right)$, leading to the normalized buckling loads P_M / P_C or P_{3D} / P_C .

For the case $d = 22$ mm, Figure 5.11 shows an excellent agreement between the flexural-torsional buckling loads P_M and P_{3D} for assemblies with $b_Y/b_X = 0.5-1.0$. As b_Y/b_X increases, the effects of distortion and shear deformation, which are captured only in the shell model, become more pronounced. These effects reduce P_{3D} by 3% compared to P_M for the assembly with a leg width ratio $b_Y/b_X = 2.0$. The close agreement between the present monolithic solution and shell model is indicative of the validity of the Vlasov theory extension developed in Section 5.5 and the corresponding sectional properties (Eqs. (5.41) and (5.42)).

Also, as shown in Figure 5.11, the P_M/P_C ratio ranges from 103% to 144% and is found to increase with b_Y/b_X and with the angle spacing d. The lowest P_M/P_C is attained for the 2L203x102x16 assembly connected by the shorter leg and spaced apart by 9.53 mm thick gusset plates with $Y_S/y_{S_i} = 0.8$ and $I_{\omega\omega}/2I_{\omega_i\omega_i} = 1.57$. At the other end of the spectrum, the maximum value for P_M/P_C corresponds to 2L203x102x16 connected by the longer legs and spaced apart by 22.2 mm gusset plates with $Y_S/y_{S_i} = 0.6$ and $I_{\omega\omega}/2I_{\omega_i\omega_i} = 5.88$.

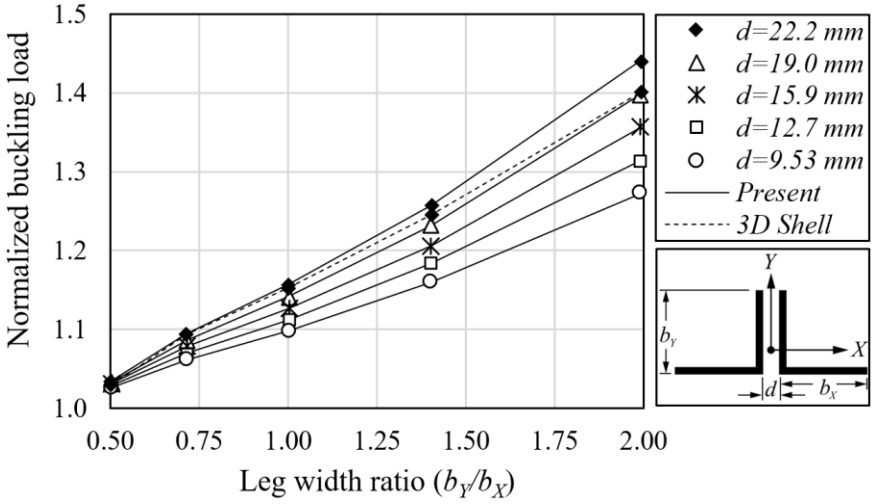

Figure 5.11 Normalized flexural-torsional buckling load (P_M/P_C or P_{3D}/P_C) versus leg width ratio for assemblies with $K_Y L_Y/r_Y = 50$ and various angles spacing

5.7.2. Effect of Interconnectors on the buckling resistance

The finite element formulation developed in Section 5.4.6 is used to investigate the influence of (i) the number of interconnectors n (ii) the global slenderness ratio (the larger of $K_Y L_Y / r_Y$ and $K_X L_X / r_X$) (iii) the leg width ratio b_Y / b_X (iv) the connected leg width-to-thickness ratio b_Y / t and (v) the angle spacing-to-thickness ratio d/t on the buckling load of back-to-back double angle assemblies. As a reference case, a 6976 mm span member is considered with 2L152x152x16 cross-section spaced at 15.9 mm with $K_Y L_Y / r_Y = 100$, $b_Y / b_X = 1.0$, $b_Y / t = 9.6$ and $d/t = 1.0$. Four sets of runs are conducted where the geometric parameters are taken to vary within the practical ranges as shown in Table 5.3. In all cases, both angles are equidistantly interconnected along the span. The number of interconnectors is varied from 0 (no interconnectors) to 5. The predicted pure flexural and flexural-torsional buckling loads for an assembly are normalized with respect to the flexural-torsional buckling load of an identical assembly continuously interconnected (i.e., a monolithic member) leading to the P_T / P_M ratio.

Table 5.3 Assembly dimensions and parameters ranges

runs	Sectional dimensions (mm)					Dimensionless parameters				
	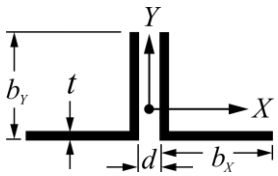					Global slenderness		Leg width	Connected leg width-to-thickness	Angle spacing-to-thickness
	b_Y	b_X	t	d	L	$0.5L/r_X$	L/r_Y	b_Y/b_X	b_Y/t	d/t
Ref.	152	152	15.9	15.9	6976	75	100	1.0	9.6	1.0
1	102	203	15.9	15.9	5438	100	51.6	0.5	6.4	1.0
	127	178	15.9	15.9	7367	100	84.6	0.7	8.0	1.0
	178	127	15.9	15.9	5468	48.5	100	1.4	11.2	1.0
	203	102	15.9	15.9	4138	31.7	100	2.0	12.8	1.0
2	152	152	15.9	15.9	3488	37.5	50	1.0	9.6	1.0
	152	152	15.9	15.9	10465	112.4	150	1.0	9.6	1.0
	152	152	15.9	15.9	13953	150	200	1.0	9.6	1.0
3	152	152	12.7	15.9	6920	69.2	100	1.0	12.0	1.3
	152	152	19.0	15.9	7034	70.2	100	1.0	8.0	0.8
	152	152	22.2	15.9	7095	70.8	100	1.0	6.8	0.7
4	152	152	15.9	9.53	6742	72.4	100	1.0	9.6	0.6
	152	152	15.9	12.7	6858	73.7	100	1.0	9.6	0.8
	152	152	15.9	19	7092	76.2	100	1.0	9.6	1.2
	152	152	15.9	22.2	7214	77.5	100	1.0	9.6	1.4
Note: Ref.= Reference case										

5.7.2.1. Results and discussion

Figure 5.12a depicts the normalized buckling load P_T/P_M versus the number of interconnectors. Members with $b_Y/b_X = 0.5$ and 0.7 with one or more interconnectors are governed by pure flexural buckling and are marked by the dotted lines in Figure 5.12a. For this mode, the increase in the number of interconnectors does not significantly alter P_T/P_M. In contrast, for members with

$b_Y/b_X \geq 1.00$, P_T/P_M is governed by flexural-torsional buckling and are marked by solid lines. For this mode, P_T/P_M is observed to noticeably increase with the number of interconnectors. Similar positive trends, between P_T/P_M and the number of interconnectors, are observed in Figure 5.12b-d. For assemblies with 2L152x152x16 angles with slenderness $K_Y L_Y/r_Y$ ranging from 100 to 200, Figure 5.12b shows nearly overlapping relationships between P_T/P_M and the number of interconnectors. However, members with a lower slenderness ($K_Y L_Y/r_Y = 50$) are influenced to a lesser extent by the number of interconnectors provided. For example, the normalized buckling load for a member without interconnectors is 0.67 when $K_Y L_Y/r_Y = 50$ and becomes 0.57 when $K_Y L_Y/r_Y = 100$. This difference decreases with the number of interconnectors. When four interconnectors are used, for example, assemblies with $K_Y L_Y/r_Y = 50,100$ yield nearly identical P_T/P_M values. For members with $K_Y L_Y/r_Y = 100$ and $b_Y/b_X = 1.0$, P_T/P_M marginally increases with the leg slenderness b_Y/t (Figure 5.12c) and marginally decreases with the normalized angle spacing d/t (Figure 5.12d). The effect of b_Y/t and d/t ratios become negligible with the increase in the number of interconnectors (Figure 5.12c,d).

In all cases, Figure 5.12a-d depicts an asymptotic behaviour in which P_T/P_M approaches unity from below as the number of interconnectors increases. The provision of two interconnectors enables the attainment of 86-91% of the monolithic flexural-torsional buckling load P_M in all cases. An exception is observed for $b_Y/b_X = 0.5$ in Figure 5.12a, where the normalized buckling load ratio attained is 63%. However, pure flexural buckling is the governing mode in this case. Providing five interconnectors in most cases increases capacity to 95-98% of the monolithic flexural-torsional buckling load.

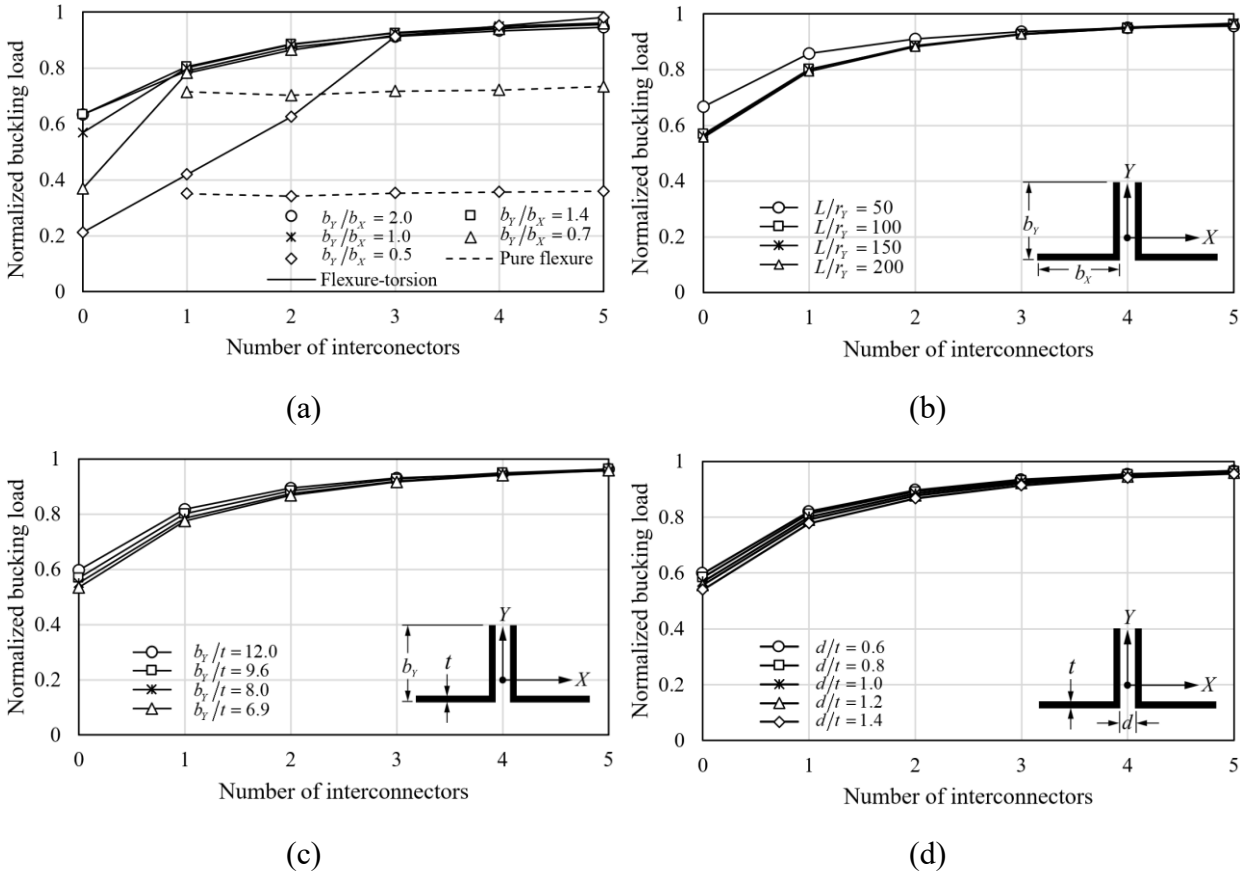

Figure 5.12 Normalized buckling load P_T/P_M versus number of interconnectors n for (a) various leg width ratios (run series 1 in Table 5.3), (b) various slenderness ratios (series 2), (c) various connected leg width-to-thickness ratios (series 3) and (d) various angle spacing-to-thickness ratio (series 4).

5.8. Design considerations

5.8.1. Assessment of current elastic buckling equations

A set of runs is conducted to compare the elastic buckling loads P_T obtained from the present finite element solution to those predicted by the modified slenderness ratio solution in ANSI/AISC 360-16, denoted as P_A. When applying the ANSI/AISC 360-16 provisions, the modified slenderness ratio considered is based on the assumption that angles are interconnected using snug-tightened bolts in Eq. (5.5). The assemblies considered have 2L152x152x16 and 2L203x102x16 cross-sections, with 15.9 mm spacing and slenderness ratios of $50, 200$ (Table 5.4). Although

ANSI/AISC 360-16 requires the assembly to be connected by at least two interconnectors (to satisfy the condition $a/r_{min} \leq 0.75 K_Y L_Y / r_Y$), cases of a single interconnector are considered in the present study for members with a slenderness ratio of 50, in which $a/r_{min} < 200$.

The buckling loads summarized in Table 5.4 show that both solutions yield very similar results when the member buckles in a pure flexural mode (denoted by an asterisk). As previously discussed, the influence of the number of interconnectors on the buckling load is insignificant for the flexural buckling mode. In contrast, in cases where the member resistance is governed by a flexural-torsional buckling mode, the present finite element solution predicts higher buckling loads than those predicted by the ANSI/AISC 360-16. The difference ranges from 4% to 82%, indicating that, in some cases, the elastic buckling equation in the present standards yields overly conservative predictions. The difference between both solutions is primarily attributed to the fact that the ANSI/AISC 360-16 solution and underlying theory by Bleich (1952) are based on a pure flexural buckling solution as opposed to a flexural-torsional buckling solution. Other reasons for the differences are (a) the approximations made in identifying the location of the shear centre and warping constant for the assembly (as discussed under Section 5.7.1), and (b) the effects of the interconnectors provided. The difference between the solutions was found to decrease as the number of interconnectors increases and tend to converge to the monolithic solution prediction, as an upper bound, when enough interconnectors are provided. The smallest difference between the flexural-torsional buckling load predictions of 4% corresponds to the assembly with 2L203x102x16 with the shorter legs connected at five intermediate locations, with $Y_S / y_{S_i} = 0.75$, $I_{\omega\omega} / 2I_{\omega_i\omega_i} = 1.84$ and a maximum slenderness ratio $L/r_Y = 50$. When the same assembly is connected through the longer legs, the maximum slenderness ratio becomes $0.5L/r_X = 50$,

$Y_{SC}/y_{SC}=0.66$ and $I_{\omega\omega}/2I_{\omega_i\omega_i}=4.36$ yielding P_T that is 32% higher than P_A. For an assembly with 2L152x152x16 with $L/r_Y=200$ having three interconnectors, P_T/P_A was found to be 1.25, also suggesting that the ANSI/AISC 360-16 solution underestimates the buckling load of assemblies with higher slenderness.

Table 5.4 Elastic buckling loads based on the present finite element and ANSI/AISC 360-16 solutions

Cross-section	Arrangement	Slenderness ratio		n	Buckling load (kN)		Ratio
		$0.5L/r_X$	L/r_Y		P_T	P_A	P_T/P_A
2L152x152x16		37.4	50	1	5020	2761	1.82
		37.4	50	3	5480	4347	1.26
		37.4	50	5	5590	4795	1.17
		149.6	200	3	417	333	1.25
		149.6	200	5	433	388	1.12
2L203x102x16		50	25.8	1	4860	3745	1.30
		50	25.8	3	5290	5094	1.04
		50	25.8	5	5320	5135	1.04
		200	103	3	449*	454*	0.99*
		200	103	5	452*	454*	1.00*
		15.9	50	1	4560	2804	1.63
		15.9	50	3	5040	3650	1.38
		15.9	50	5	5100	3851	1.32
		63.6	200	3	412	360	1.14
		63.6	200	5	429	400	1.07

Notes: * Indicates pure flexure about X axis. Otherwise, buckling modes are flexural-torsional.

n = number of interconnectors.

P_T = buckling loads based on the present finite element solution.

P_A = buckling loads based on ANSI/AISC 360-16 solution.

5.8.2. Proposed elastic buckling equation

As discussed in Section 5.8.1, current design standards generally underestimate the elastic flexural-torsional buckling load for concentrically loaded back-to-back double angle assemblies. This raises the need to develop a more accurate elastic buckling equation that captures the effect of interconnectors. The methodology sought is achieved by multiplying the elastic buckling load P_M

predicted by the present monolithic solution by a reduction factor Ω that reflects the effectiveness of the interconnectors in enforcing the monolithic action, i.e.,

$$P_R = \Omega P_M = \Omega F_{YZ} A \tag{5.43}$$

where F_{YZ} is calculated from Eq. (5.2) based on the sectional properties in Eqs. (5.4) and (5.41).

5.8.2.1. Interconnector reduction factor

A database consisting of 1250 runs (Appendix 5.A) is conducted on assemblies with slenderness ratios L/r_Y ranging from 50 to 200, leg width ratios b_Y/b_X ranging from 1.0 to 2.0, connected leg width-to-thickness ratios b_Y/t ranging from 6.0 to 14.0 and spacing-to-thickness ratios d/t ranging from 1.0 to 2.0 with n evenly spaced interconnectors, in which n was varied from 1 to 11 to cover a wide range of practical compression member geometries. The bounds for b_Y/b_X are representative of the geometries of the sections available in the database of the Handbook of Steel construction (2021). It is noted that, owing to Assumption 1 in Section 5.4.2, the solutions developed in the present study are intended for assemblies with hot-rolled angle cross-sections that are not prone to distortional effects nor local buckling. Thus, all cross-sections in the database were selected to satisfy classification requirements for Class 3 sections in CSA S16-19, i.e., $b_Y/t \le 250/\sqrt{F_y}$ for a yield strength $F_y = 300$ MPa. Similar classification rules for Class 3 sections in EN 1993-1-1:2005 are $b_Y/t \le 15\sqrt{235/F_y}$ and $(b_Y + b_X)/t \le 11.5\sqrt{235/F_y}$, and for non-slender sections in ANSI/AISC 360-16 are $b_Y/t \le 0.45\sqrt{E/F_y}$.

For all runs, full fixity end restraints about the X axis and relative to twist and pin end restraints about the Y axis were assumed. A finite element model similar to that described in Section 5.4.6 was built to predict the buckling loads P_T for all cases. The normalized buckling load P_T/P_M was

then determined by dividing the buckling loads P_T by the buckling load P_M of an identical monolithic member. Results indicated that the flexural-torsional buckling mode governs the resistance of all members with double equal-leg angles and members with double unequal-leg angles that are connected back-to-back by the longer legs.

The normalized buckling loads P_T/P_M were computed and then used to fit a regression function $\Omega = \Omega\left(b_Y/b_X, b_Y/t, L/r_Y, d/t, n\right) \approx P_T/P_M$ to approximately predict P_T/P_M based on non-linear regression analysis using TuringBot (2020), a symbolic regression analysis software. Regression results indicated that the influence of L/r_Y parameter on the sought function Ω is comparatively negligible, and hence it was discarded for simplicity. The following expression for Ω was obtained with a coefficient of determination of 0.95

$$\Omega = 1.0 - \left[\frac{\left(b_Y/b_X\right)+\left(d/t\right)}{n\left(b_Y/t\right)+1.3}\right] \tag{5.44}$$

It is noted that Eq. (5.44) is applicable only to assemblies with pin-end restraints about the Y axis and fixity end restraints relative to twist with $L/r_Y = 50-200$, $b_Y/b_X = 1.0-2.0$, $b_Y/t = 6.0-14.0$, $d/t = 1.0-2.0$ and $n = 1.0-11.0$.

5.8.2.2. Illustrative example

A 2L76x51x9.5 back-to-back compression assembly with a 2400 mm span is connected by the longer legs to a 12.7 mm thick gusset plate at both ends. The assembly has three interconnectors located at $L = 600,1200,1800$ mm. The moduli of elasticity and rigidity are taken as 200,000 MPa and 76,900 MPa, respectively. It is required to estimate the elastic and nominal inelastic buckling capacities of the assembly.

Solution:

The elastic buckling load of the assembly will be first calculated based on the proposed solution and then will be used to calculate the inelastic buckling resistance based on ANSI/AISC 360-16.

(a) Elastic buckling load

For end connections to provide full fixity restraints about X axis and relative to twist, and pin restraints about Y, one has $K_X = 0.5$, $K_Y = 1.0$ and $K_Z = 0.5$. The elastic buckling load for the given assembly is governed by the flexural-torsional buckling mode and is determined from the following steps:

Step 1: By substituting the dimensions $t = 9.53$ mm, $\tilde{b}_Y = 76.2 - 0.5 \times 9.53 = 71.4$ mm, $b_X = 50.8 - 0.5 \times 9.53 = 46.0$ mm and $\tilde{d} = 9.53 + 12.7 = 22.2$ mm into Eq. (5.41), one obtains the sectional properties $A = 2239$ mm^2, $Y_S = -10.6$ mm, $I_{YY} = 1{,}356{,}000$ mm^4, $I_{\omega\omega} = 120{,}800{,}000$ mm^6, $J = 67{,}780$ mm^4 and $r_0 = 35.8$ mm. Also, by substituting Y_S, I_{XX}, I_{YY}, A into Eq. (5.4)b, one obtains the radius of gyration $r_Y = 24.6$ mm.

Step 2: From the sectional properties determined in Step 1, and given that $L = 2400$ mm, $K_Y = 1.0$ and $K_Z = 0.5$, by substituting into Eq. (5.2), one obtains the flexural-torsional buckling stress $F_{YZ} = 205$ MPa which corresponds to a monolithic buckling load $P_M = 459$ kN.

Step 3: From the parameters $b_Y / b_X = 1.5$, $b_Y / t = 8.0$, $d/t = 1.3$ and $n = 3$, by substituting into Eq. (5.44), one obtains the reduction factor $\Omega = 0.889$.

Step 4: The flexural-torsional buckling load is obtained by multiplying the monolithic buckling load P_M by the reduction factor Ω, yielding a flexural-torsional buckling load $P_R = 408$ kN.

For comparison, the elastic buckling load of the assembly as determined by 3D shell model is $P_{3D} = 400$ kN, a 2% difference, while that determined by ANSI/AISC 360-16 solution is $P_A = 338$ kN, a 17% reduction. The pure flexural buckling load of the assembly about the X axis is $P_X = 1736$ kN which is nearly 4.25 times the flexural-torsional buckling load P_R, confirming that flexural-torsional buckling is indeed the governing buckling mode.

(b) Inelastic buckling resistance

This section is intended to illustrate possible means of integrating the elastic buckling stress equation developed in the present study into design standards to estimate the inelastic resistance of the member. The ANSI/AISC 360-16 elastic buckling stress corresponding to P_R is $F_e = P_R / A = 182$ MPa. For a yield strength $F_y = 350$ MPa, the corresponding stress ratio is $F_y / F_e = 1.92 < 2.25$ and the corresponding critical stress is $F_{cr} = 0.658^{(F_y/F_e)} F_y = 156$ MPa. Therefore, the corresponding nominal inelastic buckling resistance as estimated by the standard is $P_n = AF_{cr} = 350$ kN.

It is emphasized that the present study contributed towards a single aspect of the design of back-to-back built-up assemblies made of hot-rolled angles that satisfy non-slender/Class 3 requirements, namely their elastic buckling load/stresses. No attempt was made to investigate other factors including yielding, residual stress effects and initial out-of-straightness. Thus, while the comparisons provided suggest that the proposed elastic buckling solution is an improvement over existing elastic buckling equations, it is recommended to conduct further comparisons between inelastic buckling predictions estimated by integrating the proposed elastic buckling equation with existing standard provisions (which empirically account for yielding, residual stress effects and

initial out-of-straightness) against experimentally obtained inelastic buckling resistances and conduct a formal reliability analysis.

5.9. Summary and conclusions

The present study developed a finite element formulation to estimate the flexural-torsional buckling load of concentrically loaded back-to-back double angle assemblies with discrete interconnectors. The formulation idealized the two angles by two lines of thin-walled members while modelling the effect of the interconnectors joining them through kinematic constraints. The study also extended the Vlasov thin-walled theory, originally intended for monolithic sections, to non-monolithic assemblies consisting of double angles that are connected back-to-back. The validity of both solutions was demonstrated through comparisons with predictions of 3D finite element shell models based on ABAQUS. The solutions were then used to investigate the effect of the number of interconnectors, the slenderness ratio, the leg width ratio, the connected leg width-to-thickness, and the angle spacing-to-thickness ratio. The present model was then used to assess the accuracy of the current design practice, develop a database of result, and use the results to propose an improved elastic buckling equation for the buckling load of the assembly. The main conclusions drawn from the present study are:

1. The accurate determination of the shear centre coordinates of the assembly and the overall warping constant based on the proposed extension of the Vlasov theory was found to predict the flexural-torsional buckling resistance of monolithic-like members in agreement with finite element analysis. As a result, the extended Vlasov beam theory predicted a significant increase in the buckling loads for assemblies involving members with lower slenderness and with enough interconnectors to enforce a nearly monolithic action.

2. In agreement with past studies, the number of interconnectors was found not to noticeably influence the pure flexural buckling loads. Conversely, it heavily influences the flexural-torsional buckling loads when the number of interconnectors is low. As the number of interconnectors increases, their added beneficial effect tends to reduce.
3. For assemblies involving fewer interconnectors, the modified slenderness ratio approach in ANSI/AISC 360-16 can grossly underestimate the flexural-torsional buckling load.
4. For equal-leg angle assemblies and unequal-leg angle assemblies connected by the longer legs, the normalized flexural-torsional buckling load was found to reduce with the leg width ratio and with the spacing-to-thickness ratio and tend to increase with the connected leg width-to-thickness ratio.
5. The regression-based interconnector reduction factor Ω developed herein yields relatively accurate flexural-torsional buckling load predictions for back-to-back double angle compression members when used in conjunction with the developed monolithic buckling solution. The proposed elastic buckling equation is limited to assemblies with end conditions that are pinned about the Y axis and fixed relative to twist, in which the number of interconnectors are $n = 1.0 - 11.0$, slenderness ratios are $L/r_Y = 50 - 200$, leg width ratios are $b_Y/b_X = 1.0 - 2.0$, connected leg width-to-thickness ratio are $b_Y/t = 6.0 - 14.0$, and the spacing-to-thickness ratios are $d/t = 1.0 - 2.0$.
6. The design example provided illustrates possible means of integrating the simplified elastic buckling equation developed herein with design standard provisions to estimate the inelastic compressive resistance of back-to-back double angle assemblies.

Notation

a	Longitudinal distance between interconnectors	n	Number of interconnectors
A	Cross-sectional area for the assembly	N_p	Pre-buckling load
A_i	Cross-sectional area for angle i	P_A	Elastic buckling load based on ANSI/AISC 360-16
B_i	Sectorial origin for angle i	P_C	Elastic buckling load based on the classical solution
$b_X, \tilde{b}_X$	Nominal and centre line leg width along X axis	P_M	Elastic buckling load based on the monolithic treatment
$b_Y, \tilde{b}_Y$	Nominal and centre line leg width along Y axis	P_n	Inelastic buckling resistance
C	Centroid of the assembly	P_R	Elastic buckling load based on the reduction factor solution
C_i	Centroid of angle i	P_T	Elastic buckling load based on the present thin-walled beam element formulation
$\mathbf{C}$	Matrix of coefficients of buckling constrains	P_{3D}	Elastic buckling load based on 3D shell model (ABAQUS)
$d, \tilde{d}$	Nominal and centre line angles spacing	R_i	Pole for angle i
$\mathbf{d}, \mathbf{D}$	Element and structure nodal displacements vector	r_{min}	Minimum radius of gyration for a single angle
E	Modulus of elasticity	r_X, r_Y	Radii of gyration about X, Y axes for the assembly
F_{cr}	Inelastic critical stress	r_0	Polar radius of gyration for the assembly
F_e	Elastic stress	r_{0_i}	Polar radius of gyration for angle $.i.$
F_X, F_Y	Flexural buckling stress about X and Y axes	S	Shear centre for the assembly
F_{YZ}	Flexural-torsional buckling stresses	S_i	Shear centre for angle i
F_y	Yield stress	t	Angle thickness
F_Z	Torsional buckling stresses	u, v, w, θ	Displacements along X, Y, Z and angle of twist, respectively
G	Modulus of rigidity	X_S, Y_S	Shear centre coordinates for the assembly
I_{XX}, I_{YY}	Principal moments of inertia of the assembly	x_{S_i}, y_{S_i}	Shear centre coordinates for angle i
$I_{x_i x_i}, I_{y_i y_i}$	Moments of inertia about x_i, y_i axes for angle i	(X, Y, Z)	Global coordinate system for the assembly

$I_{x_i y_i}$	Product of inertial for angle i	(x_i, y_i, z_i)	Global coordinate system for angle i
$I_{\omega\omega}, I_{\bar{\omega}\bar{\omega}}, I_{\bar{\bar{\omega}}\bar{\bar{\omega}}}$	Total, global and local warping constants, respectively, for the assembly	(s_i, n_i, z_i)	Local coordinate system for angle i
$I_{\omega_i\omega_i}$	Total warping constant for angle i	Δ_C	Distance between the centroids of the angles
J	Saint-Venant torsional constant for the assembly	Δ_S	Distance between the shear centres of the angles
J_i	Saint-Venant torsional constant for angle i	Π_i	Total potential energy for angle i
$(K_X L/r_X)$	Assembly slenderness ratio relative to X axis	Ω	Interconnector reduction factor
$(K_Y L/r_Y)$	Assembly slenderness ratio relative to Y axis	$\omega_i, \bar{\omega}_i, \bar{\bar{\omega}}_i$	Total, global and local sectorial functions, respectively, for the angle i
$K_Z L_Z$	Assembly effective length relative to twist	$(\varepsilon_i + \lambda\varepsilon_{pi})$	Total longitudinal strain
$\mathbf{k_E}, \mathbf{K_E}$	Element and structure elastic stiffness matrix	$(\gamma_i + \lambda\gamma_{pi})$	Total shear strain
$\mathbf{k_G}, \mathbf{K_G}$	Element and structure geometric stiffness matrix	$(\sigma_i + \lambda\sigma_{pi})$	Total longitudinal stress
l	Element length	$(\tau_i + \lambda\tau_{pi})$	Total shear stress
L	Span		

References

Abbasi, M., Khezri, M., Rasmussen, K. J. R., and Schafer, B. W. (2018). "Elastic buckling analysis of cold-formed steel built-up sections with discrete fasteners using the compound strip method." *Thin Wall. Struct*., 124, 58-71.
Ádány, S. and Schafer, B. W. (2006a). "Buckling mode decomposition of single-branched open cross-section members via finite strip method: Derivation." *Thin Wall. Struct*., 44, 563-584.
Ádány, S. and Schafer, B. W. (2006b). "Buckling mode decomposition of single-branched open cross-section members via finite strip method: Application and examples." *Thin Wall. Struct*., 44, 585-600.
Ádány, S. and Schafer, B. W. (2008). "A full modal decomposition of thin-walled, single-branched open cross-section members via the constrained finite strip method." *J. Constr. Steel Res*., 64, 12-29.
Ádány, S. and Schafer, B. W. (2014). "Generalized constrained finite strip method for thin-walled members with arbitrary cross-section: primary modes." *Thin Wall. Struct*., 84, 150-169.
AISC (American Institute of Steel Construction). (2016). "Specification for Structural Steel Buildings." ANSI/AISC 360-16, Chicago, IL.
Alenezi, A. M., and Mohareb, M. (2021). "Buckling solutions for compression members with end restraints defined along non-principal directions." *J. Constr. Steel Res.*, 181, 106505.
Ananthi, G., Roy, K., and Lim, J. B. (2019a). "Experimental and numerical investigations on axial strength of back-to-back built-up cold-formed steel angle columns." *Steel Compos. Struct.*, 31(6), 601-615.
Ananthi, G., Roy, K., Chen, B., and Lim, J. B. (2019b). "Testing, simulation and design of back-to-back built-up cold-formed steel unequal angle sections under axial compression." *Steel Compos. Struct.*, 33(4), 595-614.
Ananthi, G. B. G., Deepak, M. S., Roy, K., and Lim, J. B. (2021). "Influence of intermediate stiffeners on the axial capacity of cold-formed steel back-to-back built-up unequal angle sections." *Struct*. 32, 827-848.
Anbarasu, M., and Dar, M. A. (2020). "Improved design procedure for battened cold-formed steel built-up columns composed of lipped angles." *J. Constr. Steel Res.*, 164, 105781.
Aslani, F., and Goel, S. C. (1991a). "Stitch spacing and local buckling in seismic-resistant double-angle braces." *J. Struct. Eng*., 117(8), 2442-2463.
Aslani, F., and Goel, S. C. (1991b). "An analytical criterion for buckling strength of built-up compression members." *Eng. J*., 28(4), 159-68.
Astaneh-Asl, A., Goel, S. C., and Hanson, R. D. (1985). "Cyclic out-of-plane buckling of double-angle bracing." *J. Struct. Eng.*, 111(5), 1135-1153.
Barsoum, R. S. and Gallagher, R. H. (1970). "Finite element analysis of torsional and torsional–flexural stability problems." *Int. J. Numer. Meth. Eng*., 2(3), 335-352.
Bleich, F. (1952). Buckling strength of metal structures. Mc Graw-Hill Inc., New York, NY.

Botelho, I. S., Kayser, A. M. G., Sarquis, F. R., de Lima, L. R. O., Vellasco, P. D. S., da Silva, A. T., Rodrigues M. C. and Diniz, M. G. (2021). "Starred rolled stainless steel angle sections under compression: An experimental and numerical investigation." *Thin Wall. Struct.*, 158, 107177.

Bradford, M. A. and Trahair, N. S. (1982). "Distortional buckling of thin-web beam-columns." *Eng. Struct*., 4(1), 2-10.

Camotim, D., Silvestre, N., Basaglia, C. and Bebiano, R. (2008). "GBT-based buckling analysis of thin-walled members with non-standard support conditions." *Thin Wall. Struct*., 46(7-9), 800-815.

Chan, S. L. and Kitipornchai, S. (1987). "Geometric Nonlinear Analysis of Asymmetric Thin-Walled Beam-Columns." *Eng. Struct*., 9, 243-254.

Chen, S., and Su, M. (2003). "Out-of-plane buckling and bracing requirement in double-angle trusses." *Steel Compos. Struct.*, 3(4), 261-275.

Chen, B., Roy, K., Uzzaman, A., Raftery, G., and Lim, J. B. (2020). "Axial strength of back-to-back cold-formed steel channels with edge-stiffened holes, un-stiffened holes and plain webs." *J. Constr. Steel Res.*, 174, 106313.

Chin, C.K., Al-Bermani, F.G. and Kitipornchai, S. (1993). "Finite element method for buckling analysis of plate structures." *J. Struct. Eng*., 119(4), 1048-1068.

CISC (Canadian Institute of Steel Construction). (2021). *Handbook of steel construction*. 12th ed. Markham, ON, Canada.

CSA (Canadian Standards Association). (2019). "Design of Steel Structures." CSA S16:19, Toronto, ON, Canada.

Dar, M. A., Sahoo, D. R., and Jain, A. K. (2020). "Influence of chord compactness and slenderness on axial compression behavior of built-up battened CFS columns." *J. Build. Eng*., 32, 101743.

Dar, M. A., Sahoo, D. R., Jain, A. K., and Sharma, S. (2021). "Monotonic tests and numerical validation of cold-formed steel battened built-up columns." *Thin Wall. Struct*., 159, 107275.

Davies, J.M., Leach, P. and Heinz, D. (1994). "Second-order generalised beam theory." *J. Constr. Steel Res*., 31, 221-241.

Dinis, P.B., Camotim, D. and Silvestre, N. (2006). "GBT formulation to analyse the buckling behaviour of thin-walled members with arbitrarily 'branched' open cross-sections." *Thin Wall. Struct*., 44(1), 20-38.

Dobrić, J., Marković, Z., Buđevac, D., Spremić, M., and Fric, N. (2018a). "Resistance of cold-formed built-up stainless steel columns–part I: experiment." *J. Constr. Steel Res.*, 145, 552-572.

Dobrić, J., Pavlović, M., Marković, Z., Buđevac, D., and Spremić, M. (2018b). "Resistance of cold-formed built-up stainless steel columns–Part II: Numerical simulation." *J. Constr. Steel Res.*, 140, 247-260.

Duan, L., and Chen, W. F. (1988). "Design rules of built-up members in load and resistance factor design." *J. Struct. Eng*., 114(11), 2544-2554.

Fratamico, D. C., Torabian, S., Zhao, X., Rasmussen, K. J., and Schafer, B. W. (2018). "Experimental study on the composite action in sheathed and bare built-up cold-formed steel columns." *Thin Wall. Struct*., 127, 290-305.
Haifeng, L., Xuming, W., and Junke, H. (2016). "Simplified method for Euler buckling load of closely star-battened angle column about Y axis." *Thin Wall. Struct*., 107, 620-626.
Han, J. K., Zhang, C. L., Li, Z. B., and Wang, X. M. (2017). "Stability analysis of closely star-battened member of transmission tower." *Int. J. Steel Struct.*, 17(3), 949-956.
He, B., Zhang, Y., Ge, W.Y., An, Y. and Liu, D. (2018). "Buckling analysis of thin-walled members with open-branched cross section via semi-analytical finite strip transfer matrix method." *Thin Wall. Struct*., 124, 20-31.
Hu H., He, J., Song, L., Zhan, Z. and Li, Z. (2019). "Experimental Study and Finite Element Analysis on Ultimate Strength of Dual-Angle Cross Combined Section Under Compression." *Comp. Model. Eng. Sci*., 119(3), 499-539.
Kennedy, J. B., and Murty, M. K. (1972). "Buckling of steel angle and tee struts." *J. Struct. Div*., 98(11), 2507-2522.
Kim, M. Y., Chang, S. P. and Kim, S. B. (1994). "Spatial Stability and Free Vibration of Shear II: Numerical Approach Flexible Thin-Walled Elastic Beams." *Int. J. Numer. Meth. Eng*., 37, 4117-4140.
Kitipornchai, S., and Lee, H. W. (1986a). "Inelastic buckling of single-angle, tee and double-angle struts." *J. Constr. Steel Res.*, 6(1), 3-20.
Kitipornchai, S., and Lee, H. W. (1986b). "Inelastic experiments on angle and tee struts." *J. Constr. Steel Res.*, 6(3), 219-236.
Krajcinovic, D. (1969). "A consistent discrete elements technique for thinwalled assemblages." *Int. J. Solids Struct*., 5(7), 639-662.
Lau, S. C. W. and Hancock, G. J. (1986). "Buckling of thin flat-walled structures by a spline finite strip method." *Thin Wall. Struct*., 4(4), 269-294.
Laudiero, F. and Zaccaria, D. (1988). "Finite Element Analysis of Stability of Thin-Walled Beams of Open Section." *Int. J. Mech. Sci*., 30(8), 543-557.
Li, Z., and Schafer, B. W. (2013). "Constrained finite strip method for thin-walled members with general end boundary conditions." *J. Eng. Mech*., 139(11), 1566-1576.
Li, Q. Y., and Young, B. (2022). "Experimental and numerical investigation on cold-formed steel built-up section pin-ended columns." *Thin Wall. Struct*., 170, 108444.
Li, Y., Zhou, T., Ren, L., Sang, L., and Zhang, L. (2021). "Elastic buckling of composite webs in back-to-back cold-formed steel built-up columns-Part II: Design formula." *Struct*. 33, 3515-3525.
Liu, S. W., Gao, W. L. and Ziemian, R. D. (2019). "Improved line-element formulations for the stability analysis of arbitrarily-shaped open-section beam-columns." *Thin wall. Struct*., 144, 106290.
Liu, J. L., Lue, D. M., and Lin, C. H. (2009). "Investigation on slenderness ratios of built-up compression members." *J. Constr. Steel Res.*, 65(1), 237-248.

Lue, D. M., Yen, T., and Liu, J. L. (2006). "Experimental investigation on built-up columns." *J. Constr. Steel Res.*, 62(12), 1325-1332.
Mahar, A. M., and Jayachandran, S. A. (2021). "A Computational Study on Buckling Behavior of Cold-Formed Steel Built-Up Columns Using Compound Spline Finite Strip Method." *Int. J. Struct. Stab. Dyn.*, 21(05), 2150064.
Mahar, A. M., Jayachandran, S. A., and Mahendran, M. (2021). "Global buckling strength of discretely fastened back-to-back built-up cold-formed steel columns." *J. Constr. Steel Res.*, 187, 106998.
Maia, W. F., Vieira Jr, L. C. M., Schafer, B. W., and Malite, M. (2016). "Experimental and numerical investigation of cold-formed steel double angle members under compression." *J. Constr. Steel Res.*, 121, 398-412.
Marsh, C. (1997). "Design of single and multiple angle columns and beams." *J. Struct. Eng*., 123(7), 847-856.
Naderian, H. R. and Ronagh, H. R. (2015). "Buckling analysis of thin-walled cold-formed steel structural members using complex finite strip method." *Thin Wall. Struct*., 90, 74-83.
Papangelis, J. P. and Hancock, G. J. (1995). "Computer analysis of thin-walled structural members." *Comput. Struct*., 56(1), 157-176.
Papangelis, J. P., Trahair, N. S. and Hancock, G. J. (1998). "Elastic flexural-torsional buckling of structures by computer." *Comput. Struct*., 68, 125-137.
Pezeshky, P., Sahraei, A., Rong, F., Sasibut, S., and Mohareb, M. (2020). "Generalization of the Vlasov theory for lateral torsional buckling analysis of built-up monosymmetric assemblies." *Eng. Struct*., 221, 111055.
Phan, D. K., Rasmussen, K. J., and Schafer, B. W. (2021). "Tests and design of built-up section columns." *J. Constr. Steel Res.*, 181, 106619.
Plank, R. J. and Wittrick, W. H. (1974). "Buckling under combined loading of thin, flat-walled structures by a complex finite strip method." *Int. J. Numer. Meth. Eng*., 8(2), 323-339.
Qu, S., Zhang, B., Guo, Y., Sun, Q., and Wang, Y. (2020). "Ultimate strength of pinned-end dual-angle cross combined section columns under axial compression." *Thin Wall. Struct*., 157, 107062.
Rasmussen, K. J., Khezri, M., Schafer, B. W., and Zhang, H. (2020). "The mechanics of built-up cold-formed steel members." *Thin Wall. Struct*., 154, 106756.
Roy, K., Ting, T. C. H., Lau, H. H., and Lim, J. B. (2018). "Nonlinear behaviour of back-to-back gapped built-up cold-formed steel channel sections under compression." *J. Constr. Steel Res.*, 147, 257-276.
Roy, K., Ting, T. C. H., Lau, H. H., and Lim, J. B. (2019). "Experimental and numerical investigations on the axial capacity of cold-formed steel built-up box sections." *J. Constr. Steel Res.*, 160, 411-427.
Roy, K., Lau, H. H., Ting, T. C. H., Chen, B., and Lim, J. B. (2020). "Flexural capacity of gapped built-up cold-formed steel channel sections including web stiffeners." *J. Constr. Steel Res.*, 172, 106154.

Sato, A., and Uang, C. M. (2007). "Modified slenderness ratio for built-up members." *Eng. J*., 44(3), 269-280.
Selvaraj, S., and Madhavan, M. (2021). "Design of cold-formed steel built-up columns subjected to local-global interactive buckling using direct strength method." *Thin Wall. Struct*., 159, 107305.
Sherman, D. R., and Yura, J. A. (1998). "Bolted double angle compression members." *J. Constr. Steel Res.*, 46(1-3), 470-471.
Silvestre, N. and Camotim, D. (2002). "Second-order generalised beam theory for arbitrary orthotropic materials." *Thin Wall. Struct*., 40(9), pp.791-820.
Smith, T. G. and Sridharan, S. (1978). "A finite strip method for the buckling of plate structures under arbitrary loading." *Int. J. Mech. Sci*., 20(10), 685-693.
Temple, M. C., Schepers, J. A., and Kennedy, D. L. (1986). "Interconnection of starred angle compression members." *Can. J. Civ. Eng.*, 13(6), 606-619.
Temple, M. C., McCloskey, D. C., and Calabrese, J. M. (1987). "Interconnection of boxed angle compression members." *Can. J. Civ. Eng.*, 14(4), 534-541.
Temple, M. C., and Tan, J. C. (1988). "Interconnection of widely spaced angles." *Can. J. Civ. Eng.*, 15(4), 732-741.
Ting, T. C. H., Roy, K., Lau, H. H., and Lim, J. B. (2018). "Effect of screw spacing on behavior of axially loaded back-to-back cold-formed steel built-up channel sections." *Adv. Struct. Eng*., 21(3), 474-487.
Trahair, N. S. (1993). Flexural-Torsional Buckling of Structures, CRC Press, Boca Raton, FL.
Trahair, N. S., and Rasmussen, K. J. (2005). "Flexural–torsional buckling of columns with oblique eccentric restraints." *J. Struct. Eng*., 131(11), 1731-1737.
TuringBot. (2020). "Symbolic regression software-TuringBot", < https://turingbotsoftware.com> (accessed Feb. 2, 2022)
Vlasov V. Z. (1961). Thin-Walled Elastic Beams, 2nd Ed., Israel Program for Scientific Translations, Jerusalem.
Xiang, Y., Wang, C. M. and Kitipornchai, S. (1992). "Column buckling under general loads with allowances for pre-buckling shortening and shear deformation." *Arch. Appl. Mech*., 62(8), 544-556.
Zahn, C. J., and Haaijer, G. (1987). "Effect of connector spacing on double angle compressive strength." *Proc. Materials and Member Behavior*, ASCE, 199-212.
Zandonini, R. (1985), "Stability of Compact Built-Up Struts: Experimental Investigation and Numerical Simulation," *Construzione Metalliche*, Milan, Italy, 202-224.
Zhang, J. H., and Young, B. (2015). "Numerical investigation and design of cold-formed steel built-up open section columns with longitudinal stiffeners." *Thin Wall. Struct*., 89, 178-191.
Zhou, T., Li, Y., Wu, H., Lu, Y., and Ren, L. (2020). "Analysis to determine flexural buckling of cold-formed steel built-up back-to-back section columns." *J. Constr. Steel Res.*, 166, 105898.
Zhou, T., Li, Y., Ren, L., Sang, L., and Zhang, L. (2021). "Research on the elastic buckling of composite webs in cold-formed steel back-to-back built-up columns–Part I: Experimental and numerical investigation." *Struct.*, 30, 115-133.

Appendix 5.A. Database of elastic resistances for back-to-back double angle assemblies

This appendix summarizes the buckling load database for assemblies with back-to-back double equal-leg angles and unequal-leg angles connected through the longer legs.

Table 5.5 Elastic compressive resistance database for back-to-back double angle assemblies

Run #	Geometric properties (mm)					Dimensionless parameters					Compressive resistance			
											kN		Ratio	
	b_Y	b_X	t	d	L	b_Y/b_X	b_Y/t	d/t	L/r_Y	n	P_T	P_M	P_T/P_M	Ω
1	152	152	12.7	12.7	3402	1.00	12.0	1.00	50	1	3378	3588	0.941	0.849
2	152	152	12.7	12.7	3402	1.00	12.0	1.00	50	2	3449	3588	0.961	0.921
3	152	152	12.7	12.7	3402	1.00	12.0	1.00	50	3	3488	3588	0.972	0.946
4	152	152	12.7	12.7	3402	1.00	12.0	1.00	50	4	3505	3588	0.977	0.959
5	152	152	12.7	12.7	3402	1.00	12.0	1.00	50	5	3514	3588	0.980	0.967
6	152	152	12.7	12.7	3402	1.00	12.0	1.00	50	7	3523	3588	0.982	0.976
7	152	152	12.7	12.7	3402	1.00	12.0	1.00	50	11	3528	3588	0.983	0.985
8	152	152	12.7	15.9	3460	1.00	12.0	1.25	50	1	3378	3602	0.938	0.830
9	152	152	12.7	15.9	3460	1.00	12.0	1.25	50	2	3449	3602	0.957	0.911
10	152	152	12.7	15.9	3460	1.00	12.0	1.25	50	3	3487	3602	0.968	0.939
11	152	152	12.7	15.9	3460	1.00	12.0	1.25	50	4	3504	3602	0.973	0.954
12	152	152	12.7	15.9	3460	1.00	12.0	1.25	50	5	3513	3602	0.975	0.963
13	152	152	12.7	19.0	3517	1.00	12.0	1.50	50	1	3377	3615	0.934	0.812
14	152	152	12.7	19.0	3517	1.00	12.0	1.50	50	2	3448	3615	0.954	0.901
15	152	152	12.7	19.0	3517	1.00	12.0	1.50	50	3	3486	3615	0.964	0.933
16	152	152	12.7	19.0	3517	1.00	12.0	1.50	50	4	3503	3615	0.969	0.949
17	152	152	12.7	19.0	3517	1.00	12.0	1.50	50	5	3511	3615	0.971	0.959
18	152	152	12.7	22.2	3577	1.00	12.0	1.75	50	1	3375	3627	0.931	0.793
19	152	152	12.7	22.2	3577	1.00	12.0	1.75	50	2	3446	3627	0.950	0.891
20	152	152	12.7	22.2	3577	1.00	12.0	1.75	50	3	3483	3627	0.960	0.926
21	152	152	12.7	22.2	3577	1.00	12.0	1.75	50	4	3500	3627	0.965	0.944
22	152	152	12.7	22.2	3577	1.00	12.0	1.75	50	5	3508	3627	0.967	0.955
23	152	152	12.7	25.4	3638	1.00	12.0	2.00	50	1	3373	3638	0.927	0.774
24	152	152	12.7	25.4	3638	1.00	12.0	2.00	50	2	3443	3638	0.947	0.881
25	152	152	12.7	25.4	3638	1.00	12.0	2.00	50	3	3479	3638	0.956	0.919
26	152	152	12.7	25.4	3638	1.00	12.0	2.00	50	4	3495	3638	0.961	0.939

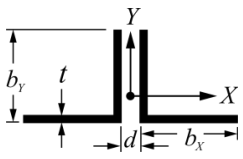

P_T = Buckling load based on the thin-walled finite element solution

P_M = Buckling load based on the monolithic solution

n = Number of interconnectors

$$\Omega = 1.0 - \left[\frac{(b_Y/b_X)+(d/t)}{n(b_Y/t)+1.3}\right]$$

Run #	b_Y	b_X	t	d	L	b_Y/b_X	b_Y/t	d/t	L/r_Y	n	P_T	P_M	P_T/P_M	Ω
27	152	152	12.7	25.4	3638	1.00	12.0	2.00	50	5	3503	3638	0.963	0.951
28	152	152	15.9	15.9	3488	1.00	9.6	1.00	50	1	5021	5842	0.859	0.816
29	152	152	15.9	15.9	3488	1.00	9.6	1.00	50	2	5323	5842	0.911	0.902
30	152	152	15.9	15.9	3488	1.00	9.6	1.00	50	3	5476	5842	0.937	0.933
31	152	152	15.9	15.9	3488	1.00	9.6	1.00	50	4	5551	5842	0.950	0.949
32	152	152	15.9	15.9	3488	1.00	9.6	1.00	50	5	5592	5842	0.957	0.959
33	152	152	15.9	15.9	3488	1.00	9.6	1.00	50	7	5630	5842	0.964	0.971
34	152	152	15.9	15.9	3488	1.00	9.6	1.00	50	11	5660	5842	0.969	0.981
35	152	152	19.0	19.0	3576	1.00	8.0	1.00	50	1	6212	7755	0.801	0.785
36	152	152	19.0	19.0	3576	1.00	8.0	1.00	50	2	6787	7755	0.875	0.884
37	152	152	19.0	19.0	3576	1.00	8.0	1.00	50	3	7083	7755	0.913	0.921
38	152	152	19.0	19.0	3576	1.00	8.0	1.00	50	4	7235	7755	0.933	0.940
39	152	152	19.0	19.0	3576	1.00	8.0	1.00	50	5	7308	7755	0.942	0.952
40	152	152	19.0	19.0	3576	1.00	8.0	1.00	50	7	7402	7755	0.955	0.965
41	152	152	19.0	19.0	3576	1.00	8.0	1.00	50	11	7471	7755	0.963	0.978
42	152	152	19.0	22.2	3637	1.00	8.0	1.17	50	1	6155	7793	0.790	0.767
43	152	152	19.0	22.2	3637	1.00	8.0	1.17	50	2	6753	7793	0.867	0.875
44	152	152	19.0	22.2	3637	1.00	8.0	1.17	50	3	7066	7793	0.907	0.914
45	152	152	19.0	22.2	3637	1.00	8.0	1.17	50	4	7225	7793	0.927	0.935
46	152	152	19.0	22.2	3637	1.00	8.0	1.17	50	5	7303	7793	0.937	0.947
47	152	152	19.0	25.4	3699	1.00	8.0	1.34	50	1	6097	7832	0.778	0.749
48	152	152	19.0	25.4	3699	1.00	8.0	1.34	50	2	6719	7832	0.858	0.865
49	152	152	19.0	25.4	3699	1.00	8.0	1.34	50	3	7046	7832	0.900	0.908
50	152	152	19.0	25.4	3699	1.00	8.0	1.34	50	4	7214	7832	0.921	0.930
51	152	152	19.0	25.4	3699	1.00	8.0	1.34	50	5	7295	7832	0.932	0.943
52	152	152	19.0	28.6	3762	1.00	8.0	1.51	50	1	6036	7869	0.767	0.731
53	152	152	19.0	28.6	3762	1.00	8.0	1.51	50	2	6682	7869	0.849	0.855
54	152	152	19.0	28.6	3762	1.00	8.0	1.51	50	3	7025	7869	0.893	0.901
55	152	152	19.0	28.6	3762	1.00	8.0	1.51	50	4	7186	7869	0.913	0.925
56	152	152	19.0	28.6	3762	1.00	8.0	1.51	50	5	7286	7869	0.926	0.939
57	152	152	19.0	31.8	3826	1.00	8.0	1.67	50	1	5973	7907	0.755	0.713
58	152	152	19.0	31.8	3826	1.00	8.0	1.67	50	2	6643	7907	0.840	0.845
59	152	152	19.0	31.8	3826	1.00	8.0	1.67	50	3	7002	7907	0.886	0.894
60	152	152	19.0	31.8	3826	1.00	8.0	1.67	50	4	7171	7907	0.907	0.920
61	152	152	19.0	31.8	3826	1.00	8.0	1.67	50	5	7276	7907	0.920	0.935
62	152	152	22.2	22.2	3670	1.00	6.8	1.00	50	1	7183	9409	0.763	0.755
63	152	152	22.2	22.2	3670	1.00	6.8	1.00	50	2	8017	9409	0.852	0.867
64	152	152	22.2	22.2	3670	1.00	6.8	1.00	50	3	8462	9409	0.899	0.908
65	152	152	22.2	22.2	3670	1.00	6.8	1.00	50	4	8672	9409	0.922	0.930
66	152	152	22.2	22.2	3670	1.00	6.8	1.00	50	5	8809	9409	0.936	0.944
67	152	152	22.2	22.2	3670	1.00	6.8	1.00	50	7	8958	9409	0.952	0.959
68	152	152	22.2	22.2	3670	1.00	6.8	1.00	50	11	9069	9409	0.964	0.974

Run #	b_Y	b_X	t	d	L	b_Y/b_X	b_Y/t	d/t	L/r_Y	n	P_T	P_M	P_T/P_M	Ω
69	152	152	25.4	25.4	3767	1.00	6.0	1.00	50	1	7992	10883	0.734	0.725
70	152	152	25.4	25.4	3767	1.00	6.0	1.00	50	2	9074	10883	0.834	0.849
71	152	152	25.4	25.4	3767	1.00	6.0	1.00	50	3	9641	10883	0.886	0.896
72	152	152	25.4	25.4	3767	1.00	6.0	1.00	50	4	9955	10883	0.915	0.921
73	152	152	25.4	25.4	3767	1.00	6.0	1.00	50	5	10144	10883	0.932	0.936
74	152	152	25.4	25.4	3767	1.00	6.0	1.00	50	7	10349	10883	0.951	0.954
75	152	152	25.4	25.4	3767	1.00	6.0	1.00	50	11	10457	10883	0.961	0.970
76	152	152	25.4	28.6	3831	1.00	6.0	1.13	50	1	7883	10907	0.723	0.708
77	152	152	25.4	28.6	3831	1.00	6.0	1.13	50	2	9001	10907	0.825	0.840
78	152	152	25.4	28.6	3831	1.00	6.0	1.13	50	3	9595	10907	0.880	0.890
79	152	152	25.4	28.6	3831	1.00	6.0	1.13	50	4	9927	10907	0.910	0.916
80	152	152	25.4	28.6	3831	1.00	6.0	1.13	50	5	10122	10907	0.928	0.932
81	152	152	25.4	31.8	3896	1.00	6.0	1.25	50	1	7775	10931	0.711	0.691
82	152	152	25.4	31.8	3896	1.00	6.0	1.25	50	2	8927	10931	0.817	0.830
83	152	152	25.4	31.8	3896	1.00	6.0	1.25	50	3	9549	10931	0.874	0.883
84	152	152	25.4	31.8	3896	1.00	6.0	1.25	50	4	9895	10931	0.905	0.911
85	152	152	25.4	31.8	3896	1.00	6.0	1.25	50	5	10099	10931	0.924	0.928
86	152	152	12.7	12.7	5103	1.00	12.0	1.00	75	1	1934	2284	0.847	0.849
87	152	152	12.7	12.7	5103	1.00	12.0	1.00	75	2	2074	2284	0.908	0.921
88	152	152	12.7	12.7	5103	1.00	12.0	1.00	75	3	2143	2284	0.939	0.946
89	152	152	12.7	12.7	5103	1.00	12.0	1.00	75	4	2179	2284	0.954	0.959
90	152	152	12.7	12.7	5103	1.00	12.0	1.00	75	5	2199	2284	0.963	0.967
91	152	152	12.7	12.7	5103	1.00	12.0	1.00	75	7	2220	2284	0.972	0.976
92	152	152	12.7	12.7	5103	1.00	12.0	1.00	75	11	2236	2284	0.979	0.985
93	152	152	15.9	15.9	5232	1.00	9.6	1.00	75	1	2453	3041	0.807	0.816
94	152	152	15.9	15.9	5232	1.00	9.6	1.00	75	2	2689	3041	0.884	0.902
95	152	152	15.9	15.9	5232	1.00	9.6	1.00	75	3	2808	3041	0.924	0.933
96	152	152	15.9	15.9	5232	1.00	9.6	1.00	75	4	2871	3041	0.944	0.949
97	152	152	15.9	15.9	5232	1.00	9.6	1.00	75	5	2907	3041	0.956	0.959
98	152	152	15.9	15.9	5232	1.00	9.6	1.00	75	7	2945	3041	0.968	0.971
99	152	152	15.9	15.9	5232	1.00	9.6	1.00	75	11	2973	3041	0.978	0.981
100	152	152	19.0	19.0	5364	1.00	8.0	1.00	75	1	2877	3692	0.779	0.785
101	152	152	19.0	19.0	5364	1.00	8.0	1.00	75	2	3202	3692	0.867	0.884
102	152	152	19.0	19.0	5364	1.00	8.0	1.00	75	3	3372	3692	0.913	0.921
103	152	152	19.0	19.0	5364	1.00	8.0	1.00	75	4	3461	3692	0.938	0.940
104	152	152	19.0	19.0	5364	1.00	8.0	1.00	75	5	3514	3692	0.952	0.952
105	152	152	19.0	19.0	5364	1.00	8.0	1.00	75	7	3569	3692	0.967	0.965
106	152	152	19.0	19.0	5364	1.00	8.0	1.00	75	11	3610	3692	0.978	0.978
107	152	152	22.2	22.2	5504	1.00	6.8	1.00	75	1	3258	4320	0.754	0.755
108	152	152	22.2	22.2	5504	1.00	6.8	1.00	75	2	3678	4320	0.851	0.867
109	152	152	22.2	22.2	5504	1.00	6.8	1.00	75	3	3903	4320	0.903	0.908
110	152	152	22.2	22.2	5504	1.00	6.8	1.00	75	4	4024	4320	0.931	0.930

Run #	b_Y	b_X	t	d	L	b_Y/b_X	b_Y/t	d/t	L/r_Y	n	P_T	P_M	P_T/P_M	Ω
111	152	152	22.2	22.2	5504	1.00	6.8	1.00	75	5	4094	4320	0.948	0.944
112	152	152	22.2	22.2	5504	1.00	6.8	1.00	75	7	4169	4320	0.965	0.959
113	152	152	22.2	22.2	5504	1.00	6.8	1.00	75	11	4224	4320	0.978	0.974
114	152	152	25.4	25.4	5650	1.00	6.0	1.00	75	1	3591	4920	0.730	0.725
115	152	152	25.4	25.4	5650	1.00	6.0	1.00	75	2	4109	4920	0.835	0.849
116	152	152	25.4	25.4	5650	1.00	6.0	1.00	75	3	4395	4920	0.893	0.896
117	152	152	25.4	25.4	5650	1.00	6.0	1.00	75	4	4548	4920	0.924	0.921
118	152	152	25.4	25.4	5650	1.00	6.0	1.00	75	5	4640	4920	0.943	0.936
119	152	152	25.4	25.4	5650	1.00	6.0	1.00	75	7	4737	4920	0.963	0.954
120	152	152	25.4	25.4	5650	1.00	6.0	1.00	75	11	4809	4920	0.977	0.970
121	152	152	12.7	12.7	6803	1.00	12.0	1.00	100	1	1143	1383	0.827	0.849
122	152	152	12.7	12.7	6803	1.00	12.0	1.00	100	2	1243	1383	0.899	0.921
123	152	152	12.7	12.7	6803	1.00	12.0	1.00	100	3	1292	1383	0.934	0.946
124	152	152	12.7	12.7	6803	1.00	12.0	1.00	100	4	1318	1383	0.953	0.959
125	152	152	12.7	12.7	6803	1.00	12.0	1.00	100	5	1332	1383	0.964	0.967
126	152	152	12.7	12.7	6803	1.00	12.0	1.00	100	7	1348	1383	0.975	0.976
127	152	152	12.7	12.7	6803	1.00	12.0	1.00	100	11	1360	1383	0.983	0.985
128	152	152	12.7	15.9	6920	1.00	12.0	1.25	100	1	1132	1387	0.816	0.830
129	152	152	12.7	15.9	6920	1.00	12.0	1.25	100	2	1236	1387	0.891	0.911
130	152	152	12.7	15.9	6920	1.00	12.0	1.25	100	3	1289	1387	0.929	0.939
131	152	152	12.7	15.9	6920	1.00	12.0	1.25	100	4	1316	1387	0.949	0.954
132	152	152	12.7	15.9	6920	1.00	12.0	1.25	100	5	1332	1387	0.960	0.963
133	152	152	12.7	19.0	7034	1.00	12.0	1.50	100	1	1121	1391	0.806	0.812
134	152	152	12.7	19.0	7034	1.00	12.0	1.50	100	2	1230	1391	0.884	0.901
135	152	152	12.7	19.0	7034	1.00	12.0	1.50	100	3	1285	1391	0.924	0.933
136	152	152	12.7	19.0	7034	1.00	12.0	1.50	100	4	1314	1391	0.945	0.949
137	152	152	12.7	19.0	7034	1.00	12.0	1.50	100	5	1331	1391	0.957	0.959
138	152	152	12.7	22.2	7154	1.00	12.0	1.75	100	1	1109	1395	0.795	0.793
139	152	152	12.7	22.2	7154	1.00	12.0	1.75	100	2	1223	1395	0.876	0.891
140	152	152	12.7	22.2	7154	1.00	12.0	1.75	100	3	1281	1395	0.918	0.926
141	152	152	12.7	22.2	7154	1.00	12.0	1.75	100	4	1312	1395	0.940	0.944
142	152	152	12.7	22.2	7154	1.00	12.0	1.75	100	5	1330	1395	0.953	0.955
143	152	152	12.7	25.4	7275	1.00	12.0	2.00	100	1	1098	1399	0.784	0.774
144	152	152	12.7	25.4	7275	1.00	12.0	2.00	100	2	1216	1399	0.869	0.881
145	152	152	12.7	25.4	7275	1.00	12.0	2.00	100	3	1277	1399	0.913	0.919
146	152	152	12.7	25.4	7275	1.00	12.0	2.00	100	4	1310	1399	0.936	0.939
147	152	152	12.7	25.4	7275	1.00	12.0	2.00	100	5	1328	1399	0.949	0.951
148	152	152	15.9	15.9	6976	1.00	9.6	1.00	100	1	1408	1762	0.799	0.816
149	152	152	15.9	15.9	6976	1.00	9.6	1.00	100	2	1554	1762	0.882	0.902
150	152	152	15.9	15.9	6976	1.00	9.6	1.00	100	3	1628	1762	0.924	0.933
151	152	152	15.9	15.9	6976	1.00	9.6	1.00	100	4	1667	1762	0.946	0.949
152	152	152	15.9	15.9	6976	1.00	9.6	1.00	100	5	1690	1762	0.959	0.959

Run #	b_Y	b_X	t	d	L	b_Y/b_X	b_Y/t	d/t	L/r_Y	n	P_T	P_M	P_T/P_M	Ω
153	152	152	15.9	15.9	6976	1.00	9.6	1.00	100	7	1714	1762	0.973	0.971
154	152	152	15.9	15.9	6976	1.00	9.6	1.00	100	11	1732	1762	0.983	0.981
155	152	152	19.0	19.0	7151	1.00	8.0	1.00	100	1	1635	2107	0.776	0.785
156	152	152	19.0	19.0	7151	1.00	8.0	1.00	100	2	1828	2107	0.867	0.884
157	152	152	19.0	19.0	7151	1.00	8.0	1.00	100	3	1928	2107	0.915	0.921
158	152	152	19.0	19.0	7151	1.00	8.0	1.00	100	4	1982	2107	0.940	0.940
159	152	152	19.0	19.0	7151	1.00	8.0	1.00	100	5	2013	2107	0.955	0.952
160	152	152	19.0	19.0	7151	1.00	8.0	1.00	100	7	2046	2107	0.971	0.965
161	152	152	19.0	19.0	7151	1.00	8.0	1.00	100	11	2071	2107	0.983	0.978
162	152	152	19.0	22.2	7274	1.00	8.0	1.17	100	1	1614	2109	0.765	0.767
163	152	152	19.0	22.2	7274	1.00	8.0	1.17	100	2	1814	2109	0.860	0.875
164	152	152	19.0	22.2	7274	1.00	8.0	1.17	100	3	1919	2109	0.910	0.914
165	152	152	19.0	22.2	7274	1.00	8.0	1.17	100	4	1976	2109	0.937	0.935
166	152	152	19.0	22.2	7274	1.00	8.0	1.17	100	5	2009	2109	0.952	0.947
167	152	152	19.0	25.4	7399	1.00	8.0	1.34	100	1	1593	2112	0.754	0.749
168	152	152	19.0	25.4	7399	1.00	8.0	1.34	100	2	1799	2112	0.852	0.865
169	152	152	19.0	25.4	7399	1.00	8.0	1.34	100	3	1911	2112	0.905	0.908
170	152	152	19.0	25.4	7399	1.00	8.0	1.34	100	4	1970	2112	0.933	0.930
171	152	152	19.0	25.4	7399	1.00	8.0	1.34	100	5	2005	2112	0.949	0.943
172	152	152	19.0	28.6	7524	1.00	8.0	1.51	100	1	1572	2114	0.744	0.731
173	152	152	19.0	28.6	7524	1.00	8.0	1.51	100	2	1785	2114	0.844	0.855
174	152	152	19.0	28.6	7524	1.00	8.0	1.51	100	3	1901	2114	0.899	0.901
175	152	152	19.0	28.6	7524	1.00	8.0	1.51	100	4	1964	2114	0.929	0.925
176	152	152	19.0	28.6	7524	1.00	8.0	1.51	100	5	2000	2114	0.946	0.939
177	152	152	19.0	31.8	7651	1.00	8.0	1.67	100	1	1550	2116	0.733	0.713
178	152	152	19.0	31.8	7651	1.00	8.0	1.67	100	2	1770	2116	0.837	0.845
179	152	152	19.0	31.8	7651	1.00	8.0	1.67	100	3	1892	2116	0.894	0.894
180	152	152	19.0	31.8	7651	1.00	8.0	1.67	100	4	1957	2116	0.925	0.920
181	152	152	19.0	31.8	7651	1.00	8.0	1.67	100	5	1996	2116	0.943	0.935
182	152	152	22.2	22.2	7339	1.00	6.8	1.00	100	1	1843	2449	0.753	0.755
183	152	152	22.2	22.2	7339	1.00	6.8	1.00	100	2	2086	2449	0.852	0.867
184	152	152	22.2	22.2	7339	1.00	6.8	1.00	100	3	2217	2449	0.905	0.908
185	152	152	22.2	22.2	7339	1.00	6.8	1.00	100	4	2288	2449	0.934	0.930
186	152	152	22.2	22.2	7339	1.00	6.8	1.00	100	5	2329	2449	0.951	0.944
187	152	152	22.2	22.2	7339	1.00	6.8	1.00	100	7	2373	2449	0.969	0.959
188	152	152	22.2	22.2	7339	1.00	6.8	1.00	100	11	2406	2449	0.982	0.974
189	152	152	25.4	25.4	7533	1.00	6.0	1.00	100	1	2027	2780	0.729	0.725
190	152	152	25.4	25.4	7533	1.00	6.0	1.00	100	2	2324	2780	0.836	0.849
191	152	152	25.4	25.4	7533	1.00	6.0	1.00	100	3	2487	2780	0.895	0.896
192	152	152	25.4	25.4	7533	1.00	6.0	1.00	100	4	2577	2780	0.927	0.921
193	152	152	25.4	25.4	7533	1.00	6.0	1.00	100	5	2630	2780	0.946	0.936
194	152	152	25.4	25.4	7533	1.00	6.0	1.00	100	7	2686	2780	0.966	0.954

Run #	b_Y	b_X	t	d	L	b_Y/b_X	b_Y/t	d/t	L/r_Y	n	P_T	P_M	P_T/P_M	Ω
195	152	152	25.4	25.4	7533	1.00	6.0	1.00	100	11	2729	2780	0.982	0.970
196	152	152	25.4	28.6	7662	1.00	6.0	1.13	100	1	1997	2781	0.718	0.708
197	152	152	25.4	28.6	7662	1.00	6.0	1.13	100	2	2302	2781	0.828	0.840
198	152	152	25.4	28.6	7662	1.00	6.0	1.13	100	3	2474	2781	0.890	0.890
199	152	152	25.4	28.6	7662	1.00	6.0	1.13	100	4	2567	2781	0.923	0.916
200	152	152	25.4	28.6	7662	1.00	6.0	1.13	100	5	2623	2781	0.943	0.932
201	152	152	25.4	31.8	7792	1.00	6.0	1.25	100	1	1967	2782	0.707	0.691
202	152	152	25.4	31.8	7792	1.00	6.0	1.25	100	2	2281	2782	0.820	0.830
203	152	152	25.4	31.8	7792	1.00	6.0	1.25	100	3	2459	2782	0.884	0.883
204	152	152	25.4	31.8	7792	1.00	6.0	1.25	100	4	2558	2782	0.919	0.911
205	152	152	25.4	31.8	7792	1.00	6.0	1.25	100	5	2616	2782	0.940	0.928
206	152	152	12.7	12.7	10205	1.00	12.0	1.00	150	1	521	636	0.819	0.849
207	152	152	12.7	12.7	10205	1.00	12.0	1.00	150	2	571	636	0.897	0.921
208	152	152	12.7	12.7	10205	1.00	12.0	1.00	150	3	595	636	0.936	0.946
209	152	152	12.7	12.7	10205	1.00	12.0	1.00	150	4	607	636	0.955	0.959
210	152	152	12.7	12.7	10205	1.00	12.0	1.00	150	5	615	636	0.966	0.967
211	152	152	12.7	12.7	10205	1.00	12.0	1.00	150	7	622	636	0.978	0.976
212	152	152	12.7	12.7	10205	1.00	12.0	1.00	150	11	628	636	0.988	0.985
213	152	152	15.9	15.9	10465	1.00	9.6	1.00	150	1	633	795	0.796	0.816
214	152	152	15.9	15.9	10465	1.00	9.6	1.00	150	2	702	795	0.883	0.902
215	152	152	15.9	15.9	10465	1.00	9.6	1.00	150	3	736	795	0.925	0.933
216	152	152	15.9	15.9	10465	1.00	9.6	1.00	150	4	755	795	0.949	0.949
217	152	152	15.9	15.9	10465	1.00	9.6	1.00	150	5	765	795	0.962	0.959
218	152	152	15.9	15.9	10465	1.00	9.6	1.00	150	7	777	795	0.976	0.971
219	152	152	15.9	15.9	10465	1.00	9.6	1.00	150	11	785	795	0.987	0.981
220	152	152	19.0	19.0	10727	1.00	8.0	1.00	150	1	732	945	0.774	0.785
221	152	152	19.0	19.0	10727	1.00	8.0	1.00	150	2	820	945	0.868	0.884
222	152	152	19.0	19.0	10727	1.00	8.0	1.00	150	3	866	945	0.916	0.921
223	152	152	19.0	19.0	10727	1.00	8.0	1.00	150	4	890	945	0.943	0.940
224	152	152	19.0	19.0	10727	1.00	8.0	1.00	150	5	905	945	0.958	0.952
225	152	152	19.0	19.0	10727	1.00	8.0	1.00	150	7	920	945	0.974	0.965
226	152	152	19.0	19.0	10727	1.00	8.0	1.00	150	11	932	945	0.986	0.978
227	152	152	22.2	22.2	11009	1.00	6.8	1.00	150	1	822	1094	0.752	0.755
228	152	152	22.2	22.2	11009	1.00	6.8	1.00	150	2	932	1094	0.852	0.867
229	152	152	22.2	22.2	11009	1.00	6.8	1.00	150	3	992	1094	0.907	0.908
230	152	152	22.2	22.2	11009	1.00	6.8	1.00	150	4	1024	1094	0.936	0.930
231	152	152	22.2	22.2	11009	1.00	6.8	1.00	150	5	1043	1094	0.953	0.944
232	152	152	22.2	22.2	11009	1.00	6.8	1.00	150	7	1063	1094	0.972	0.959
233	152	152	22.2	22.2	11009	1.00	6.8	1.00	150	11	1078	1094	0.985	0.974
234	152	152	25.4	25.4	11300	1.00	6.0	1.00	150	1	903	1239	0.729	0.725
235	152	152	25.4	25.4	11300	1.00	6.0	1.00	150	2	1036	1239	0.836	0.849
236	152	152	25.4	25.4	11300	1.00	6.0	1.00	150	3	1111	1239	0.896	0.896

Run #	b_Y	b_X	t	d	L	b_Y/b_X	b_Y/t	d/t	L/r_Y	n	P_T	P_M	P_T/P_M	Ω
237	152	152	25.4	25.4	11300	1.00	6.0	1.00	150	4	1152	1239	0.929	0.921
238	152	152	25.4	25.4	11300	1.00	6.0	1.00	150	5	1175	1239	0.948	0.936
239	152	152	25.4	25.4	11300	1.00	6.0	1.00	150	7	1200	1239	0.969	0.954
240	152	152	25.4	25.4	11300	1.00	6.0	1.00	150	11	1220	1239	0.984	0.970
241	152	152	12.7	12.7	13607	1.00	12.0	1.00	200	1	295	361	0.817	0.849
242	152	152	12.7	12.7	13607	1.00	12.0	1.00	200	2	324	361	0.897	0.921
243	152	152	12.7	12.7	13607	1.00	12.0	1.00	200	3	338	361	0.936	0.946
244	152	152	12.7	12.7	13607	1.00	12.0	1.00	200	4	345	361	0.956	0.959
245	152	152	12.7	12.7	13607	1.00	12.0	1.00	200	5	350	361	0.968	0.967
246	152	152	12.7	12.7	13607	1.00	12.0	1.00	200	7	354	361	0.980	0.976
247	152	152	12.7	12.7	13607	1.00	12.0	1.00	200	11	357	361	0.989	0.985
248	152	152	12.7	15.9	13839	1.00	12.0	1.25	200	1	292	361	0.807	0.830
249	152	152	12.7	15.9	13839	1.00	12.0	1.25	200	2	322	361	0.890	0.911
250	152	152	12.7	15.9	13839	1.00	12.0	1.25	200	3	337	361	0.932	0.939
251	152	152	12.7	15.9	13839	1.00	12.0	1.25	200	4	345	361	0.953	0.954
252	152	152	12.7	15.9	13839	1.00	12.0	1.25	200	5	349	361	0.965	0.963
253	152	152	12.7	19.0	14068	1.00	12.0	1.50	200	1	288	362	0.797	0.812
254	152	152	12.7	19.0	14068	1.00	12.0	1.50	200	2	320	362	0.884	0.901
255	152	152	12.7	19.0	14068	1.00	12.0	1.50	200	3	335	362	0.927	0.933
256	152	152	12.7	19.0	14068	1.00	12.0	1.50	200	4	344	362	0.950	0.949
257	152	152	12.7	19.0	14068	1.00	12.0	1.50	200	5	348	362	0.963	0.959
258	152	152	12.7	22.2	14308	1.00	12.0	1.75	200	1	285	362	0.787	0.793
259	152	152	12.7	22.2	14308	1.00	12.0	1.75	200	2	317	362	0.877	0.891
260	152	152	12.7	22.2	14308	1.00	12.0	1.75	200	3	334	362	0.923	0.926
261	152	152	12.7	22.2	14308	1.00	12.0	1.75	200	4	342	362	0.946	0.944
262	152	152	12.7	22.2	14308	1.00	12.0	1.75	200	5	348	362	0.960	0.955
263	152	152	12.7	25.4	14550	1.00	12.0	2.00	200	1	281	362	0.776	0.774
264	152	152	12.7	25.4	14550	1.00	12.0	2.00	200	2	315	362	0.870	0.881
265	152	152	12.7	25.4	14550	1.00	12.0	2.00	200	3	332	362	0.918	0.919
266	152	152	12.7	25.4	14550	1.00	12.0	2.00	200	4	341	362	0.942	0.939
267	152	152	12.7	25.4	14550	1.00	12.0	2.00	200	5	347	362	0.957	0.951
268	152	152	15.9	15.9	13953	1.00	9.6	1.00	200	1	358	450	0.795	0.816
269	152	152	15.9	15.9	13953	1.00	9.6	1.00	200	2	397	450	0.883	0.902
270	152	152	15.9	15.9	13953	1.00	9.6	1.00	200	3	417	450	0.927	0.933
271	152	152	15.9	15.9	13953	1.00	9.6	1.00	200	4	427	450	0.949	0.949
272	152	152	15.9	15.9	13953	1.00	9.6	1.00	200	5	433	450	0.963	0.959
273	152	152	15.9	15.9	13953	1.00	9.6	1.00	200	7	440	450	0.978	0.971
274	152	152	15.9	15.9	13953	1.00	9.6	1.00	200	11	444	450	0.989	0.981
275	152	152	19.0	19.0	14303	1.00	8.0	1.00	200	1	412	533	0.774	0.785
276	152	152	19.0	19.0	14303	1.00	8.0	1.00	200	2	463	533	0.869	0.884
277	152	152	19.0	19.0	14303	1.00	8.0	1.00	200	3	488	533	0.917	0.921
278	152	152	19.0	19.0	14303	1.00	8.0	1.00	200	4	503	533	0.944	0.940

Run #	b_Y	b_X	t	d	L	b_Y/b_X	b_Y/t	d/t	L/r_Y	n	P_T	P_M	P_T/P_M	Ω
279	152	152	19.0	19.0	14303	1.00	8.0	1.00	200	5	511	533	0.959	0.952
280	152	152	19.0	19.0	14303	1.00	8.0	1.00	200	7	519	533	0.975	0.965
281	152	152	19.0	19.0	14303	1.00	8.0	1.00	200	11	526	533	0.988	0.978
282	152	152	19.0	22.2	14549	1.00	8.0	1.17	200	1	407	533	0.763	0.767
283	152	152	19.0	22.2	14549	1.00	8.0	1.17	200	2	459	533	0.861	0.875
284	152	152	19.0	22.2	14549	1.00	8.0	1.17	200	3	486	533	0.912	0.914
285	152	152	19.0	22.2	14549	1.00	8.0	1.17	200	4	501	533	0.940	0.935
286	152	152	19.0	22.2	14549	1.00	8.0	1.17	200	5	510	533	0.956	0.947
287	152	152	19.0	25.4	14797	1.00	8.0	1.34	200	1	401	533	0.753	0.749
288	152	152	19.0	25.4	14797	1.00	8.0	1.34	200	2	455	533	0.853	0.865
289	152	152	19.0	25.4	14797	1.00	8.0	1.34	200	3	484	533	0.907	0.908
290	152	152	19.0	25.4	14797	1.00	8.0	1.34	200	4	499	533	0.936	0.930
291	152	152	19.0	25.4	14797	1.00	8.0	1.34	200	5	508	533	0.954	0.943
292	152	152	19.0	28.6	15049	1.00	8.0	1.51	200	1	396	533	0.742	0.731
293	152	152	19.0	28.6	15049	1.00	8.0	1.51	200	2	451	533	0.846	0.855
294	152	152	19.0	28.6	15049	1.00	8.0	1.51	200	3	481	533	0.902	0.901
295	152	152	19.0	28.6	15049	1.00	8.0	1.51	200	4	497	533	0.933	0.925
296	152	152	19.0	28.6	15049	1.00	8.0	1.51	200	5	507	533	0.951	0.939
297	152	152	19.0	31.8	15303	1.00	8.0	1.67	200	1	390	533	0.731	0.713
298	152	152	19.0	31.8	15303	1.00	8.0	1.67	200	2	447	533	0.838	0.845
299	152	152	19.0	31.8	15303	1.00	8.0	1.67	200	3	478	533	0.897	0.894
300	152	152	19.0	31.8	15303	1.00	8.0	1.67	200	4	496	533	0.929	0.920
301	152	152	19.0	31.8	15303	1.00	8.0	1.67	200	5	506	533	0.948	0.935
302	152	152	22.2	22.2	14678	1.00	6.8	1.00	200	1	463	616	0.751	0.755
303	152	152	22.2	22.2	14678	1.00	6.8	1.00	200	2	525	616	0.853	0.867
304	152	152	22.2	22.2	14678	1.00	6.8	1.00	200	3	559	616	0.907	0.908
305	152	152	22.2	22.2	14678	1.00	6.8	1.00	200	4	577	616	0.936	0.930
306	152	152	22.2	22.2	14678	1.00	6.8	1.00	200	5	588	616	0.954	0.944
307	152	152	22.2	22.2	14678	1.00	6.8	1.00	200	7	599	616	0.972	0.959
308	152	152	22.2	22.2	14678	1.00	6.8	1.00	200	11	607	616	0.985	0.974
309	152	152	22.2	25.4	15067	1.00	6.8	1.14	200	1	508	698	0.728	0.737
310	152	152	22.2	25.4	15067	1.00	6.8	1.14	200	2	584	698	0.837	0.857
311	152	152	22.2	25.4	15067	1.00	6.8	1.14	200	3	625	698	0.897	0.902
312	152	152	22.2	25.4	15067	1.00	6.8	1.14	200	4	648	698	0.929	0.925
313	152	152	22.2	25.4	15067	1.00	6.8	1.14	200	5	662	698	0.949	0.940
314	152	152	22.2	25.4	15067	1.00	6.8	1.14	200	7	676	698	0.969	0.956
315	152	152	22.2	25.4	15067	1.00	6.8	1.14	200	11	687	698	0.985	0.972
316	152	152	25.4	28.6	15324	1.00	6.0	1.13	200	1	501	698	0.717	0.708
317	152	152	25.4	28.6	15324	1.00	6.0	1.13	200	2	578	698	0.829	0.840
318	152	152	25.4	28.6	15324	1.00	6.0	1.13	200	3	622	698	0.891	0.890
319	152	152	25.4	28.6	15324	1.00	6.0	1.13	200	4	646	698	0.926	0.916
320	152	152	25.4	28.6	15324	1.00	6.0	1.13	200	5	660	698	0.946	0.932

Run #	b_Y	b_X	t	d	L	b_Y/b_X	b_Y/t	d/t	L/r_Y	n	P_T	P_M	P_T/P_M	Ω
321	152	152	25.4	31.8	15583	1.00	6.0	1.25	200	1	493	698	0.707	0.691
322	152	152	25.4	31.8	15583	1.00	6.0	1.25	200	2	573	698	0.821	0.830
323	152	152	25.4	31.8	15583	1.00	6.0	1.25	200	3	618	698	0.886	0.883
324	152	152	25.4	31.8	15583	1.00	6.0	1.25	200	4	644	698	0.923	0.911
325	152	152	25.4	31.8	15583	1.00	6.0	1.25	200	5	658	698	0.943	0.928
326	102	88.9	7.9	7.9	1933	1.15	12.8	1.00	50	1	1307	1397	0.935	0.848
327	102	88.9	7.9	7.9	1933	1.15	12.8	1.00	50	2	1343	1397	0.961	0.920
328	102	88.9	7.9	7.9	1933	1.15	12.8	1.00	50	3	1357	1397	0.971	0.946
329	102	88.9	7.9	7.9	1933	1.15	12.8	1.00	50	4	1363	1397	0.976	0.959
330	102	88.9	7.9	7.9	1933	1.15	12.8	1.00	50	5	1366	1397	0.978	0.967
331	102	88.9	7.9	7.9	1933	1.15	12.8	1.00	50	7	1369	1397	0.980	0.976
332	102	88.9	7.9	7.9	1933	1.15	12.8	1.00	50	11	1371	1397	0.981	0.985
333	102	88.9	9.5	9.5	1976	1.15	10.7	1.00	50	1	1821	2081	0.875	0.821
334	102	88.9	9.5	9.5	1976	1.15	10.7	1.00	50	2	1921	2081	0.923	0.905
335	102	88.9	9.5	9.5	1976	1.15	10.7	1.00	50	3	1965	2081	0.944	0.936
336	102	88.9	9.5	9.5	1976	1.15	10.7	1.00	50	4	1986	2081	0.954	0.951
337	102	88.9	9.5	9.5	1976	1.15	10.7	1.00	50	5	1997	2081	0.960	0.961
338	102	88.9	9.5	9.5	1976	1.15	10.7	1.00	50	7	2008	2081	0.965	0.972
339	102	88.9	9.5	9.5	1976	1.15	10.7	1.00	50	11	2016	2081	0.969	0.982
340	102	88.9	7.9	7.9	2900	1.15	12.8	1.00	75	1	748	876	0.854	0.848
341	102	88.9	7.9	7.9	2900	1.15	12.8	1.00	75	2	801	876	0.915	0.920
342	102	88.9	7.9	7.9	2900	1.15	12.8	1.00	75	3	826	876	0.943	0.946
343	102	88.9	7.9	7.9	2900	1.15	12.8	1.00	75	4	838	876	0.956	0.959
344	102	88.9	7.9	7.9	2900	1.15	12.8	1.00	75	5	845	876	0.964	0.967
345	102	88.9	7.9	7.9	2900	1.15	12.8	1.00	75	7	852	876	0.972	0.976
346	102	88.9	7.9	7.9	2900	1.15	12.8	1.00	75	11	857	876	0.978	0.985
347	102	88.9	9.5	9.5	2964	1.15	10.7	1.00	75	1	918	1120	0.820	0.821
348	102	88.9	9.5	9.5	2964	1.15	10.7	1.00	75	2	1001	1120	0.894	0.905
349	102	88.9	9.5	9.5	2964	1.15	10.7	1.00	75	3	1041	1120	0.929	0.936
350	102	88.9	9.5	9.5	2964	1.15	10.7	1.00	75	4	1061	1120	0.947	0.951
351	102	88.9	9.5	9.5	2964	1.15	10.7	1.00	75	5	1072	1120	0.958	0.961
352	102	88.9	9.5	9.5	2964	1.15	10.7	1.00	75	7	1084	1120	0.968	0.972
353	102	88.9	9.5	9.5	2964	1.15	10.7	1.00	75	11	1093	1120	0.976	0.982
354	102	88.9	7.9	7.9	3867	1.15	12.8	1.00	100	1	447	535	0.834	0.848
355	102	88.9	7.9	7.9	3867	1.15	12.8	1.00	100	2	485	535	0.905	0.920
356	102	88.9	7.9	7.9	3867	1.15	12.8	1.00	100	3	503	535	0.939	0.946
357	102	88.9	7.9	7.9	3867	1.15	12.8	1.00	100	4	512	535	0.955	0.959
358	102	88.9	7.9	7.9	3867	1.15	12.8	1.00	100	5	517	535	0.965	0.967
359	102	88.9	7.9	7.9	3867	1.15	12.8	1.00	100	7	522	535	0.975	0.976
360	102	88.9	7.9	7.9	3867	1.15	12.8	1.00	100	11	526	535	0.983	0.985
361	102	88.9	7.9	9.5	3924	1.15	12.8	1.20	100	1	443	537	0.825	0.834
362	102	88.9	7.9	9.5	3924	1.15	12.8	1.20	100	2	483	537	0.899	0.913

Run #	b_Y	b_X	t	d	L	b_Y/b_X	b_Y/t	d/t	L/r_Y	n	P_T	P_M	P_T/P_M	Ω
363	102	88.9	7.9	9.5	3924	1.15	12.8	1.20	100	3	502	537	0.934	0.941
364	102	88.9	7.9	9.5	3924	1.15	12.8	1.20	100	4	511	537	0.952	0.955
365	102	88.9	7.9	9.5	3924	1.15	12.8	1.20	100	5	517	537	0.962	0.964
366	102	88.9	7.9	12.7	4040	1.15	12.8	1.60	100	1	436	541	0.807	0.806
367	102	88.9	7.9	12.7	4040	1.15	12.8	1.60	100	2	479	541	0.886	0.898
368	102	88.9	7.9	12.7	4040	1.15	12.8	1.60	100	3	500	541	0.925	0.931
369	102	88.9	7.9	12.7	4040	1.15	12.8	1.60	100	4	510	541	0.944	0.948
370	102	88.9	7.9	12.7	4040	1.15	12.8	1.60	100	5	517	541	0.955	0.958
371	102	88.9	7.9	15.9	4160	1.15	12.8	2.00	100	1	429	544	0.788	0.777
372	102	88.9	7.9	15.9	4160	1.15	12.8	2.00	100	2	475	544	0.873	0.883
373	102	88.9	7.9	15.9	4160	1.15	12.8	2.00	100	3	498	544	0.915	0.921
374	102	88.9	7.9	15.9	4160	1.15	12.8	2.00	100	4	509	544	0.936	0.940
375	102	88.9	7.9	15.9	4160	1.15	12.8	2.00	100	5	516	544	0.949	0.952
376	102	88.9	9.5	9.5	3951	1.15	10.7	1.00	100	1	532	657	0.810	0.821
377	102	88.9	9.5	9.5	3951	1.15	10.7	1.00	100	2	585	657	0.891	0.905
378	102	88.9	9.5	9.5	3951	1.15	10.7	1.00	100	3	611	657	0.930	0.936
379	102	88.9	9.5	9.5	3951	1.15	10.7	1.00	100	4	624	657	0.950	0.951
380	102	88.9	9.5	9.5	3951	1.15	10.7	1.00	100	5	631	657	0.961	0.961
381	102	88.9	9.5	9.5	3951	1.15	10.7	1.00	100	7	639	657	0.973	0.972
382	102	88.9	9.5	9.5	3951	1.15	10.7	1.00	100	11	645	657	0.982	0.982
383	102	88.9	9.5	12.7	4069	1.15	10.7	1.33	100	1	522	659	0.792	0.793
384	102	88.9	9.5	12.7	4069	1.15	10.7	1.33	100	2	579	659	0.878	0.891
385	102	88.9	9.5	12.7	4069	1.15	10.7	1.33	100	3	607	659	0.921	0.926
386	102	88.9	9.5	12.7	4069	1.15	10.7	1.33	100	4	622	659	0.943	0.944
387	102	88.9	9.5	12.7	4069	1.15	10.7	1.33	100	5	630	659	0.956	0.955
388	102	88.9	9.5	15.9	4191	1.15	10.7	1.67	100	1	512	662	0.773	0.765
389	102	88.9	9.5	15.9	4191	1.15	10.7	1.67	100	2	573	662	0.865	0.876
390	102	88.9	9.5	15.9	4191	1.15	10.7	1.67	100	3	604	662	0.912	0.916
391	102	88.9	9.5	15.9	4191	1.15	10.7	1.67	100	4	619	662	0.936	0.936
392	102	88.9	9.5	15.9	4191	1.15	10.7	1.67	100	5	629	662	0.950	0.949
393	102	88.9	9.5	19.0	4311	1.15	10.7	1.99	100	1	501	664	0.755	0.738
394	102	88.9	9.5	19.0	4311	1.15	10.7	1.99	100	2	566	664	0.852	0.862
395	102	88.9	9.5	19.0	4311	1.15	10.7	1.99	100	3	599	664	0.902	0.906
396	102	88.9	9.5	19.0	4311	1.15	10.7	1.99	100	4	617	664	0.929	0.929
397	102	88.9	9.5	19.0	4311	1.15	10.7	1.99	100	5	627	664	0.944	0.943
398	102	88.9	7.9	7.9	5800	1.15	12.8	1.00	150	1	205	248	0.826	0.848
399	102	88.9	7.9	7.9	5800	1.15	12.8	1.00	150	2	224	248	0.903	0.920
400	102	88.9	7.9	7.9	5800	1.15	12.8	1.00	150	3	233	248	0.939	0.946
401	102	88.9	7.9	7.9	5800	1.15	12.8	1.00	150	4	238	248	0.958	0.959
402	102	88.9	7.9	7.9	5800	1.15	12.8	1.00	150	5	240	248	0.968	0.967
403	102	88.9	7.9	7.9	5800	1.15	12.8	1.00	150	7	243	248	0.979	0.976
404	102	88.9	7.9	7.9	5800	1.15	12.8	1.00	150	11	245	248	0.988	0.985

Run #	b_Y	b_X	t	d	L	b_Y/b_X	b_Y/t	d/t	L/r_Y	n	P_T	P_M	P_T/P_M	Ω
405	102	88.9	9.5	9.5	5927	1.15	10.7	1.00	150	1	241	299	0.806	0.821
406	102	88.9	9.5	9.5	5927	1.15	10.7	1.00	150	2	266	299	0.891	0.905
407	102	88.9	9.5	9.5	5927	1.15	10.7	1.00	150	3	278	299	0.932	0.936
408	102	88.9	9.5	9.5	5927	1.15	10.7	1.00	150	4	285	299	0.953	0.951
409	102	88.9	9.5	9.5	5927	1.15	10.7	1.00	150	5	288	299	0.965	0.961
410	102	88.9	9.5	9.5	5927	1.15	10.7	1.00	150	7	292	299	0.978	0.972
411	102	88.9	9.5	9.5	5927	1.15	10.7	1.00	150	11	295	299	0.987	0.982
412	102	88.9	7.9	7.9	7733	1.15	12.8	1.00	200	1	116	141	0.824	0.848
413	102	88.9	7.9	7.9	7733	1.15	12.8	1.00	200	2	128	141	0.903	0.920
414	102	88.9	7.9	7.9	7733	1.15	12.8	1.00	200	3	133	141	0.940	0.946
415	102	88.9	7.9	7.9	7733	1.15	12.8	1.00	200	4	136	141	0.959	0.959
416	102	88.9	7.9	7.9	7733	1.15	12.8	1.00	200	5	137	141	0.970	0.967
417	102	88.9	7.9	7.9	7733	1.15	12.8	1.00	200	7	139	141	0.981	0.976
418	102	88.9	7.9	7.9	7733	1.15	12.8	1.00	200	11	140	141	0.990	0.985
419	102	88.9	9.5	9.5	7903	1.15	10.7	1.00	200	1	136	169	0.805	0.821
420	102	88.9	9.5	9.5	7903	1.15	10.7	1.00	200	2	151	169	0.891	0.905
421	102	88.9	9.5	9.5	7903	1.15	10.7	1.00	200	3	158	169	0.932	0.936
422	102	88.9	9.5	9.5	7903	1.15	10.7	1.00	200	4	161	169	0.954	0.951
423	102	88.9	9.5	9.5	7903	1.15	10.7	1.00	200	5	163	169	0.966	0.961
424	102	88.9	9.5	9.5	7903	1.15	10.7	1.00	200	7	166	169	0.979	0.972
425	102	88.9	9.5	9.5	7903	1.15	10.7	1.00	200	11	167	169	0.989	0.982
426	203	152	15.9	15.9	3231	1.34	12.8	1.00	50	1	5116	5640	0.907	0.834
427	203	152	15.9	15.9	3231	1.34	12.8	1.00	50	2	5330	5640	0.945	0.913
428	203	152	15.9	15.9	3231	1.34	12.8	1.00	50	3	5407	5640	0.959	0.941
429	203	152	15.9	15.9	3231	1.34	12.8	1.00	50	4	5442	5640	0.965	0.955
430	203	152	15.9	15.9	3231	1.34	12.8	1.00	50	5	5459	5640	0.968	0.964
431	203	152	15.9	15.9	3231	1.34	12.8	1.00	50	7	5477	5640	0.971	0.974
432	203	152	15.9	15.9	3231	1.34	12.8	1.00	50	11	5488	5640	0.973	0.984
433	203	152	22.2	22.2	3407	1.34	9.1	1.00	50	1	8256	10292	0.802	0.776
434	203	152	22.2	22.2	3407	1.34	9.1	1.00	50	2	8998	10292	0.874	0.881
435	203	152	22.2	22.2	3407	1.34	9.1	1.00	50	3	9352	10292	0.909	0.919
436	203	152	22.2	22.2	3407	1.34	9.1	1.00	50	4	9529	10292	0.926	0.938
437	203	152	22.2	22.2	3407	1.34	9.1	1.00	50	5	9631	10292	0.936	0.950
438	203	152	22.2	22.2	3407	1.34	9.1	1.00	50	7	9708	10292	0.943	0.964
439	203	152	22.2	22.2	3407	1.34	9.1	1.00	50	11	9806	10292	0.953	0.977
440	203	152	15.9	15.9	4847	1.34	12.8	1.00	75	1	2781	3292	0.845	0.834
441	203	152	15.9	15.9	4847	1.34	12.8	1.00	75	2	2986	3292	0.907	0.913
442	203	152	15.9	15.9	4847	1.34	12.8	1.00	75	3	3081	3292	0.936	0.941
443	203	152	15.9	15.9	4847	1.34	12.8	1.00	75	4	3126	3292	0.949	0.955
444	203	152	15.9	15.9	4847	1.34	12.8	1.00	75	5	3155	3292	0.958	0.964
445	203	152	15.9	15.9	4847	1.34	12.8	1.00	75	7	3186	3292	0.968	0.974
446	203	152	15.9	15.9	4847	1.34	12.8	1.00	75	11	3206	3292	0.974	0.984

Run #	b_Y	b_X	t	d	L	b_Y/b_X	b_Y/t	d/t	L/r_Y	n	P_T	P_M	P_T/P_M	Ω
447	203	152	22.2	22.2	5110	1.34	9.1	1.00	75	1	3879	4963	0.782	0.776
448	203	152	22.2	22.2	5110	1.34	9.1	1.00	75	2	4300	4963	0.867	0.881
449	203	152	22.2	22.2	5110	1.34	9.1	1.00	75	3	4511	4963	0.909	0.919
450	203	152	22.2	22.2	5110	1.34	9.1	1.00	75	4	4625	4963	0.932	0.938
451	203	152	22.2	22.2	5110	1.34	9.1	1.00	75	5	4692	4963	0.946	0.950
452	203	152	22.2	22.2	5110	1.34	9.1	1.00	75	7	4764	4963	0.960	0.964
453	203	152	22.2	22.2	5110	1.34	9.1	1.00	75	11	4804	4963	0.968	0.977
454	203	152	15.9	15.9	6462	1.34	12.8	1.00	100	1	1650	1990	0.829	0.834
455	203	152	15.9	15.9	6462	1.34	12.8	1.00	100	2	1791	1990	0.900	0.913
456	203	152	15.9	15.9	6462	1.34	12.8	1.00	100	3	1858	1990	0.934	0.941
457	203	152	15.9	15.9	6462	1.34	12.8	1.00	100	4	1893	1990	0.951	0.955
458	203	152	15.9	15.9	6462	1.34	12.8	1.00	100	5	1913	1990	0.961	0.964
459	203	152	15.9	15.9	6462	1.34	12.8	1.00	100	7	1933	1990	0.971	0.974
460	203	152	15.9	15.9	6462	1.34	12.8	1.00	100	11	1950	1990	0.980	0.984
461	203	152	15.9	19.0	6575	1.34	12.8	1.19	100	1	1635	1998	0.818	0.820
462	203	152	15.9	19.0	6575	1.34	12.8	1.19	100	2	1783	1998	0.893	0.906
463	203	152	15.9	19.0	6575	1.34	12.8	1.19	100	3	1854	1998	0.928	0.936
464	203	152	15.9	19.0	6575	1.34	12.8	1.19	100	4	1891	1998	0.947	0.952
465	203	152	15.9	19.0	6575	1.34	12.8	1.19	100	5	1913	1998	0.957	0.961
466	203	152	15.9	22.2	6693	1.34	12.8	1.40	100	1	1619	2005	0.807	0.806
467	203	152	15.9	22.2	6693	1.34	12.8	1.40	100	2	1775	2005	0.885	0.898
468	203	152	15.9	22.2	6693	1.34	12.8	1.40	100	3	1850	2005	0.922	0.931
469	203	152	15.9	22.2	6693	1.34	12.8	1.40	100	4	1889	2005	0.942	0.948
470	203	152	15.9	22.2	6693	1.34	12.8	1.40	100	5	1912	2005	0.954	0.958
471	203	152	15.9	25.4	6812	1.34	12.8	1.60	100	1	1602	2013	0.796	0.792
472	203	152	15.9	25.4	6812	1.34	12.8	1.60	100	2	1766	2013	0.877	0.891
473	203	152	15.9	25.4	6812	1.34	12.8	1.60	100	3	1845	2013	0.917	0.926
474	203	152	15.9	25.4	6812	1.34	12.8	1.60	100	4	1887	2013	0.937	0.944
475	203	152	15.9	25.4	6812	1.34	12.8	1.60	100	5	1911	2013	0.950	0.955
476	203	152	15.9	28.6	6933	1.34	12.8	1.80	100	1	1585	2020	0.785	0.777
477	203	152	15.9	28.6	6933	1.34	12.8	1.80	100	2	1756	2020	0.869	0.883
478	203	152	15.9	28.6	6933	1.34	12.8	1.80	100	3	1840	2020	0.911	0.921
479	203	152	15.9	28.6	6933	1.34	12.8	1.80	100	4	1884	2020	0.933	0.940
480	203	152	15.9	28.6	6933	1.34	12.8	1.80	100	5	1910	2020	0.945	0.952
481	203	152	15.9	31.8	7056	1.34	12.8	2.00	100	1	1568	2028	0.773	0.763
482	203	152	15.9	31.8	7056	1.34	12.8	2.00	100	2	1746	2028	0.861	0.876
483	203	152	15.9	31.8	7056	1.34	12.8	2.00	100	3	1834	2028	0.905	0.916
484	203	152	15.9	31.8	7056	1.34	12.8	2.00	100	4	1881	2028	0.928	0.936
485	203	152	15.9	31.8	7056	1.34	12.8	2.00	100	5	1909	2028	0.941	0.949
486	203	152	22.2	22.2	6814	1.34	9.1	1.00	100	1	2218	2851	0.778	0.776
487	203	152	22.2	22.2	6814	1.34	9.1	1.00	100	2	2476	2851	0.868	0.881
488	203	152	22.2	22.2	6814	1.34	9.1	1.00	100	3	2605	2851	0.914	0.919

Run #	b_Y	b_X	t	d	L	b_Y/b_X	b_Y/t	d/t	L/r_Y	n	P_T	P_M	P_T/P_M	Ω
489	203	152	22.2	22.2	6814	1.34	9.1	1.00	100	4	2669	2851	0.936	0.938
490	203	152	22.2	22.2	6814	1.34	9.1	1.00	100	5	2710	2851	0.950	0.950
491	203	152	22.2	22.2	6814	1.34	9.1	1.00	100	7	2755	2851	0.966	0.964
492	203	152	22.2	22.2	6814	1.34	9.1	1.00	100	11	2783	2851	0.976	0.977
493	203	152	15.9	15.9	9693	1.34	12.8	1.00	150	1	757	921	0.822	0.834
494	203	152	15.9	15.9	9693	1.34	12.8	1.00	150	2	827	921	0.898	0.913
495	203	152	15.9	15.9	9693	1.34	12.8	1.00	150	3	861	921	0.935	0.941
496	203	152	15.9	15.9	9693	1.34	12.8	1.00	150	4	879	921	0.954	0.955
497	203	152	15.9	15.9	9693	1.34	12.8	1.00	150	5	889	921	0.965	0.964
498	203	152	15.9	15.9	9693	1.34	12.8	1.00	150	7	900	921	0.977	0.974
499	203	152	15.9	15.9	9693	1.34	12.8	1.00	150	11	908	921	0.986	0.984
500	203	152	22.2	22.2	10220	1.34	9.1	1.00	150	1	996	1284	0.776	0.776
501	203	152	22.2	22.2	10220	1.34	9.1	1.00	150	2	1116	1284	0.869	0.881
502	203	152	22.2	22.2	10220	1.34	9.1	1.00	150	3	1177	1284	0.916	0.919
503	203	152	22.2	22.2	10220	1.34	9.1	1.00	150	4	1209	1284	0.941	0.938
504	203	152	22.2	22.2	10220	1.34	9.1	1.00	150	5	1228	1284	0.957	0.950
505	203	152	22.2	22.2	10220	1.34	9.1	1.00	150	7	1249	1284	0.972	0.964
506	203	152	22.2	22.2	10220	1.34	9.1	1.00	150	11	1264	1284	0.984	0.977
507	203	152	15.9	15.9	12925	1.34	12.8	1.00	200	1	430	525	0.820	0.834
508	203	152	15.9	15.9	12925	1.34	12.8	1.00	200	2	471	525	0.898	0.913
509	203	152	15.9	15.9	12925	1.34	12.8	1.00	200	3	491	525	0.935	0.941
510	203	152	15.9	15.9	12925	1.34	12.8	1.00	200	4	501	525	0.955	0.955
511	203	152	15.9	15.9	12925	1.34	12.8	1.00	200	5	507	525	0.967	0.964
512	203	152	15.9	15.9	12925	1.34	12.8	1.00	200	7	514	525	0.979	0.974
513	203	152	15.9	15.9	12925	1.34	12.8	1.00	200	11	518	525	0.988	0.984
514	203	152	22.2	22.2	13627	1.34	9.1	1.00	200	1	562	725	0.775	0.776
515	203	152	22.2	22.2	13627	1.34	9.1	1.00	200	2	631	725	0.870	0.881
516	203	152	22.2	22.2	13627	1.34	9.1	1.00	200	3	665	725	0.917	0.919
517	203	152	22.2	22.2	13627	1.34	9.1	1.00	200	4	684	725	0.943	0.938
518	203	152	22.2	22.2	13627	1.34	9.1	1.00	200	5	695	725	0.958	0.950
519	203	152	22.2	22.2	13627	1.34	9.1	1.00	200	7	707	725	0.974	0.964
520	203	152	22.2	22.2	13627	1.34	9.1	1.00	200	11	716	725	0.986	0.977
521	178	127	12.7	12.7	2648	1.40	14.0	1.00	50	1	3245	3506	0.926	0.843
522	178	127	12.7	12.7	2648	1.40	14.0	1.00	50	2	3365	3506	0.960	0.918
523	178	127	12.7	12.7	2648	1.40	14.0	1.00	50	3	3398	3506	0.969	0.945
524	178	127	12.7	12.7	2648	1.40	14.0	1.00	50	4	3412	3506	0.973	0.958
525	178	127	12.7	12.7	2648	1.40	14.0	1.00	50	5	3419	3506	0.975	0.966
526	178	127	12.7	12.7	2648	1.40	14.0	1.00	50	7	3425	3506	0.977	0.976
527	178	127	12.7	12.7	2648	1.40	14.0	1.00	50	11	3430	3506	0.978	0.985
528	178	127	15.9	15.9	2734	1.40	11.2	1.00	50	1	4817	5621	0.857	0.808
529	178	127	15.9	15.9	2734	1.40	11.2	1.00	50	2	5128	5621	0.912	0.899
530	178	127	15.9	15.9	2734	1.40	11.2	1.00	50	3	5254	5621	0.935	0.931

Run #	b_Y	b_X	t	d	L	b_Y/b_X	b_Y/t	d/t	L/r_Y	n	P_T	P_M	P_T/P_M	Ω
531	178	127	15.9	15.9	2734	1.40	11.2	1.00	50	4	5309	5621	0.945	0.948
532	178	127	15.9	15.9	2734	1.40	11.2	1.00	50	5	5342	5621	0.950	0.958
533	178	127	15.9	15.9	2734	1.40	11.2	1.00	50	7	5375	5621	0.956	0.970
534	178	127	15.9	15.9	2734	1.40	11.2	1.00	50	11	5397	5621	0.960	0.981
535	178	127	19.0	19.0	2823	1.40	9.4	1.00	50	1	6031	7521	0.802	0.775
536	178	127	19.0	19.0	2823	1.40	9.4	1.00	50	2	6584	7521	0.875	0.880
537	178	127	19.0	19.0	2823	1.40	9.4	1.00	50	3	6824	7521	0.907	0.918
538	178	127	19.0	19.0	2823	1.40	9.4	1.00	50	4	6954	7521	0.925	0.938
539	178	127	19.0	19.0	2823	1.40	9.4	1.00	50	5	7027	7521	0.934	0.950
540	178	127	19.0	19.0	2823	1.40	9.4	1.00	50	7	7101	7521	0.944	0.964
541	178	127	19.0	19.0	2823	1.40	9.4	1.00	50	11	7153	7521	0.951	0.977
542	178	127	22.2	22.2	2918	1.40	8.0	1.00	50	1	7015	9243	0.759	0.742
543	178	127	22.2	22.2	2918	1.40	8.0	1.00	50	2	7824	9243	0.847	0.861
544	178	127	22.2	22.2	2918	1.40	8.0	1.00	50	3	8221	9243	0.889	0.905
545	178	127	22.2	22.2	2918	1.40	8.0	1.00	50	4	8432	9243	0.912	0.928
546	178	127	22.2	22.2	2918	1.40	8.0	1.00	50	5	8553	9243	0.925	0.942
547	178	127	22.2	22.2	2918	1.40	8.0	1.00	50	7	8680	9243	0.939	0.958
548	178	127	22.2	22.2	2918	1.40	8.0	1.00	50	11	8760	9243	0.948	0.973
549	178	127	25.4	25.4	3018	1.40	7.0	1.00	50	1	7797	10789	0.723	0.711
550	178	127	25.4	25.4	3018	1.40	7.0	1.00	50	2	8886	10789	0.824	0.843
551	178	127	25.4	25.4	3018	1.40	7.0	1.00	50	3	9442	10789	0.875	0.892
552	178	127	25.4	25.4	3018	1.40	7.0	1.00	50	4	9744	10789	0.903	0.918
553	178	127	25.4	25.4	3018	1.40	7.0	1.00	50	5	9919	10789	0.919	0.934
554	178	127	25.4	25.4	3018	1.40	7.0	1.00	50	7	10106	10789	0.937	0.952
555	178	127	25.4	25.4	3018	1.40	7.0	1.00	50	11	10227	10789	0.948	0.969
556	178	127	12.7	12.7	3972	1.40	14.0	1.00	75	1	1863	2163	0.861	0.843
557	178	127	12.7	12.7	3972	1.40	14.0	1.00	75	2	1985	2163	0.918	0.918
558	178	127	12.7	12.7	3972	1.40	14.0	1.00	75	3	2040	2163	0.943	0.945
559	178	127	12.7	12.7	3972	1.40	14.0	1.00	75	4	2068	2163	0.956	0.958
560	178	127	12.7	12.7	3972	1.40	14.0	1.00	75	5	2083	2163	0.963	0.966
561	178	127	12.7	12.7	3972	1.40	14.0	1.00	75	7	2100	2163	0.971	0.976
562	178	127	12.7	12.7	3972	1.40	14.0	1.00	75	11	2111	2163	0.976	0.985
563	178	127	15.9	15.9	4101	1.40	11.2	1.00	75	1	2410	2955	0.816	0.808
564	178	127	15.9	15.9	4101	1.40	11.2	1.00	75	2	2627	2955	0.889	0.899
565	178	127	15.9	15.9	4101	1.40	11.2	1.00	75	3	2729	2955	0.924	0.931
566	178	127	15.9	15.9	4101	1.40	11.2	1.00	75	4	2782	2955	0.942	0.948
567	178	127	15.9	15.9	4101	1.40	11.2	1.00	75	5	2813	2955	0.952	0.958
568	178	127	15.9	15.9	4101	1.40	11.2	1.00	75	7	2845	2955	0.963	0.970
569	178	127	15.9	15.9	4101	1.40	11.2	1.00	75	11	2868	2955	0.971	0.981
570	178	127	19.0	19.0	4234	1.40	9.4	1.00	75	1	2843	3638	0.781	0.775
571	178	127	19.0	19.0	4234	1.40	9.4	1.00	75	2	3158	3638	0.868	0.880
572	178	127	19.0	19.0	4234	1.40	9.4	1.00	75	3	3312	3638	0.910	0.918

Run #	b_Y	b_X	t	d	L	b_Y/b_X	b_Y/t	d/t	L/r_Y	n	P_T	P_M	P_T/P_M	Ω
573	178	127	19.0	19.0	4234	1.40	9.4	1.00	75	4	3394	3638	0.933	0.938
574	178	127	19.0	19.0	4234	1.40	9.4	1.00	75	5	3441	3638	0.946	0.950
575	178	127	19.0	19.0	4234	1.40	9.4	1.00	75	7	3488	3638	0.959	0.964
576	178	127	19.0	19.0	4234	1.40	9.4	1.00	75	11	3527	3638	0.969	0.977
577	178	127	22.2	22.2	4377	1.40	8.0	1.00	75	1	3217	4292	0.750	0.742
578	178	127	22.2	22.2	4377	1.40	8.0	1.00	75	2	3639	4292	0.848	0.861
579	178	127	22.2	22.2	4377	1.40	8.0	1.00	75	3	3852	4292	0.898	0.905
580	178	127	22.2	22.2	4377	1.40	8.0	1.00	75	4	3968	4292	0.925	0.928
581	178	127	22.2	22.2	4377	1.40	8.0	1.00	75	5	4036	4292	0.940	0.942
582	178	127	22.2	22.2	4377	1.40	8.0	1.00	75	7	4104	4292	0.956	0.958
583	178	127	22.2	22.2	4377	1.40	8.0	1.00	75	11	4159	4292	0.969	0.973
584	178	127	25.4	25.4	4527	1.40	7.0	1.00	75	1	3528	4910	0.719	0.711
585	178	127	25.4	25.4	4527	1.40	7.0	1.00	75	2	4064	4910	0.828	0.843
586	178	127	25.4	25.4	4527	1.40	7.0	1.00	75	3	4346	4910	0.885	0.892
587	178	127	25.4	25.4	4527	1.40	7.0	1.00	75	4	4492	4910	0.915	0.918
588	178	127	25.4	25.4	4527	1.40	7.0	1.00	75	5	4582	4910	0.933	0.934
589	178	127	25.4	25.4	4527	1.40	7.0	1.00	75	7	4681	4910	0.953	0.952
590	178	127	25.4	25.4	4527	1.40	7.0	1.00	75	11	4757	4910	0.969	0.969
591	178	127	12.7	12.7	5296	1.40	14.0	1.00	100	1	1126	1339	0.841	0.843
592	178	127	12.7	12.7	5296	1.40	14.0	1.00	100	2	1216	1339	0.908	0.918
593	178	127	12.7	12.7	5296	1.40	14.0	1.00	100	3	1257	1339	0.939	0.945
594	178	127	12.7	12.7	5296	1.40	14.0	1.00	100	4	1278	1339	0.954	0.958
595	178	127	12.7	12.7	5296	1.40	14.0	1.00	100	5	1290	1339	0.963	0.966
596	178	127	12.7	12.7	5296	1.40	14.0	1.00	100	7	1303	1339	0.973	0.976
597	178	127	12.7	12.7	5296	1.40	14.0	1.00	100	11	1312	1339	0.980	0.985
598	178	127	15.9	15.9	5468	1.40	11.2	1.00	100	1	1401	1736	0.807	0.808
599	178	127	15.9	15.9	5468	1.40	11.2	1.00	100	2	1539	1736	0.887	0.899
600	178	127	15.9	15.9	5468	1.40	11.2	1.00	100	3	1606	1736	0.925	0.931
601	178	127	15.9	15.9	5468	1.40	11.2	1.00	100	4	1641	1736	0.945	0.948
602	178	127	15.9	15.9	5468	1.40	11.2	1.00	100	5	1661	1736	0.957	0.958
603	178	127	15.9	15.9	5468	1.40	11.2	1.00	100	7	1682	1736	0.969	0.970
604	178	127	15.9	15.9	5468	1.40	11.2	1.00	100	11	1698	1736	0.978	0.981
605	178	127	19.0	19.0	5645	1.40	9.4	1.00	100	1	1627	2093	0.777	0.775
606	178	127	19.0	19.0	5645	1.40	9.4	1.00	100	2	1817	2093	0.868	0.880
607	178	127	19.0	19.0	5645	1.40	9.4	1.00	100	3	1912	2093	0.913	0.918
608	178	127	19.0	19.0	5645	1.40	9.4	1.00	100	4	1962	2093	0.937	0.938
609	178	127	19.0	19.0	5645	1.40	9.4	1.00	100	5	1992	2093	0.951	0.950
610	178	127	19.0	19.0	5645	1.40	9.4	1.00	100	7	2023	2093	0.966	0.964
611	178	127	19.0	19.0	5645	1.40	9.4	1.00	100	11	2046	2093	0.977	0.977
612	178	127	22.2	22.2	5837	1.40	8.0	1.00	100	1	1827	2444	0.747	0.742
613	178	127	22.2	22.2	5837	1.40	8.0	1.00	100	2	2075	2444	0.849	0.861
614	178	127	22.2	22.2	5837	1.40	8.0	1.00	100	3	2203	2444	0.901	0.905

Run #	b_Y	b_X	t	d	L	b_Y/b_X	b_Y/t	d/t	L/r_Y	n	P_T	P_M	P_T/P_M	Ω
615	178	127	22.2	22.2	5837	1.40	8.0	1.00	100	4	2271	2444	0.929	0.928
616	178	127	22.2	22.2	5837	1.40	8.0	1.00	100	5	2312	2444	0.946	0.942
617	178	127	22.2	22.2	5837	1.40	8.0	1.00	100	7	2355	2444	0.964	0.958
618	178	127	22.2	22.2	5837	1.40	8.0	1.00	100	11	2387	2444	0.977	0.973
619	178	127	25.4	25.4	6037	1.40	7.0	1.00	100	1	1996	2781	0.718	0.711
620	178	127	25.4	25.4	6037	1.40	7.0	1.00	100	2	2306	2781	0.829	0.843
621	178	127	25.4	25.4	6037	1.40	7.0	1.00	100	3	2471	2781	0.888	0.892
622	178	127	25.4	25.4	6037	1.40	7.0	1.00	100	4	2560	2781	0.921	0.918
623	178	127	25.4	25.4	6037	1.40	7.0	1.00	100	5	2614	2781	0.940	0.934
624	178	127	25.4	25.4	6037	1.40	7.0	1.00	100	7	2671	2781	0.961	0.952
625	178	127	25.4	25.4	6037	1.40	7.0	1.00	100	11	2714	2781	0.976	0.969
626	178	127	12.7	12.7	7944	1.40	14.0	1.00	150	1	523	629	0.831	0.843
627	178	127	12.7	12.7	7944	1.40	14.0	1.00	150	2	569	629	0.905	0.918
628	178	127	12.7	12.7	7944	1.40	14.0	1.00	150	3	590	629	0.939	0.945
629	178	127	12.7	12.7	7944	1.40	14.0	1.00	150	4	602	629	0.957	0.958
630	178	127	12.7	12.7	7944	1.40	14.0	1.00	150	5	608	629	0.967	0.966
631	178	127	12.7	12.7	7944	1.40	14.0	1.00	150	7	614	629	0.977	0.976
632	178	127	12.7	12.7	7944	1.40	14.0	1.00	150	11	620	629	0.986	0.985
633	178	127	15.9	15.9	8202	1.40	11.2	1.00	150	1	636	792	0.803	0.808
634	178	127	15.9	15.9	8202	1.40	11.2	1.00	150	2	703	792	0.887	0.899
635	178	127	15.9	15.9	8202	1.40	11.2	1.00	150	3	735	792	0.928	0.931
636	178	127	15.9	15.9	8202	1.40	11.2	1.00	150	4	751	792	0.949	0.948
637	178	127	15.9	15.9	8202	1.40	11.2	1.00	150	5	761	792	0.961	0.958
638	178	127	15.9	15.9	8202	1.40	11.2	1.00	150	7	772	792	0.975	0.970
639	178	127	15.9	15.9	8202	1.40	11.2	1.00	150	11	780	792	0.985	0.981
640	178	127	19.0	19.0	8468	1.40	9.4	1.00	150	1	732	944	0.775	0.775
641	178	127	19.0	19.0	8468	1.40	9.4	1.00	150	2	821	944	0.870	0.880
642	178	127	19.0	19.0	8468	1.40	9.4	1.00	150	3	864	944	0.916	0.918
643	178	127	19.0	19.0	8468	1.40	9.4	1.00	150	4	888	944	0.941	0.938
644	178	127	19.0	19.0	8468	1.40	9.4	1.00	150	5	902	944	0.956	0.950
645	178	127	19.0	19.0	8468	1.40	9.4	1.00	150	7	917	944	0.972	0.964
646	178	127	19.0	19.0	8468	1.40	9.4	1.00	150	11	928	944	0.984	0.977
647	178	127	22.2	22.2	8755	1.40	8.0	1.00	150	1	817	1095	0.746	0.742
648	178	127	22.2	22.2	8755	1.40	8.0	1.00	150	2	931	1095	0.850	0.861
649	178	127	22.2	22.2	8755	1.40	8.0	1.00	150	3	990	1095	0.904	0.905
650	178	127	22.2	22.2	8755	1.40	8.0	1.00	150	4	1022	1095	0.933	0.928
651	178	127	22.2	22.2	8755	1.40	8.0	1.00	150	5	1041	1095	0.950	0.942
652	178	127	22.2	22.2	8755	1.40	8.0	1.00	150	7	1061	1095	0.969	0.958
653	178	127	22.2	22.2	8755	1.40	8.0	1.00	150	11	1076	1095	0.983	0.973
654	178	127	25.4	25.4	9055	1.40	7.0	1.00	150	1	891	1242	0.717	0.711
655	178	127	25.4	25.4	9055	1.40	7.0	1.00	150	2	1031	1242	0.830	0.843
656	178	127	25.4	25.4	9055	1.40	7.0	1.00	150	3	1106	1242	0.891	0.892

Run #	b_Y	b_X	t	d	L	b_Y/b_X	b_Y/t	d/t	L/r_Y	n	P_T	P_M	P_T/P_M	Ω
657	178	127	25.4	25.4	9055	1.40	7.0	1.00	150	4	1148	1242	0.924	0.918
658	178	127	25.4	25.4	9055	1.40	7.0	1.00	150	5	1172	1242	0.944	0.934
659	178	127	25.4	25.4	9055	1.40	7.0	1.00	150	7	1198	1242	0.965	0.952
660	178	127	25.4	25.4	9055	1.40	7.0	1.00	150	11	1219	1242	0.981	0.969
661	178	127	12.7	12.7	10591	1.40	14.0	1.00	200	1	298	359	0.829	0.843
662	178	127	12.7	12.7	10591	1.40	14.0	1.00	200	2	325	359	0.904	0.918
663	178	127	12.7	12.7	10591	1.40	14.0	1.00	200	3	338	359	0.940	0.945
664	178	127	12.7	12.7	10591	1.40	14.0	1.00	200	4	344	359	0.958	0.958
665	178	127	12.7	12.7	10591	1.40	14.0	1.00	200	5	348	359	0.969	0.966
666	178	127	12.7	12.7	10591	1.40	14.0	1.00	200	7	352	359	0.980	0.976
667	178	127	12.7	12.7	10591	1.40	14.0	1.00	200	11	355	359	0.988	0.985
668	178	127	15.9	15.9	10936	1.40	11.2	1.00	200	1	360	449	0.802	0.808
669	178	127	15.9	15.9	10936	1.40	11.2	1.00	200	2	399	449	0.888	0.899
670	178	127	15.9	15.9	10936	1.40	11.2	1.00	200	3	417	449	0.929	0.931
671	178	127	15.9	15.9	10936	1.40	11.2	1.00	200	4	427	449	0.951	0.948
672	178	127	15.9	15.9	10936	1.40	11.2	1.00	200	5	433	449	0.964	0.958
673	178	127	15.9	15.9	10936	1.40	11.2	1.00	200	7	439	449	0.977	0.970
674	178	127	15.9	15.9	10936	1.40	11.2	1.00	200	11	443	449	0.987	0.981
675	178	127	19.0	19.0	11290	1.40	9.4	1.00	200	1	413	533	0.775	0.775
676	178	127	19.0	19.0	11290	1.40	9.4	1.00	200	2	464	533	0.870	0.880
677	178	127	19.0	19.0	11290	1.40	9.4	1.00	200	3	490	533	0.918	0.918
678	178	127	19.0	19.0	11290	1.40	9.4	1.00	200	4	503	533	0.943	0.938
679	178	127	19.0	19.0	11290	1.40	9.4	1.00	200	5	511	533	0.958	0.950
680	178	127	19.0	19.0	11290	1.40	9.4	1.00	200	7	519	533	0.974	0.964
681	178	127	19.0	19.0	11290	1.40	9.4	1.00	200	11	526	533	0.986	0.977
682	178	127	22.2	22.2	11673	1.40	8.0	1.00	200	1	461	618	0.746	0.742
683	178	127	22.2	22.2	11673	1.40	8.0	1.00	200	2	526	618	0.852	0.861
684	178	127	22.2	22.2	11673	1.40	8.0	1.00	200	3	559	618	0.905	0.905
685	178	127	22.2	22.2	11673	1.40	8.0	1.00	200	4	577	618	0.934	0.928
686	178	127	22.2	22.2	11673	1.40	8.0	1.00	200	5	588	618	0.952	0.942
687	178	127	22.2	22.2	11673	1.40	8.0	1.00	200	7	599	618	0.971	0.958
688	178	127	22.2	22.2	11673	1.40	8.0	1.00	200	11	608	618	0.985	0.973
689	178	127	25.4	25.4	12073	1.40	7.0	1.00	200	1	502	700	0.717	0.711
690	178	127	25.4	25.4	12073	1.40	7.0	1.00	200	2	581	700	0.831	0.843
691	178	127	25.4	25.4	12073	1.40	7.0	1.00	200	3	624	700	0.892	0.892
692	178	127	25.4	25.4	12073	1.40	7.0	1.00	200	4	647	700	0.925	0.918
693	178	127	25.4	25.4	12073	1.40	7.0	1.00	200	5	661	700	0.945	0.934
694	178	127	25.4	25.4	12073	1.40	7.0	1.00	200	7	676	700	0.967	0.952
695	178	127	25.4	25.4	12073	1.40	7.0	1.00	200	11	688	700	0.983	0.969
696	152	102	15.9	15.9	2248	1.49	9.6	1.00	50	1	4171	5224	0.798	0.771
697	152	102	15.9	15.9	2248	1.49	9.6	1.00	50	2	4561	5224	0.873	0.878
698	152	102	15.9	15.9	2248	1.49	9.6	1.00	50	3	4735	5224	0.906	0.917

Run #	b_Y	b_X	t	d	L	b_Y/b_X	b_Y/t	d/t	L/r_Y	n	P_T	P_M	P_T/P_M	Ω
699	152	102	15.9	15.9	2248	1.49	9.6	1.00	50	4	4822	5224	0.923	0.937
700	152	102	15.9	15.9	2248	1.49	9.6	1.00	50	5	4871	5224	0.932	0.949
701	152	102	15.9	15.9	2248	1.49	9.6	1.00	50	7	4919	5224	0.942	0.963
702	152	102	15.9	15.9	2248	1.49	9.6	1.00	50	11	4952	5224	0.948	0.977
703	152	102	22.2	22.2	2444	1.49	6.8	1.00	50	1	5540	7870	0.704	0.694
704	152	102	22.2	22.2	2444	1.49	6.8	1.00	50	2	6391	7870	0.812	0.834
705	152	102	22.2	22.2	2444	1.49	6.8	1.00	50	3	6828	7870	0.868	0.886
706	152	102	22.2	22.2	2444	1.49	6.8	1.00	50	4	7062	7870	0.897	0.913
707	152	102	22.2	22.2	2444	1.49	6.8	1.00	50	5	7199	7870	0.915	0.930
708	152	102	22.2	22.2	2444	1.49	6.8	1.00	50	7	7336	7870	0.932	0.949
709	152	102	22.2	22.2	2444	1.49	6.8	1.00	50	11	7445	7870	0.946	0.967
710	152	102	15.9	15.9	3372	1.49	9.6	1.00	75	1	1969	2529	0.779	0.771
711	152	102	15.9	15.9	3372	1.49	9.6	1.00	75	2	2191	2529	0.867	0.878
712	152	102	15.9	15.9	3372	1.49	9.6	1.00	75	3	2299	2529	0.909	0.917
713	152	102	15.9	15.9	3372	1.49	9.6	1.00	75	4	2354	2529	0.931	0.937
714	152	102	15.9	15.9	3372	1.49	9.6	1.00	75	5	2387	2529	0.944	0.949
715	152	102	15.9	15.9	3372	1.49	9.6	1.00	75	7	2421	2529	0.957	0.963
716	152	102	15.9	15.9	3372	1.49	9.6	1.00	75	11	2446	2529	0.967	0.977
717	152	102	22.2	22.2	3666	1.49	6.8	1.00	75	1	2499	3566	0.701	0.694
718	152	102	22.2	22.2	3666	1.49	6.8	1.00	75	2	2908	3566	0.816	0.834
719	152	102	22.2	22.2	3666	1.49	6.8	1.00	75	3	3125	3566	0.876	0.886
720	152	102	22.2	22.2	3666	1.49	6.8	1.00	75	4	3245	3566	0.910	0.913
721	152	102	22.2	22.2	3666	1.49	6.8	1.00	75	5	3315	3566	0.930	0.930
722	152	102	22.2	22.2	3666	1.49	6.8	1.00	75	7	3391	3566	0.951	0.949
723	152	102	22.2	22.2	3666	1.49	6.8	1.00	75	11	3447	3566	0.967	0.967
724	152	102	15.9	15.9	4495	1.49	9.6	1.00	100	1	1128	1456	0.774	0.771
725	152	102	15.9	15.9	4495	1.49	9.6	1.00	100	2	1263	1456	0.867	0.878
726	152	102	15.9	15.9	4495	1.49	9.6	1.00	100	3	1329	1456	0.913	0.917
727	152	102	15.9	15.9	4495	1.49	9.6	1.00	100	4	1364	1456	0.937	0.937
728	152	102	15.9	15.9	4495	1.49	9.6	1.00	100	5	1384	1456	0.951	0.949
729	152	102	15.9	15.9	4495	1.49	9.6	1.00	100	7	1405	1456	0.965	0.963
730	152	102	15.9	15.9	4495	1.49	9.6	1.00	100	11	1422	1456	0.976	0.977
731	152	102	15.9	19.0	4615	1.49	9.6	1.19	100	1	1106	1460	0.758	0.753
732	152	102	15.9	19.0	4615	1.49	9.6	1.19	100	2	1249	1460	0.855	0.868
733	152	102	15.9	19.0	4615	1.49	9.6	1.19	100	3	1321	1460	0.904	0.910
734	152	102	15.9	19.0	4615	1.49	9.6	1.19	100	4	1359	1460	0.930	0.932
735	152	102	15.9	19.0	4615	1.49	9.6	1.19	100	5	1381	1460	0.946	0.945
736	152	102	15.9	22.2	4741	1.49	9.6	1.40	100	1	1083	1464	0.740	0.734
737	152	102	15.9	22.2	4741	1.49	9.6	1.40	100	2	1234	1464	0.843	0.859
738	152	102	15.9	22.2	4741	1.49	9.6	1.40	100	3	1311	1464	0.896	0.904
739	152	102	15.9	22.2	4741	1.49	9.6	1.40	100	4	1353	1464	0.924	0.927
740	152	102	15.9	22.2	4741	1.49	9.6	1.40	100	5	1376	1464	0.940	0.941

Run #	b_Y	b_X	t	d	L	b_Y/b_X	b_Y/t	d/t	L/r_Y	n	P_T	P_M	P_T/P_M	Ω
741	152	102	15.9	25.4	4869	1.49	9.6	1.60	100	1	1060	1468	0.722	0.716
742	152	102	15.9	25.4	4869	1.49	9.6	1.60	100	2	1219	1468	0.831	0.849
743	152	102	15.9	25.4	4869	1.49	9.6	1.60	100	3	1302	1468	0.887	0.897
744	152	102	15.9	25.4	4869	1.49	9.6	1.60	100	4	1346	1468	0.917	0.922
745	152	102	15.9	25.4	4869	1.49	9.6	1.60	100	5	1371	1468	0.934	0.937
746	152	102	15.9	28.6	4999	1.49	9.6	1.80	100	1	1037	1471	0.705	0.697
747	152	102	15.9	28.6	4999	1.49	9.6	1.80	100	2	1204	1471	0.818	0.839
748	152	102	15.9	28.6	4999	1.49	9.6	1.80	100	3	1291	1471	0.878	0.890
749	152	102	15.9	28.6	4999	1.49	9.6	1.80	100	4	1338	1471	0.909	0.917
750	152	102	15.9	28.6	4999	1.49	9.6	1.80	100	5	1367	1471	0.929	0.933
751	152	102	15.9	31.8	5131	1.49	9.6	2.00	100	1	1013	1474	0.687	0.679
752	152	102	15.9	31.8	5131	1.49	9.6	2.00	100	2	1187	1474	0.805	0.829
753	152	102	15.9	31.8	5131	1.49	9.6	2.00	100	3	1281	1474	0.869	0.884
754	152	102	15.9	31.8	5131	1.49	9.6	2.00	100	4	1331	1474	0.903	0.912
755	152	102	15.9	31.8	5131	1.49	9.6	2.00	100	5	1361	1474	0.923	0.929
756	152	102	22.2	22.2	4888	1.49	6.8	1.00	100	1	1413	2017	0.700	0.694
757	152	102	22.2	22.2	4888	1.49	6.8	1.00	100	2	1651	2017	0.818	0.834
758	152	102	22.2	22.2	4888	1.49	6.8	1.00	100	3	1776	2017	0.880	0.886
759	152	102	22.2	22.2	4888	1.49	6.8	1.00	100	4	1845	2017	0.915	0.913
760	152	102	22.2	22.2	4888	1.49	6.8	1.00	100	5	1887	2017	0.935	0.930
761	152	102	22.2	22.2	4888	1.49	6.8	1.00	100	7	1932	2017	0.957	0.949
762	152	102	22.2	22.2	4888	1.49	6.8	1.00	100	11	1966	2017	0.974	0.967
763	152	102	15.9	15.9	6743	1.49	9.6	1.00	150	1	507	657	0.772	0.771
764	152	102	15.9	15.9	6743	1.49	9.6	1.00	150	2	570	657	0.868	0.878
765	152	102	15.9	15.9	6743	1.49	9.6	1.00	150	3	602	657	0.916	0.917
766	152	102	15.9	15.9	6743	1.49	9.6	1.00	150	4	618	657	0.941	0.937
767	152	102	15.9	15.9	6743	1.49	9.6	1.00	150	5	628	657	0.956	0.949
768	152	102	15.9	15.9	6743	1.49	9.6	1.00	150	7	638	657	0.971	0.963
769	152	102	15.9	15.9	6743	1.49	9.6	1.00	150	11	646	657	0.983	0.977
770	152	102	22.2	22.2	7332	1.49	6.8	1.00	150	1	630	900	0.700	0.694
771	152	102	22.2	22.2	7332	1.49	6.8	1.00	150	2	738	900	0.820	0.834
772	152	102	22.2	22.2	7332	1.49	6.8	1.00	150	3	796	900	0.884	0.886
773	152	102	22.2	22.2	7332	1.49	6.8	1.00	150	4	827	900	0.919	0.913
774	152	102	22.2	22.2	7332	1.49	6.8	1.00	150	5	846	900	0.940	0.930
775	152	102	22.2	22.2	7332	1.49	6.8	1.00	150	7	866	900	0.962	0.949
776	152	102	22.2	22.2	7332	1.49	6.8	1.00	150	11	882	900	0.980	0.967
777	152	102	15.9	15.9	8991	1.49	9.6	1.00	200	1	287	371	0.772	0.771
778	152	102	15.9	15.9	8991	1.49	9.6	1.00	200	2	323	371	0.870	0.878
779	152	102	15.9	15.9	8991	1.49	9.6	1.00	200	3	341	371	0.917	0.917
780	152	102	15.9	15.9	8991	1.49	9.6	1.00	200	4	350	371	0.943	0.937
781	152	102	15.9	15.9	8991	1.49	9.6	1.00	200	5	356	371	0.958	0.949
782	152	102	15.9	15.9	8991	1.49	9.6	1.00	200	7	362	371	0.974	0.963

Run #	b_Y	b_X	t	d	L	b_Y/b_X	b_Y/t	d/t	L/r_Y	n	P_T	P_M	P_T/P_M	Ω
783	152	102	15.9	15.9	8991	1.49	9.6	1.00	200	11	366	371	0.986	0.977
784	152	102	22.2	22.2	9776	1.49	6.8	1.00	200	1	355	507	0.700	0.694
785	152	102	22.2	22.2	9776	1.49	6.8	1.00	200	2	416	507	0.820	0.834
786	152	102	22.2	22.2	9776	1.49	6.8	1.00	200	3	449	507	0.885	0.886
787	152	102	22.2	22.2	9776	1.49	6.8	1.00	200	4	467	507	0.920	0.913
788	152	102	22.2	22.2	9776	1.49	6.8	1.00	200	5	478	507	0.942	0.930
789	152	102	22.2	22.2	9776	1.49	6.8	1.00	200	7	489	507	0.965	0.949
790	152	102	22.2	22.2	9776	1.49	6.8	1.00	200	11	498	507	0.982	0.967
791	127	76.2	9.5	9.5	1561	1.67	13.3	1.00	50	1	1754	1986	0.883	0.818
792	127	76.2	9.5	9.5	1561	1.67	13.3	1.00	50	2	1856	1986	0.935	0.905
793	127	76.2	9.5	9.5	1561	1.67	13.3	1.00	50	3	1885	1986	0.949	0.935
794	127	76.2	9.5	9.5	1561	1.67	13.3	1.00	50	4	1897	1986	0.955	0.951
795	127	76.2	9.5	9.5	1561	1.67	13.3	1.00	50	5	1903	1986	0.958	0.961
796	127	76.2	9.5	9.5	1561	1.67	13.3	1.00	50	7	1909	1986	0.961	0.972
797	127	76.2	9.5	9.5	1561	1.67	13.3	1.00	50	11	1913	1986	0.963	0.982
798	127	76.2	12.7	12.7	1652	1.67	10.0	1.00	50	1	2621	3308	0.792	0.764
799	127	76.2	12.7	12.7	1652	1.67	10.0	1.00	50	2	2876	3308	0.869	0.875
800	127	76.2	12.7	12.7	1652	1.67	10.0	1.00	50	3	2984	3308	0.902	0.915
801	127	76.2	12.7	12.7	1652	1.67	10.0	1.00	50	4	3037	3308	0.918	0.935
802	127	76.2	12.7	12.7	1652	1.67	10.0	1.00	50	5	3066	3308	0.927	0.948
803	127	76.2	12.7	12.7	1652	1.67	10.0	1.00	50	7	3095	3308	0.936	0.963
804	127	76.2	12.7	12.7	1652	1.67	10.0	1.00	50	11	3115	3308	0.942	0.976
805	127	76.2	9.5	9.5	2341	1.67	13.3	1.00	75	1	934	1117	0.836	0.818
806	127	76.2	9.5	9.5	2341	1.67	13.3	1.00	75	2	1009	1117	0.903	0.905
807	127	76.2	9.5	9.5	2341	1.67	13.3	1.00	75	3	1041	1117	0.932	0.935
808	127	76.2	9.5	9.5	2341	1.67	13.3	1.00	75	4	1057	1117	0.946	0.951
809	127	76.2	9.5	9.5	2341	1.67	13.3	1.00	75	5	1066	1117	0.954	0.961
810	127	76.2	9.5	9.5	2341	1.67	13.3	1.00	75	7	1075	1117	0.962	0.972
811	127	76.2	9.5	9.5	2341	1.67	13.3	1.00	75	11	1081	1117	0.968	0.982
812	127	76.2	12.7	12.7	2478	1.67	10.0	1.00	75	1	1242	1607	0.773	0.764
813	127	76.2	12.7	12.7	2478	1.67	10.0	1.00	75	2	1387	1607	0.863	0.875
814	127	76.2	12.7	12.7	2478	1.67	10.0	1.00	75	3	1456	1607	0.906	0.915
815	127	76.2	12.7	12.7	2478	1.67	10.0	1.00	75	4	1490	1607	0.927	0.935
816	127	76.2	12.7	12.7	2478	1.67	10.0	1.00	75	5	1510	1607	0.940	0.948
817	127	76.2	12.7	12.7	2478	1.67	10.0	1.00	75	7	1532	1607	0.953	0.963
818	127	76.2	12.7	12.7	2478	1.67	10.0	1.00	75	11	1547	1607	0.963	0.976
819	127	76.2	9.5	9.5	3121	1.67	13.3	1.00	100	1	555	675	0.822	0.818
820	127	76.2	9.5	9.5	3121	1.67	13.3	1.00	100	2	606	675	0.897	0.905
821	127	76.2	9.5	9.5	3121	1.67	13.3	1.00	100	3	629	675	0.931	0.935
822	127	76.2	9.5	9.5	3121	1.67	13.3	1.00	100	4	640	675	0.948	0.951
823	127	76.2	9.5	9.5	3121	1.67	13.3	1.00	100	5	647	675	0.958	0.961
824	127	76.2	9.5	9.5	3121	1.67	13.3	1.00	100	7	654	675	0.968	0.972

Run #	b_Y	b_X	t	d	L	b_Y/b_X	b_Y/t	d/t	L/r_Y	n	P_T	P_M	P_T/P_M	Ω
825	127	76.2	9.5	9.5	3121	1.67	13.3	1.00	100	11	659	675	0.975	0.982
826	127	76.2	9.5	12.7	3238	1.67	13.3	1.33	100	1	545	682	0.799	0.795
827	127	76.2	9.5	12.7	3238	1.67	13.3	1.33	100	2	600	682	0.881	0.893
828	127	76.2	9.5	12.7	3238	1.67	13.3	1.33	100	3	626	682	0.919	0.927
829	127	76.2	9.5	12.7	3238	1.67	13.3	1.33	100	4	639	682	0.938	0.945
830	127	76.2	9.5	12.7	3238	1.67	13.3	1.33	100	5	647	682	0.949	0.956
831	127	76.2	9.5	15.9	3360	1.67	13.3	1.67	100	1	533	687	0.775	0.772
832	127	76.2	9.5	15.9	3360	1.67	13.3	1.67	100	2	594	687	0.864	0.881
833	127	76.2	9.5	15.9	3360	1.67	13.3	1.67	100	3	623	687	0.906	0.919
834	127	76.2	9.5	15.9	3360	1.67	13.3	1.67	100	4	638	687	0.928	0.939
835	127	76.2	9.5	15.9	3360	1.67	13.3	1.67	100	5	646	687	0.940	0.951
836	127	76.2	9.5	19.0	3481	1.67	13.3	1.99	100	1	521	693	0.752	0.750
837	127	76.2	9.5	19.0	3481	1.67	13.3	1.99	100	2	587	693	0.847	0.869
838	127	76.2	9.5	19.0	3481	1.67	13.3	1.99	100	3	619	693	0.894	0.911
839	127	76.2	9.5	19.0	3481	1.67	13.3	1.99	100	4	636	693	0.918	0.933
840	127	76.2	9.5	19.0	3481	1.67	13.3	1.99	100	5	646	693	0.932	0.946
841	127	76.2	12.7	12.7	3304	1.67	10.0	1.00	100	1	713	928	0.769	0.764
842	127	76.2	12.7	12.7	3304	1.67	10.0	1.00	100	2	801	928	0.864	0.875
843	127	76.2	12.7	12.7	3304	1.67	10.0	1.00	100	3	844	928	0.910	0.915
844	127	76.2	12.7	12.7	3304	1.67	10.0	1.00	100	4	866	928	0.934	0.935
845	127	76.2	12.7	12.7	3304	1.67	10.0	1.00	100	5	879	928	0.948	0.948
846	127	76.2	12.7	12.7	3304	1.67	10.0	1.00	100	7	892	928	0.962	0.963
847	127	76.2	12.7	12.7	3304	1.67	10.0	1.00	100	11	903	928	0.973	0.976
848	127	76.2	12.7	15.9	3429	1.67	10.0	1.25	100	1	694	931	0.745	0.742
849	127	76.2	12.7	15.9	3429	1.67	10.0	1.25	100	2	789	931	0.847	0.863
850	127	76.2	12.7	15.9	3429	1.67	10.0	1.25	100	3	837	931	0.898	0.907
851	127	76.2	12.7	15.9	3429	1.67	10.0	1.25	100	4	862	931	0.925	0.929
852	127	76.2	12.7	15.9	3429	1.67	10.0	1.25	100	5	876	931	0.940	0.943
853	127	76.2	12.7	19.0	3552	1.67	10.0	1.50	100	1	674	935	0.721	0.720
854	127	76.2	12.7	19.0	3552	1.67	10.0	1.50	100	2	777	935	0.831	0.852
855	127	76.2	12.7	19.0	3552	1.67	10.0	1.50	100	3	829	935	0.886	0.899
856	127	76.2	12.7	19.0	3552	1.67	10.0	1.50	100	4	856	935	0.915	0.923
857	127	76.2	12.7	19.0	3552	1.67	10.0	1.50	100	5	872	935	0.933	0.938
858	127	76.2	12.7	22.2	3683	1.67	10.0	1.75	100	1	654	938	0.697	0.698
859	127	76.2	12.7	22.2	3683	1.67	10.0	1.75	100	2	763	938	0.813	0.840
860	127	76.2	12.7	22.2	3683	1.67	10.0	1.75	100	3	820	938	0.874	0.891
861	127	76.2	12.7	22.2	3683	1.67	10.0	1.75	100	4	850	938	0.905	0.917
862	127	76.2	12.7	22.2	3683	1.67	10.0	1.75	100	5	868	938	0.925	0.933
863	127	76.2	12.7	25.4	3815	1.67	10.0	2.00	100	1	634	941	0.673	0.676
864	127	76.2	12.7	25.4	3815	1.67	10.0	2.00	100	2	749	941	0.796	0.828
865	127	76.2	12.7	25.4	3815	1.67	10.0	2.00	100	3	810	941	0.860	0.883
866	127	76.2	12.7	25.4	3815	1.67	10.0	2.00	100	4	843	941	0.896	0.911

Run #	b_Y	b_X	t	d	L	b_Y/b_X	b_Y/t	d/t	L/r_Y	n	P_T	P_M	P_T/P_M	Ω
867	127	76.2	12.7	25.4	3815	1.67	10.0	2.00	100	5	863	941	0.917	0.929
868	127	76.2	9.5	9.5	4682	1.67	13.3	1.00	150	1	256	314	0.816	0.818
869	127	76.2	9.5	9.5	4682	1.67	13.3	1.00	150	2	281	314	0.896	0.905
870	127	76.2	9.5	9.5	4682	1.67	13.3	1.00	150	3	293	314	0.933	0.935
871	127	76.2	9.5	9.5	4682	1.67	13.3	1.00	150	4	299	314	0.952	0.951
872	127	76.2	9.5	9.5	4682	1.67	13.3	1.00	150	5	302	314	0.963	0.961
873	127	76.2	9.5	9.5	4682	1.67	13.3	1.00	150	7	306	314	0.975	0.972
874	127	76.2	9.5	9.5	4682	1.67	13.3	1.00	150	11	309	314	0.983	0.982
875	127	76.2	12.7	12.7	4955	1.67	10.0	1.00	150	1	321	419	0.767	0.764
876	127	76.2	12.7	12.7	4955	1.67	10.0	1.00	150	2	363	419	0.865	0.875
877	127	76.2	12.7	12.7	4955	1.67	10.0	1.00	150	3	383	419	0.914	0.915
878	127	76.2	12.7	12.7	4955	1.67	10.0	1.00	150	4	394	419	0.939	0.935
879	127	76.2	12.7	12.7	4955	1.67	10.0	1.00	150	5	400	419	0.954	0.948
880	127	76.2	12.7	12.7	4955	1.67	10.0	1.00	150	7	407	419	0.970	0.963
881	127	76.2	12.7	12.7	4955	1.67	10.0	1.00	150	11	411	419	0.981	0.976
882	127	76.2	9.5	9.5	6242	1.67	13.3	1.00	200	1	146	179	0.814	0.818
883	127	76.2	9.5	9.5	6242	1.67	13.3	1.00	200	2	161	179	0.896	0.905
884	127	76.2	9.5	9.5	6242	1.67	13.3	1.00	200	3	167	179	0.935	0.935
885	127	76.2	9.5	9.5	6242	1.67	13.3	1.00	200	4	171	179	0.955	0.951
886	127	76.2	9.5	9.5	6242	1.67	13.3	1.00	200	5	173	179	0.966	0.961
887	127	76.2	9.5	9.5	6242	1.67	13.3	1.00	200	7	175	179	0.978	0.972
888	127	76.2	9.5	9.5	6242	1.67	13.3	1.00	200	11	177	179	0.987	0.982
889	127	76.2	12.7	12.7	6607	1.67	10.0	1.00	200	1	182	237	0.766	0.764
890	127	76.2	12.7	12.7	6607	1.67	10.0	1.00	200	2	205	237	0.866	0.875
891	127	76.2	12.7	12.7	6607	1.67	10.0	1.00	200	3	217	237	0.916	0.915
892	127	76.2	12.7	12.7	6607	1.67	10.0	1.00	200	4	223	237	0.942	0.935
893	127	76.2	12.7	12.7	6607	1.67	10.0	1.00	200	5	227	237	0.957	0.948
894	127	76.2	12.7	12.7	6607	1.67	10.0	1.00	200	7	231	237	0.973	0.963
895	127	76.2	12.7	12.7	6607	1.67	10.0	1.00	200	11	234	237	0.985	0.976
896	178	102	15.9	15.9	2150	1.75	11.2	1.00	50	1	4411	5383	0.819	0.780
897	178	102	15.9	15.9	2150	1.75	11.2	1.00	50	2	4780	5383	0.888	0.884
898	178	102	15.9	15.9	2150	1.75	11.2	1.00	50	3	4922	5383	0.914	0.921
899	178	102	15.9	15.9	2150	1.75	11.2	1.00	50	4	4989	5383	0.927	0.940
900	178	102	15.9	15.9	2150	1.75	11.2	1.00	50	5	5024	5383	0.933	0.952
901	178	102	15.9	15.9	2150	1.75	11.2	1.00	50	7	5057	5383	0.939	0.966
902	178	102	15.9	15.9	2150	1.75	11.2	1.00	50	11	5081	5383	0.944	0.978
903	178	102	22.2	22.2	2346	1.75	8.0	1.00	50	1	6111	8561	0.714	0.705
904	178	102	22.2	22.2	2346	1.75	8.0	1.00	50	2	6992	8561	0.817	0.842
905	178	102	22.2	22.2	2346	1.75	8.0	1.00	50	3	7404	8561	0.865	0.892
906	178	102	22.2	22.2	2346	1.75	8.0	1.00	50	4	7631	8561	0.891	0.918
907	178	102	22.2	22.2	2346	1.75	8.0	1.00	50	5	7758	8561	0.906	0.934
908	178	102	22.2	22.2	2346	1.75	8.0	1.00	50	7	7893	8561	0.922	0.952

Run #	b_Y	b_X	t	d	L	b_Y/b_X	b_Y/t	d/t	L/r_Y	n	P_T	P_M	P_T/P_M	Ω
909	178	102	22.2	22.2	2346	1.75	8.0	1.00	50	11	7990	8561	0.933	0.969
910	178	102	15.9	15.9	3225	1.75	11.2	1.00	75	1	2153	2718	0.792	0.780
911	178	102	15.9	15.9	3225	1.75	11.2	1.00	75	2	2374	2718	0.873	0.884
912	178	102	15.9	15.9	3225	1.75	11.2	1.00	75	3	2477	2718	0.911	0.921
913	178	102	15.9	15.9	3225	1.75	11.2	1.00	75	4	2530	2718	0.931	0.940
914	178	102	15.9	15.9	3225	1.75	11.2	1.00	75	5	2560	2718	0.942	0.952
915	178	102	15.9	15.9	3225	1.75	11.2	1.00	75	7	2592	2718	0.953	0.966
916	178	102	15.9	15.9	3225	1.75	11.2	1.00	75	11	2614	2718	0.962	0.978
917	178	102	22.2	22.2	3520	1.75	8.0	1.00	75	1	2786	3929	0.709	0.705
918	178	102	22.2	22.2	3520	1.75	8.0	1.00	75	2	3222	3929	0.820	0.842
919	178	102	22.2	22.2	3520	1.75	8.0	1.00	75	3	3446	3929	0.877	0.892
920	178	102	22.2	22.2	3520	1.75	8.0	1.00	75	4	3569	3929	0.908	0.918
921	178	102	22.2	22.2	3520	1.75	8.0	1.00	75	5	3639	3929	0.926	0.934
922	178	102	22.2	22.2	3520	1.75	8.0	1.00	75	7	3712	3929	0.945	0.952
923	178	102	22.2	22.2	3520	1.75	8.0	1.00	75	11	3770	3929	0.959	0.969
924	178	102	15.9	15.9	4300	1.75	11.2	1.00	100	1	1248	1589	0.785	0.780
925	178	102	15.9	15.9	4300	1.75	11.2	1.00	100	2	1387	1589	0.873	0.884
926	178	102	15.9	15.9	4300	1.75	11.2	1.00	100	3	1453	1589	0.915	0.921
927	178	102	15.9	15.9	4300	1.75	11.2	1.00	100	4	1487	1589	0.936	0.940
928	178	102	15.9	15.9	4300	1.75	11.2	1.00	100	5	1507	1589	0.949	0.952
929	178	102	15.9	15.9	4300	1.75	11.2	1.00	100	7	1528	1589	0.962	0.966
930	178	102	15.9	15.9	4300	1.75	11.2	1.00	100	11	1544	1589	0.972	0.978
931	178	102	15.9	19.0	4419	1.75	11.2	1.19	100	1	1225	1595	0.768	0.765
932	178	102	15.9	19.0	4419	1.75	11.2	1.19	100	2	1373	1595	0.861	0.876
933	178	102	15.9	19.0	4419	1.75	11.2	1.19	100	3	1445	1595	0.906	0.916
934	178	102	15.9	19.0	4419	1.75	11.2	1.19	100	4	1482	1595	0.929	0.936
935	178	102	15.9	19.0	4419	1.75	11.2	1.19	100	5	1504	1595	0.943	0.949
936	178	102	15.9	22.2	4544	1.75	11.2	1.40	100	1	1201	1602	0.750	0.749
937	178	102	15.9	22.2	4544	1.75	11.2	1.40	100	2	1359	1602	0.848	0.867
938	178	102	15.9	22.2	4544	1.75	11.2	1.40	100	3	1435	1602	0.896	0.910
939	178	102	15.9	22.2	4544	1.75	11.2	1.40	100	4	1477	1602	0.922	0.932
940	178	102	15.9	22.2	4544	1.75	11.2	1.40	100	5	1501	1602	0.937	0.945
941	178	102	15.9	25.4	4671	1.75	11.2	1.60	100	1	1176	1608	0.731	0.732
942	178	102	15.9	25.4	4671	1.75	11.2	1.60	100	2	1343	1608	0.835	0.859
943	178	102	15.9	25.4	4671	1.75	11.2	1.60	100	3	1426	1608	0.886	0.904
944	178	102	15.9	25.4	4671	1.75	11.2	1.60	100	4	1471	1608	0.914	0.927
945	178	102	15.9	25.4	4671	1.75	11.2	1.60	100	5	1497	1608	0.931	0.942
946	178	102	15.9	28.6	4800	1.75	11.2	1.80	100	1	1151	1614	0.713	0.716
947	178	102	15.9	28.6	4800	1.75	11.2	1.80	100	2	1327	1614	0.822	0.850
948	178	102	15.9	28.6	4800	1.75	11.2	1.80	100	3	1415	1614	0.877	0.898
949	178	102	15.9	28.6	4800	1.75	11.2	1.80	100	4	1464	1614	0.907	0.923
950	178	102	15.9	28.6	4800	1.75	11.2	1.80	100	5	1493	1614	0.925	0.938

Run #	b_Y	b_X	t	d	L	b_Y/b_X	b_Y/t	d/t	L/r_Y	n	P_T	P_M	P_T/P_M	Ω
951	178	102	15.9	31.8	4931	1.75	11.2	2.00	100	1	1125	1620	0.695	0.700
952	178	102	15.9	31.8	4931	1.75	11.2	2.00	100	2	1310	1620	0.809	0.842
953	178	102	15.9	31.8	4931	1.75	11.2	2.00	100	3	1405	1620	0.867	0.893
954	178	102	15.9	31.8	4931	1.75	11.2	2.00	100	4	1457	1620	0.900	0.919
955	178	102	15.9	31.8	4931	1.75	11.2	2.00	100	5	1488	1620	0.919	0.935
956	178	102	22.2	22.2	4693	1.75	8.0	1.00	100	1	1580	2233	0.708	0.705
957	178	102	22.2	22.2	4693	1.75	8.0	1.00	100	2	1836	2233	0.822	0.842
958	178	102	22.2	22.2	4693	1.75	8.0	1.00	100	3	1969	2233	0.882	0.892
959	178	102	22.2	22.2	4693	1.75	8.0	1.00	100	4	2042	2233	0.915	0.918
960	178	102	22.2	22.2	4693	1.75	8.0	1.00	100	5	2085	2233	0.934	0.934
961	178	102	22.2	22.2	4693	1.75	8.0	1.00	100	7	2131	2233	0.955	0.952
962	178	102	22.2	22.2	4693	1.75	8.0	1.00	100	11	2165	2233	0.970	0.969
963	178	102	15.9	15.9	6450	1.75	11.2	1.00	150	1	566	724	0.782	0.780
964	178	102	15.9	15.9	6450	1.75	11.2	1.00	150	2	632	724	0.874	0.884
965	178	102	15.9	15.9	6450	1.75	11.2	1.00	150	3	665	724	0.919	0.921
966	178	102	15.9	15.9	6450	1.75	11.2	1.00	150	4	682	724	0.942	0.940
967	178	102	15.9	15.9	6450	1.75	11.2	1.00	150	5	692	724	0.956	0.952
968	178	102	15.9	15.9	6450	1.75	11.2	1.00	150	7	702	724	0.970	0.966
969	178	102	15.9	15.9	6450	1.75	11.2	1.00	150	11	710	724	0.981	0.978
970	178	102	22.2	22.2	7039	1.75	8.0	1.00	150	1	706	999	0.707	0.705
971	178	102	22.2	22.2	7039	1.75	8.0	1.00	150	2	824	999	0.825	0.842
972	178	102	22.2	22.2	7039	1.75	8.0	1.00	150	3	886	999	0.887	0.892
973	178	102	22.2	22.2	7039	1.75	8.0	1.00	150	4	919	999	0.920	0.918
974	178	102	22.2	22.2	7039	1.75	8.0	1.00	150	5	939	999	0.940	0.934
975	178	102	22.2	22.2	7039	1.75	8.0	1.00	150	7	961	999	0.962	0.952
976	178	102	22.2	22.2	7039	1.75	8.0	1.00	150	11	977	999	0.978	0.969
977	178	102	15.9	15.9	8600	1.75	11.2	1.00	200	1	320	410	0.781	0.780
978	178	102	15.9	15.9	8600	1.75	11.2	1.00	200	2	359	410	0.875	0.884
979	178	102	15.9	15.9	8600	1.75	11.2	1.00	200	3	378	410	0.920	0.921
980	178	102	15.9	15.9	8600	1.75	11.2	1.00	200	4	388	410	0.945	0.940
981	178	102	15.9	15.9	8600	1.75	11.2	1.00	200	5	393	410	0.959	0.952
982	178	102	15.9	15.9	8600	1.75	11.2	1.00	200	7	400	410	0.974	0.966
983	178	102	15.9	15.9	8600	1.75	11.2	1.00	200	11	404	410	0.985	0.978
984	178	102	22.2	22.2	9385	1.75	8.0	1.00	200	1	398	563	0.707	0.705
985	178	102	22.2	22.2	9385	1.75	8.0	1.00	200	2	465	563	0.826	0.842
986	178	102	22.2	22.2	9385	1.75	8.0	1.00	200	3	500	563	0.888	0.892
987	178	102	22.2	22.2	9385	1.75	8.0	1.00	200	4	520	563	0.922	0.918
988	178	102	22.2	22.2	9385	1.75	8.0	1.00	200	5	531	563	0.942	0.934
989	178	102	22.2	22.2	9385	1.75	8.0	1.00	200	7	543	563	0.964	0.952
990	178	102	22.2	22.2	9385	1.75	8.0	1.00	200	11	553	563	0.981	0.969
991	203	102	15.9	15.9	2069	1.99	12.8	1.00	50	1	4558	5455	0.836	0.787
992	203	102	15.9	15.9	2069	1.99	12.8	1.00	50	2	4922	5455	0.902	0.889

Run #	b_Y	b_X	t	d	L	b_Y/b_X	b_Y/t	d/t	L/r_Y	n	P_T	P_M	P_T/P_M	Ω
993	203	102	15.9	15.9	2069	1.99	12.8	1.00	50	3	5036	5455	0.923	0.924
994	203	102	15.9	15.9	2069	1.99	12.8	1.00	50	4	5078	5455	0.931	0.943
995	203	102	15.9	15.9	2069	1.99	12.8	1.00	50	5	5103	5455	0.936	0.954
996	203	102	15.9	15.9	2069	1.99	12.8	1.00	50	7	5128	5455	0.940	0.967
997	203	102	15.9	15.9	2069	1.99	12.8	1.00	50	11	5145	5455	0.943	0.979
998	203	102	15.9	19.0	2128	1.99	12.8	1.19	50	1	4546	5592	0.813	0.774
999	203	102	15.9	19.0	2128	1.99	12.8	1.19	50	2	4950	5592	0.885	0.881
1000	203	102	15.9	19.0	2128	1.99	12.8	1.19	50	3	5082	5592	0.909	0.920
1001	203	102	15.9	19.0	2128	1.99	12.8	1.19	50	4	5130	5592	0.917	0.939
1002	203	102	15.9	19.0	2128	1.99	12.8	1.19	50	5	5159	5592	0.923	0.951
1003	203	102	15.9	22.2	2190	1.99	12.8	1.40	50	1	4522	5731	0.789	0.759
1004	203	102	15.9	22.2	2190	1.99	12.8	1.40	50	2	4971	5731	0.867	0.874
1005	203	102	15.9	22.2	2190	1.99	12.8	1.40	50	3	5112	5731	0.892	0.914
1006	203	102	15.9	22.2	2190	1.99	12.8	1.40	50	4	5176	5731	0.903	0.935
1007	203	102	15.9	22.2	2190	1.99	12.8	1.40	50	5	5209	5731	0.909	0.948
1008	203	102	15.9	25.4	2254	1.99	12.8	1.60	50	1	4491	5867	0.765	0.745
1009	203	102	15.9	25.4	2254	1.99	12.8	1.60	50	2	4978	5867	0.848	0.866
1010	203	102	15.9	25.4	2254	1.99	12.8	1.60	50	3	5143	5867	0.877	0.909
1011	203	102	15.9	25.4	2254	1.99	12.8	1.60	50	4	5216	5867	0.889	0.931
1012	203	102	15.9	25.4	2254	1.99	12.8	1.60	50	5	5253	5867	0.895	0.945
1013	203	102	15.9	28.6	2318	1.99	12.8	1.80	50	1	4449	6000	0.741	0.731
1014	203	102	15.9	28.6	2318	1.99	12.8	1.80	50	2	4981	6000	0.830	0.859
1015	203	102	15.9	28.6	2318	1.99	12.8	1.80	50	3	5166	6000	0.861	0.904
1016	203	102	15.9	28.6	2318	1.99	12.8	1.80	50	4	5249	6000	0.875	0.928
1017	203	102	15.9	28.6	2318	1.99	12.8	1.80	50	5	5291	6000	0.882	0.942
1018	203	102	15.9	31.8	2383	1.99	12.8	2.00	50	1	4400	6130	0.718	0.716
1019	203	102	15.9	31.8	2383	1.99	12.8	2.00	50	2	4977	6130	0.812	0.851
1020	203	102	15.9	31.8	2383	1.99	12.8	2.00	50	3	5182	6130	0.845	0.899
1021	203	102	15.9	31.8	2383	1.99	12.8	2.00	50	4	5275	6130	0.861	0.924
1022	203	102	15.9	31.8	2383	1.99	12.8	2.00	50	5	5323	6130	0.868	0.939
1023	203	102	19.0	19.0	2163	1.99	10.7	1.00	50	1	5711	7366	0.775	0.750
1024	203	102	19.0	19.0	2163	1.99	10.7	1.00	50	2	6307	7366	0.856	0.868
1025	203	102	19.0	19.0	2163	1.99	10.7	1.00	50	3	6547	7366	0.889	0.910
1026	203	102	19.0	19.0	2163	1.99	10.7	1.00	50	4	6664	7366	0.905	0.932
1027	203	102	19.0	19.0	2163	1.99	10.7	1.00	50	5	6728	7366	0.913	0.945
1028	203	102	19.0	19.0	2163	1.99	10.7	1.00	50	7	6792	7366	0.922	0.961
1029	203	102	19.0	19.0	2163	1.99	10.7	1.00	50	11	6836	7366	0.928	0.975
1030	203	102	22.2	22.2	2266	1.99	9.1	1.00	50	1	6607	9145	0.722	0.714
1031	203	102	22.2	22.2	2266	1.99	9.1	1.00	50	2	7494	9145	0.819	0.847
1032	203	102	22.2	22.2	2266	1.99	9.1	1.00	50	3	7899	9145	0.864	0.896
1033	203	102	22.2	22.2	2266	1.99	9.1	1.00	50	4	8108	9145	0.887	0.921
1034	203	102	22.2	22.2	2266	1.99	9.1	1.00	50	5	8225	9145	0.899	0.936

Run #	b_Y	b_X	t	d	L	b_Y/b_X	b_Y/t	d/t	L/r_Y	n	P_T	P_M	P_T/P_M	Ω
1035	203	102	22.2	22.2	2266	1.99	9.1	1.00	50	7	8346	9145	0.913	0.954
1036	203	102	22.2	22.2	2266	1.99	9.1	1.00	50	11	8430	9145	0.922	0.971
1037	203	102	22.2	25.4	2332	1.99	9.1	1.14	50	1	6482	9239	0.702	0.700
1038	203	102	22.2	25.4	2332	1.99	9.1	1.14	50	2	7426	9239	0.804	0.840
1039	203	102	22.2	25.4	2332	1.99	9.1	1.14	50	3	7862	9239	0.851	0.891
1040	203	102	22.2	25.4	2332	1.99	9.1	1.14	50	4	8088	9239	0.875	0.917
1041	203	102	22.2	25.4	2332	1.99	9.1	1.14	50	5	8221	9239	0.890	0.933
1042	203	102	22.2	28.6	2398	1.99	9.1	1.29	50	1	6347	9327	0.680	0.686
1043	203	102	22.2	28.6	2398	1.99	9.1	1.29	50	2	7352	9327	0.788	0.833
1044	203	102	22.2	28.6	2398	1.99	9.1	1.29	50	3	7838	9327	0.840	0.886
1045	203	102	22.2	28.6	2398	1.99	9.1	1.29	50	4	8074	9327	0.866	0.913
1046	203	102	22.2	28.6	2398	1.99	9.1	1.29	50	5	8212	9327	0.880	0.930
1047	203	102	22.2	31.8	2465	1.99	9.1	1.43	50	1	6212	9411	0.660	0.672
1048	203	102	22.2	31.8	2465	1.99	9.1	1.43	50	2	7272	9411	0.773	0.825
1049	203	102	22.2	31.8	2465	1.99	9.1	1.43	50	3	7780	9411	0.827	0.881
1050	203	102	22.2	31.8	2465	1.99	9.1	1.43	50	4	8045	9411	0.855	0.910
1051	203	102	22.2	31.8	2465	1.99	9.1	1.43	50	5	8207	9411	0.872	0.927
1052	203	102	25.4	25.4	2374	1.99	8.0	1.00	50	1	7261	10748	0.676	0.678
1053	203	102	25.4	25.4	2374	1.99	8.0	1.00	50	2	8473	10748	0.788	0.827
1054	203	102	25.4	25.4	2374	1.99	8.0	1.00	50	3	9060	10748	0.843	0.882
1055	203	102	25.4	25.4	2374	1.99	8.0	1.00	50	4	9382	10748	0.873	0.910
1056	203	102	25.4	25.4	2374	1.99	8.0	1.00	50	5	9569	10748	0.890	0.928
1057	203	102	25.4	25.4	2374	1.99	8.0	1.00	50	7	9744	10748	0.907	0.948
1058	203	102	25.4	25.4	2374	1.99	8.0	1.00	50	11	9878	10748	0.919	0.966
1059	203	102	15.9	15.9	3104	1.99	12.8	1.00	75	1	2304	2866	0.804	0.787
1060	203	102	15.9	15.9	3104	1.99	12.8	1.00	75	2	2523	2866	0.880	0.889
1061	203	102	15.9	15.9	3104	1.99	12.8	1.00	75	3	2620	2866	0.914	0.924
1062	203	102	15.9	15.9	3104	1.99	12.8	1.00	75	4	2669	2866	0.931	0.943
1063	203	102	15.9	15.9	3104	1.99	12.8	1.00	75	5	2696	2866	0.941	0.954
1064	203	102	15.9	15.9	3104	1.99	12.8	1.00	75	7	2723	2866	0.950	0.967
1065	203	102	15.9	15.9	3104	1.99	12.8	1.00	75	11	2743	2866	0.957	0.979
1066	203	102	19.0	19.0	3245	1.99	10.7	1.00	75	1	2715	3582	0.758	0.750
1067	203	102	19.0	19.0	3245	1.99	10.7	1.00	75	2	3047	3582	0.851	0.868
1068	203	102	19.0	19.0	3245	1.99	10.7	1.00	75	3	3203	3582	0.894	0.910
1069	203	102	19.0	19.0	3245	1.99	10.7	1.00	75	4	3281	3582	0.916	0.932
1070	203	102	19.0	19.0	3245	1.99	10.7	1.00	75	5	3328	3582	0.929	0.945
1071	203	102	19.0	19.0	3245	1.99	10.7	1.00	75	7	3378	3582	0.943	0.961
1072	203	102	19.0	19.0	3245	1.99	10.7	1.00	75	11	3414	3582	0.953	0.975
1073	203	102	22.2	22.2	3400	1.99	9.1	1.00	75	1	3045	4261	0.715	0.714
1074	203	102	22.2	22.2	3400	1.99	9.1	1.00	75	2	3504	4261	0.822	0.847
1075	203	102	22.2	22.2	3400	1.99	9.1	1.00	75	3	3727	4261	0.875	0.896
1076	203	102	22.2	22.2	3400	1.99	9.1	1.00	75	4	3850	4261	0.904	0.921

Run #	b_Y	b_X	t	d	L	b_Y/b_X	b_Y/t	d/t	L/r_Y	n	P_T	P_M	P_T/P_M	Ω
1077	203	102	22.2	22.2	3400	1.99	9.1	1.00	75	5	3923	4261	0.921	0.936
1078	203	102	22.2	22.2	3400	1.99	9.1	1.00	75	7	3999	4261	0.939	0.954
1079	203	102	22.2	22.2	3400	1.99	9.1	1.00	75	11	4053	4261	0.951	0.971
1080	203	102	25.4	25.4	3562	1.99	8.0	1.00	75	1	3294	4896	0.673	0.678
1081	203	102	25.4	25.4	3562	1.99	8.0	1.00	75	2	3886	4896	0.794	0.827
1082	203	102	25.4	25.4	3562	1.99	8.0	1.00	75	3	4196	4896	0.857	0.882
1083	203	102	25.4	25.4	3562	1.99	8.0	1.00	75	4	4366	4896	0.892	0.910
1084	203	102	25.4	25.4	3562	1.99	8.0	1.00	75	5	4469	4896	0.913	0.928
1085	203	102	25.4	25.4	3562	1.99	8.0	1.00	75	7	4578	4896	0.935	0.948
1086	203	102	25.4	25.4	3562	1.99	8.0	1.00	75	11	4658	4896	0.951	0.966
1087	203	102	15.9	15.9	4138	1.99	12.8	1.00	100	1	1353	1704	0.794	0.787
1088	203	102	15.9	15.9	4138	1.99	12.8	1.00	100	2	1494	1704	0.877	0.889
1089	203	102	15.9	15.9	4138	1.99	12.8	1.00	100	3	1560	1704	0.916	0.924
1090	203	102	15.9	15.9	4138	1.99	12.8	1.00	100	4	1594	1704	0.936	0.943
1091	203	102	15.9	15.9	4138	1.99	12.8	1.00	100	5	1614	1704	0.947	0.954
1092	203	102	15.9	15.9	4138	1.99	12.8	1.00	100	7	1634	1704	0.959	0.967
1093	203	102	15.9	15.9	4138	1.99	12.8	1.00	100	11	1649	1704	0.968	0.979
1094	203	102	15.9	19.0	4257	1.99	12.8	1.19	100	1	1330	1714	0.776	0.774
1095	203	102	15.9	19.0	4257	1.99	12.8	1.19	100	2	1481	1714	0.864	0.881
1096	203	102	15.9	19.0	4257	1.99	12.8	1.19	100	3	1553	1714	0.906	0.920
1097	203	102	15.9	19.0	4257	1.99	12.8	1.19	100	4	1591	1714	0.928	0.939
1098	203	102	15.9	19.0	4257	1.99	12.8	1.19	100	5	1612	1714	0.941	0.951
1099	203	102	15.9	22.2	4381	1.99	12.8	1.40	100	1	1305	1724	0.757	0.759
1100	203	102	15.9	22.2	4381	1.99	12.8	1.40	100	2	1467	1724	0.851	0.874
1101	203	102	15.9	22.2	4381	1.99	12.8	1.40	100	3	1545	1724	0.896	0.914
1102	203	102	15.9	22.2	4381	1.99	12.8	1.40	100	4	1586	1724	0.920	0.935
1103	203	102	15.9	22.2	4381	1.99	12.8	1.40	100	5	1610	1724	0.934	0.948
1104	203	102	15.9	25.4	4507	1.99	12.8	1.60	100	1	1280	1734	0.738	0.745
1105	203	102	15.9	25.4	4507	1.99	12.8	1.60	100	2	1452	1734	0.837	0.866
1106	203	102	15.9	25.4	4507	1.99	12.8	1.60	100	3	1536	1734	0.886	0.909
1107	203	102	15.9	25.4	4507	1.99	12.8	1.60	100	4	1581	1734	0.912	0.931
1108	203	102	15.9	25.4	4507	1.99	12.8	1.60	100	5	1607	1734	0.927	0.945
1109	203	102	15.9	28.6	4636	1.99	12.8	1.80	100	1	1253	1743	0.719	0.731
1110	203	102	15.9	28.6	4636	1.99	12.8	1.80	100	2	1436	1743	0.824	0.859
1111	203	102	15.9	28.6	4636	1.99	12.8	1.80	100	3	1526	1743	0.876	0.904
1112	203	102	15.9	28.6	4636	1.99	12.8	1.80	100	4	1575	1743	0.904	0.928
1113	203	102	15.9	28.6	4636	1.99	12.8	1.80	100	5	1603	1743	0.920	0.942
1114	203	102	15.9	31.8	4767	1.99	12.8	2.00	100	1	1226	1752	0.700	0.716
1115	203	102	15.9	31.8	4767	1.99	12.8	2.00	100	2	1419	1752	0.810	0.851
1116	203	102	15.9	31.8	4767	1.99	12.8	2.00	100	3	1516	1752	0.865	0.899
1117	203	102	15.9	31.8	4767	1.99	12.8	2.00	100	4	1568	1752	0.895	0.924
1118	203	102	15.9	31.8	4767	1.99	12.8	2.00	100	5	1599	1752	0.913	0.939

Run #	b_Y	b_X	t	d	L	b_Y/b_X	b_Y/t	d/t	L/r_Y	n	P_T	P_M	P_T/P_M	Ω
1119	203	102	19.0	19.0	4327	1.99	10.7	1.00	100	1	1563	2074	0.754	0.750
1120	203	102	19.0	19.0	4327	1.99	10.7	1.00	100	2	1766	2074	0.851	0.868
1121	203	102	19.0	19.0	4327	1.99	10.7	1.00	100	3	1864	2074	0.899	0.910
1122	203	102	19.0	19.0	4327	1.99	10.7	1.00	100	4	1917	2074	0.925	0.932
1123	203	102	19.0	19.0	4327	1.99	10.7	1.00	100	5	1948	2074	0.939	0.945
1124	203	102	19.0	19.0	4327	1.99	10.7	1.00	100	7	1979	2074	0.954	0.961
1125	203	102	19.0	19.0	4327	1.99	10.7	1.00	100	11	2004	2074	0.966	0.975
1126	203	102	22.2	22.2	4533	1.99	9.1	1.00	100	1	1734	2433	0.713	0.714
1127	203	102	22.2	22.2	4533	1.99	9.1	1.00	100	2	2007	2433	0.825	0.847
1128	203	102	22.2	22.2	4533	1.99	9.1	1.00	100	3	2146	2433	0.882	0.896
1129	203	102	22.2	22.2	4533	1.99	9.1	1.00	100	4	2221	2433	0.913	0.921
1130	203	102	22.2	22.2	4533	1.99	9.1	1.00	100	5	2264	2433	0.930	0.936
1131	203	102	22.2	22.2	4533	1.99	9.1	1.00	100	7	2313	2433	0.950	0.954
1132	203	102	22.2	22.2	4533	1.99	9.1	1.00	100	11	2348	2433	0.965	0.971
1133	203	102	22.2	25.4	4664	1.99	9.1	1.14	100	1	1692	2439	0.694	0.700
1134	203	102	22.2	25.4	4664	1.99	9.1	1.14	100	2	1979	2439	0.811	0.840
1135	203	102	22.2	25.4	4664	1.99	9.1	1.14	100	3	2127	2439	0.872	0.891
1136	203	102	22.2	25.4	4664	1.99	9.1	1.14	100	4	2209	2439	0.906	0.917
1137	203	102	22.2	25.4	4664	1.99	9.1	1.14	100	5	2255	2439	0.924	0.933
1138	203	102	22.2	28.6	4796	1.99	9.1	1.29	100	1	1649	2445	0.675	0.686
1139	203	102	22.2	28.6	4796	1.99	9.1	1.29	100	2	1950	2445	0.797	0.833
1140	203	102	22.2	28.6	4796	1.99	9.1	1.29	100	3	2108	2445	0.862	0.886
1141	203	102	22.2	28.6	4796	1.99	9.1	1.29	100	4	2195	2445	0.898	0.913
1142	203	102	22.2	28.6	4796	1.99	9.1	1.29	100	5	2246	2445	0.919	0.930
1143	203	102	22.2	31.8	4931	1.99	9.1	1.43	100	1	1606	2450	0.656	0.672
1144	203	102	22.2	31.8	4931	1.99	9.1	1.43	100	2	1920	2450	0.784	0.825
1145	203	102	22.2	31.8	4931	1.99	9.1	1.43	100	3	2088	2450	0.852	0.881
1146	203	102	22.2	31.8	4931	1.99	9.1	1.43	100	4	2179	2450	0.890	0.910
1147	203	102	22.2	31.8	4931	1.99	9.1	1.43	100	5	2235	2450	0.913	0.927
1148	203	102	25.4	25.4	4749	1.99	8.0	1.00	100	1	1866	2776	0.672	0.678
1149	203	102	25.4	25.4	4749	1.99	8.0	1.00	100	2	2214	2776	0.798	0.827
1150	203	102	25.4	25.4	4749	1.99	8.0	1.00	100	3	2400	2776	0.864	0.882
1151	203	102	25.4	25.4	4749	1.99	8.0	1.00	100	4	2498	2776	0.900	0.910
1152	203	102	25.4	25.4	4749	1.99	8.0	1.00	100	5	2560	2776	0.922	0.928
1153	203	102	25.4	25.4	4749	1.99	8.0	1.00	100	7	2626	2776	0.946	0.948
1154	203	102	25.4	25.4	4749	1.99	8.0	1.00	100	11	2677	2776	0.964	0.966
1155	203	102	15.9	15.9	6208	1.99	12.8	1.00	150	1	620	785	0.789	0.787
1156	203	102	15.9	15.9	6208	1.99	12.8	1.00	150	2	689	785	0.878	0.889
1157	203	102	15.9	15.9	6208	1.99	12.8	1.00	150	3	723	785	0.920	0.924
1158	203	102	15.9	15.9	6208	1.99	12.8	1.00	150	4	740	785	0.943	0.943
1159	203	102	15.9	15.9	6208	1.99	12.8	1.00	150	5	750	785	0.955	0.954
1160	203	102	15.9	15.9	6208	1.99	12.8	1.00	150	7	760	785	0.968	0.967

Run #	b_Y	b_X	t	d	L	b_Y/b_X	b_Y/t	d/t	L/r_Y	n	P_T	P_M	P_T/P_M	Ω
1161	203	102	15.9	15.9	6208	1.99	12.8	1.00	150	11	768	785	0.979	0.979
1162	203	102	19.0	19.0	6490	1.99	10.7	1.00	150	1	706	940	0.751	0.750
1163	203	102	19.0	19.0	6490	1.99	10.7	1.00	150	2	802	940	0.854	0.868
1164	203	102	19.0	19.0	6490	1.99	10.7	1.00	150	3	850	940	0.904	0.910
1165	203	102	19.0	19.0	6490	1.99	10.7	1.00	150	4	875	940	0.932	0.932
1166	203	102	19.0	19.0	6490	1.99	10.7	1.00	150	5	890	940	0.947	0.945
1167	203	102	19.0	19.0	6490	1.99	10.7	1.00	150	7	906	940	0.965	0.961
1168	203	102	19.0	19.0	6490	1.99	10.7	1.00	150	11	918	940	0.977	0.975
1169	203	102	22.2	22.2	6799	1.99	9.1	1.00	150	1	778	1093	0.712	0.714
1170	203	102	22.2	22.2	6799	1.99	9.1	1.00	150	2	904	1093	0.827	0.847
1171	203	102	22.2	22.2	6799	1.99	9.1	1.00	150	3	969	1093	0.887	0.896
1172	203	102	22.2	22.2	6799	1.99	9.1	1.00	150	4	1005	1093	0.920	0.921
1173	203	102	22.2	22.2	6799	1.99	9.1	1.00	150	5	1027	1093	0.939	0.936
1174	203	102	22.2	22.2	6799	1.99	9.1	1.00	150	7	1049	1093	0.960	0.954
1175	203	102	22.2	22.2	6799	1.99	9.1	1.00	150	11	1066	1093	0.976	0.971
1176	203	102	25.4	25.4	7123	1.99	8.0	1.00	150	1	834	1241	0.672	0.678
1177	203	102	25.4	25.4	7123	1.99	8.0	1.00	150	2	993	1241	0.800	0.827
1178	203	102	25.4	25.4	7123	1.99	8.0	1.00	150	3	1078	1241	0.869	0.882
1179	203	102	25.4	25.4	7123	1.99	8.0	1.00	150	4	1126	1241	0.907	0.910
1180	203	102	25.4	25.4	7123	1.99	8.0	1.00	150	5	1155	1241	0.931	0.928
1181	203	102	25.4	25.4	7123	1.99	8.0	1.00	150	7	1185	1241	0.955	0.948
1182	203	102	25.4	25.4	7123	1.99	8.0	1.00	150	11	1208	1241	0.974	0.966
1183	203	102	15.9	15.9	8277	1.99	12.8	1.00	200	1	352	447	0.788	0.787
1184	203	102	15.9	15.9	8277	1.99	12.8	1.00	200	2	393	447	0.879	0.889
1185	203	102	15.9	15.9	8277	1.99	12.8	1.00	200	3	412	447	0.922	0.924
1186	203	102	15.9	15.9	8277	1.99	12.8	1.00	200	4	423	447	0.945	0.943
1187	203	102	15.9	15.9	8277	1.99	12.8	1.00	200	5	429	447	0.959	0.954
1188	203	102	15.9	15.9	8277	1.99	12.8	1.00	200	7	435	447	0.973	0.967
1189	203	102	15.9	15.9	8277	1.99	12.8	1.00	200	11	440	447	0.983	0.979
1190	203	102	15.9	19.0	8513	1.99	12.8	1.19	200	1	345	448	0.770	0.774
1191	203	102	15.9	19.0	8513	1.99	12.8	1.19	200	2	388	448	0.867	0.881
1192	203	102	15.9	19.0	8513	1.99	12.8	1.19	200	3	409	448	0.915	0.920
1193	203	102	15.9	19.0	8513	1.99	12.8	1.19	200	4	421	448	0.940	0.939
1194	203	102	15.9	19.0	8513	1.99	12.8	1.19	200	5	427	448	0.954	0.951
1195	203	102	15.9	22.2	8762	1.99	12.8	1.40	200	1	337	448	0.752	0.759
1196	203	102	15.9	22.2	8762	1.99	12.8	1.40	200	2	383	448	0.855	0.874
1197	203	102	15.9	22.2	8762	1.99	12.8	1.40	200	3	406	448	0.906	0.914
1198	203	102	15.9	22.2	8762	1.99	12.8	1.40	200	4	419	448	0.934	0.935
1199	203	102	15.9	22.2	8762	1.99	12.8	1.40	200	5	426	448	0.950	0.948
1200	203	102	15.9	25.4	9015	1.99	12.8	1.60	200	1	329	449	0.733	0.745
1201	203	102	15.9	25.4	9015	1.99	12.8	1.60	200	2	378	449	0.842	0.866
1202	203	102	15.9	25.4	9015	1.99	12.8	1.60	200	3	403	449	0.898	0.909

Run #	b_Y	b_X	t	d	L	b_Y/b_X	b_Y/t	d/t	L/r_Y	n	P_T	P_M	P_T/P_M	Ω
1203	203	102	15.9	25.4	9015	1.99	12.8	1.60	200	4	416	449	0.927	0.931
1204	203	102	15.9	25.4	9015	1.99	12.8	1.60	200	5	424	449	0.944	0.945
1205	203	102	15.9	28.6	9272	1.99	12.8	1.80	200	1	321	449	0.715	0.731
1206	203	102	15.9	28.6	9272	1.99	12.8	1.80	200	2	373	449	0.830	0.859
1207	203	102	15.9	28.6	9272	1.99	12.8	1.80	200	3	399	449	0.889	0.904
1208	203	102	15.9	28.6	9272	1.99	12.8	1.80	200	4	414	449	0.921	0.928
1209	203	102	15.9	28.6	9272	1.99	12.8	1.80	200	5	422	449	0.939	0.942
1210	203	102	15.9	31.8	9533	1.99	12.8	2.00	200	1	313	450	0.697	0.716
1211	203	102	15.9	31.8	9533	1.99	12.8	2.00	200	2	367	450	0.817	0.851
1212	203	102	15.9	31.8	9533	1.99	12.8	2.00	200	3	396	450	0.880	0.899
1213	203	102	15.9	31.8	9533	1.99	12.8	2.00	200	4	411	450	0.913	0.924
1214	203	102	15.9	31.8	9533	1.99	12.8	2.00	200	5	420	450	0.934	0.939
1215	203	102	19.0	19.0	8654	1.99	10.7	1.00	200	1	399	532	0.750	0.750
1216	203	102	19.0	19.0	8654	1.99	10.7	1.00	200	2	455	532	0.855	0.868
1217	203	102	19.0	19.0	8654	1.99	10.7	1.00	200	3	483	532	0.907	0.910
1218	203	102	19.0	19.0	8654	1.99	10.7	1.00	200	4	497	532	0.935	0.932
1219	203	102	19.0	19.0	8654	1.99	10.7	1.00	200	5	506	532	0.951	0.945
1220	203	102	19.0	19.0	8654	1.99	10.7	1.00	200	7	515	532	0.968	0.961
1221	203	102	19.0	19.0	8654	1.99	10.7	1.00	200	11	522	532	0.982	0.975
1222	203	102	22.2	22.2	9066	1.99	9.1	1.00	200	1	439	617	0.711	0.714
1223	203	102	22.2	22.2	9066	1.99	9.1	1.00	200	2	511	617	0.829	0.847
1224	203	102	22.2	22.2	9066	1.99	9.1	1.00	200	3	549	617	0.890	0.896
1225	203	102	22.2	22.2	9066	1.99	9.1	1.00	200	4	569	617	0.922	0.921
1226	203	102	22.2	22.2	9066	1.99	9.1	1.00	200	5	581	617	0.942	0.936
1227	203	102	22.2	22.2	9066	1.99	9.1	1.00	200	7	594	617	0.964	0.954
1228	203	102	22.2	22.2	9066	1.99	9.1	1.00	200	11	605	617	0.980	0.971
1229	203	102	22.2	25.4	9327	1.99	9.1	1.14	200	1	427	617	0.693	0.700
1230	203	102	22.2	25.4	9327	1.99	9.1	1.14	200	2	504	617	0.816	0.840
1231	203	102	22.2	25.4	9327	1.99	9.1	1.14	200	3	543	617	0.880	0.891
1232	203	102	22.2	25.4	9327	1.99	9.1	1.14	200	4	565	617	0.916	0.917
1233	203	102	22.2	25.4	9327	1.99	9.1	1.14	200	5	579	617	0.937	0.933
1234	203	102	22.2	28.6	9593	1.99	9.1	1.29	200	1	416	618	0.674	0.686
1235	203	102	22.2	28.6	9593	1.99	9.1	1.29	200	2	496	618	0.802	0.833
1236	203	102	22.2	28.6	9593	1.99	9.1	1.29	200	3	538	618	0.871	0.886
1237	203	102	22.2	28.6	9593	1.99	9.1	1.29	200	4	561	618	0.909	0.913
1238	203	102	22.2	28.6	9593	1.99	9.1	1.29	200	5	576	618	0.932	0.930
1239	203	102	22.2	31.8	9861	1.99	9.1	1.43	200	1	405	618	0.655	0.672
1240	203	102	22.2	31.8	9861	1.99	9.1	1.43	200	2	487	618	0.789	0.825
1241	203	102	22.2	31.8	9861	1.99	9.1	1.43	200	3	532	618	0.861	0.881
1242	203	102	22.2	31.8	9861	1.99	9.1	1.43	200	4	558	618	0.902	0.910
1243	203	102	22.2	31.8	9861	1.99	9.1	1.43	200	5	573	618	0.927	0.927
1244	203	102	25.4	25.4	9498	1.99	8.0	1.00	200	1	470	699	0.672	0.678

Run #	b_Y	b_X	t	d	L	b_Y/b_X	b_Y/t	d/t	L/r_Y	n	P_T	P_M	P_T/P_M	Ω
1245	203	102	25.4	25.4	9498	1.99	8.0	1.00	200	2	561	699	0.802	0.827
1246	203	102	25.4	25.4	9498	1.99	8.0	1.00	200	3	609	699	0.871	0.882
1247	203	102	25.4	25.4	9498	1.99	8.0	1.00	200	4	636	699	0.910	0.910
1248	203	102	25.4	25.4	9498	1.99	8.0	1.00	200	5	652	699	0.933	0.928
1249	203	102	25.4	25.4	9498	1.99	8.0	1.00	200	7	670	699	0.958	0.948
1250	203	102	25.4	25.4	9498	1.99	8.0	1.00	200	11	684	699	0.978	0.966

Chapter 6: Summary, conclusions, and recommendations

6.1. Summary

The present dissertation contributed to advancing methods of quantifying the elastic and inelastic resistance of compression members with single and back-to-back double angles, as summarized in the following:

a) The study developed the variational principle, governing equations, boundary conditions, and closed form buckling solutions for determining the elastic buckling resistance of compression members with asymmetric cross-sections with end restraints defined along non-principal axes, which fall outside of the scope of the classical buckling solution.

b) The study developed a database of inelastic compressive resistance for 936 eccentrically loaded single angle compression members with end conditions that simulate gusset plate end conditions based on 3D shell-based finite element models based on ABAQUS that capture initial out-of-straightness, geometric and material nonlinear effects and load eccentricity. The database was then used to develop a simple design method capable of predicting the compressive resistance of such members.

c) The study formulated a finite element buckling solution for the elastic compressive resistance of back-to-back double angle assemblies featuring non-principal end restraints and user-defined multi-point constraints needed to model the discrete interconnectors between the individual angles. The study also extended the generalized Vlasov theory to predict the elastic buckling resistance of back-to-back double angle assemblies for the limiting case where enough interconnectors are provided to enforce a monolithic action between both angles. Both solutions were used to generate a database of flexural-torsional buckling resistance for 1250 back-to-back double angle assemblies and develop a simple and reliable expression for

predicting the elastic buckling resistance of double angle assemblies. Possible means for integrating the new expression into design standards to predict the inelastic compressive resistance of such assemblies were demonstrated through a design example.

6.2. Main conclusions

The main conclusions of the present dissertation are

a) The elastic buckling load for a compression member with a pin-end restraint about a non-principal axis and a fixity end restraint about the orthogonal axis is significantly influenced by the angle of inclination between the fixity axis and the minor principal axis. In compression members with angle cross-sections, the angle of inclination is related to the leg width ratio of the outstanding leg to that of the connected leg.

b) While the effective slenderness method implemented in CSA S16-19 involves relatively simple procedure, it can overestimate the compressive resistance of eccentrically loaded single angle compression members. Conversely, the beam-column interaction method in CSA S16-19 involves a lengthy design procedure and can grossly underestimate the compressive resistance of the member. The design methodology based on the reduction factor proposed in the present study offers a simple and more accurate prediction of the member resistance when compared to present methods in design standards.

c) The proposed extension of Vlasov theory provided a formal means to determine the location of the shear centre of back-to-back double angle assemblies as well as the overall warping constant of the assemblies. These properties were shown to highly influence the elastic flexural-torsional buckling resistance for compression members with relatively short spans in which warping effects are significant in the limiting case where enough interconnectors are provided to enforce a monolithic response.

d) The modified slenderness approach for double angel members available in CSA S16-19 and ANSI/AISC 360-16 can noticeably underestimate the elastic flexural-torsional buckling resistance for assemblies with a few interconnectors. In this context, an improved prediction of the buckling load can be predicted from the solution proposed in the present study based on the reduction factor expression.

6.3. Recommendations for future research

a) The elastic buckling solutions of the characteristic equations obtained in the present study for members with non-principal end restraints involve an iterative technique. The procedure can be simplified by developing effective length factors that capture the effect of non-principal end conditions on the elastic buckling resistance.

b) The Vlasov theory extension for back-to-back double angle assemblies can be extended to determine the overall warping constant for other types of assemblies such as those with star-shaped angles, back-to-back channels, etc.

c) The finite element formulation developed for the elastic buckling resistance of asymmetric cross-sections can be extended to beam-columns to enable the modelling of load eccentricities. The formulation can be also used/extended for the elastic buckling analysis of compression chords in trusses and open-web steel joists.

d) The present study has conservatively omitted the partial rotational restraints provided by the gusset plates. While such a conservative approach is appropriate from a design perspective, it is possible to further refine the solutions by incorporating the rotational restraint effects provided by the gusset plates to the models, and possibly develop effective length factors that reflect their beneficial effects. Experimental verifications for such models and effective lengths are also recommended.